Cymantren- und Ferrocen-basierte Poly(pyrazol-1-yl)borate: Kation-π Wechselwirkungen und Multidecker-Sandwichkomplexe

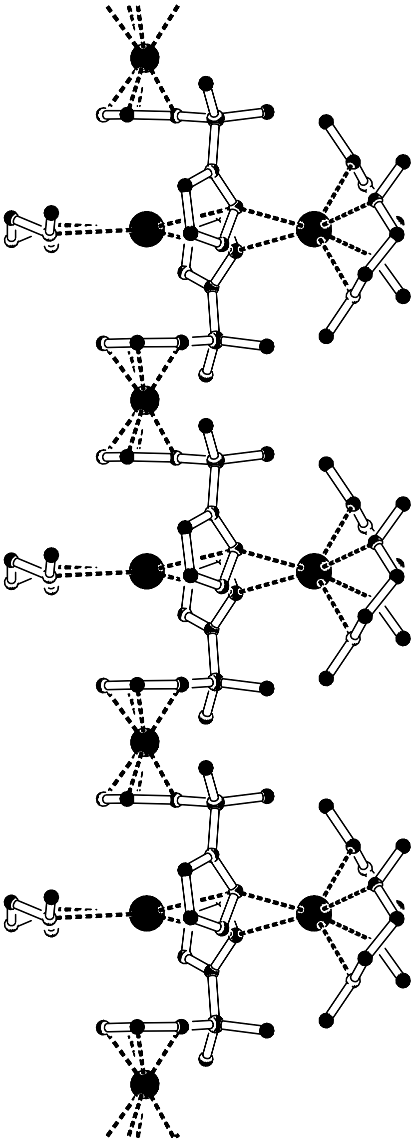

Alireza Haghiri Ilkhechi

Cymantren- und Ferrocen-basierte Poly(pyrazol-1-yl)borate: Kation-π Wechselwirkungen und Multidecker-Sandwichkomplexe

Dissertation
zur Erlangung des Doktorgrades
der Naturwissenschaften

vorgelegt beim Fachbereich chemische und pharmazeutische Wissenschaften
der Johann Wolfgang Goethe-Universität
in Frankfurt am Main

von

Alireza Haghiri Ilkhechi
aus Teheran
Frankfurt am Main, 2005

Vom Fachbereich chemische und pharmazeutische Wissenschaften der Johann Wolfgang Goethe-Universität als Dissertation angenommen.

Dekan: Prof. Dr. H. Schwalbe

Gutachter: (1) Prof. Dr. M. Wagner
(2) Prof. Dr. B. O. Kolbesen

Datum der Disputation: 17.06.2005

Die vorliegende Arbeit entstand in der Zeit von August 2002 bis März 2005 am Institut für Anorganische und Analytische Chemie der Johann Wolfgang Goethe-Universität in Frankfurt am Main.

Danksagung

Mein besonderer Dank gebührt meinem sehr verehrten Lehrer

Herrn Prof. Dr. Matthias Wagner

für sein mir entgegengebrachtes Vertrauen, die Aufnahme in den Arbeitskreis, die Überlassung eines Laborplatzes, sein großes Interesse an der vorliegenden Arbeit, zahlreiche konstruktive Diskussionen, die ständige Hilfsbereitschaft, welche in besonderem Maße zum Gelingen dieser Arbeit beigetragen hat und nicht zuletzt die mir gewährte wissenschaftliche Freiheit.

Herzlich bedanken möchte ich mich bei Herrn Dr. Hans Wolfram Lerner für die stets angenehme und freundschaftliche Atmosphäre und gute Zusammenarbeit mit vielen interessanten Diskussionen.

Ein besonders herzliches Dankeschön gebührt Frau Beate Wagner und Frau Angelika Lerner, die für große und etwas weniger weltbewegende Probleme immer ein offenes Ohr hatten.

Ganz besonderen Dank schulde ich meinen Laborkollegen – Susanne Bieller, Dr. Fang Chenije, Franz Dornhaus, Birgit Dissinger, Oliver Dietz, Dr. Shengli Guo, Monika Haberecht, Julia Heilmann, Theresa Kückmann, Tonia Kretz, Dr. Kuangbiao Ma, Dr. Li Ding, Dr. Günter Margraf, Gabriele Otto, Kai Ruth, Ingeborg Sänger, Frauke Schödel, Matthias Scheibitz, Dr. Stefan Scholz, Hans-Peter Weiß und Dr. Fan Zhang – die mich zwei Jahre begleitet haben. Das humorvolle Miteinander und die angenehme Arbeitsatmosphäre werde ich nicht vergessen.

Mein Dank gilt ferner:

Herrn Dr. Michael Bolte und Herrn Dr. Jan W. Bats für die Durchführung der Röntgenstrukturanalysen,

Herrn Dr. J. Gottfried Zimmermann, Herrn Reinhard Olbrich, Frau Eva-Maria Schmid und Frau Bärbel Langer für die Hilfe bei NMR- spektroskopischen Fragestellungen und die Durchführung zahlreicher Heterokern-Spektren,

Herrn Michael Röder und Herrn Reinhold Gutberlet für die Herstellung und Bearbeitung der hoch komplizierten Glasapparaturen für meine Versuche,

Frau Ilona Brill und Frau Hannelore Priess für die Aufnahme der ESI- und MALDI-Massenspektren,

Frau Marianne Christoph für die Durchführung der Elementaranalysen.

Ganz besonders danke ich meinen Eltern, die mich während meines gesamten Studiums und der Promotion nach Kräften unterstützt haben. Ihnen sei daher diese Arbeit in tiefster Dankbarkeit gewidmet.

Ein reines Aug' nur kann erschaun,

hell wie des Neumonds Licht,

Das Mondlein dort, es spiegelt sich

in jedem Auge nicht.

Gedicht von Hafez

Verwendete Abkürzungen:

Å	Angström
Abb.	Abbildung
Äquiv.	Äquivalent (e)
ber.	berechnet
br	breit (NMR)
bzw.	beziehungsweise
COG	Center of gravity (Schwerpunkt eines cyclischen π-Systems)
Cp	Cyclopentadienyl
Cp´	Methylcyclopentadienyl
Cp*	Pentamethylcyclopentadienyl
CV	Cyclovoltammetrie
Cym	Cymantrenyl
Cym´	Methylcymantrenyl
d	Tag (e); Dublett (NMR)
DFT	Dichtefunktionaltheorie
d.h.	das heißt
DME	Dimethoxyethan
DMF	N,N-Dimethylformamid
DMSO	Dimethylsulfoxid
δ	chemische Verschiebung in der Kernresonanzspektroskopie [ppm]
Et	Ethyl, $-CH_2-CH_3$
Et_2O	Diethylether
exc.	Überschuss
Fc	Ferrocenyl, $-C_5H_4FeC_5H_5$
fc	1,1´-Ferrocendiyl, $(-C_5H_4)_2Fe$
FcH	Ferrocen, $C_5H_5FeC_5H_5$
ggf.	gegebenenfalls
h	Stunde (n)
$h_{1/2}$	Halbhöhenbreite
HOMO	highest occupied molecular orbital
Hpz	Pyrazol

HV	Hochvakuum
Hz	Hertz
IR	Infrarot (Spektroskopie)
J	skalare Kopplungskonstante in der Kernresonanzspektroskopie [Hz]
K	Kelvin
12-Krone-4	1,4,7,10-Tetraoxacyclododecan
KZ	Koordinationszahl
Lit.	Literaturstelle
LM	Lösungsmittel
LUMO	lowest unoccupied molecular orbital
M	Metallatom
MALDI	Matrix Assisted Laser Desorption/Ionization
Me	Methyl, -CH_3
MeCN	Acetonitril
MHz	Megahertz
min	Minute (n)
ml	Milliliter
mmol	Millimol
MS	Massenspektrometrie
m/z	Verhältnis von Masse zu Ladung
n.a.	Multiplett im NMR-Spektrum erwartet, aber nicht aufgelöst
n.b.	nicht beobachtet (NMR)
NEt_3	Triethylamin
NMR	Kernresonanzspektroskopie
ÖV	Ölpumpenvakuum
Ph	Phenyl, -C_6H_5
PPh_3	Triphenylphosphan
ppm	parts per million
pz	Pyrazolyl
R	beliebiger Rest
rel.	relativ
RT	Raumtemperatur
s	Sekunde (n); Singulett (NMR)
$SiMe_3$	Trimethylsilyl

sept	Septett (NMR)
Tab.	Tabelle
^{t}Bu	*tert*-Butyl, $-C(CH_3)_3$
TG	Thermogravimetrie
THF	Tetrahydrofuran
TlOEt	Thalliumethanolat
Tol	Tolyl
Tp	Tris(pyrazol-1-yl)borat
tr	Triplett (NMR)
u.a.	unter anderem
UV	Ultraviolett (Spektroskopie)
υ	Wellenzahl [cm^{-1}]
V	Volt
vgl.	vergleiche
vs.	versus
vtr	virtuelles Triplett (NMR)
z.B.	zum Beispiel

Inhaltsverzeichnis

1 Übersicht über die experimentellen Ergebnisse

1.1 Einleitung und Aufgabenstellung

Trofimenko hat im Jahre 1966 Tris(pyrazol-1-yl)borate als Liganden in die Übergangsmetallchemie eingeführt.[1] Er prägte für diese Verbindungsklasse den Trivialnamen „Skorpionate“, der sich auch in der Literatur durchgesetzt hat. Die Bezeichnung leitet sich von der Molekülstruktur der Tris(pyrazol-1-yl)borate **1** ab, die an einen Skorpion erinnert: Zwei Pyrazolreste bilden gleichsam die Scheren des Skorpions, während der dritte den Stachel darstellt (Abb. **1**).

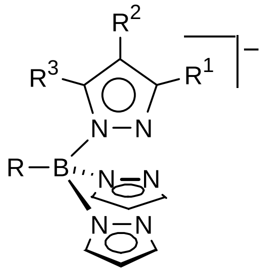

1

Abb. **1**: Schematische Darstellung eines Tris(pyrazol-1-yl)borats (Skorpionats) **1**. Aus Gründen der Übersichtlichkeit wurden die Reste R^1 – R^3 an zwei der drei Pyrazolylliganden nicht dargestellt.

Skorpionate haben in der Koordinationschemie sehr schnell eine breit gefächerte Anwendung gefunden.[2] Das liegt zum einen daran, dass es sich um äußerst stabile Einheiten handelt, zum anderen lassen sie sich aus Pyrazolbausteinen mit unterschiedlichsten Substitutionsmustern (R^1 – R^3) zusammensetzen. Weitere Derivatisierungsmöglichkeiten ergeben sich durch Variation des Substituenten R am Borzentrum. Dadurch ist es möglich, sowohl die elektronische Umgebung des komplexierten Metallions als auch den sterischen Anspruch des Liganden gezielt einzustellen.[3] Beispielweise lassen sich durch die Einführung raumerfüllender Reste in die R^1-Position des Pyrazols reaktive Komplexfragmente durch sterische Abschirmung kinetisch stabilisieren.

Die Zähnigkeit der Skorpionatliganden kann zwischen eins und drei variieren, und auch der Bißwinkel kann sich den Anforderungen des koordinierten Metallkomplexfragments anpassen. Die Skorpionateinheit wird in der Literatur oft mit dem Cyclopentadienylring verglichen. Bei beiden Systemen handelt es sich um monoanionische Liganden, die sechs Elektronen für die Bindung des Metallzentrums zur Verfügung stellen können und einen Koordinationshalbraum vollständig abschirmen. Diese Betrachtungsweise vernachlässigt jedoch wichtige Unterschiede.[4] So koordiniert das Skorpionatfragment das Zentralmetall meist dreizähnig, während der Cyclopentadienylring als η^5-Ligand wirkt. Daraus resultieren für analoge Komplexe unterschiedliche Symmetrien. Zudem lassen sich die sterischen und elektronischen Eigenschaften der Tris(pyrazol-1-yl)borat-Liganden durch Wahl eines geeigneten Substitutionsmusters mit wesentlich geringerem Syntheseaufwand einstellen, als das bei Cyclopentadienylresten möglich ist.

Die klassische Synthese von Tris(pyrazol-1-yl)boraten erfolgt durch Erhitzen von Natriumboranat ($NaBH_4$) mit dem gewählten Pyrazolderivat (Hpz) in Substanz.[5] Dazu benötigt man Temperaturen von bis zu 200 °C, so dass nur solche Pyrazolderivate verwendet werden können, die ausreichend temperaturstabil sind. Die entstehenden Produkte tragen dann, je nach eingesetzter Stöchiometrie, als vierten Substituenten am Bor entweder Wasserstoff (drei Äquiv. Hpz) oder einen weiteren Pyrazolrest (vier Äquiv. Hpz). Es sind darüber hinaus auch einige Beispiele bekannt, bei denen das Borzentrum eine Phenyl- oder Alkylgruppe trägt.

$$3\,\text{Hpz} + [\text{BH}_4]^- \rightarrow [\text{HB(pz)}_3]^- + 3\,\text{H}_2\uparrow$$

$$\text{Hpz} + [\text{HB(pz)}_3]^- \rightarrow [\text{B(pz)}_4]^- + \text{H}_2\uparrow$$

Schema **1**: Der klassische Darstellungsweg für Poly(pyrazol-1-yl)borate.

In unserem Arbeitskreis ist es gelungen, auf einem anderen Weg und unter milden Bedingungen Tris(pyrazol-1-yl)borat-Einheiten an (Methyl)Cymantren und Ferrocen zu knüpfen.[6-9] Auf diese Weise entstanden die Cymantrenyltris(pyrazol-1-yl)borate **2** und **3** mit einer Skorpionateinheit und die Ferrocenyltris(pyrazol-1-yl)borate (**4**) bzw. (**5**) mit einer bzw. zwei Skorpionateinheiten (Abb. **2**).

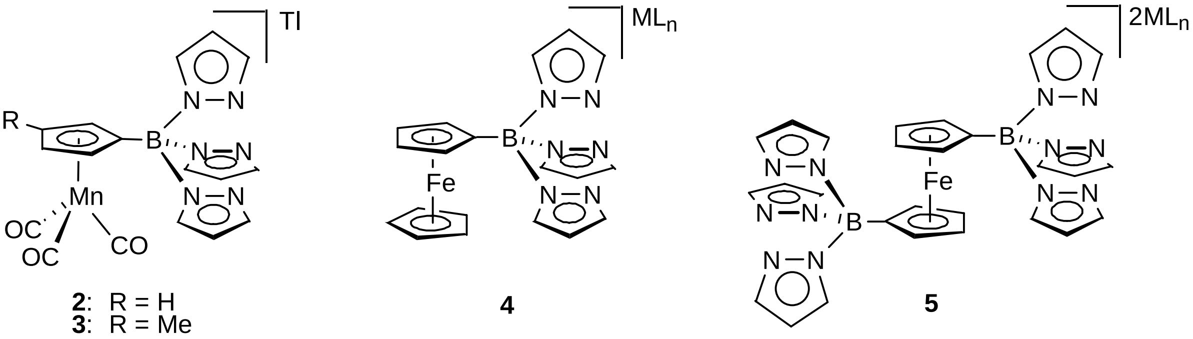

2: R = H
3: R = Me

4

5

Abb. **2**: Mono- (**2**, **3**, **4**) und difunktionelle (**5**) Tris(pyrazol-1-yl)borat-Liganden auf (Methyl)Cymantren- und Ferrocenbasis; $ML_n = Tl^+$, $Mo(CO)_3$, $Mo(CO)_2(\eta^3\text{-methylallyl})^+$, $ZrCl_3^+$.

Von den ferrocenhaltigen Skorpionatverbindungen **4** und **5** sind Tl^+-, $Mo(CO)_3$-, $Mo(CO)_2(\eta^3\text{-methylallyl})^+$-, $ZrCl_3^+$-Komplexe bekannt, wohingegen die Cymantrenyltris(pyrazol-1-yl)borate **2** und **3** bislang nur als Thallium(I)-Verbindungen erhalten wurden.

In zwei wesentlichen Punkten unterscheiden sich **4** und **5** von den meisten bislang beschriebenen Skorpionaten. Bei beiden Molekülen handelt es sich um redoxaktive Liganden, und **5** trägt darüber hinaus mehr als ein Tris(pyrazol-1-yl)borat-Fragment. Gerade die Kombination dieser beiden Eigenschaften macht die Ferrocenyltris(pyrazol-1-yl)borate **4** und **5** zu viel versprechenden Bausteinen für die Darstellung oligonuklearer Komplexe **6** und metallorganischer Polymere **7** (Abb. **3**).

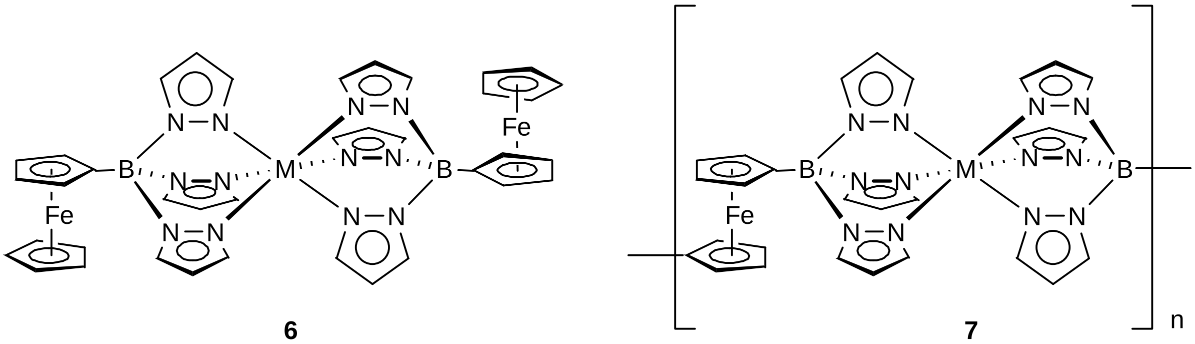

6

7

Abb. **3**: Trinukleare Komplexe **6** ($M^{(II)}$ = Mn, Fe, Co, Ni, Cu, Zn) und metallorganische Polymere **7** (M = Fe, Zn).

Aufgabenstellung

Mit den Ferrocen- und Cymantren-basierten Tris(pyrazol-1-yl)boraten **2 – 5** wurden erstmalig Hybridmoleküle geschaffen, die gleichzeitig zwei der bedeutendsten Liganden in der Koordinationschemie – den Cyclopentadienylring und die Skorpionatfunktion – enthalten. Die Aufgabe der vorliegenden Arbeit bestand darin, das Potential dieser Ligandsysteme im Hinblick auf die Darstellung oligonuclearer Komplexe und Koordinationspolymere auszuloten. Konkret waren folgende Fragestellungen zu untersuchen:

1) Anhand des Mangantricarbonylkomplexes $Mn(CO)_3[CymB(pz)_3]$ sollten die elektronischen Eigenschaften des Cp-gebundenen Mangantricarbonylfragments mit denen des Skorpionat-gebundenen verglichen werden, um Aufschlüsse über Ähnlichkeiten und Unterschiede der beiden Liganden zu erhalten. Darüber hinaus galt es zu klären, ob durch Abspaltung der CO-Liganden eine Selbstpolymerisation der $[CymBpz_3]^-$ Einheit erreicht werden kann.
2) Mit Hilfe von Ferrocenyltris(pyrazol-1-yl)borat-Liganden lassen sich zwar mehrkernige Metallkomplexe darstellen, der Grad der elektronischen Wechselwirkung zwischen der Ferroceneinheit und dem komplexierten Metallion M ist jedoch gering. Dies könnte sich ändern, wenn man die Zahl der Pyrazolyldonoren im System schrittweise verringert, so dass M nicht mehr vollständig koordinativ abgesättigt wird und in der Folge auch an den Ferrocen-Cyclopentadienylring bindet. Vor dem Hintergrund dieser Überlegung stellte sich die Aufgabe, mono- und difunktionelle Ferrocenylscorpionate des Typs $[FcB(R)pz_2]^-$, $[1,1'\text{-}fc(B(R)pz_2)_2]^{2-}$, $[FcB(R)_2pz]^-$ und $[1,1'\text{-}fc(B(R)_2pz)_2]^{2-}$ (R = Fc, Me) zu synthetisieren und deren Komplexbildungseigenschaften zu studieren.
3) Im Zusammenhang mit der unter 2) skizzierten Problematik ergab sich die weiterführende Frage, ob Multidecker-Sandwichkomplexe des Ferrocens bzw. des Benzols auch ohne stabilisierende Lewis-basische Seitenketten allein durch elektrostatische Wechselwirkungen zusammengehalten werden können. Aus diesem Grund sollten Ferrocen- und Benzol-basierte Borate des Typs $[FcBR_3]^-$, $[1,1'\text{-}fc(BR_3)_2]^{2-}$, $[C_6H_5BR_3]^-$, $[1,4\text{-}C_6H_4(BR_3)_2]^{2-}$ und $[1,3,5\text{-}C_6H_3(BR_3)_3]^{3-}$ (R = H, Me) präpariert und anschließend versucht werden, durch Zugabe geeigneter Metallionen eindimensionale stapelförmige Strukturen zu erzeugen.

1.2 Liganden auf (Methyl)Cymantrenbasis

(Methyl)Cymantren lässt sich wie Ferrocen mit Bortribromid in einem Schritt borylieren (**10**, **11**; Schema **2**).[10] Zudem trägt es drei Carbonylgruppen, die für eine nachfolgende Derivatisierung am Manganzentrum und als Sonde in der IR-Spektroskopie genutzt werden können. Aufgrund dieser Tatsache ist Cymantren eine interessante Alternative zu Ferrocen für die Darstellung von Metallocenyltris(pyrazol-1-yl)boraten.

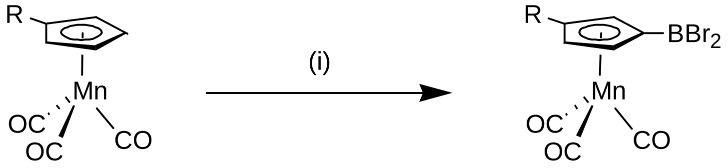

8: R = H
9: R = Me

10:R = H
11:R = Me

Schema **2**: Synthese von **10**, **11**: (i) + exc. BBr_3, Hexan, Erhitzen am Rückfluss (3d).

1.2.1 (Methyl)Cymantrenylborane als Bausteine zur Synthese von Skorpionatliganden

Die Skorpionatliganden **12** und **13** wurden erstmals von Dr. Shengli Guo in unserem Arbeitskreis dargestellt (Schema **3**).[11] Die Verbindungen sind in guten Ausbeuten durch Reaktion des borylierten (Methyl)Cymantrens **10**, **11** mit drei Äquivalenten Pyrazol, zwei Äquivalenten NEt_3 und anschließender Deprotonierung der freien Säure mit TlOEt zugänglich.

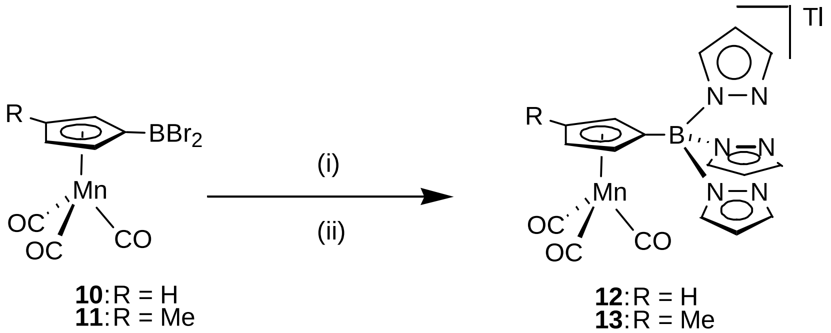

Schema **3**: Synthese von **12**, **13**: (i) + 3 Hpz, + 2 NEt_3 in Toluol; (ii) + TlOEt in Toluol.

Die resultierenden Thallium(I)-Skorpionate zeigen im Festkörper ungewöhnliche Strukturen: $[CymB(pz)_3Tl]_\infty$ (**12**, monokline Raumgruppe $P2_1/c$) bildet polymere Ketten, während $[Cym'B(pz)_3Tl]_4$ (**13**, tetragonale Raumgruppe $I4_1/a$) in Form eines cyclischen Tetramers vorliegt.[11] In beiden Fällen bindet jedes Skorpionat mit zwei Pyrazolylliganden an dasselbe Thallium(I)-Ion, während der dritte Pyrazolring an ein anderes Thallium(I)-Ion koordiniert ist. Der sperrige Cymantrenyl-Substituent am Borzentrum destabilisiert eine η^3-Koordination des Skorpionatliganden wahrscheinlich aus sterischen Gründen (vgl. auch die Kristallstruktur[12] von $[FcBpz_3Tl]_\infty$).[11] Obwohl die Carbonylliganden des Cymantrens durch Lewis Basen thermisch oder photochemisch leicht substituiert werden können, sind **12** und **13** bei Raumtemperatur im Tageslicht stabil. Man beobachtet keine Selbstpolymerisation unter Bildung von $[\text{-}MnCpB(pz)_3MnCpB(pz)_3\text{-}]_\infty$ und Freisetzung von CO-Liganden.[11]

1.2.2 Synthese und Charakterisierung der di- und trinuklearen Cymantrenyltris(pyrazol-1-yl)borate 14 – 16

Ausgehend vom Thallium(I)-Skorpionat **12** und Mangan(I)-pentacarbonylbromid ist der zweikernige Mangankomplex **14** zugänglich (Schema **4**). Dabei muss unter Luftausschluss gearbeitet werden.

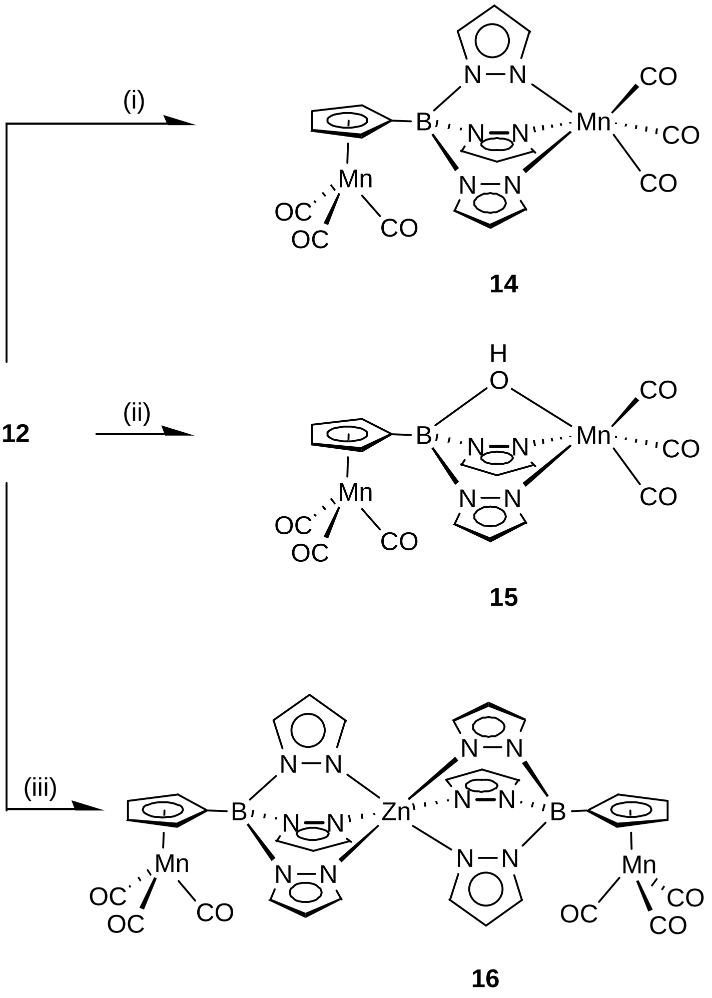

Schema **4**: Synthese von **14** - **16**: (i) + $Mn(CO)_5Br$ in THF, RT, Inertgasatmosphäre; (ii) + $Mn(CO)_5Br$ in THF, RT, keine Inertgasatmosphäre; (iii) + 0.5 $ZnBr_2$ in THF, RT, Inertgasatmophäre.[13]

Verbindung **12** besitzt in THF-Lösung eine blassgelbe Farbe. Zugabe von $Mn(CO)_5Br$ führt zu einer Farbvertiefung. Im festen Zustand ist **14** stabil und kann unter Inertgasatmosphäre und Ausschluss von UV-Licht (Sonnenlicht) ohne merkliche Zersetzung gelagert werden. Der gelbe Feststoff **14** ist in allen gängigen Lösungsmitteln nur schlecht löslich, lässt sich jedoch aus Chloroform umkristallisieren.[13]

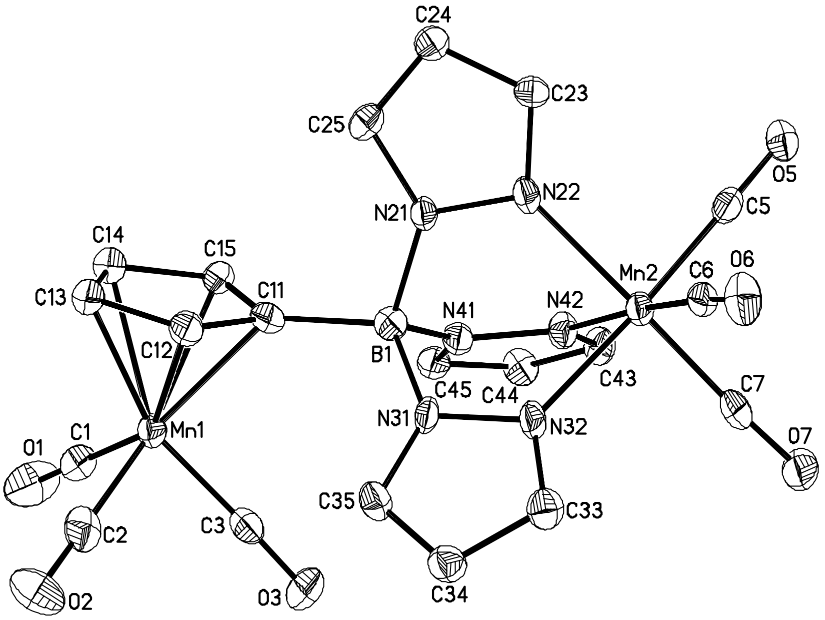

Abb. **4**: Struktur des zweikernigen Mangankomplexes **14** im Kristall. Die anisotropen Auslenkungsparameter entsprechen 50 % Aufenthaltswahrscheinlichkeit.

Abbildung **4** gibt die Struktur des Homoskorpionatkomplexes **14** im Kristall wieder (monokline Raumgruppe $P2_1$; zwei kristallographisch unabhängige Moleküle in der asymmetrischen Einheit).[13] Molekül **14** besitzt eine interessante Struktur, da hier zwei Mangantricarbonylfragmente an verschiedene Donorgruppen [Cyclopentadienyl und Tris(pyrazol-1-yl)borat] gebunden sind. Um herauszufinden, welches der beiden Manganzentren von **14** elektronenreicher ist, wurde die Verbindung nicht nur mittels Einkristall-Röntgenstrukturanalyse sondern auch mittels IR-Spektroskopie untersucht.

Besonders aufschlußreich sind die Bindungslängen zwischen den beiden Manganzentren und ihren jeweiligen Carbonylliganden sowie die C-O-Bindungslängen (starke π-Rückbindung: kurze Mn-C-Bindungslänge, langer C-O-Abstand).[13] Die durchschnittliche Bindungslänge des Mn(1)-Zentrums zu seinen Carbonylliganden beträgt 1.795(6) Å; beim Mn(2)-Zentrum sind es 1.806(5) Å. Diese Werte sind im Rahmen der Standardabweichungen gleich. Die C-O-

Bindungslängen bewegen sich in einem Intervall von C(2)-O(2) = 1.153(7) Å bis C(1)-O(1) = 1.165(7) Å mit Mittelwerten am Mn(1)-Zentrum von 1.157(6) Å und am Mn(2)-Zentrum von 1.156(6) Å. Daraus lässt sich schließen, dass der Cp-Ring und der Skorpionatligand in der Tat eine vergleichbar große Ligandenfeldstärke besitzen.

Eine zweite Sonde liefern die Valenzschwingungen der Carbonylliganden (starke Rückbindung: Verschiebung der Bande zu kleineren Wellenzahlen). Für **14** treten drei Banden bei υ(CO) = 2030, 2023, 1933 cm^{-1} (in KBr) auf.[13] Eventuelle Unterschiede in den CO-Schwingungen der beiden $Mn(CO)_3$-Fragmente sind demnach nicht aufgelöst. Die Schwingungsfrequenzen liegen bei geringfügig höheren Wellenzahlen als im Falle von **12** [υ(CO) = 2019, 1944, 1922 cm^{-1} (in TlBr)]. Im Vergleich zu Cymantren (**8**) [υ(CO) = 2035, 1949 cm^{-1} (in KBr)] sind die Werte nahezu unverändert, d.h. der $B(pz)_3Mn(CO)_3$-Substituent wirkt gegenüber dem Cymantrenyl-Fragment weder als Elektronendonor noch als Elektronenakzeptor. Aus den Befunden der Röntgenstrukturanalyse und der IR-spektroskopischen Untersuchung lässt sich schließen, dass der Cp-Ring und der Skorpionatligand in der Tat einen ähnlichen elektronischen Einfluss auf das $Mn(CO)_3$-Fragment ausüben und beide Manganzentren eine ähnliche Elektronendichte besitzen.

Führt man die Umsetzung des Thallium(I)-Skorpionats **12** mit $Mn(CO)_5Br$ ohne Luftausschluss durch, so bildet sich nicht der Homoskorpionatkomplex **14**, sondern man isoliert den Heteroskorpionatkomplex (**15**·pzH)$_2$ (Abb **5**).

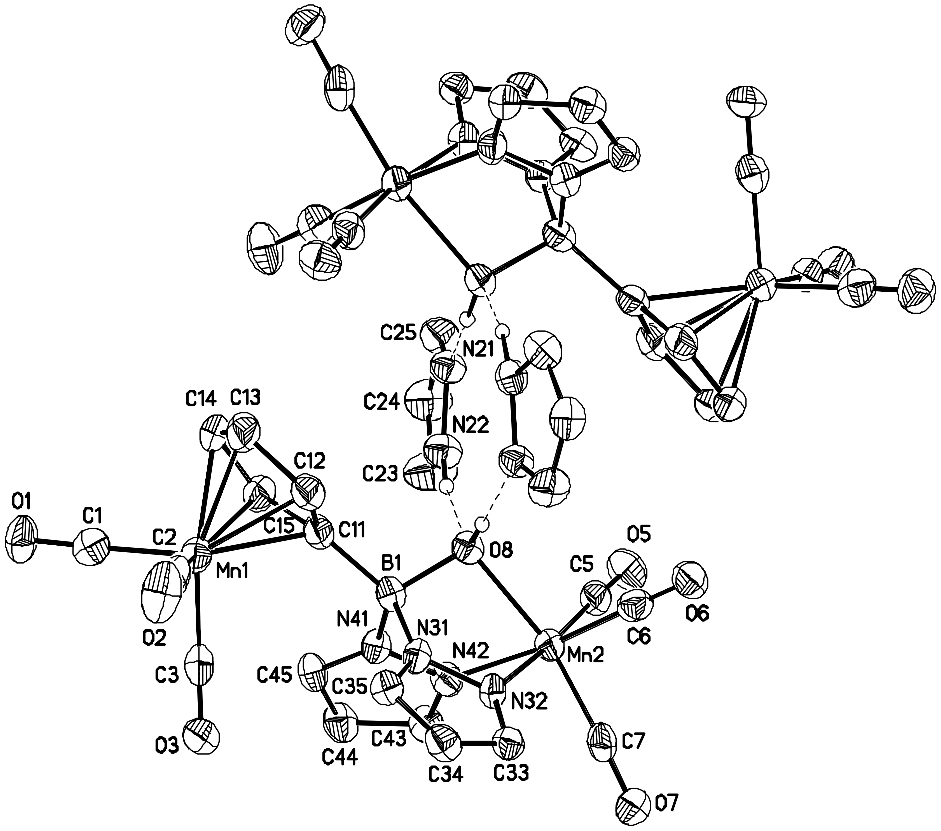

Abb. **5**: Struktur des Heteroskorpionatkomplexes (**15c**·pzH)$_2$ im Kristall. Die anisotropen Auslenkungsparameter entsprechen 50 % Aufenthaltswahrscheinlichkeit.

Abbildung **5** gibt die Struktur von (**15**·pzH)$_2$ im Kristall wieder (monokline Raumgruppe *C*2/*c*; drei unabhängige Moleküle (**15a**·pzH)$_2$, (**15b**·pzH)$_2$ und (**15c**·pzH)$_2$ in der asymmetrischen Einheit).[13] Infolge von Hydrolyse des Skorpionatliganden wurde ein Pyrazolring am Borzentrum durch eine Hydroxylgruppe verdrängt, so dass das zweite Mn(CO)$_3$-Fragment von zwei Stickstoff– und einem Sauerstoffatom koordiniert ist. Der Dimangankomplex (**15**·pzH)$_2$ kristallisiert mit einem Äquivalent Pyrazol aus. Im Festkörper liegt eine dimere Struktur vor, welche durch zwei OH···N und zwei NH···O Wasserstoffbrückenbindungen zusammengehalten wird.

Ausgehend vom Thallium(I)-Skorpionat **12** ist durch Umsetzung mit ZnBr$_2$ in THF auch die heterotrinucleare Verbindung **16** zugänglich, die in allen gängigen Lösungsmitteln nur schlecht löslich ist, sich jedoch aus C$_6$D$_6$ umkristallisieren lässt (Abb. **6**).

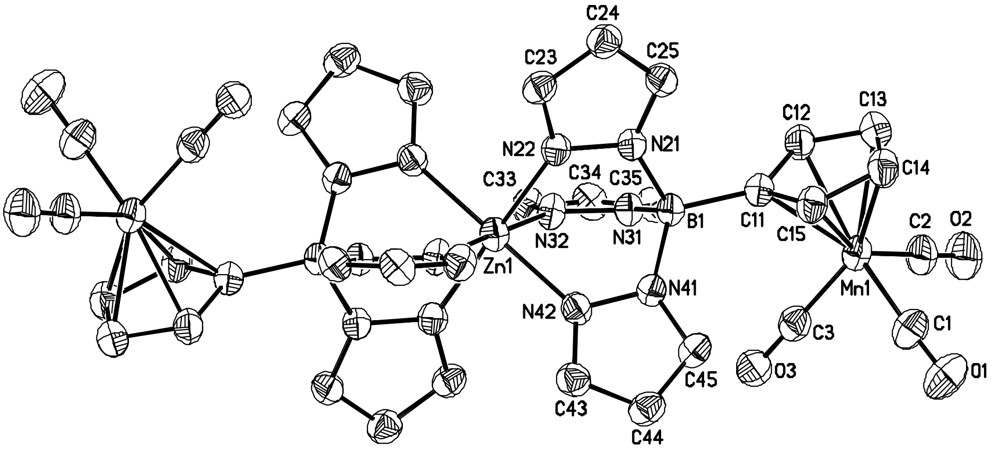

Abb. **6**: Struktur des heterotrinuclearen Komplexes **16** im Kristall. Die anisotropen Auslenkungsparameter entsprechen 50 % Aufenthaltswahrscheinlichkeit.

Abbildung **6** gibt die Struktur des heterotrinuclearen Komplexes **16** im Kristall wieder (trikline Raumgruppe $P\bar{1}$). Das Zn-Atom liegt auf einem Inversionszentrum und ist oktaedrisch von sechs Pyrazolringen umgeben. Die Konformation der $CymBpz_3$-Fragmente von **16** ist der in Molekül **14** sehr ähnlich.[13]

1.2.2.1 Photochemische Untersuchungen

Die Reaktivität der Verbindung **14** wurde durch Bestrahlung mit UV Licht (λ = 254 nm) in $CHCl_3$ in Gegenwart der Lewis-Basen CD_3CN bzw. PPh_3 untersucht.
Im ersten Fall zeigte das IR-Spektrum neben Banden bei $\upsilon(CO) = 2019$ und $1933\ cm^{-1}$ eine weitere Bande bei $\upsilon(CO) = 1862\ cm^{-1}$ (KBr-Preßling), die nicht der Verbindung **14** zuzuordnen ist.[13] Die Tatsache, dass im Vergleichssystem $C_5H_5Mn(CO)_2CH_3CN$ eine Bande bei $\upsilon(CO) = 1886\ cm^{-1}$ beobachtet wird[14], deutet auf den Austausch eines CO- gegen ein CD_3CN Molekül hin. Die gebildeten Mikrokristalle des Photolyseprodukts waren in allen gängigen Lösungsmitteln unlöslich, so dass die Molekülstruktur nicht bestimmt werden konnte. Die Bestrahlung von **14** in Gegenwart eines Äquivalents PPh_3 ergab ein qualitativ ähnliches Ergebnis (IR-Banden in KBr: $\upsilon(CO) = 2019, 1948, 1927, 1913, 1856\ cm^{-1}$; vgl. $C_5H_5Mn(CO)_2PPh_3$ in CH_2Cl_2: $\upsilon(CO) = 1931, 1864\ cm^{-1}$.[15]).

1.3 Auf dem Weg zu Ferrocen-basierten Multidecker-Sandwichkomplexen

Ähnlich wie Koordinationsverbindungen der Ferrocenylskorpionate **4** und **5** (Abb. **2**) enthalten die Komplexe **14** – **16** (Schema **4**) neuartige Cyclopentadienyl/Tris(pyrazol-1-yl)borat-Hybridliganden. In den bislang untersuchten Fällen binden beide Donorfunktionalitäten stets an unterschiedliche Übergangsmetallionen [vgl. **16**: Cyclopentadienyl-Mn(I); Tris(pyrazol-1-yl)borat-Zn(II)]. Um die elektronische (und ggf. auch magnetische) Kommunikation der koordinierten Metallionen zu maximieren, könnte es jedoch von Vorteil sein, *beide* Ionen von unterschiedlichen Seiten an *denselben* Cyclopentadienylliganden zu binden, so dass ein Doppeldecker-Sandwichkomplex entstünde. Ausgehend von 1,1´-disubstituierten Ferrocenderivaten könnte man auf diese Weise prinzipiell sogar Koordinationspolymere mit Multideckerstruktur darstellen, die interessante elektronische und magnetische Festkörpereigenschaften erwarten lassen.

Das folgende Kapitel widmet sich der Entwicklung eines entsprechenden Ferrocen-basierten Ligandensystems und beschreibt erste Ergebnisse zur Strukturchemie seiner Alkalimetallkomplexe.

1.3.1 Liganden auf Ferrocenbasis

1.3.1.1 Darstellung der Startmaterialien

Die Synthese der Ferrocenylborane nach *Siebert*[10, 16] geht von Ferrocen aus, das bei geeigneter Wahl der Reaktionsbedingungen in einem einzigen Schritt mit Bortribromid ein-, zwei-, oder viermal selektiv und mit guten Ausbeuten boryliert werden kann (Schema **5**).[16] Zahlreiche Derivate lassen sich durch nachfolgende Substitution eines oder beider Bromoliganden am Bor erzeugen. Damit wird auch die Lewis-Acidität der Borylgruppe über einen weiten Bereich einstellbar (Schema **5**). Ferrocenylborane sind vor allem wegen ihres Redoxverhaltens im Hinblick auf die hier bearbeitete Themenstellung aus mehreren Gründen attraktiv. Erstens verläuft die Oxidation am Eisenzentrum der meisten Ferrocenderivate reversibel. Zweitens kann über die Zahl und den Koordinationszustand der Borylgruppen am Ferrocen das Redoxpotential für den Fe(II)/Fe(III)-Übergang beeinflusst werden. Ein zunehmender Borylierungsgrad erschwert die Oxidation, solange die Borylsubstituenten dreifach koordiniert sind und als π-Akzeptoren wirken. Nach Zugabe von Lewis-Basen führt die Adduktbildung am Bor jedoch zu einer ausgeprägten kathodischen Verschiebung des Fe(II)/Fe(III)-Redoxpotentials.[17] Im Schema **5** sind alle Ferrocenylborane (**17** – **25**) zusammengestellt, die im folgenden als Synthesebausteine genutzt werden sollen. Die Borylierungen laufen in der Regel in Hexanlösung ab. Mit steigender Zahl der Borsubstituenten wird das Ferrocengerüst jedoch immer elektronenärmer, was den elektrophilen Angriff durch weiteres Bortribromid zunehmend erschwert. Daher führt man die Darstellung von Verbindungen mit vier Borsubstituenten am Ferrocen am besten in überschüssigem Bortribromid als Lösungsmittel durch. Der Austausch von Bromosubstituenten durch Methylgruppen gelingt mit Zinntetramethyl bei Temperaturen zwischen 60 und 90 °C. Über die stöchiometrischen Verhältnisse lassen sich gezielt eine oder auch zwei Methylgruppen pro Boratom einführen. Die Darstellung von **24** und **25** erfolgt durch Umsetzung von **21** bzw. **23** mit N,N-Dimethyltrimethylsilylamin in CH_2Cl_2.

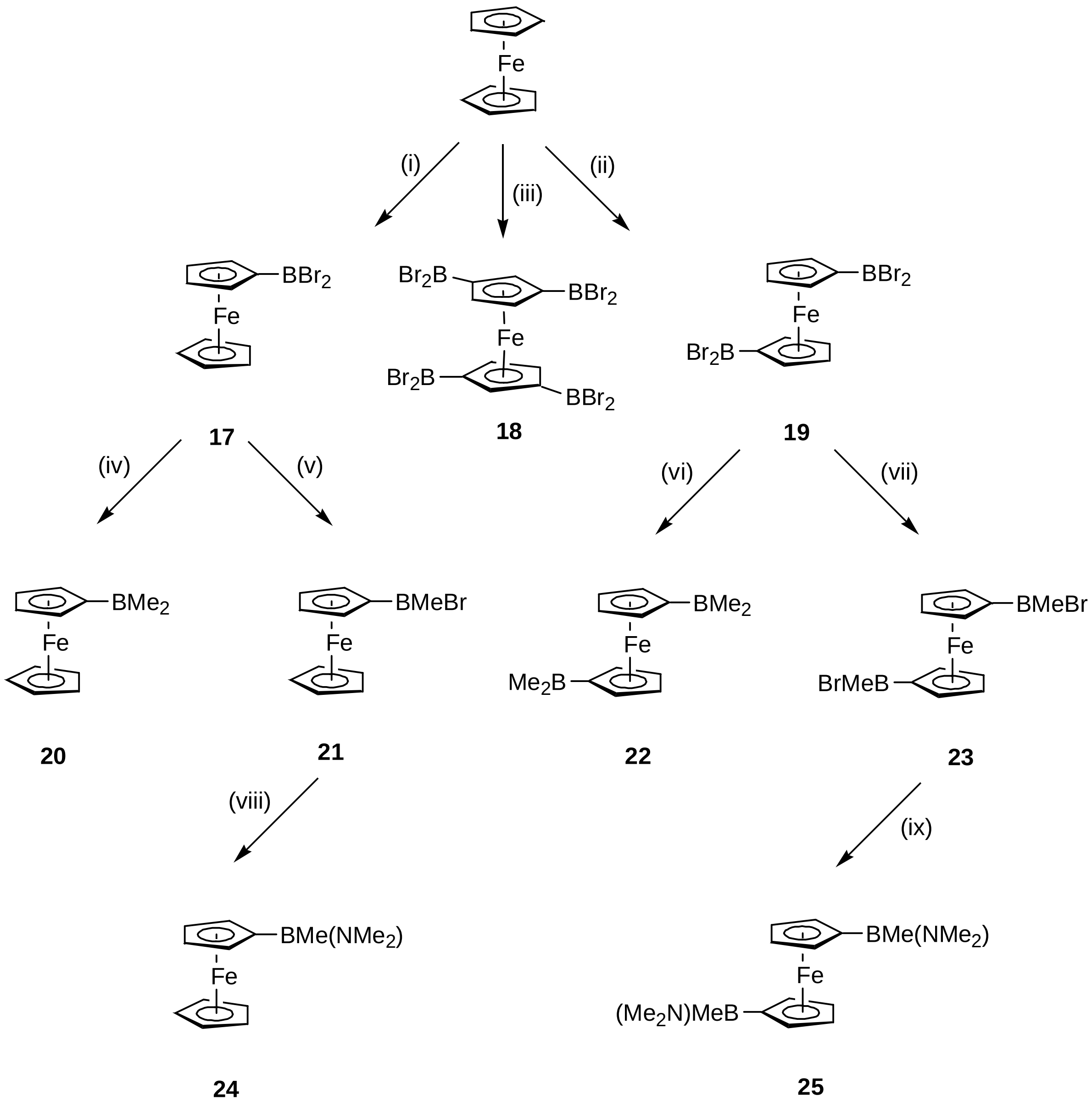

Schema **5**: Darstellung der in dieser Arbeit verwendeten Ferrocenylborane.
(i) + BBr_3, Hexan, 68 °C, 5h; (ii) + 2.5 BBr_3, Hexan, 68 °C, 5h; (iii) + 10 BBr_3, 91 °C, 48h; (iv) + 2 $SnMe_4$, 90 °C, 5h; (v) + $SnMe_4$, $CHCl_3$, 61 °C, 3h; (vi) + 5 $SnMe_4$, 90 °C, 5h; (vii) + 2 $SnMe_4$, $CHCl_3$, 61 °C, 3h; (viii) + Me_3SiNMe_2, CH_2Cl_2, 2h; (ix) + 2 Me_3SiNMe_2, CH_2Cl_2, 2h.

1.3.1.2 Konzipierung des Ligandensystems

Seit mehr als 30 Jahren werden Multidecker-Sandwichkomplexe aufgrund ihres Potentials für die Anwendungen in der Nanotechnik (z.B. als eindimensionale Drähte oder Spinketten) untersucht.[18] Ein besonders bemerkenswerter Vertreter dieser Verbindungsklasse wurde 1985 von *Siebert*[19] veröffentlicht, dem die Synthese ausgedehnter säulenartiger Strukturen von Nickelionen und η^5,µ-2,3-dihydro-1,3-diboroyl-Liganden gelang. Später konnten für dieses eindimensionale System Halbleitereigenschaften in fester Phase nachgewiesen werden. [20, 21] Aus praktischen Gründen wäre es wünschenswert, einfache Cyclopentadienylliganden anstelle der komplizierten Borheterocyclen zu verwenden. Es wurden bereits einige Tripeldecker-Sandwichkomplexe des permethylierten Cyclopentadienylderivates $[C_5Me_5]^-$ isoliert und strukturell charakterisiert.[18] Für den unsubstituierten $[C_5H_5]^-$ Liganden gibt es hingegen in dieser Hinsicht nur wenige bekannte Beispiele: $[Ni_2(C_5H_5)_3]^+$ [22], $[Tl_2(C_5H_5)_3]^-$. [23]

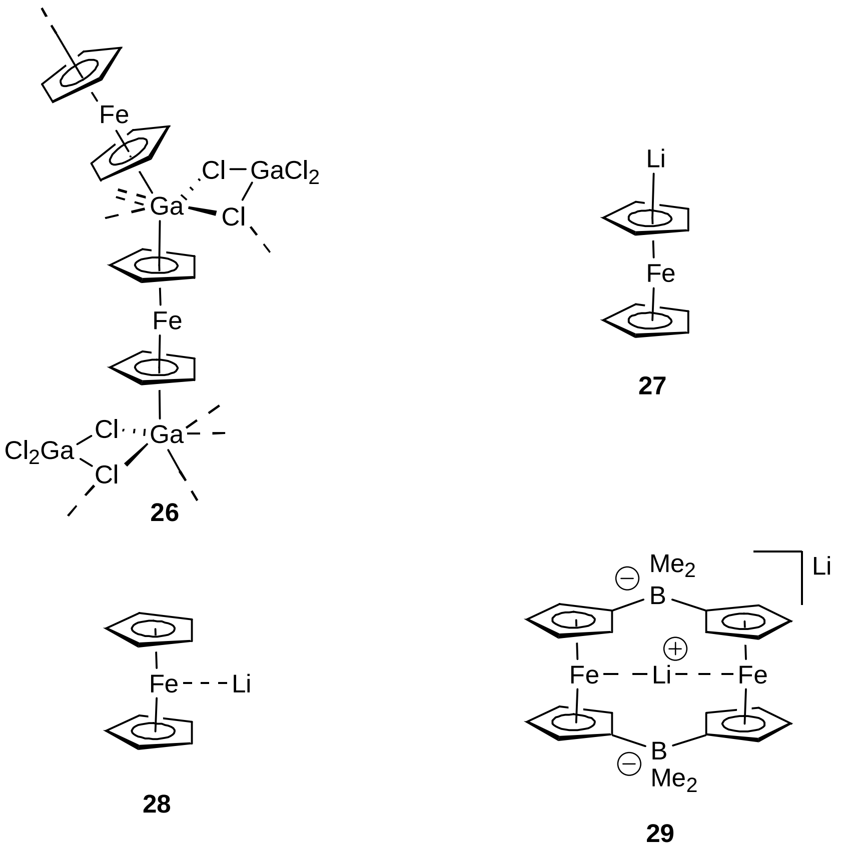

Abb. 7: Der Ga^+-Ferrocen-Multidecker-Sandwichkomplex **26**, zwei berechnete Strukturen **27** und **28** des Li^+···Ferrocen-Komplexes in der Gasphase[24] und das Lithium-[1.1]diborataferrocenophan **29**.

Unsere Gruppe hat die Synthese und Röntgenstrukturanalyse des Polydecker-Sandwichkomplexes **26** veröffentlicht, in dem Ga(I)- und Fe(II)-Ionen abwechselnd durch

η^5,μ-$[C_5H_5]^-$ Einheiten verbunden sind.[25] Hierbei wurden die Ga(I)-Ionen aus $GaCl_3$ durch Reduktion mit Ferrocen in *situ* erzeugt. Dichtefunktionalrechnungen ergaben, dass die Bindungsenergie zweier Ferrocenmoleküle an ein Ga(I)-Ion ca. 213 kJ/mol beträgt. Dies sind ca. 80 kJ/mol mehr, als bei der Bildung von $[Ga(C_6H_6)_2]^+$ aus Ga(I) und zwei Benzolmolekülen frei werden. Durch Fragmentanalyse von $\{[Fe(C_5H_5)_2]_2Ga\}^+$ ergibt sich eine Übertragung von 0.4 Elektronen vom Ferrocen auf das 4p Orbital des Ga(I)-Ions. Tieferen Einblick in die Gasphasenbasizität des Ferrocens gegenüber Hauptgruppenmetallkationen liefern weitere theoretische Untersuchungen von *Ugalde* et al:[24] Es ist bekannt, dass das Lithiumkation in der Gasphase Addukte mit polaren Molekülen eingeht.[24] *Ugalde* et al. haben kürzlich die (in der Gasphase) stabilen Isomere des Ferrocen-Lithium-Kations ($Cp_2Fe\cdots Li^+$) mittels Dichtefunktionalrechnung vorhergesagt.[24] Für das stabilste Isomer **27** ergibt sich eine η^5-Koordination des Lithiumions an einen der Cp-Ringe des Ferrocens, während es im weniger stabilen Isomer **28** zu einer direkten Fe-Li-Wechselwirkung kommen sollte. Beide Isomere entsprechen Minima der Potentialhyperfläche; die Energiedifferenz zwischen ihnen ist gering (ΔE = 33 kJ/mol). Wir fanden ein dem hypothetischen Komplex **28** ähnliches Strukturmotiv beim [1.1]Diborataferrocenophan **29**, welches mit einem Lithiumkation im molekularen Hohlraum kristallisiert.

Der Ferrocen-Ga(I) Multidecker-Sandwichkomplex **26** wurde als Sonderfall im schwach koordinierenden Lösungsmittel Benzol synthetisiert, so dass die Ferrocendonoren nicht mit Lewis-basischen Solvensmolekülen (z.B. CH_3CN, THF) um das Metallion konkurrieren müssen.

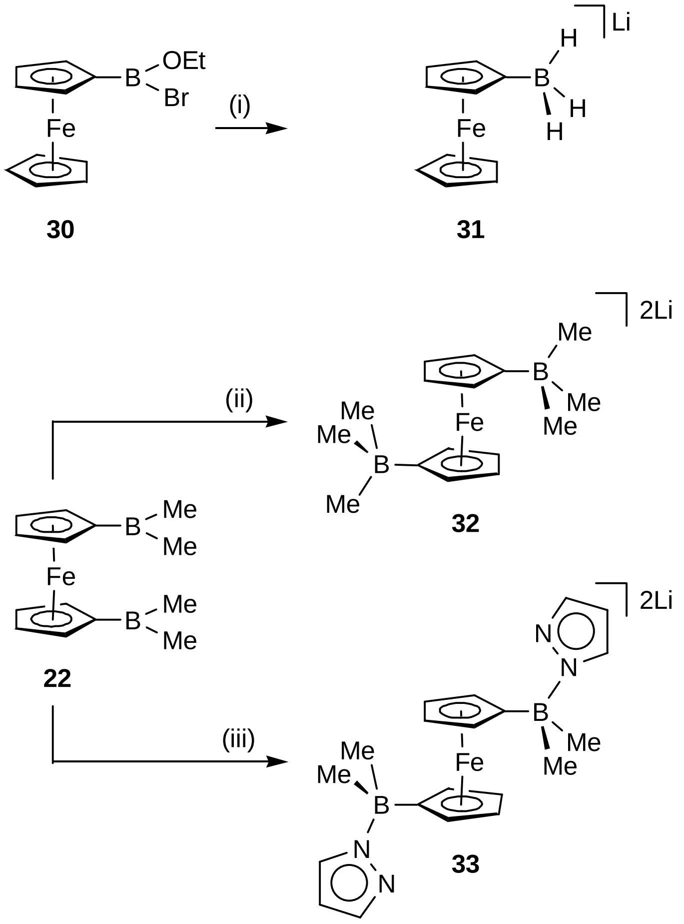

Schema **6**: Synthese der Lithium-Ferrocenylborate **31**, **32** und **33**: (i) + Li[AlH$_4$], Et$_2$O/C$_5$H$_{12}$, 0 °C; (ii) + 2 MeLi, Et$_2$O, -78 °C: (iii) + 2 Lipz, Et$_2$O, -78 °C.

Um das im hypothetischen Aggregat **27** (Abb. **7**) enthaltene Strukturmotiv zu erzeugen, wurden im Rahmen dieser Arbeit zunächst die Ferrocenderivate **31** und **32** synthetisiert (Schema **6**).[26] Das Konzept bestand darin, eine potentielle Wechselwirkung zwischen Li$^+$ und Ferrocen allein durch Einführung negativ geladener Substituenten in das Ferrocengerüst auf elektrostatischem Wege zu stabilisieren. Aufgrund der guten Zugänglichkeit der Ferrocenylborane wurden Borat-Substituenten für diese Untersuchungen verwendet. Die Kristallstrukturanalyse von Li[FcBH$_3$]·(12-Krone-4) **31** zeigte ein hexakoordiniertes Li$^+$-Ion, welches an ein Molekül 12-Krone-4 und zwei Wasserstoffatome des [FcBH$_3$]$^-$ Fragmentes gebunden ist.[26] Folglich wird das Hydridoborat-Fragment gegenüber dem Cp-π-System für die Li$^+$-Koordination bevorzugt. Versuche, diese Koordinationsstelle durch Substitution der

Wasserstoffatome mit Methylgruppen zu blockieren, scheiterten, da die entsprechenden Methylborate aus THF als solvens-separierte Ionenpaare $\{[Li(THF)_4]^+\}_2[1,1'\text{-fc}(BMe_3)_2]^{2-}$ [**32**·(THF)$_8$ Abb. **8**] kristallisierten. Einkristalle dieser Verbindung aus weniger stark koordinierenden Lösungsmitteln (z.B. Diethylether) konnten bisher nicht erhalten werden.

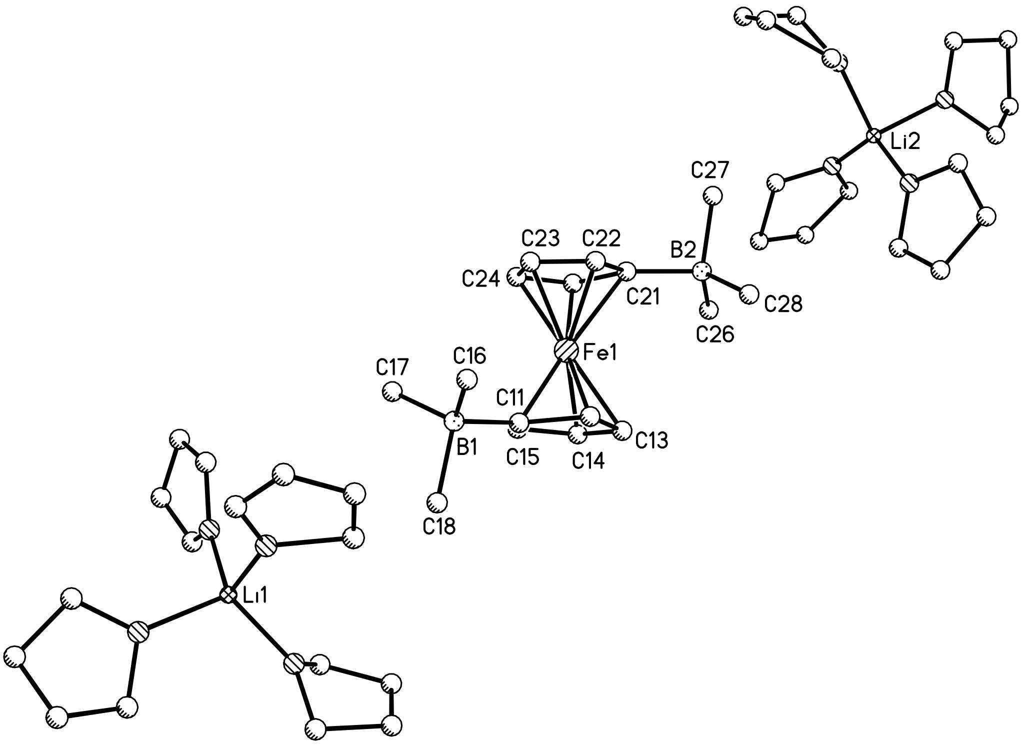

Abb. **8**: Struktur von **32**·(THF)$_8$ im Kristall.

Die Struktur der Verbindung **32**·(THF)$_8$ (orthorhombisch, $Pca2_1$) konnte röntgenstrukturanalytisch bestimmt werden. Im Festkörper ist jedes der beiden Li^+-Ionen an vier THF-Moleküle gebunden. Das $[1,1'\text{-fc}(BMe_3)_2]^{2-}$-Ion nimmt eine *anti* Konformation ein, in der die BMe_3-Substituenten voneinander abgewandt sind (C(11)-COG[C(11)C(12)C(13)-C(14)C(15)]-COG[C(21)C(22)C(23)C(24)C(25)]-C(21) = 154.1°).[26]

Daraus ergab sich die Schlussfolgerung, dass eine chelatisierende Seitenkette für die Stabilisierung des gewünschten Li^+-Ferrocen Komplexes förderlich sein könnte, welche das Li^+-Ion über dem Cyclopentadienylring positioniert. Molecular-Modelling-Rechnungen zeigten, dass sich der starre Pyrazolring gut für diesen Zweck eignet. Auf Grundlage unserer Erfahrungen mit Ferrocen-basierten Tris(pyrazol-1-yl)boraten wurde daher das Ligandsystem

$[1,1'\text{-fc}(BMe_2pz)_2]^{2-}$ dargestellt (Schema **6**), in der Erwartung, dass dessen Li^+-Salz **33Li** im Festkörper das gesuchte Strukturmotiv (Abb. **9**) aufweisen könnte.[26]

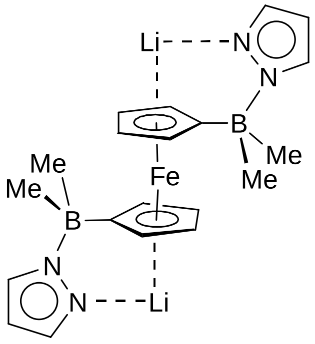

33Li

Abb. **9**: Ligandkonzept zur Erhöhung der Wahrscheinlichkeit einer η^5-Koordination von Lithiumionen an die Cp-Ringe des Ferrocenrückgrates.

Unser Liganddesign stützt sich auch auf zwei Arbeiten aus der Literatur, bei denen ein ähnliches Konzept verwirklicht wurde:

Enders et al. synthetisierten den Liganden η^5-1-(8-Chinolyl)-2,3,4,5-tetramethyl-cyclopentadienyl-η^5-cyclopentadienyleisen, **34** (Schema **7**). Sterische Wechselwirkungen mit den benachbarten Methylgruppen bzw. dem unsubstituierten Cp-Ring begünstigen eine Konformation, bei der die Ebene des 8-Chinolylsubstituenten senkrecht zum Tetramethylcyclopentadienylliganden orientiert ist. An das Chinolyl-Stickstoffatom koordinierte Metallionen werden somit in eine Position unmittelbar oberhalb des Ferrocen-π-Systems dirigiert. Dies wird anhand des $ZnCl_2$ Komplexes **35** (Schema **7**) deutlich, in dem das Zink(II)-Ion tetraedrisch von zwei Chloroliganden, dem Stickstoffdonor und einem Kohlenstoffatom des substituierten Cyclopentadienylliganden umgeben ist. Interessanterweise führten analoge Komplexierungsversuche mit der stärkeren Lewis-Säure BCl_3 zum Bruch der Fe-C Bindungen unter Bildung des eisenfreien Derivats **36** (Schema **7**).[27]

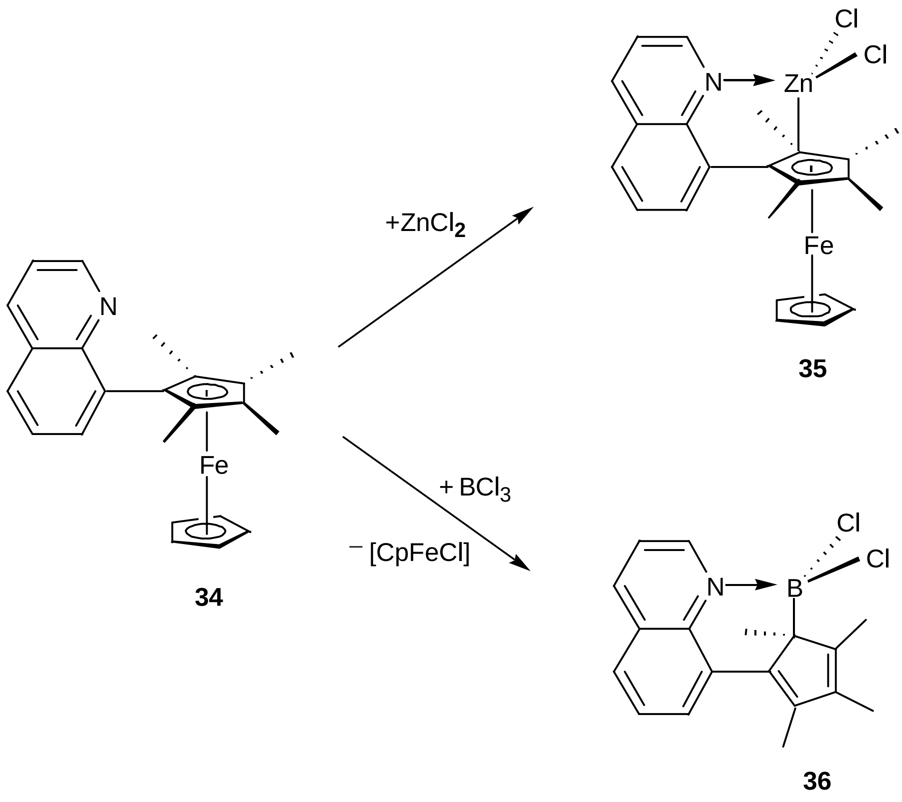

Schema **7**: Schematische Darstellung des Ferrocenderivates **34** und dessen Reaktivität gegenüber Zinkdichlorid und Bortribromid.

Laguna et al. gelang die Darstellung des Multidecker-Sandwichkomplexes des Ferrocens durch Komplexierung des zweifach substituierten Dithiocarbamatliganden 1,1′-fc(S_2CNEt_2)$_2$ mit $AgClO_4$ (**37**; Abb. **10**).[28]

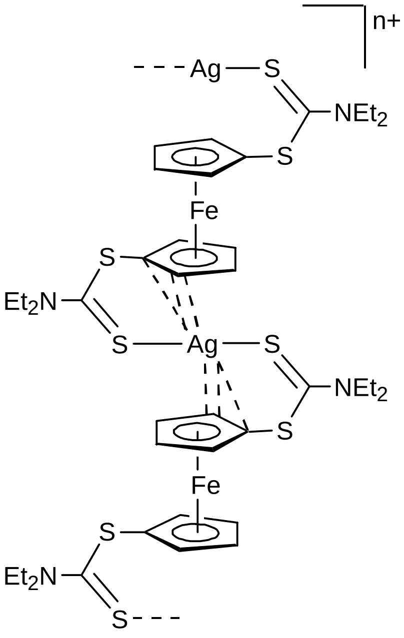

37

Abb. **10**: Darstellung des Silber(I)-Komplexes $[Ag\{1,1'\text{-}fc(S_2CNEt_2)_2\}]_n[ClO_4]_n$ (**37**).

Die in das System **33Li** (Abb. **9**) gesetzten Erwartungen bestätigten sich nach einer Röntgenstrukturanalyse an Kristallen von **33Li**$\cdot(Et_2O)_4$, die aus Diethylether gewonnen wurden.

Abbildung **11** gibt die Struktur von **33Li**$\cdot(Et_2O)_4$ im Festkörper wieder (triklin, $P\bar{1}$). Jedes Li^+-Ion ist an zwei Diethylether-Moleküle, an den Lewis-basischen Pyrazolylseitenarm und an einen Cp-Ring des Ferrocens koordiniert.[26]

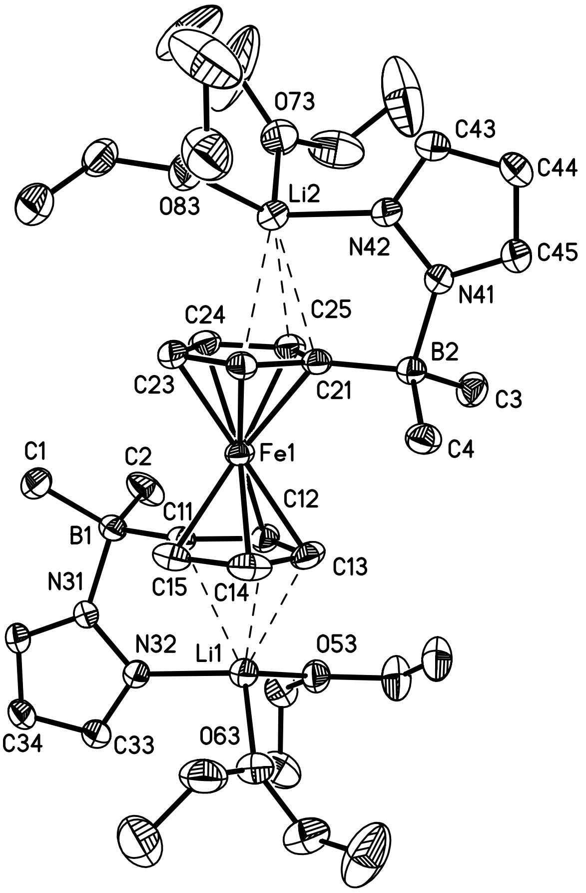

Abb. **11**: Struktur von **33Li**·$(Et_2O)_4$ im Kristall. Die anisotropen Auslenkungsparameter entsprechen 30 % Aufenthaltswahrscheinlichkeit.

Die kürzesten Li-Cp(C) Abstände betragen: Li(1)-C(11) = 2.646(5) Å, Li(1)-C(12) = 2.395(5) Å, Li(1)-C(13) = 2.910(6) Å und Li(2)-C(21) = 2.475(5) Å, Li(2)-C(22) = 2.496(5) Å, Li(2)-C(25) = 2.730(6) Å. Als Abstand zwischen dem jeweiligen Li^+-Ion und dem Schwerpunkt (COG) des koordinierenden Cyclopentadienylrings ergibt sich: COG[C(11)C(12)C(13)C(14)-C(15)]···Li(1) = 2.663 Å, COG[C(21)C(22)C(23)C(24)C(25)]···Li(2) = 2.401 Å. Die Li^+-Ionen sind nicht nur im Festkörper an den Pyrazolring gebunden, sondern auch in Lösung. Diese Schlussfolgerung ergibt sich aus dem ^{7}Li-NMR-Spektrum von **33Li** (Abb. **9**), welches in d_8-THF ein Signal bei $\delta(^7\mathrm{Li}) = -1.30$ ($h_{1/2}$ = 37 Hz) aufweist. LiCl in d_8-THF zeigt hingegen eine ^{7}Li-NMR-Resonanz bei $\delta(^7\mathrm{Li}) = -1.54$ ($h_{1/2}$ = 0.6 Hz). Setzt man dieser Lösung ein

Äquivalent Pyrazol zu, so verschiebt sich das ^{7}Li-NMR Signal nach $\delta(^7\text{Li}) = -1.26$ ($h_{1/2} = 0.6$ Hz).

1.3.2 Synthese und strukturelle Charakterisierung von 33M·(DME)$_x$ (M = Li, Na, K, Rb, Cs), (x = 2, 3)

Die Kristallstrukturanalyse von **33Li**·(Et$_2$O)$_4$ hat bewiesen, dass Tripeldecker-Sandwichkomplexe aus Li$^+$-Kationen und Ferrocen auf der Basis des Liganden [**33**]$^{2-}$ zugänglich sind. Als nächstes galt es daher, auch die analogen Komplexe der schwereren Alkalimetallionen zu synthetisieren, um deren Festkörperstrukturen bestimmen zu können. Die Verbindungen **33M** (M = Na, K, Rb, Cs) wurden auf dieselbe Weise wie **33Li** durch Umsetzung von **22** mit den entsprechenden Alkalimetallpyrazoliden gewonnen (Schema **8**). Die Bor-Stickstoff-Addukte präzipitieren aus Diethylether in nahezu quantitativer Ausbeute.[29]

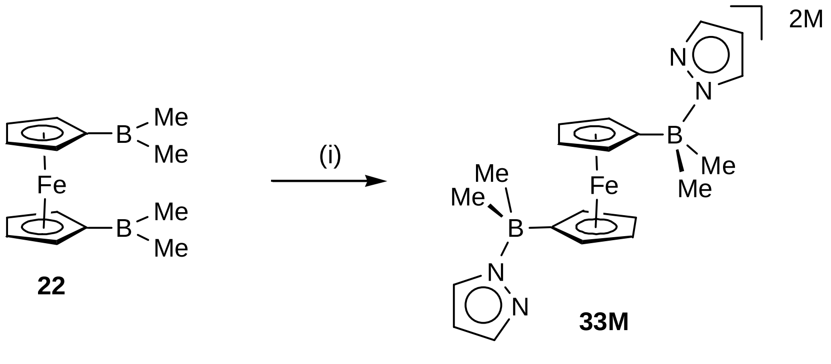

M = Li, Na, K, Rb, Cs

Schema **8**: Synthese der Alkalimetall-Ferrocenylborate **33M** (M = Li, Na, K, Rb, Cs): (i) + 2 Mpz, Et$_2$O, -78 °C.

Um maximale Vergleichbarkeit der Kristallstrukturen zu gewährleisten, wurden Löslichkeitsversuche für **33M** (M = Li, Na, K, Rb, Cs) in unterschiedlichen organischen

Solventien durchgeführt und Dimethoxiethan (DME) als geeignetes Lösungsmittel identifiziert, aus dem sich alle Komplexe umkristallisieren ließen.

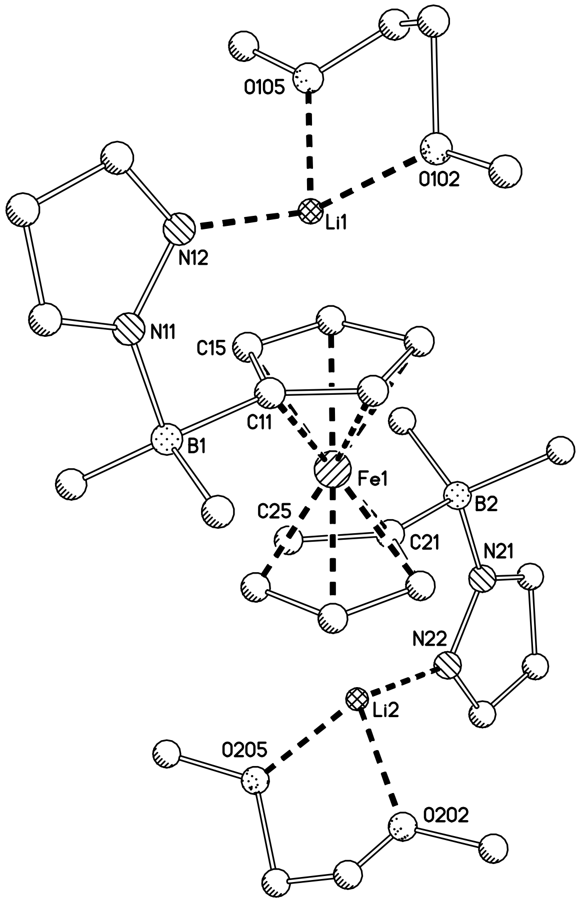

Abb. **12**: Struktur von **33Li**·(DME)$_2$ im Kristall.

Die asymmetrische Einheit des Kristallgitters der Verbindung **33Li**·(DME)$_2$ (trikline Raumgruppe *P*-1; Abb. **12**) enthält zwei ganze und zwei halbe Moleküle; letztere liegen auf Inversionszentren. Folglich gibt es in der Elementarzelle sechs Moleküle. Die Strukturparameter der vier kristallographisch unabhängigen Moleküle sind sehr ähnlich. Jedes Li^+-Ion ist an einen chelatisierenden DME-Liganden und an das freie Elektronenpaar eines Pyrazolylsubstituenten koordiniert, der es über dem jeweiligen Cyclopentadienylring platziert [mittlerer Abstand zwischen den Li^+-Ionen und den Schwerpunkten (COG) der Cyclopentadienylringe: 2.35 Å]. Dieser Li^+···COG Kontakt ist um 0.18 Å kürzer, als im analogen Komplex **33Li**·(Et$_2$O)$_4$. Dies ist vermutlich darauf zurückzuführen, dass der sterische Anspruch von zwei Ethermolekülen größer ist als von einem Molekül DME.[29]

Das Kristallgitter des Natriumkomplexes **33Na**·(DME)$_3$ (orthorhombische Raumgruppe *Pbca*) besteht aus polyanionischen Zick-Zack Ketten [**33**Na]$_n^{n-}$ und [Na(DME)$_3$]$^+$ Gegenionen von verzerrt oktaedrischer Struktur (Abb. **13**).

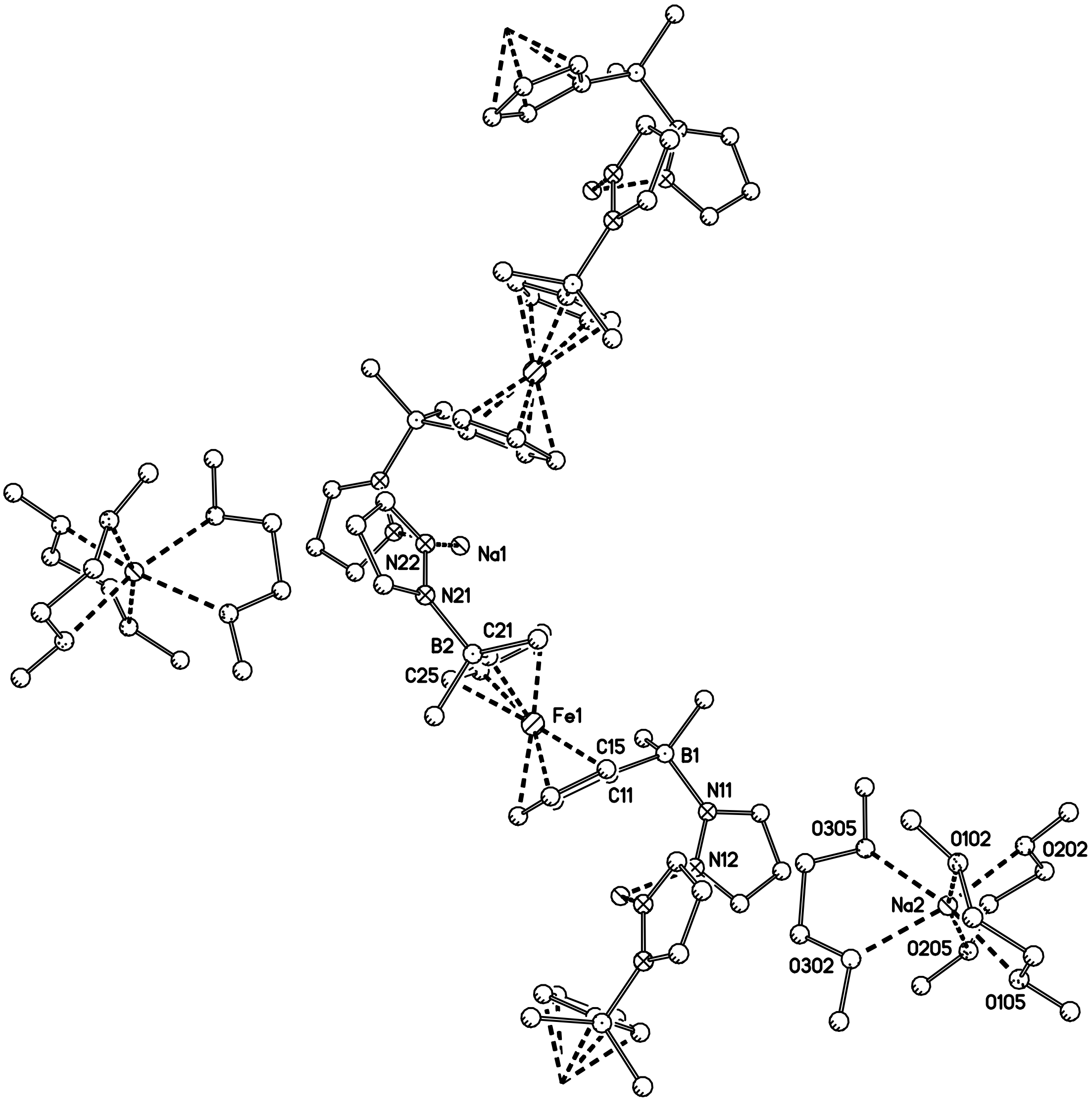

Abb. **13**: Struktur von **33Na**·(DME)$_3$ im Kristall.

Ein wesentlicher Unterschied zwischen der Konformation des Ferrocenliganden [**33**]$^{2-}$ in **33Na**·(DME)$_3$ und **33Li**·(DME)$_2$ liegt im Torsionswinkel C(11)-COG[C(11)C(12)C(13)-

C(14)C(15)]-COG[C(21)C(22)C(23)C(24)C(25)]-C(21), der im ersten Fall -135.4° und im zweiten 178.8° beträgt. Innerhalb der Zick-Zack Ketten von [**33**Na]$_n^{n-}$ ist jedes Na$^+$-Ion an zwei Pyrazolylsubstituenten benachbarter Liganden [**33**]$^{2-}$ gebunden und bildet kurze Kontakte zu zwei Cyclopentadienylringen aus (Na(1)···COG[C(11$^\#$)C(12$^\#$)C(13$^\#$)C(14$^\#$)-C(15$^\#$)] = 2.561 Å, Na(1)···COG[C(21)C(22) C(23)C(24)C(25)] = 2.590 Å). Somit kann die polymere Untereinheit [**33**Na]$_n^{n-}$ als gewinkelter Multidecker-Sandwichkomplex des Ferrocens mit Na$^+$-Ionen betrachtet werden.[29]

Die Verbindung **33K**·(DME)$_3$ kristallisiert aus DME in der triklinen Raumgruppe *P*-1. Die Komplexe der schweren Alkalimetallionen **33Rb**·(DME)$_3$ (triklin, *P*-1) und **33Cs**·(DME)$_3$ (monoklin, *C*2/*c*) sind zu **33K**·(DME)$_3$ weitestgehend isostrukturell. Stellvertretend für alle drei Verbindungen wird daher nur die Molekülstruktur von **33K**·(DME)$_3$ in Abbildung **14** gezeigt.

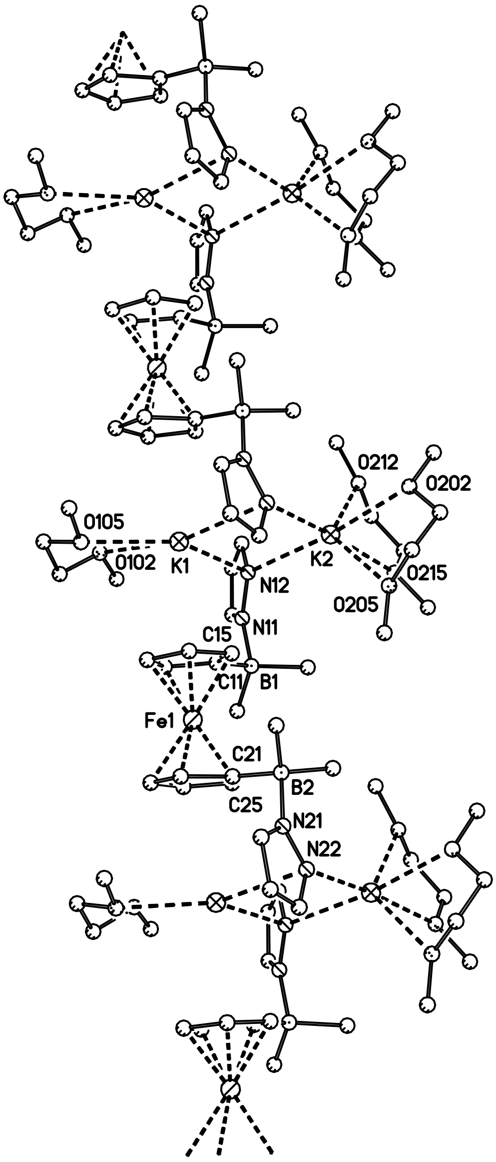

Abb. **14**: Struktur von **33K**·(DME)$_3$ im Kristall.

Im Gegensatz zu den gewinkelten Polymeren von **33Na**·(DME)$_3$ bilden die höheren Homologen lineare Säulen bestehend aus alternierenden Ferroceneinheiten und Alkalimetallionen aus. Die Konformation der Ferrocenylenfragmente führt zu einer größeren Annäherung der Borylsubstituenten in **33K**·(DME)$_3$, **33Rb**·(DME)$_3$ und **33Cs**·(DME)$_3$ im Vergleich zu **33Na**·(DME)$_3$ und **33Li**·(DME)$_3$. Die Pyrazolyl-Substituenten koordinieren nicht mehr nur jeweils ein Alkalimetallion, sondern fungieren als verbrückende Liganden zwischen zwei Alkalimetallionen. Bei **33K**·(DME)$_3$ und **33Rb**·(DME)$_3$ besitzt eine der M^+-pz-M^+-Brücken eine annähernd symmetrische Struktur [Torsionswinkel B(1)-N(11)-N(12)-K(1) = -66.0(4)°, B(1)-N(11)-N(12)-K(2) = 47.3(4)°; B(1)-N(11)-N(12)-Rb(1) = 68.3(13)°, B(1)-N(11)-N(12)-Rb(2) = -43.9(15)°], während der andere Pyrazolylring eine π-Bindung (η^5) und eine σ-Bindung (η^1) ausbildet. Diesen unsymmetrischen Koordinationsmodus findet man auch in **33Cs**·(DME)$_3$. Zusätzlich zu den beiden Stickstoff-Donoren sind die $M(1)^+$ Ionen jeweils an ein DME-Molekül und zwei Cyclopentadienylringe gebunden, wogegen die Ionen $M(2)^+$ von zwei DME-Liganden koordinativ abgesättigt werden (M = K, Rb, Cs). Die Abstände zwischen $M(1)^+$ und dem Schwerpunkt der benachbarten C_5H_4-Liganden betragen 3.228 Å/3.298 Å [K(1)], 3.265 Å/3.285 Å [Rb(1)] und 3.283 Å/3.283 Å [Cs(1)].

Abgesehen von **33K**·(DME)$_3$ gibt es nur ein Beispiel eines η^5-Ferrocen-K^+-Komplexes, das in der Literatur bekannt ist, nämlich $[K(Ferrocen)_2(Toluol)_2]^+[Mg(HMDS)_3]^-$ [HMDS = Bis(trimethylsilyl)amid].[30] Die Verbindung entstand ungeplant beim Versuch, Ferrocenylkalium durch Deprotonierung von Ferrocen mit Hilfe des Kalium/Magnesium Amids $KMg(HMDS)_3$ darzustellen (Schema **9**).

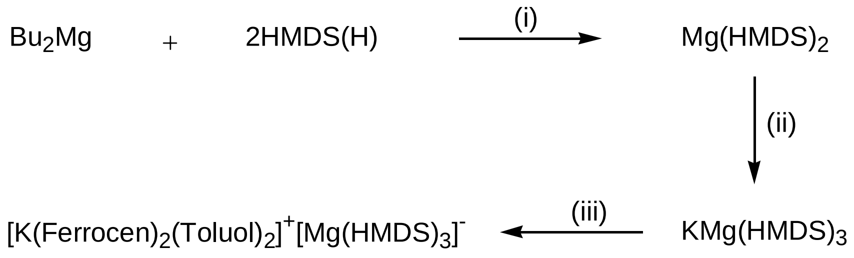

Schema **9**: Synthese von $[K(Ferrocen)_2(Toluol)_2]^+[Mg(HMDS)_3]^-$:[30] (i) Heptan/Hexan, 25 °C, -2 BuH; (ii) + KHMDS, Toluol; (iii) + Ferrocen, 120 °C.

Die kationische Einheit besteht aus einem Kaliumion, das von zwei Toluol-π-Systemen und zwei Ferrocenyl-Cyclopentadienylringen verzerrt tetraedrisch umgeben ist (Abb. **15**). $[K(Ferrocen)_2(Toluol)_2]^+$ stellt ein exzellentes Vergleichssystem für **33K**·(DME)$_3$ dar, da es freie $K^+\cdots\eta^5$-Ferrocen Bindungen enthält, die nicht durch stabilisierende Seitenketten oder elektrostatische Wechselwirkungen beeinflusst werden. Der durchschnittliche Abstand $K^+\cdots COG(C_5H_5)$ beträgt 2.964 Å und ist damit um 0.3 Å (etwa 10%) kürzer als der entsprechende Abstand in **33K**·(DME)$_3$ (3.228 Å). Der Bindungswinkel $COG(C_5H_5)$-K^+-$COG(C_5H_5')$ beträgt 106.08° (FcH = Ferrocen: vgl. COG[C(11)C(12)C(13)C(14)C(15)]-Na^+-COG[C(21)C(22)C(23)C(24)C(25)] im gewinkelten Polymer **33Na**·(DME)$_3$: 132.0°). Die unterschiedlichen Bindungslängen von $K^+\cdots COG(C_5H_5)$ in $[K(Ferrocen)_2(Toluol)_2]^+$ und $K^+\cdots COG(C_5H_4)$ in **33K**·(DME)$_3$ können mehrere Gründe haben: (i) Die BMe$_2$pz Seitenkette ist den geometrischen Erfordernissen der $K^+\cdots\eta^5$-(C_5H_4) Aggregate nicht ideal angepasst, (ii) der sterische Anspruch des DME-Liganden an K(1) führt zu einem verlängerten $K^+\cdots COG(C_5H_4)$ Abstand, (iii) die Sauerstoff- und Stickstoff-Donoren setzen die Lewis-Acidität des K^+-Ions so weit herab, dass die $K^+\cdots\eta^5$-(C_5H_4) Wechselwirkung geschwächt wird, (iv) im Gegensatz zu $[K(Ferrocen)_2(Toluol)_2]^+$, in dem nur ein K^+-Ion an jedes Ferrocen gebunden ist, wird die Elektronendichte der Ferrocenylenfragmente in **33K**·(DME)$_3$ von zwei Kaliumionen geteilt.

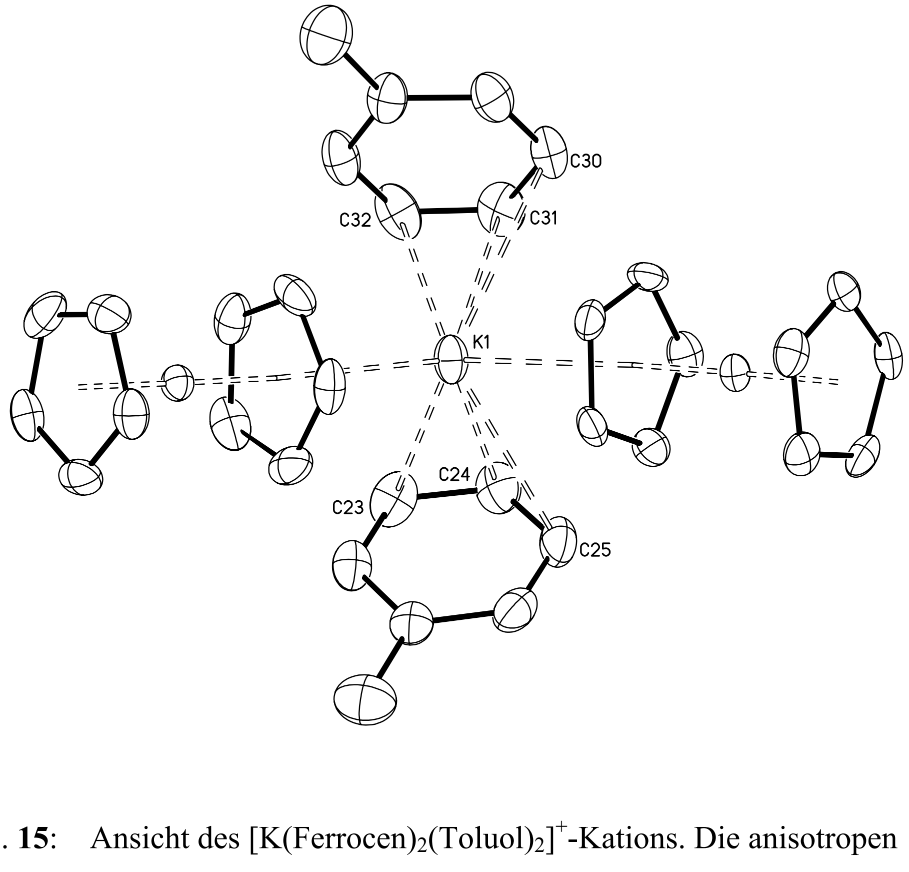

Abb. **15**: Ansicht des $[K(Ferrocen)_2(Toluol)_2]^+$-Kations. Die anisotropen Auslenkungsparameter entsprechen 40 % Aufenthaltswahrscheinlichkeit.

1.3.3 Strukturelle Charakterisierung der Komplexe 33M·(THF)$_4$ (M = Na, K, Rb)

Da in die Komplexe **33M**·(DME)$_3$ (M = Li, Na, K, Rb, Cs) Lösungsmittelmoleküle als Liganden eingebunden sind, ergab sich die Frage, in welchem Ausmaß diese Liganden strukturbildend wirken. Aus diesem Grund wurden die Verbindungen **33Na**, **33K** und **33Rb** auch aus dem Lösungsmittel Tetrahydrofuran kristallisiert. Man erhält wiederum Koordinationspolymere, die sich jedoch in wesentlichen Strukturmerkmalen von den aus DME gewonnenen Polymeren unterscheiden.

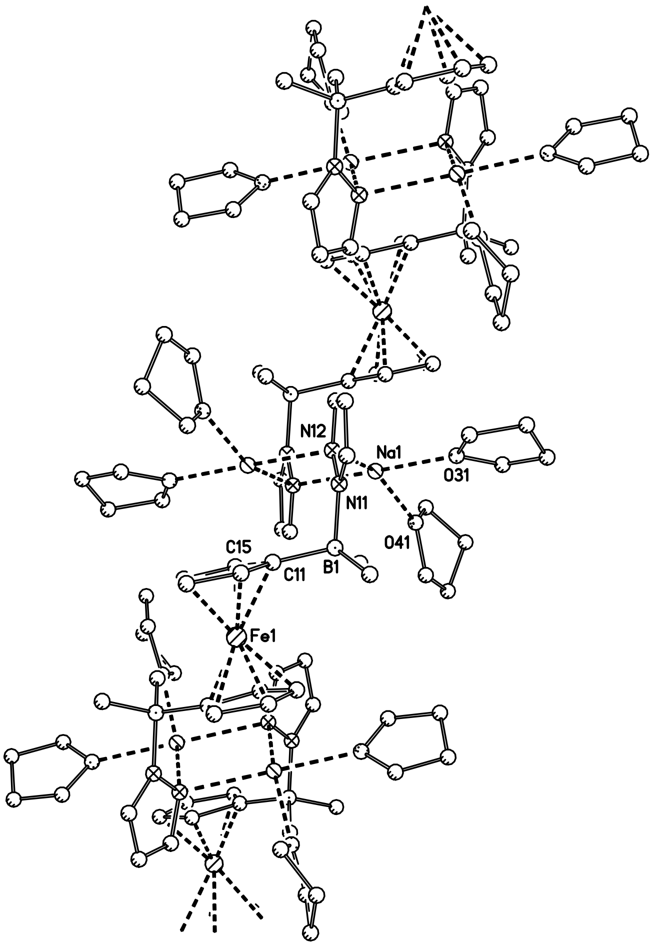

Abb. **16**: Struktur von **33Na**·(THF)$_4$ im Kristall.

In allen drei Fällen enthalten die Kristalle vier Äquivalente THF: **33Na**·$(THF)_4$ (orthorhombisch, *Pbcn*), **33K**·$(THF)_4$ (monoklin, $P2_1/n$) und **33Rb**·$(THF)_4$ (monoklin, $P2_1/n$). Wegen der ausgeprägten Ähnlichkeit dieser drei Strukturen ist nur **33Na·**$(THF)_4$ in Abbildung **16** dargestellt. Im Gegensatz zu **33Na**·$(DME)_3$ mit seiner polyanionischen Zick-Zack-Kette und den säulenförmigen Aggregaten **33M**·$(DME)_3$ (M = K, Rb, Cs) bilden **33Na**·$(THF)_4$, **33K**·$(THF)_4$ und **33Rb**·$(THF)_4$ treppenförmige Strukturen in fester Phase. Analog zu **33K**·$(DME)_3$ verbrücken die Pyrazolylsubstituenten jeweils zwei Alkalimetallionen, die, anders als bei **33K**·$(DME)_3$, noch an zwei Moleküle THF koordiniert sind. Der wichtigste Unterschied in den Kristallstrukturen von **33M**·$(DME)_3$ und **33M**·$(THF)_3$ (M = Na, K, Rb) ergibt sich aus der Art, in der die M^+-Ionen an die Ferrocenfragmente koordiniert sind. Im Fall der THF-Komplexe ist jedes Alkalimetallion an genau einen Cyclopentadienylring gebunden, ähnlich wie man es beim trimetallischen Aggregat **33Li**·$(DME)_2$ beobachtet (Abb. **12**). Bei den DME-Komplexen der höheren Homologen hingegen gehen alle M^+-Ionen Wechselwirkungen mit zwei Cyclopentadienylringen ein. Weiterhin sind die Alkalimetallionen in **33Na**·$(THF)_4$, **33K**·$(THF)_4$ und **33Rb**·$(THF)_4$ vom Zentrum des Cyclopentadienylrings zum Borylsubstituenten hin verschoben, was zu großen Unterschieden zwischen den einzelnen $M^+\cdots$Cp(C) Abständen führt. Die kürzesten $M^+\cdots$Cp(C) Abstände betragen: Na(1)-C($15^{\#}$) = 2.848(3) Å, K(1)-C(12) = 2.953(4) Å, und Rb(1)-C(12) = 3.156(12) Å.[29]

1.4 Synthese und strukturelle Charakterisierung Ferrocen-basierter Bis(pyrazol-1-yl)borat-Liganden

Ausgehend von den Ferrocen-basierten Mono(pyrazol-1-yl)boraten $[\mathbf{33}]^{2-}$ gelang es im Rahmen dieser Arbeit, Multidecker-Sandwichkomplexe des Ferrocens mit den Alkalimetallionen Li^+ – Cs^+ darzustellen. In Zukunft soll diese Materialklasse auch auf andere – insbesondere paramagnetische – Metallionen ausgeweitet werden. Daher stellte sich die Frage, ob die angestrebten Multidecker-Strukturen durch Einführung eines zweiten chelatisierenden Pyrazolylsubstituenten zusätzliche Stabilität gewinnen. Aus diesem Grund sollten die entsprechenden Liganden $[FcB(Me)pz_2]^-$, $[Fc_2Bpz_2]^-$ und $[1,1'\text{-}fc(B(Me)pz_2)_2]^{2-}$ dargestellt werden.

1.4.1 Literaturübersicht: Synthese und strukturelle Charakterisierung eines difunktionellen Ferrocenylen-verbrückten Bis(pyrazol-1-yl)methanliganden und dessen Ag(I)-Koordinations-Polymere

Der difunktionelle Ligand 1,1′-Bis(dipyrazol-1-ylmethyl)ferrocen, $Fe[C_5H_4CH(pz)_2]_2$ (**40**)[31] wurde von *Reger* et al. durch Reaktion von 1,1′-Ferrocendicarbaldehyd (**38**)[32] mit 1,1′-Carbonyldipyrazol (**39**)[33] in Anwesenheit katalytischer Mengen Cobalt(II)chlorid synthetisiert (Schema **10**). Verbindung **40** ist luftstabil und gut löslich in Aceton, THF, Methylenchlorid, Toluol und Acetonitril, aber nur schlecht löslich in Diethylether und Hexan. Im Festkörper sind die Bis(pyrazolyl)methaneinheiten antiperiplanar ekliptisch orientiert. Die Moleküle werden in ihrer dreidimensionalen Anordnung durch $\pi\cdots\pi$ und $C\text{-}H\cdots\pi$ Wechselwirkungen sowie schwache $C\text{-}H\cdots N$ Wasserstoffbrückenbindungen zusammengehalten.

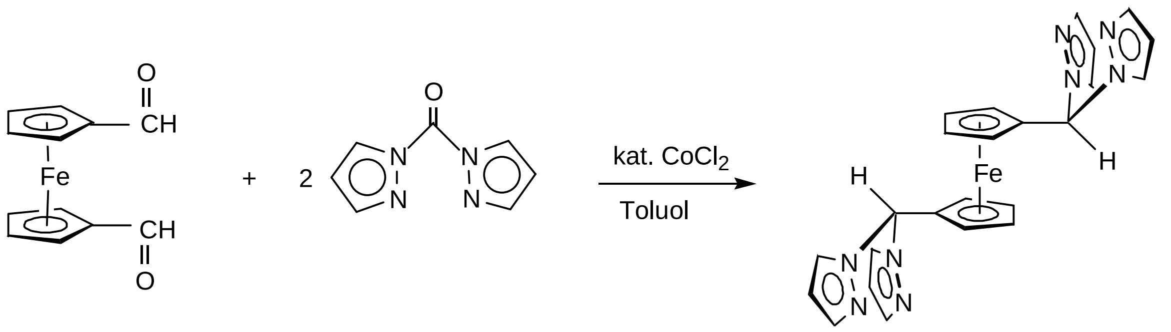

38 **39** **40**

Schema **10**: Darstellung des difunktionellen Liganden 1,1′-Bis(dipyrazol-1-ylmethyl)ferrocen, $Fe[C_5H_4CH(pz)_2]_2$ (**40**).

Die Umsetzung von **40** mit $AgBF_4$, $AgPF_6$, $AgSO_3CF_3$ oder $AgSbF_6$ ergab $\{Fe[C_5H_4CH(pz)_2]_2AgBF_4\}_n$, $\{Fe[C_5H_4CH(pz)_2]_2AgPF_6\}_n$, $\{Fe[C_5H_4CH(pz)_2]_2AgSO_3CF_3\}_n$ und $\{Fe[C_5H_4CH(pz)_2]_2AgSbF_6\}_n$ (**41X**; Schema **11**).[31] Die Silberkomplexe **41X** bilden zwei unterschiedliche Strukturen aus: Helicale und nichthelicale Ketten. Der Hauptunterschied zwischen den beiden Strukturtypen liegt in der relativen Orientierung der Ferrocenyleinheiten in den Polymersträngen. Bei der helicalen Form nehmen sie eine abwechselnde AB-Orientierung ein, während sie in der nichthelicalen Form alle die gleiche AA-Orientierung besitzen. Beide Formen bilden sehr hoch organisierte supramolekulare Strukturen aus, die sich aus schwachen Wasserstoffbrückenbindungen, $\pi\cdots\pi$ Stapeleffekten und $CH\cdots\pi$ Wechselwirkungen ergeben. Es scheint, dass die kleineren Anionen (BF_4^- und PF_6^-) die Entstehung der helicalen Struktur fördern, da sie besser in die Spiralketten hineinpassen.[31] Im Fall des PF_6^--Anions kristallisieren jedoch beide Formen. Hieraus wird klar, dass die Größe des Anions nicht der einzige bestimmende Faktor für die Bildung helicaler bzw. nichthelicaler Ketten ist.

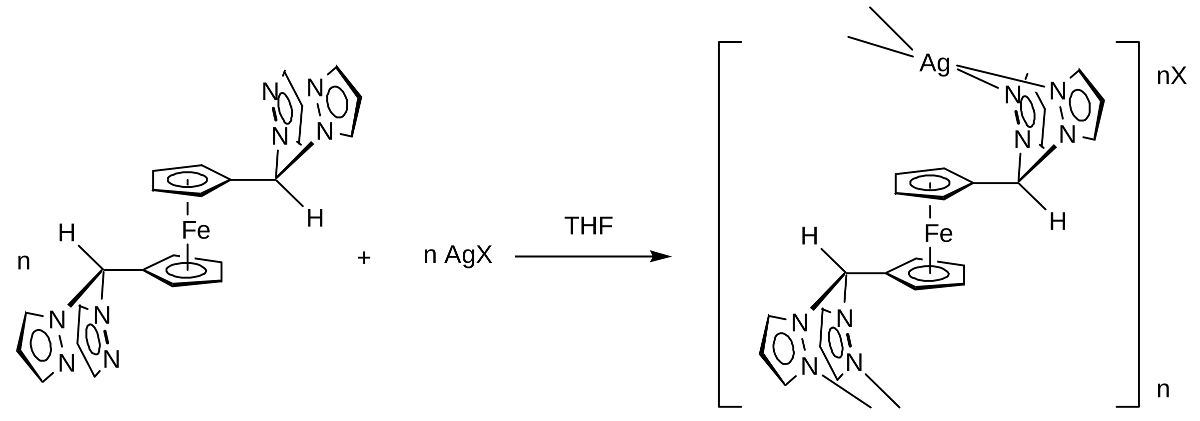

40 $X = BF_4^-, PF_6^-, SO_3CF_3^-, SbF_6^-$ **41X**

Schema **11**: Darstellung der Silberkomplexe $\{Fe[C_5H_4CH(pz)_2]_2AgX\}_n$ (**41X**).

1.4.2 Synthese und strukturelle Charakterisierung der Ferrocen-basierten Bis(pyrazol-1-yl)borat-Liganden $FcB(Me)pz_2K$ (43), Fc_2Bpz_2K (44) und 1,1′-$fc[B(Me)pz_2]_2K_2$ (45)

Umsetzung der Ferrocenyl(dimethylamino)borane $FcB(Me)NMe_2$ (**24**), Fc_2BNMe_2 (**42**)[34] und 1,1′-$fc[B(Me)NMe_2]_2$ (**25**) mit einer 1:1 Mischung aus Hpz und Kpz in THF bei Rückflusstemperatur liefert in guten Ausbeuten die jeweiligen Heteroskorpionate $FcB(Me)pz_2K$ (**43**), Fc_2Bpz_2K (**44**) und 1,1′-$fc[B(Me)pz_2]_2K_2$ (**45**).[34]

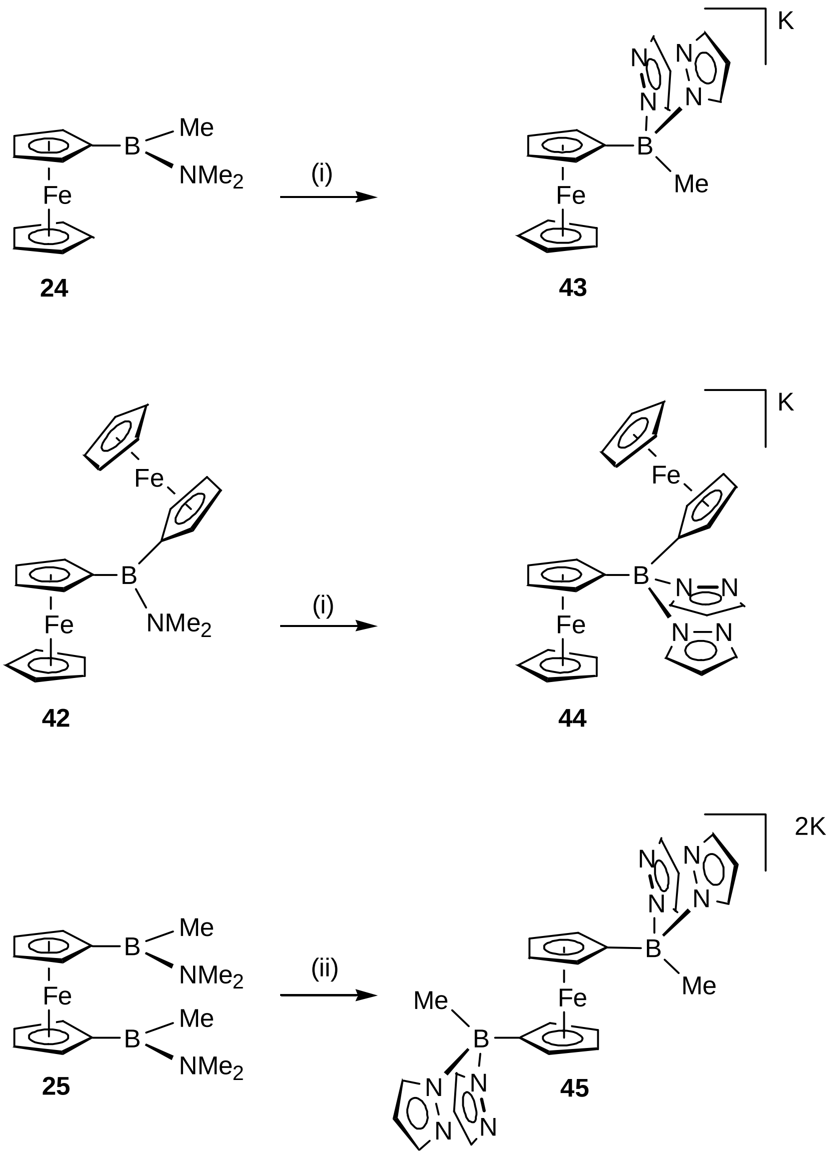

Schema **12**: Synthese der difunktionellen Bis(pyrazol-1-yl)liganden **43**, **44** und **45**: (i) + Kpz/Hpz, THF, -78 °C → RT, 24h Erhitzen am Rückfluss; (ii) + 2 Kpz/2 Hpz, THF, -78 °C → RT, 34h Erhitzen am Rückfluss.[34]

Die Verbindungen sind etwas luftempfindlich. FcB(Me)pz_2K (**43**) und Fc_2Bpz_2K (**44**) lösen sich gut in THF, wogegen 1,1′-fc[B(Me)$pz_2]_2K_2$ (**45**) in allen gängigen organischen Lösungsmitteln nur mäßig löslich ist. Die ^{11}B-NMR-Signale von **43** – **45** liegen im Intervall zwischen -1.4 ppm und 1.0 ppm und sind somit charakteristisch für vierfach koordinierte Borzentren. In allen drei Fällen wird nur ein Satz von Signalen für die Pyrazolylringe in den ^{1}H- wie auch in den ^{13}C-NMR-Spektren beobachtet. Das gleiche gilt für die

Ferrocenylresonanzen von Verbindung **44**. Obwohl **44** und **45** sterisch stark belastet sind, ist die Rotation sowohl um die B-N- als auch um die B-C-Bindungen offensichtlich schnell auf der NMR-Zeitskala. Alle ^{1}H- und ^{13}C-NMR-Verschiebungen liegen im erwarteten Bereich.[34] Die Struktur der Verbindung (**43**THF)$_2$ konnte röntgenstrukturanalytisch bestimmt werden (monoklin, $P2_1/n$). Das K$^+$-Ion ist an ein THF-Molekül, an den Lewis-basischen N(22)-Pyrazolylseitenarm und an den Cp-Ring des Ferrocens koordiniert. (**43**THF)$_2$ bildet im Feststoff zentrosymmetrische Dimere (Abb. **17**).

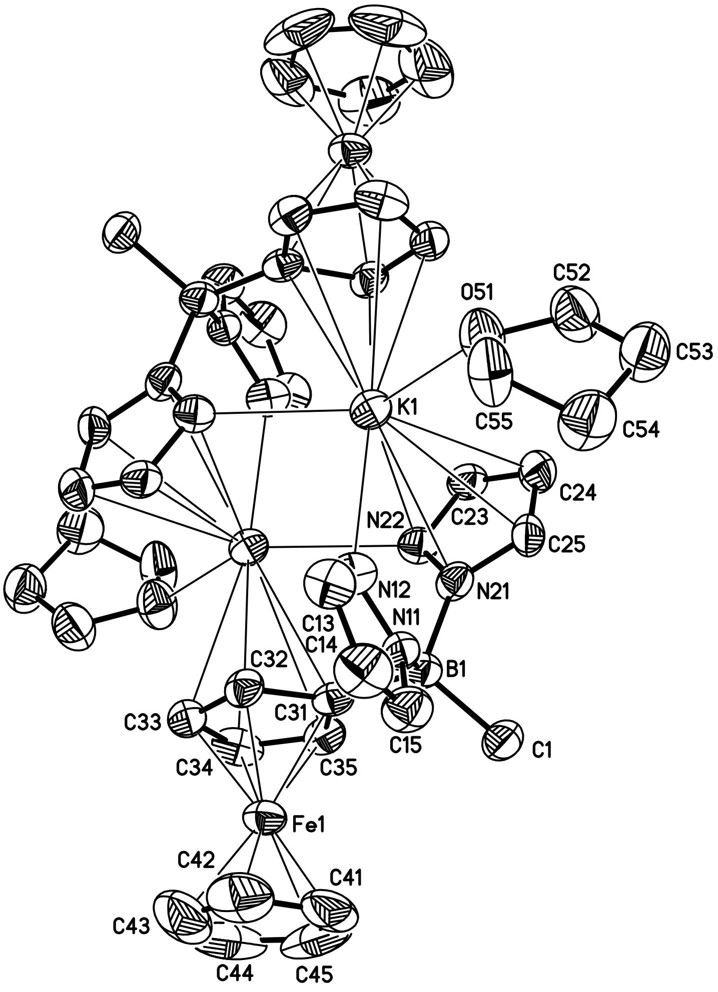

Abb. **17**: Struktur von (**43**THF)$_2$ im Kristall. Die anisotropen Auslenkungsparameter entsprechen 50 % Aufenthaltswahrscheinlichkeit.

Abbildung **18** gibt die Struktur des Heteroskorpionatkomplexes [**44**·(THF)$_2$]$_2$ im Kristall wieder (triklin, *P*-1). Die Geometrie der zentrosymmetrischen Struktur ist der von (**43**THF)$_2$ sehr ähnlich, abgesehen davon, dass jedes K$^+$-Ion nunmehr *zwei* THF-Liganden trägt (Abb. **18**).

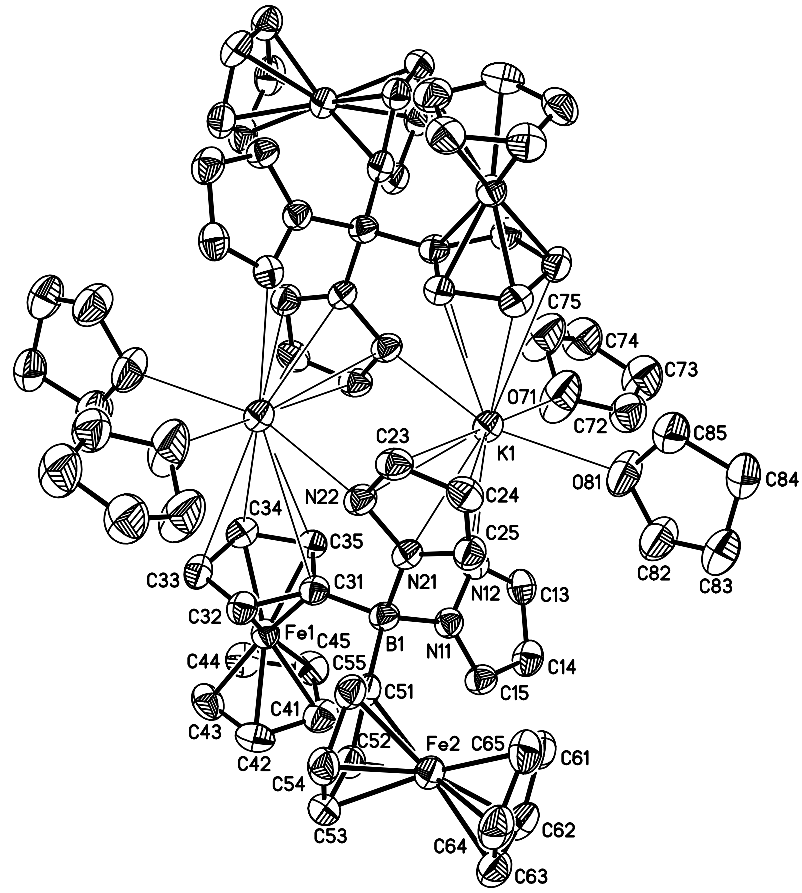

Abb. **18**: Struktur von [**44**·(THF)$_2$]$_2$ im Kristall. Die anisotropen Auslenkungsparameter entsprechen 50 % Aufenthaltswahrscheinlichkeit.

Verbindung [**45**·(THF)$_4$]$_\infty$ kristallisiert aus THF in der monoklinen Raumgruppe *P*2$_1$/n. Das Kristallgitter besteht aus Koordinationspolymeren. Innerhalb dieser Stränge sind die einzelnen CpB(Me)pz$_2$K-Fragmente wiederum zu dinuklearen Kaliumkomplexen angeordnet, die im wesentlichen die strukturellen Merkmale aufweisen, die schon für (**43**THF)$_2$ beschrieben wurden.

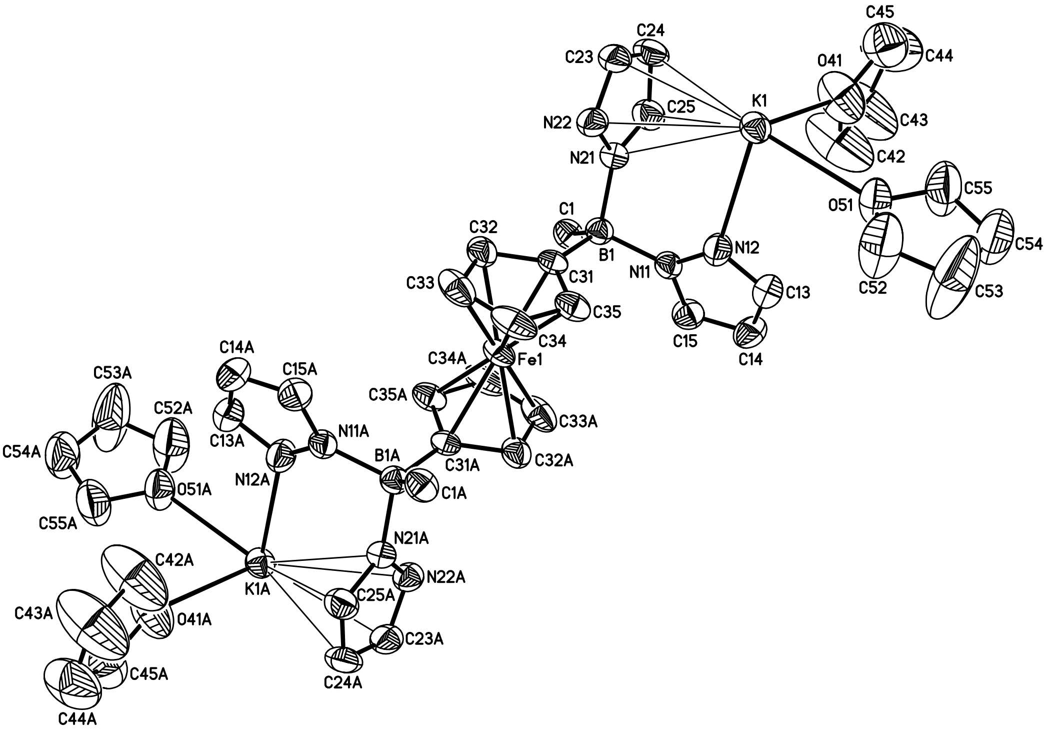

Abb. **19**: Struktur von [**45**·(THF)$_4$]$_\infty$ im Kristall. Die anisotropen Auslenkungsparameter entsprechen 50 % Aufenthaltswahrscheinlichkeit.

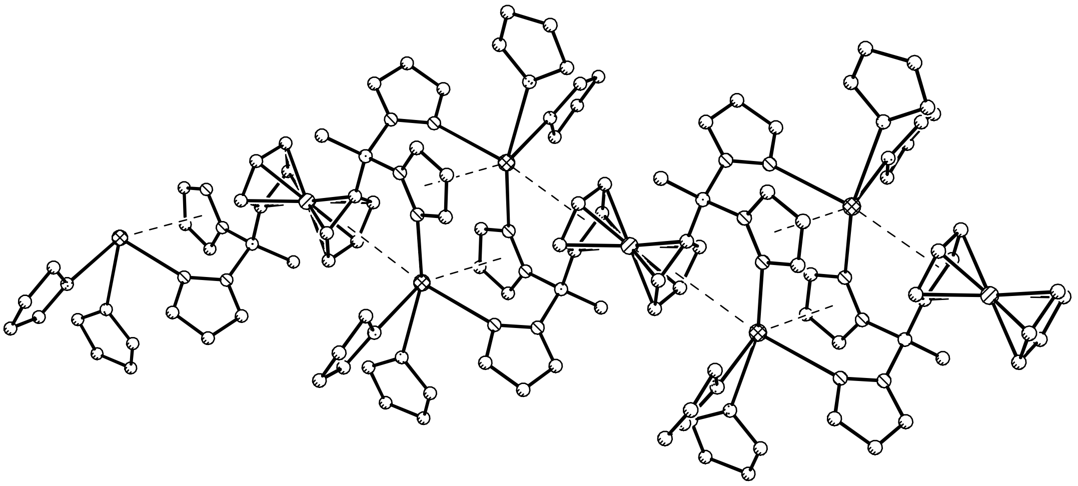

Abb. **20**: Ansicht eines Polymerstranges von [**45**·(THF)$_4$]$_\infty$.

In allen drei Fällen $FcB(Me)pz_2K$ (**43**), Fc_2Bpz_2K (**44**) und 1,1´-fc$[B(Me)pz_2]_2K_2$ (**45**) wird jedes Kaliumion nicht nur von den Pyrazolylringen gebunden, sondern auch von einem Ferrocenfragment über dessen Cyclopentadienylring koordiniert. Die Abstände zwischen den Kaliumionen und dem Schwerpunkt des jeweiligen gebundenen Cyclopentadienylrings betragen 2.942 Å (**43**), 3.171 Å (**44**) und 3.020 Å (**45**).

Alle drei Skorpionatliganden sind somit aussichtsreiche Bausteine für die Herstellung Ferrocen-basierter Multideckerkomplexe. Außerdem kann man bei Verbindung **44** erwarten, dass aufgrund der Anwesenheit von zwei Ferrocenyl-Substituenten im Liganden die Wahrscheinlichkeit für eine M···Cp Koordination gesteigert wird.[34]

1.5 Wechselwirkungen von Arenkomplexen mit dem Li$^+$-Ion

Das im vorangegangenen Kapitel vorgestellte Konzept, mittels anionischer Chelatbrücken eine η^5-Koordination von Metallionen an die Cyclopentadienylringe von Ferrocen zu erzwingen, sollte sich auch auf rein organische π-Systeme übertragen lassen. Da borylierte Benzole ähnlich gut zugänglich sind wie borylierte Ferrocenderivate, konnten in unserem Arbeitskreis bereits erste Versuche zum Komplexierungsverhalten von 1,3-$[C_6H_4(BRpz_2)_2]^{2-}$ und 1,4-$[C_6H_4(BRpz_2)_2]^{2-}$ unternommen werden (R = ^{t}Bu, Ph). Die genannten Verbindungen sind den oben beschriebenen Ferrocenliganden (**43**THF)$_2$, [**44**·(THF)$_2$]$_2$ und [**45**·(THF)$_4$]$_\infty$ verwandt.[35] In der Tat zeigten Tl$^+$- und $Ag(PPh_3)^+$-Komplexe von 1,3-$[C_6H_4(B^tBupz_2)_2]^{2-}$ im festen Zustand zwischen den Metallionen und einigen Kohlenstoffatomen des Phenylrings kurze Abstände, die im Bereich bindender Wechselwirkungen liegen.[36] Im Gegensatz zu Ferrocen, das an jedem Cyclopentadienylring maximal zweifach boryliert werden kann, ist das dreifach borylierte Benzolderivat 1,3,5-$C_6H_3(BI_2)_3$ literaturbekannt.[37] Durch Umwandlung in das entsprechende Borat ließen sich demnach in diesem Fall drei negative Ladungen in unmittelbarer Nähe zum aromatischen π-System platzieren. Hieraus ergibt sich die Möglichkeit, die gewünschte Metallion···Aren-Wechselwirkung diesmal auf rein elektrostatischem Wege ohne Einführung chelatisierender Seitengruppen auch für solche Metallionen herbeizuführen, die normalerweise nicht zur Bildung von Arenkomplexen neigen. Gegenstand der im folgenden beschriebenen Untersuchung war daher die Darstellung einer vollständigen Reihe gleichartig substituierter mono-, di- und triborylierter Benzole, deren Umwandlung in die entsprechenden Methylborate und eine erste Untersuchung der Komplexbildungseigenschaften gegenüber Alkalimetallionen.

1.5.1 Mehrfach borylierte Arene

Die starken Lewis-Säuren 4-(Dibromoboryl)toluol (**46**), 1,4-Bis(dibromoboryl)benzol (**47**) und 1,3,5-Tris(dibromoboryl)benzol (**48**) wurden aus den entsprechenden Trimethylsilyl-Derivaten und Bortriboromid synthetisiert (Schema **13**) und mittels Röntgenkristallographie untersucht.[10, 16, 38] Jedes dieser Moleküle besitzt im festen Zustand eine planare Konformation [vgl. **46**, orthorhombische Raumgruppe *Pca*2$_1$; Abb. **21**]. Dieses Strukturmotiv ermöglicht maximalen Überlapp zwischen den leeren p-Orbitalen der BBr_2-Substituenten und den gefüllten p-Orbitalen der C*ipso*-Atome. Es war daher interessant zu untersuchen, wie sich die Einführung der stark elektronenziehenden Borylgruppen auf die Elektronenverteilung im aromatischen Ring auswirkt. Zu diesem Zweck wurden an den Verbindungen **46** – **48** Hartree-Fock (HF) und Dichtefunktionaltheorierechnungen durchgeführt. Ein Vergleich der optimierten Geometrien und berechneten NMR-Verschiebungen mit den entsprechenden experimentellen Daten dient als Test für die Qualität der unterschiedlichen theoretischen Methoden im Hinblick auf eine zuverlässige theoretische Behandlung der Verbindungsklasse.[38] Alle eingesetzten DFT-Methoden liefern optimierte Molekülstrukturen der höchst möglichen Symmetriepunktgruppen (C_s, C_{2v} und D_{3h} für **46**, **47**, und **48**). Die erhaltenen Bindungslängen stimmen im Rahmen des 3σ-Fehlerintervalls mit dem Experiment überein.[38] Bei der Berechnung der NMR-Verschiebungen jedoch treten signifikante Abweichungen zwischen den einzelnen theoretischen Methoden auf.

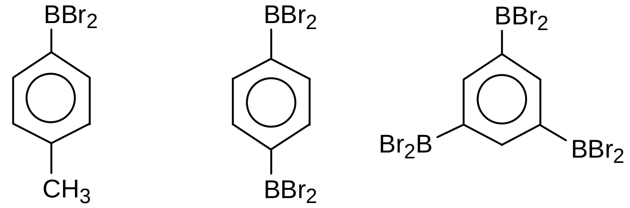

46 **47** **48**

$$\text{Aryl-SiMe}_3 + \text{BBr}_3 \longrightarrow \text{Aryl-BBr}_2 + \text{BrSiMe}_3$$

Schema **13**: Borylierte Arene **46** – **48** und die generelle Syntheseroute über einen Silyl/Boryl-Austausch.

Zusammenfassend empfielt sich für die Untersuchungen borylierter aromatischer Verbindungen die Verwendung der B3LYP/SVP Kombination als zuverlässiges und effizientes theoretisches Niveau zur Berechnung von Molekülstrukturen sowie absoluter und relativer ^{1}H-, ^{13}C- und ^{11}B-NMR-Verschiebungen. Die experimentell bestimmten ^{11}B-NMR-Signale von **46 – 48** liegen alle in dem sehr schmalen Bereich zwischen 56.6 ppm (**46**) und 58.3 ppm (**48**).[39] Da der größte Einfluss auf die magnetische Abschirmung des dreifach koordinierten Borkerns in der Regel von der Elektronendichte im p-Orbital des Boratoms ausgeht, kann man folgern, dass die p-Orbitale aller vier Borverbindungen annähernd gleich stark besetzt sind. Diese Deutung wird unterstützt durch die berechneten NBO Ladungen an den Bor Atomen, die für **46** (+0.41), **47** (+0.40) und **48** (+0.40) fast identisch sind.

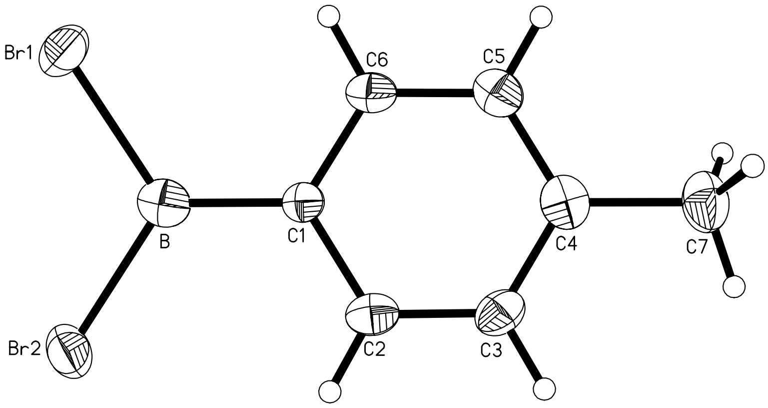

Abb. **21**: Struktur von **46** im Kristall. Die anisotropen Auslenkungsparameter entsprechen 50 % Aufenthaltswahrscheinlichkeit.

1.5.2 Mehrfach borylierte Arene als Bausteine zur Synthese von Arenkomplexen

Für die Synthese der Borate **49** – **50** wurde von den entsprechenden Dibromoborylbenzolen **46** – **48** ausgegangen.

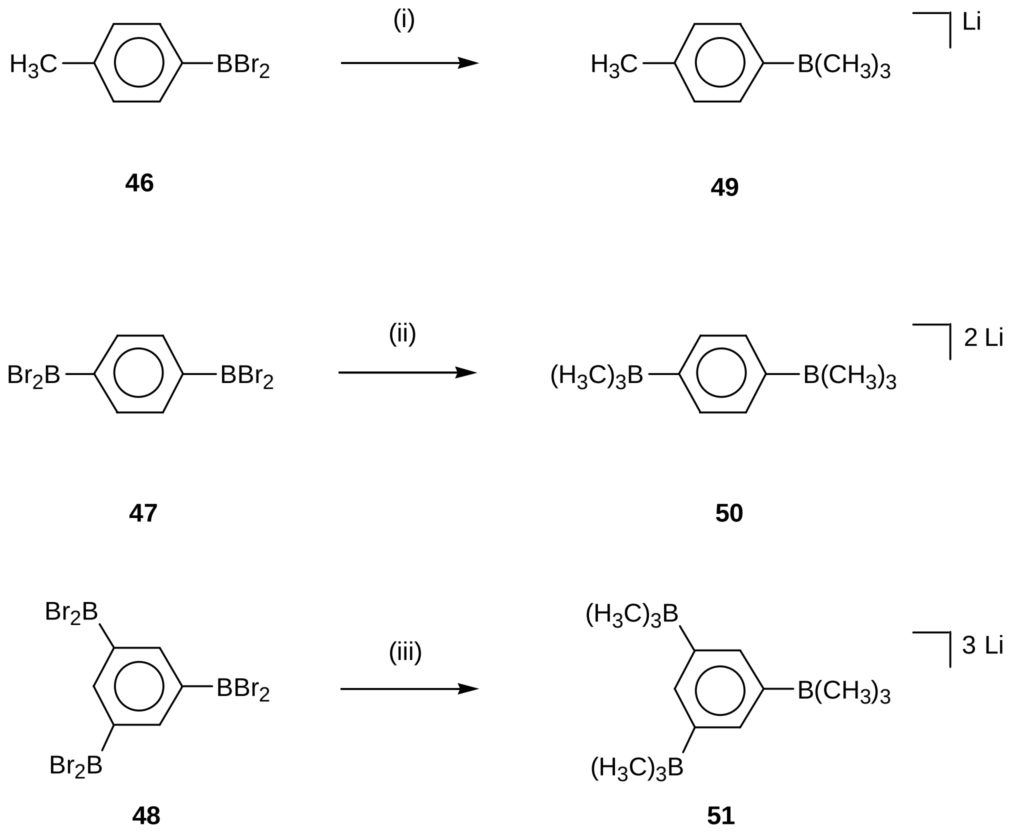

$$\text{Aryl-BBr}_2 + 3\ \text{LiMe} \longrightarrow \text{Aryl-B(Me)}_3\text{Li} + 2\ \text{LiBr}$$

Schema **14**: Die Borate **49** – **51** und ihre generelle Syntheseroute über nucleophile Substitution (i) + 3 LiMe, Toluol, -78 °C,1h; (ii) + 6 LiMe, Toluol, -78 °C, 1h; (iii) + 9 LiMe, Toluol, -78 °C, 1h.

Zur Röntgenstrukturanalyse geeignete Einkristalle von **49**, **50** und **51** wurden durch Diffusion von Diethylether in eine THF-Lösung erhalten, der zwei, vier und sechs Äquivalente 12-Krone-4 zugesetzt worden waren. Die Züchtung von Einkristallen ohne Zusatz von 12-Krone-4 war bislang nicht erfolgreich. Abbildung **22** zeigt die Struktur der Verbindung **49** im Kristall (monokline Raumgruppe $P2_1/c$). Alle Bindungslängen und -winkel bewegen sich im normalen Bereich und bedürfen daher keiner Diskussion. Eine Methylgruppe des Trimethylboratsubstituenten liegt annähernd in der Ebene des Phenylenrings [Torsionswinkel C(9)-B(1)-C(1)-C(2) = -157.0(5)°]. Im Festkörper findet man solvens-separierte Ionenpaare $[Li(12\text{-Krone-}4)_2]^+$ $[Me_3B\text{-}C_6H_4\text{-}Me]^-$. Direkte Li$^+$···Aren Kontakte treten nicht auf.

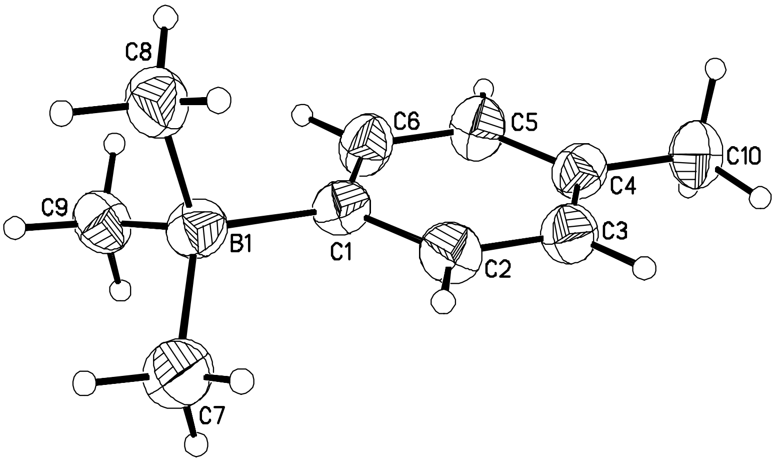

Abb. **22**: Struktur von **49**·(12-Krone-4)$_2$ im Kristall. Die anisotropen Auslenkungsparameter entsprechen 50 % Aufenthaltswahrscheinlichkeit. Das Li·(12-Krone-4)$_2$$^+$-Ion ist nicht dargestellt.

Auch in Verbindung **50** (monokline Raumgruppe $P2_1/c$) liegen vom dianionischen Fragment 1,4-[$C_6H_4(BMe_3)_2$]$^{2-}$ isolierte Li·(12-Krone-4)$_2$$^+$-Ionen vor. Das Molekül 1,4-[$C_6H_4(BMe_3)_2$]$^{2-}$ liegt auf einem kristallographischen Inversionszentrum. Wie bei **49** befindet sich auch hier eine Methylgruppe fast in der Ebene des Phenylenrings [Torsionswinkel C(4)-B(1)-C(1)-C(2) = 22.7(3)°].

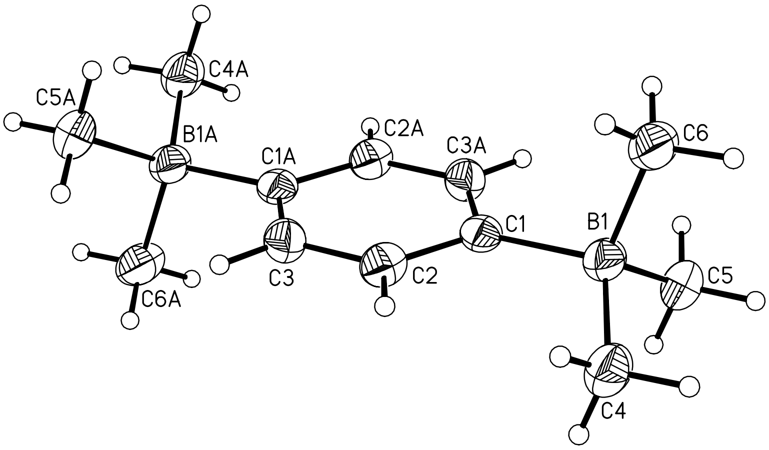

Abb. **23**: Struktur von **50**·(12-Krone-4)$_4$ im Kristall. Die anisotropen Auslenkungsparameter entsprechen 50 % Aufenthaltswahrscheinlichkeit. Die Li·(12-Krone-4)$_2$$^+$-Ionen sind nicht dargestellt.

Nach Einführung eines dritten Trimethylboratsubstituenten in den aromatischen Ring tritt ein direkter Li$^+$···Aren Kontakt auf (**51**). Verbindung **51** kristallisiert aus THF in Anwesenheit von 12-Krone-4 in der monoklinen Raumgruppe $P2_1/n$. In diesem Fall liegen zwei Lithiumionen an 12-Krone-4 gebunden vor, während das dritte, wie gewünscht, an das π-System des Aromaten koordiniert (Abb. **24**). Als Abstand zwischen dem Li$^+$-Ion und dem Schwerpunkt (COG) des koordinierenden Phenylenrings ergibt sich COG[C(1)C(2)C(3)C(4)-C(5)C(6)]···Li(2) = 1.784 Å.

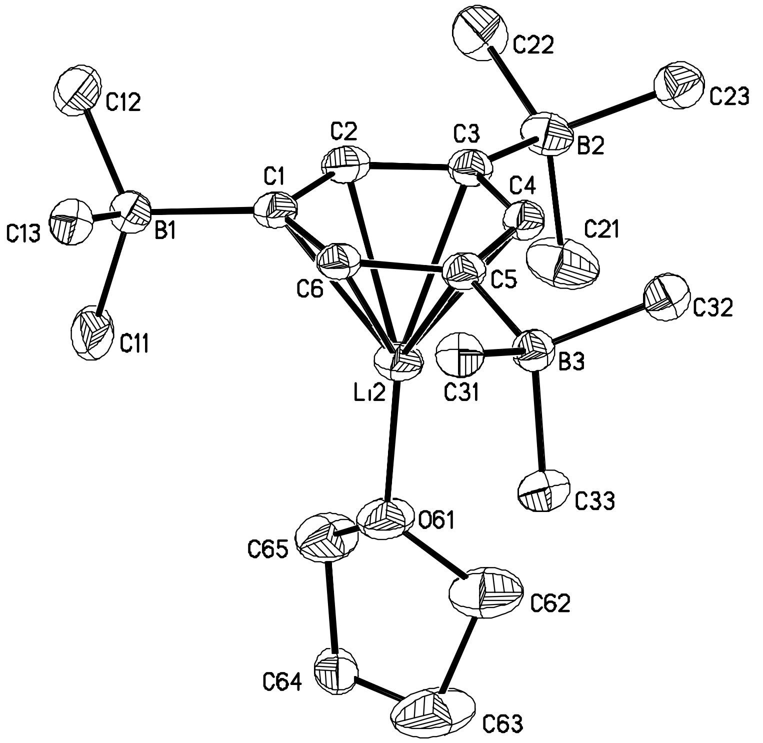

Abb. **24**: Struktur von **51**·THF(12-Krone-4)$_4$ im Kristall. Die anisotropen Auslenkungsparameter entsprechen 30 % Aufenthaltswahrscheinlichkeit. Die Li·(12-Krone-4)$_2^+$-Ionen sind nicht dargestellt.

2 Experimenteller Teil

2.1 Synthese und Charakterisierung der noch unpublizierten Verbindungen 49 – 51

2.1.1 Synthese von 49

Zu einer Lösung von **46** (2.40 g, 9.16 mmol) in Toluol (20 ml) wurden bei –78 °C drei Äquiv. LiMe-Lösung in Diethylether (1.6 M, 27.48 mmol, 17.18 ml) zugetropft. Nach 30 min lässt man die Mischung auf RT erwärmen und rührt 1h. Das Reaktionsgemisch wurde über eine G4-Fritte von unlöslichem LiBr abfiltriert. Nach Entfernen des Lösungsmittels vom Filtrat im Vakuum wurde ein farbloser Feststoff erhalten. Ausbeute: 1.30 g (92 %). Kristalle für die Röntgenstrukturanalyse wurden durch Diffusion von Diethylether in eine THF-Lösung von **49** mit zwei Äquiv. 12-Krone-4 bei RT erhalten. ^{11}B NMR (80.3 MHz, C_6D_6): δ -19.2 ($h_{1/2}$ = 11 Hz). ^{1}H NMR (250.1 MHz, C_6D_6): δ 0.00 (s, 9H, BCH_3), 2.07 (s, 3H, CH_3), 6.92 (d, 2H, ^3J(H,H) = 7.7 Hz; H-2,6), 7.43 (d, 2H, ^3J(H,H) = 6.9 Hz; H-3,5). ^{13}C NMR (62.9 MHz, C_6D_6): δ 13.9 (BCH_3), 20.7 (CH_3), 130.7 (C-2,6), 134.1 (C-3,5), 135.2 (C-1), n.b. (C-4).

2.1.1.1 Kristallstrukturanalyse von 49

$C_{26}H_{48}BLiO_8$, M_r = 506.39, monoklin, Raumgruppe $P2_1/c$, a = 12.7833(12), b = 14.5154(11), c = 16.2812(14) Å, β = 111.498(7)°, V = 2810.9(4) Å^3, Z = 4, $\rho_{\text{ber.}}$ = 1.197 Mg m^{-3}, μ = 0.085 mm^{-1}, F(000) = 1104, $\lambda(\text{Mo}_{K\alpha})$ = 0.71073 Å, T = 100(2) K, Kristallabmessungen 0.24 × 0.12 × 0.05 mm^3, $2\Theta_{\text{max}}$ = 25.35°, 33353 gemessene Reflexe, 5146 unabhängige Reflexe (R_{int} = 0.0698), 5146 berücksichtigte Reflexe, semiempirische Absorptionskorrektur, max./min. Transmission 0.9958/0.9799, 402 Parameter, $R1$= 0.0987 (alle Daten), $wR2$ = 0.3257 (alle Daten), max./min. Restelektronendichte 0.420/-0.266 e Å^{-3}. Die Daten wurden auf einem STOE-IPDS-II Zweikreis-Diffraktometer an einem im Öltropfen gekühlten Kristall gesammelt. Zur Strukturlösung und -verfeinerung wurden die Programme SHELXS-97 und SHELXL-97 (G. M. Sheldrick, Universität Göttingen, 1997) benutzt. Die Struktur wurde mit Direkten Methoden gelöst und mit anisotropen Auslenkungsparametern für Nicht-H-Atome gegen F^2 verfeinert. Alle H-Atome wurden mit dem Reiter-Modell verfeinert.

B(1)-C(9) = 1.640(8), B(1)-C(1) = 1.641(8), B(1)-C(7) = 1.643(8), B(1)-C(8) = 1.651(8); C(9)-B(1)-C(1) = 111.5(4), C(9)-B(1)-C(7) = 110.2(5), C(1)-B(1)-C(7) = 111.7(4), C(9)-B(1)-

C(8) = 107.7(4), C(1)-B(1)-C(8) = 108.5(4), C(7)-B(1)-C(8) = 106.9(4), C(6)-C(1)-B(1) = 123.4(4), C(2)-C(1)-B(1) = 122.4(4); C(8)-B(1)-C(1)-C(6) = -93.2(6), C(9)-B(1)-C(1)-C(2) = -157.0(5), C(7)-B(1)-C(1)-C(2) = -33.1(7), C(9)-B(1)-C(1)-C(6) = 25.3(7), C(7)-B(1)-C(1)-C(6) = 149.2(5).

2.1.2 Synthese von 50

Die Synthese von **50** wurde analog zu der Vorschrift für **49** durchgeführt, indem zu einer Lösung von **47** (9.56 g, 22.90 mmol) in Toluol (40 ml) bei -78 °C sechs Äquiv. LiMe-Lösung in Diethylether (1.6 M, 85.90 ml, 137.44 mmol) zugetropft wurden. Nach 30 min lässt man die Mischung auf RT erwärmen und rührt 1h. Das Reaktionsgemisch wurde über eine G4-Fritte von unlöslichem LiBr abfiltriert. Nach Entfernen des Lösungsmittels vom Filtrat im Vakuum bleibt ein farbloser Feststoff zurück. Ausbeute: 4.0 g (86 %). Kristalle für die Röntgenstrukturanalyse wurden durch Diffusion von Dietylether in eine THF-Lösung von **50** mit vier Äquiv. 12-Krone-4 bei RT erhalten. ^{11}B NMR (128.4 MHz, C_6D_6): δ -18.4 ($h_{1/2}$ = 20 Hz). ^{1}H NMR (400.1 MHz, C_6D_6): δ 0.30 (s, 18H, CH_3), 7.77 (s, 4H, H-2,3,5,6). ^{13}C NMR (100.6 MHz, C_6D_6): δ 14.3 (CH_3), 134.0 (C-2,3,5,6), n.b. (C-1,4).

2.1.2.1 Kristallstrukturanalyse von 50

$C_{44}H_{86}B_2Li_2O_{16}$, M_r = 906.63, monoklin, Raumgruppe $P2_1/c$, a = 9.9258(9), b = 10.1313(10), c = 24.879(2) Å, β = 93.520(7)°, V = 2497.1(4) Å^3, Z = 2, $\rho_{\text{ber.}}$ = 1.206 Mg m^{-3}, μ = 0.088 mm^{-1}, F(000) = 988, $\lambda(\text{Mo}_{K\alpha})$ = 0.71073 Å, T = 100(2) K, Kristallabmessungen 0.38 × 0.35 × 0.28 mm^3, $2\Theta_{\max}$ = 26.60°, 17803 gemessene Reflexe, 5017 unabhängige Reflexe (R_{int} = 0.0572), 5017 berücksichtigte Reflexe, semiempirische Absorptionskorrektur, max./min. Transmission 0.9758/0.9674, 507 Parameter, $R1$= 0.0534 (alle Daten), $wR2$ = 0.1286 (alle Daten), max./min. Restelektronendichte 0.234/-0.221 e Å^{-3}. Die Daten wurden auf einem STOE-IPDS-II Zweikreis-Diffraktometer an einem im Öltropfen gekühlten Kristall gesammelt. Zur Strukturlösung und -verfeinerung wurden die Programme SHELXS-97 und SHELXL-97 (G. M. Sheldrick, Universität Göttingen, 1997) benutzt. Die Struktur wurde mit Direkten Methoden gelöst und mit anisotropen Auslenkungsparametern für Nicht-H-Atome gegen F^2 verfeinert. Alle H-Atome wurden mit dem Reiter-Modell verfeinert.

B(1)-C(4) = 1.650(3), B(1)-C(6) = 1.652(3), B(1)-C(1) = 1.652(3), B(1)-C(5) = 1.654(3); C(4)-B(1)-C(6) = 109.8(2), C(4)-B(1)-C(1) = 111.50(2), C(6)-B(1)-C(1) = 107.83(2), C(4)-B(1)-C(5) = 108.47(2), C(6)-B(1)-C(5) = 108.36(2), C(1)-B(1)-C(5) = 110.82(2), C(2)-C(1)-B(1) = 123.96(2); C(5)-B(1)-C(1)-C(2) = 143.64(2), C(4)-B(1)-C(1)-C(2) = 22.7(3), C(6)-B(1)-C(1)-C(3A) = 81.1(2), C(5)-B(1)-C(1)-C(3A) = -37.4(2), B(1)-C(1)-C(2)-C(3) = 179.38(2),

2.1.3 Synthese von 51

Verbindung **51** wurde auf dem gleichen Weg hergestellt wie **49** und **50**. Hierzu wurden zu einer Lösung von **48** (6.21 g, 10.58 mmol) in Toluol (30 ml) bei –78 °C neun Äquiv. LiMe-Lösung in Diethylether (1.6 M, 59.5 ml, 95.2 mmol) zugetropft. Nach 30 min lässt man die Mischung auf RT erwärmen und rührt 1h. Das Reaktionsgemisch wurde über eine G4-Fritte von unlöslichem LiBr abfiltriert. Nach Entfernen des Lösungsmittels vom Filtrat im Vakuum verbleibt ein farbloser Feststoff. Ausbeute: 2.40 g (85 %). Kristalle, die sich für eine Röntgenstrukturanalyse eigneten, wurden durch Diffusion von Diethylether in eine THF-Lösung von **51** mit sechs Äquiv. 12-Krone-4 bei RT hergestellt. ^{11}B NMR (128.4 MHz, DMSO): δ -17.3 ($h_{1/2}$ = 30 Hz). ^{1}H NMR (400.1 MHz, DMSO): δ -0.53 (s, 27H, CH_3), 6.78 (s, 3H, H-2,4,6). ^{13}C NMR (62.9 MHz, DMSO): δ 14.8 (CH_3), 129.9 (C-2,4,6), n.b. (C-1,3,5).

2.1.3.1 Kristallstrukturanalyse von 51

$C_{51}H_{102}B_3Li_3O_{17}$, M_r = 1040.58, monoklin, Raumgruppe $P2_1/n$, a = 19.9648(14), b = 13.5601(14), c = 24.0737(17) Å, β = 113.062(5)°, V = 5996.5(9) Å^3, Z = 4, $\rho_{\text{ber.}}$ = 1.153 Mg m^{-3}, μ = 0.082 mm^{-1}, $F(000)$ = 2272, $\lambda(\text{Mo}_{K\alpha})$ = 0.71073 Å, T = 100(2) K, Kristallabmessungen 0.44 × 0.43 × 0.37 mm^3, $2\Theta_{\text{max}}$ = 25.40°, 57572 gemessene Reflexe, 10960 unabhängige Reflexe (R_{int} = 0.0623), 10960 berücksichtigte Reflexe, semiempirische Absorptionskorrektur, max./min. Transmission 0.9703/0.9648, 907 Parameter, $R1$= 0.0955 (alle Daten), $wR2$ = 0.2646 (alle Daten), max./min. Restelektronendichte 0.830/-0.404 e Å^{-3}. Die Daten wurden auf einem STOE-IPDS-II Zweikreis-Diffraktometer an einem im Öltropfen gekühlten Kristall gesammelt. Zur Strukturlösung und -verfeinerung wurden die Programme SHELXS-97 und SHELXL-97 (G. M. Sheldrick, Universität Göttingen, 1997) benutzt. Die

Struktur wurde mit Direkten Methoden gelöst und mit anisotropen Auslenkungsparametern für Nicht-H-Atome gegen F^2 verfeinert. Alle H-Atome wurden mit dem Reiter-Modell verfeinert.

B(1)-C(1) = 1.645(6), B(1)-C(11) = 1.649(6), B(1)-C(12) = 1.649(7), B(1)-C(13) = 1.652(8), B(2)-C(3) = 1.644(6), B(2)-C(21) = 1.643(6), B(2)-C(22) = 1.638(7), B(2)-C(23) = 1.633(6), C(1)-Li(2) = 2.307(7), C(2)-Li(2) = 2.251(7), C(3)-Li(2) = 2.293(7), C(4)-Li(2) = 2.250(7), C(5)-Li(2) = 2.288(7), C(6)-Li(2) = 2.257(7), B(3)-C(5) = 1.635(6), B(3)-C(31) = 1.643(6), B(3)-C(32) = 1.642(6), B(3)-C(33) = 1.644(5), Li(2)-O(61) = 1.891(6); C(6)-C(1)-B(1) = 122.5(4), C(2)-C(1)-B(1) = 122.5(4), C(6)-C(1)-Li(2) = 70.2(3), C(2)-C(1)-Li(2) = 69.8(3), B(1)-C(1)-Li(2) = 125.3(3), C(2)-C(3)-B(2) = 123.7(3), B(2)-C(3)-Li(2) = 120.6(3), C(2)-C(3)-Li(2) = 70.3(3), C(4)-C(3)-Li(2) = 70.3(3), C(4)-C(5)-B(3) = 121.6(3), C(6)-C(5)-B(3) = 123.8(3), C(4)-C(5)-Li(2) = 70.3(3), C(6)-C(5)-Li(2) = 70.6(3); C(2)-C(1)-B(1)-C(12) = -37.3(5), C(6)-C(1)-B(1)-C(13) = 25.5(5), C(2)-C(1)-B(1)-C(13) = -159.8(3), C(6)-C(1)-B(1)-C(11) = -94.3(5), C(2)-C(3)-B(2)-C(22) = 30.2(5), C(4)-C(3)-B(2)-C(21) = 80.3(4), C(2)-C(3)-B(2)-C(23) = 153.8(3), C(4)-C(3)-B(2)-C(23) = -36.2(5), C(4)-C(5)-B(3)-C(32) = 35.8(4), C(6)-C(5)-B(3)-C(31) = 158.7(3), C(6)-C(5)-B(3)-C(33) = 87.6(4), C(4)-C(5)-B(3)-C(33) = -83.4(4).

3 Zusammenfassung

Cyclopentadienylderivate und Tris(pyrazol-1-yl)borate („Skorpionate“) gehören zu den wichtigsten Liganden für Übergangsmetallionen. In zahlreichen Publikationen wurde die Frage diskutiert,[40] inwieweit sich diese Liganden in Ihrem Koordinationsverhalten ähneln, da beide monoanionische Sechselektronendonoren sind, jedoch unterschiedliche Symmetrie besitzen. Am zuverlässigsten lässt sich diese Frage klären, indem man Komplexe der beiden Liganden, die dieselben Fragmente ML_n enthalten, zu einem Molekül vereinigt, weil nur dann identische Untersuchungsbedingungen gewährleistet sind. Da keine derartige Verbindung literaturbekannt war, wurde im Rahmen dieser Arbeit mit dem Mangantricarbonylkomplex **14** (Abb. **25**) ein erster Vertreter synthetisiert.

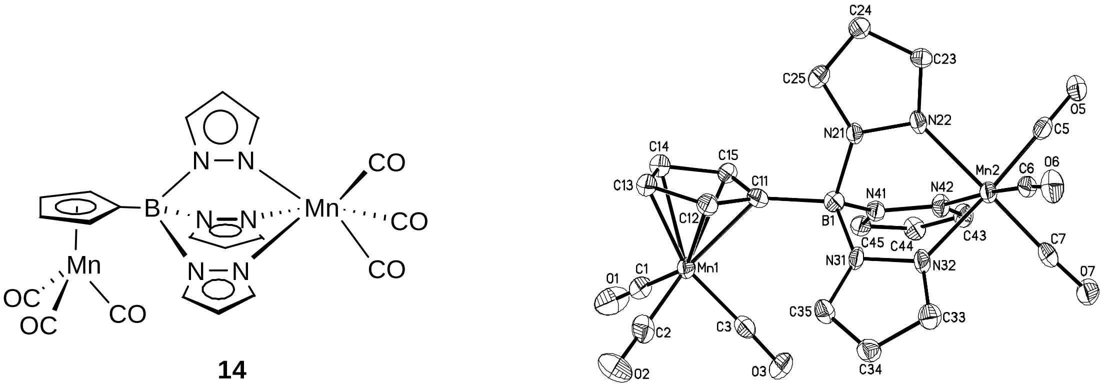

14

Abb. **25**

Zum Zeitpunkt dieser Untersuchung standen freie Cyclopentadienyl/Skorpionat-Hybridliganden nicht zur Verfügung, so dass man gezwungen war, von einem präformierten Cyclopentadienylkomplex ausgehend den Tris(pyrazol-1-yl)boratsubstituenten aufzubauen. Der erste Schritt, die elektrophile Borylierung mittels BBr_3, lässt sich nur an Ferrocen, Ruthenocen und Cymantren problemlos durchführen. Aufgrund der Tatsache, dass andererseits auch $RBpz_3MnCO_3$-Komplexe gut darstellbar sind, wurde Cymantren als metallorganische Komponente für dieses Projekt ausgewählt. Die beiden $Mn(CO)_3$-Fragmente besitzen darüber hinaus noch den Vorteil, dass ihre Carbonylliganden als Sonden zur IR-spektroskopischen Bestimmung der Ladungsdichten am jeweiligen Manganatom genutzt werden konnten. Sowohl die Röntgenstrukturanalyse von **14** (Abb. **25**; alle Mn-C- und alle C-O-Bindungslängen sind im Rahmen der Messgenauigkeit gleich) als auch die IR-Spektroskopie (Unterschiede in den Wellenzahlen der Carbonylstreckschwingungen beider $Mn(CO)_3$-Einheiten sind nicht aufgelöst) deuten auf sehr ähnliche Ladungsdichten an den beiden Manganzentren und damit auf ein ähnliches Donorvermögen des Cp-Rings und der

RBpz$_3$-Gruppe hin. Versuche, durch Photolyse Acetonitril oder Triphenylphosphan als Liganden in **14** einzuführen und auf diesem Wege eventuelle Reaktivitätsunterschiede beider Manganzentren aufzudecken, scheiterten an der mangelhaften Löslichkeit der entstandenen Reaktionsprodukte. Auch war es nicht möglich, durch Oxidation von CymBpz$_3$Tl (u.a. mit elementarem Iod) eine gezielte Selbstpolymerisation unter Bildung von $[\text{-CpMnpz}_3\text{B-}]_\infty$ auszulösen.

Durch Synthese und strukturelle Charakterisierung der Ferrocen-basierten Mono- und Bis(pyrazol-1-yl)borate **33M**, **43** – **45** (Abb. **26**) sollte die Frage geklärt werden, ob in diesen Verbindungen eine koordinative Wechselwirkung zwischen dem jeweiligen Alkalimetall und einem Ferrocen-Cyclopentadienylring durch den dirigierenden Einfluß der chelatisierenden Pyrazolylboratsubstituenten erreicht werden kann. Diese Frage ist in allen Fällen positiv zu beantworten, obwohl – je nach eingesetztem Liganden und Kristallisationsmedium – unterschiedliche supramolekulare Strukturen im Festkörper entstehen: Beide Bis(pyrazol-1-yl)borate **43** und **44** bilden zentrosymmetrische Dimere aus, in denen jedes Kaliumion an genau einen Cp-Ring bindet. Als Beispiel sei hier auf die Kristallstrukturanalyse von Verbindung (**43**THF)$_2$ verwiesen (Abb. **27**).

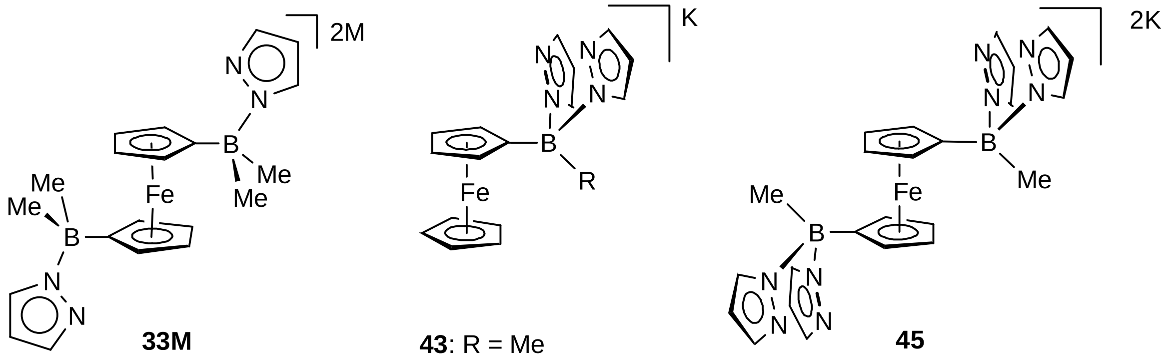

33M

M = Li, Na, K, Rb, Cs

43: R = Me

44: R = Fc

45

Abb. **26**

Das difunktionelle Skorpionat [**45**·(THF)$_4$]$_\infty$ bildet Koordinationspolymere (Abb. **27**). Diese setzen sich aus zentrosymmetrischen dinuklearen Kaliumkomplexen zusammen, wie man sie auch im Falle des monofunktionellen Analogons (**43**THF)$_2$ (Abb. **27**) findet und welche über 1,1´-Ferrocenylenbrücken miteinander verknüpft sind.

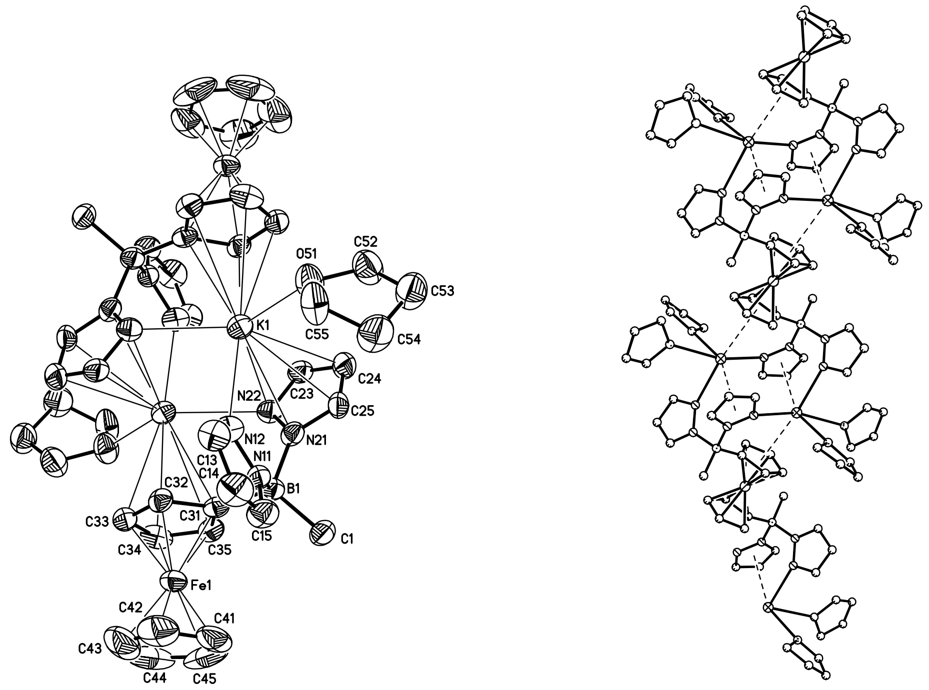

Abb. **27**

Die vollständige Reihe der Alkalimetallsalze **33M** (M = Li, Na, K, Rb, Cs) des Mono(pyrazol-1-yl)borat-Liganden [**33**]$^{2-}$ wurde aus Dimethoxyethan kristallisiert.

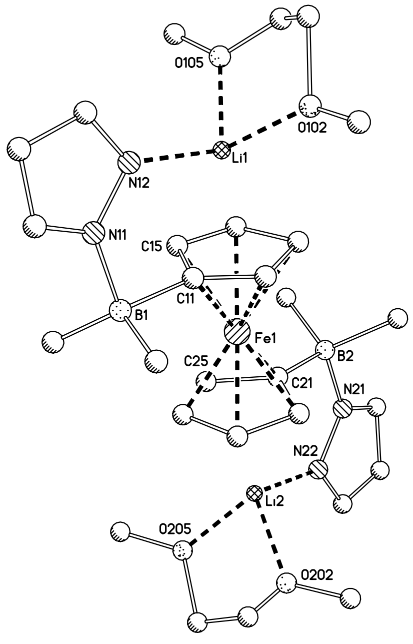

Abb. **28**

Während der Lithiumkomplex **33Li**(DME)$_2$ in Form diskreter Tripeldecker-Sandwichkomplexe anfällt (Abb **28**), bildet das Natriumsalz **33Na**(DME)$_3$ polyanionische Zick-Zack-Ketten, innerhalb derer jedes Natriumion mit *zwei* Ferrocen-Cyclopentadienylringen wechselwirkt (Abb. **29**). Solvensmoleküle koordinieren ausschließlich an die Na$^+$-Gegenionen, die als verzerrt-oktaedrische Komplexe [Na(DME)$_3$]$^+$ im Kristallgitter vorliegen.

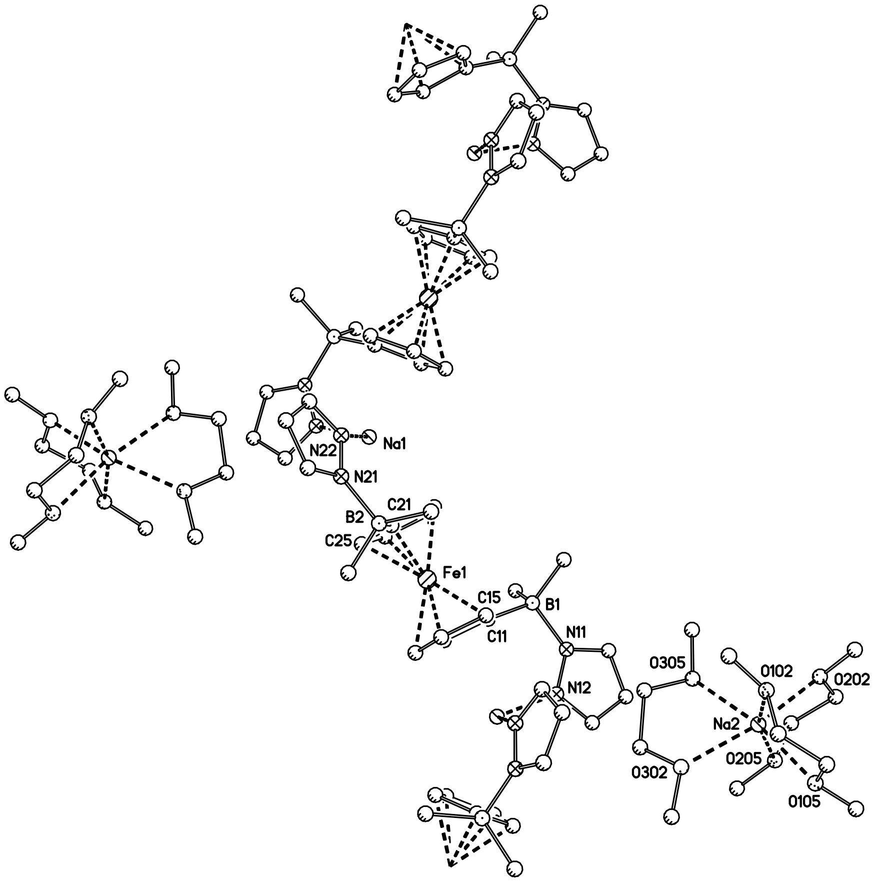

Abb. **29**

Die Salze der höheren Homologen **33M**(DME)$_3$ (M = K, Rb, Cs) sind weitgehend isostrukturell und bilden lineare Multidecker-Sandwichstapel (vgl. **33K**(DME)$_3$, Abb. **30** links). Aus Tetrahydrofuran konnten Kristalle der Salze **33M**(THF)$_4$ (M = Na, K, Rb) gewonnen werden. Auch diese drei Verbindungen besitzen untereinander sehr ähnliche polymere Strukturen, welche sich jedoch von denen der analogen DME-Komplexe **33M**(DME)$_3$ dahingehend wesentlich unterscheiden, dass jedes Alkalimetallion nur an eine

Ferroceneinheit bindet, so dass eine treppenförmige Struktur entsteht (vgl. **33Na**(THF)$_4$, Abb. **30** rechts).

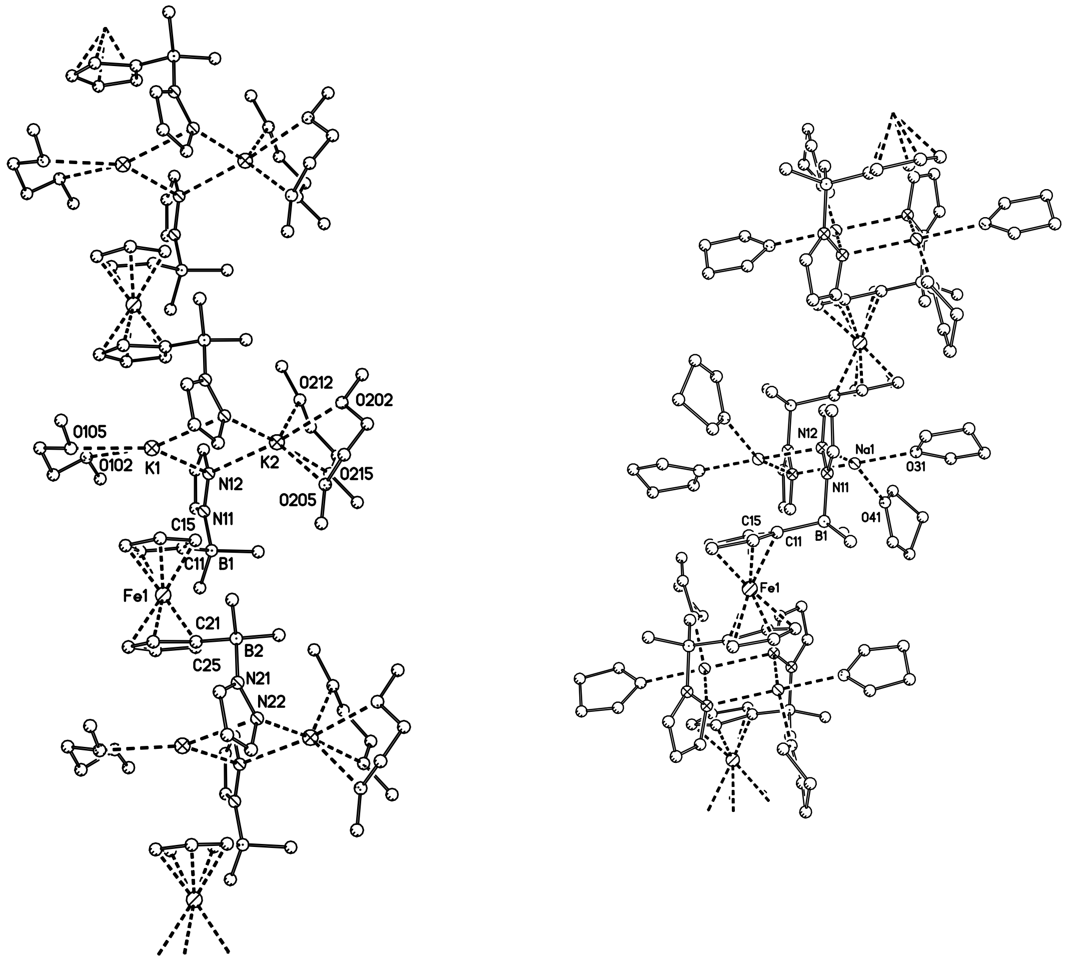

Abb. **30**

Im Falle des Ferrocenderivats **32** (Abb. **31**) reicht die elektrostatische Anziehung durch zwei anionische Boratgruppen *ohne* Lewis-basische Seitenketten nicht aus, um in Anwesenheit konkurrierender THF-Liganden eine Li$^+$···Ferrocen-Koordination herbeizuführen.

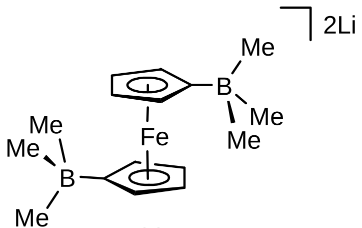

32

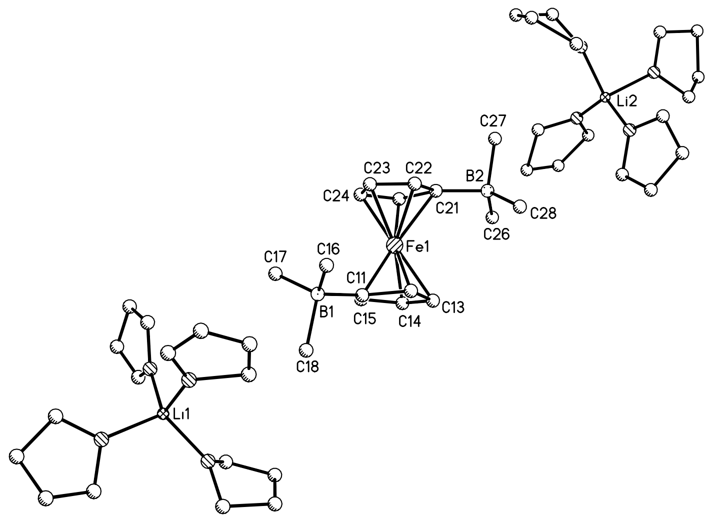

Abb. **31**

Ähnliches gilt für die Benzol-basierten Systeme **49** und **50** (Abb. **32**), die aus THF in Anwesenheit von 12-Krone-4 nur als solvens-separierte Ionenpaare kristallisieren. Dieser Befund ändert sich nach Einführung eines dritten Trimethylboratsubstituenten in den aromatischen Ring. Im Falle von **51** liegen zwei Lithiumionen an 12-Krone-4 gebunden vor, während das dritte, wie gewünscht, an das π-System des Aromaten koordiniert (Abb. **32**).

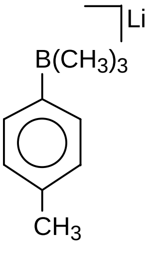

49

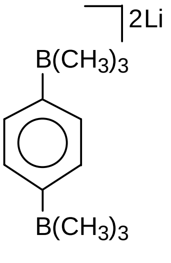

50

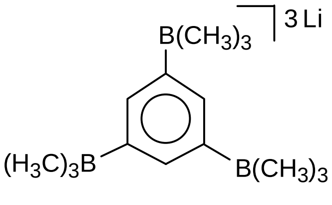

51

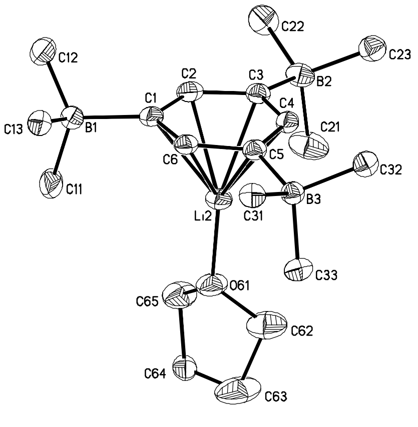

Abb. **32**

In der vorliegenden Arbeit wurde eine neuartige Klasse von Ferrocenylpoly(pyrazol-1-yl)boratliganden erschlossen, deren Alkalimetallkomplexe zu Multidecker-Sandwichstrukturen führen. Damit wurden die Grundlagen für eine weitergehende Entwicklung niedrigdimensionaler metallorganischer Festkörper erarbeitet, die sich durch interessante elektronische oder magnetische Eigenschaften auszeichnen sollten.

4 Literaturverzeichnis

[1] S. Trofimenko, *J. Am. Chem. Soc.* **1966**, *88*, 1842.

[2] S. Trofimenko, *Prog. Inorg. Chem.* **1986**, *34*, 115.

[3] S. Trofimenko, J. C. Calabrese, J. S. Thompson, *Inorg. Chem.* **1987**, *26*, 1507.

[4] S. Trofimenko, *Chem. Rev.* **1993**, *93*, 943.

[5] S. Trofimenko, *J. Am. Chem. Soc.* **1967**, *89*, 3170.

[6] F. Jäkle, K. Polborn, M. Wagner, *Chem. Ber.* **1996**, *129*, 603.

[7] F. Fabrizi de Biani, F. Jäkle, M. Spiegler, M. Wagner, P. Zanello, *Inorg. Chem.* **1997**, *36*, 2103.

[8] E. Herdtweck, F. Peters, W. Scherer, M. Wagner, *Polyhedron.* **1998**, *17*, 1149.

[9] S. L. Guo, F. Peters, F. Fabrizi de Biani, J. W. Bats, E. Herdtweck, P. Zanello, M. Wagner, *Inorg. Chem.* **2001**, *40*, 4928.

[10] T. Renk, W. Ruf, W. Siebert, *J. Organomet. Chem.* **1976**, *120*, 1.

[11] S. L. Guo, J. W. Bats, M. Bolte, M. Wagner, *J. Chem. Soc., Dalton Trans.* **2001**, 3572.

[12] F. Jäkle, F. Polborn, M. Wagner, *Chem. Ber.* **1996**, *129*, 603.

[13] A. Haghiri Ilkhechi, S. L.Guo, M. Bolte, M. Wagner, *Dalton Trans.* **2003**, 2303.

[14] J. W. Hershberger, R. J. Klingler, J. K. Kochi, *J. Am. Chem. Soc.* **1983**, *105*, 61.

[15] C. G. Atwood, W. E. Geiger, T. E. Bitterwolf, *J. of Electroanal. Chem.* **1995**, *397*, 279.

[16] W. Ruf, T. Renk, W. Siebert, *Z. Naturforsch.* **1976**, *31b*, 1028.

[17] M. Fontani, F. Peters, W. Scherer, W. Wachter, M. Wagner, P. Zanello, *Eur. J. Inorg. Chem.* **1998**, 1453.

[18] N. J. Long, *Metallocenes*, Blackwell Science, London, **1998**.

[19] W. Siebert, *Angew. Chem.* **1985**, *97*, 924.

[20] T. Kuhlmann, S. Roth, J. Rozière, W. Siebert, *Angew. Chem.* **1986**, *98*, 87.

[21] M. Y. Lavrentiev, H. Köppel, M. C. Böhm, *Chem. Phys.* **1993**, *169*, 85.

[22] A. Salzer, H. Werner, *Angew. Chem.* **1972**, *84*, 949.

[23] D. R. Armstrong, A. J. Edwards, D. Moncrieff, M. A. Paver, P. R. Raithby, M.-A. Rennie, C. A. Russell, D. S. Wright, *Chem. Comm.* **1995**, 927.

[24] A. Irigoras, J. M. Mercero, I. Silanes, J. M. Ugalde, *J. Am. Chem. Soc.* **2001**, *123*, 5040.

[25] S. Scholz, J. C. Green, H.-W. Lerner, M. Bolte, M. Wagner, *Chem. Comm.* **2002**, *36.*

[26] A. Haghiri Ilkhechi, M. Scheibitz, M. Bolte, H.-W. Lerner, M. Wagner, *Polyhedron.* **2004**, *23*, 2597.

[27] M. Enders, G. Ludwig, H. Pritzkow, *Organometallics* **2002**, *21*, 3856.

[28] O. Crespo, M. C. Gimeno, P. G. Jones, A. Laguna, C. Sarroca, *Chem. Comm.* **1998**, 1481.

[29] A. Haghiri Ilkhechi, J. M. Mercero, I. Silanes, M. Bolte, M. Scheibitz, H.-W. Lerner, J. M. Ugalde, M. Wagner, *J. Am. Chem. Soc.* **2005**, im Druck.

[30] G. W. Honeyman, A. R. Kennedy, R. E. Mulvey, D. C. Sherrington, *Organometallics* **2004**, *23*, 1197.

[31] D. L. Reger, K. J. Brown, J. R. Gardinier, M. D. Smith, *Organometallics* **2003**, *22*, 4973.

[32] G. G. A. Balavoine, G. Doisneau, F.-Khan, *J. Organomet. Chem.* **1991**, *412*, 381.

[33] P. K. Byers, A. J. Canty, R. T. Honeyman, *J. Organomet. Chem.* **1990**, *385*, 417.

[34] A. Haghiri Ilkhechi, M. Bolte, H.-W. Lerner, M. Wagner, *J. Organomet. Chem.* **2005**, 690, 1971-1977.

[35] S. Bieller, F. Zhang, M. Bolte, J. W. Bats, H.-W. Lerner, M. Wagner, *Organometallics* **2004**, *23*, 2107.

[36] F. Zhang, M. Bolte, H.-W. Lerner, M. Wagner, *Organometallics* **2004**, 23, 5075.

[37] M. Bluhm, H. Pritzkow, W. Siebert, R. N. Grimes, *Angew. Chem.* **2000**, *112*, 4736.

[38] M. C. Haberecht, J. B. Heilmann, A. Haghiri Ilkhechi, M. Bolte, J. W. Bats, H.-W. Lerner, M. C. Holthausen, M. Wagner, *Z. Anorg. Allg. Chem.* **2004**, *630*, 904.

[39] H. Nöth, B. Wrackmeyer, in *NMR Basic Principles and Progress,* ed., P. Diehl, E. Fluck, R. Kosfeld, Springer, Berlin, **1978**.

[40] S. Trofimenko, *Scorpionates-the Coordination Chemistry of Polypyrazolylborate Ligands.*, Imperial College Press, London, **1999**.

5 Vollständige Publikationsliste

5.1 Veröffentlichungen in wissenschaftlichen Journalen

1. Alireza Haghiri Ilkhechi, ShengLi Guo, Michael Bolte and Matthias Wagner, *Dalton Trans.*, **2003**, 2303-2307.

   „Cymantrene-based tris(1-pyrazolyl)borates: synthesis and structural characterization of di- and trimetallic complexes“

   Faksimile in Kapitel 6.1, Seite 69

2. Alireza Haghiri Ilkhechi, Matthias Scheibitz, Michael Bolte, Hans-Wolfram Lerner, Matthias Wagner, *Polyhedron.*, **2004**, 23, 2597-2604.

   „On the way to ferrocene-based multiple-decker sandwich complexes“

   Faksimile in Kapitel 6.2, Seite 75

3. Alireza Haghiri Ilkhechi, Jose M. Mercero, Iñaki Silanes, Michael Bolte, Matthias Scheibitz, Hans-Wolfram Lerner, Jesus M. Ugalde and Matthias Wagner, *J. Am. Chem. Soc.,* **2005**, im Druck.

   „A Joint Experimental and Theoretical Study of Cations-π Interactions: Multiple-Decker Sandwich Complexes of Ferrocene with Alkali Metal Ions (Li^+, Na^+, K^+, Rb^+, Cs^+)“

   Faksimile in Kapitel 6.3, Seite 84

4. Alireza Haghiri Ilkhechi, Michael Bolte, Hans-Wolfram Lerner and Matthias Wagner, *J. Organomet. Chem.*, **2005**, 690, 1971-1977.

   „Synthesis and structural characterization of ferrocene-based bis(pyrazol-1-yl)borate ligands: $FcB(Me)pz_2K$, Fc_2Bpz_2K, and $1,1'$-$fc[B(Me)pz_2]_2K_2$ (Fc: ferrocenyl, fc: ferrocenylene, pz: pyrazolyl)“

   Faksimile in Kapitel 6.4, Seite 137

5. Monika C. Haberecht, Julia B. Heilmann, Alireza Haghiri Ilkhechi, Michael Bolte, Jan W. Bats, Hans-Wolfram Lerner, Max C. Holthausen and Matthias Wagner, *Z. Anorg. Allg. Chem.*, **2004**, 630, 904-913.

   „Multiply Borylated Arenes: X-ray Crystal Structure Analyses and Quantum Chemical Calculations“

Faksimile in Kapitel 6.5, Seite 145

6. Hans-Wolfram Lerner, Alireza Haghiri Ilkhechi, Michael Bolte, and Matthias Wagner, *Z. Naturforsch.*, **2005**, 60b, 413-415.

   „Structure of the Adduct of Trimethyltin Chloride Me_3SnCl with Trimethyltin Hydroxide Me_3SnOH“

7. Alireza Haghiri Ilkhechi, Hans-Wolfram Lerner, Matthias Wagner and Jan W. Bats, *Acta Cryst.*, **2002**, E58, o1378-o1380.

   „3-Phenylpyrazole, a pseudosymmetric structure with Z´ = 6“

8. Alireza Haghiri Ilkhechi, Hans-Wolfram Lerner and Michael Bolte, *Acta Cryst.*, **2003**, E59, o873-o874.

   „A new polymorph of 3-phenylpyrazole“

9. Alireza Haghiri Ilkhechi, Matthias Wagner and Michael Bolte, *Acta Cryst.*, **2003**, E59, i129-i130.

   „Bromopentacarbonylmanganese“

10. Alireza Haghiri Ilkhechi, Hans-Wolfram Lerner, Matthias Wagner and Michael Bolte, *Acta Cryst.*, **2004**, E60, o876-o877.

    „3-phenylpyrazolium nitrate“

5.2 Vorträge und Posterpräsentationen

1. Alireza Haghiri Ilkhechi, Matthias Wagner

   Deutsche Borchemikertagung, 11. – 13. Oktober 2002, Rothenfels:

   Vortrag: „Übergangsmetallkomplexe mit schaltbaren Spinzuständen“

6 Ausgewählte Veröffentlichungen

6.1 „Cymantrene-based tris(1-pyrazolyl)borates: synthesis and structural characterization of di- and trimetallic complexes“

Alireza Haghiri Ilkhechi, ShengLi Guo, Michael Bolte and Matthias Wagner,

Dalton Trans., **2003**, 2303-2307.

FULL PAPER

Dalton
www.rsc.org/dalton

Cymantrene-based tris(1-pyrazolyl)borates: synthesis and structural characterization of di- and trimetallic complexes

Alireza Haghiri Ilkhechi,[a] ShengLi Guo,[a] Michael Bolte[b] and Matthias Wagner *[a]

[a] *Institut für Anorganische Chemie, J. W. Goethe-Universität Frankfurt, Marie-Curie-Str. 11, D-60439 Frankfurt (Main), Germany. E-mail: Matthias.Wagner@chemie.uni-frankfurt.de*

[b] *Institut für Organische Chemie, J. W. Goethe-Universität Frankfurt, Marie-Curie-Strasse 11, D-60439 Frankfurt (Main), Germany*

Received 16th December 2002, Accepted 3rd April 2003
First published as an Advance Article on the web 29th April 2003

The di- and trinuclear complexes $Mn(CO)_3[CymB(pz)_3]$ **6**, $Mn(CO)_3[CymB(pz)_2(OH)]$ **7** and $Zn[CymB(pz)_3]_2$ **8** have been synthesized and structurally characterized by X-ray crystallography (Cym = cymantrenyl, pz = pyrazolyl). **6** and **8** are easily accessible from the corresponding Tl^I salt $Tl[CymB(pz)_3]$ **2** and $Mn(CO)_5Br$ or $ZnBr_2$, respectively. IR spectroscopy and X-ray crystallography on **6**, which features a cyclopentadienyl ring together with a scorpionate moiety in the same molecule, indicate both ligand types to exert a very similar electronic influence on the respective $Mn(CO)_3$ fragment. The heteroscorpionate complex **7** is obtained when the reaction of $Tl[CymB(pz)_3]$ **2** and $Mn(CO)_5Br$ is performed without exclusion of air and moisture. Complex **6** undergoes photolysis (with UV light, $\lambda = 254$ nm) leading to the liberation of carbon monoxide and the formation of larger aggregates of unknown molecular structure.

Introduction

Tris(1-pyrazolyl)borates ("scorpionates") **1**[1,2] (Fig. 1) have established themselves as a most important class of ligands in coordination chemistry, since they can readily be modified sterically and electronically through appropriate substitution both on the pyrazole rings (R^1–R^3) and on the boron centre (R). The denticity of scorpionate ligands ranges between one and three, and the bite angle is adjustable to the specific requirements of the coordinated metal complex fragment. Nowadays, scorpionates find applications in various fields such as analytical chemistry, homogeneous catalysis and materials science.[3]

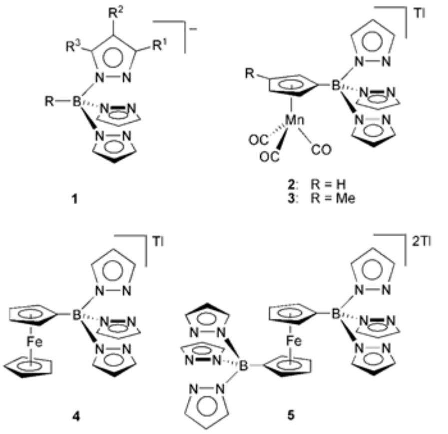

Fig. 1 Tris(1-pyrazolyl)borate **1** (substituents R^1–R^3 on two of the three pyrazolyl rings are omitted for clarity) and its cymantrene- (**2**, **3**) and ferrocene-based derivatives (**4**, **5**).

In order to supply versatile building blocks for the generation of oligonuclear transition metal complexes, our group has recently prepared the cymantrenyl tris(1-pyrazolyl)borates **2** and **3**,[4] as well as the corresponding mono- (**4**) and difunctional (**5**) ferrocene-based derivatives (Fig. 1).[5–8]

Results and discussion

Synthesis and spectroscopy

The dinuclear manganese complex **6** is accessible in high yield from the reaction of $Mn(CO)_5Br$ with the Tl^I scorpionate **2** in dry THF at ambient temperature under an argon atmosphere (Scheme 1). X-Ray quality crystals of **6** were grown from $CDCl_3$ in an NMR tube upon slow evaporation of the solvent. After the reaction had been performed without rigorous exclusion of air and moisture, the heteroscorpionate complex **7** was

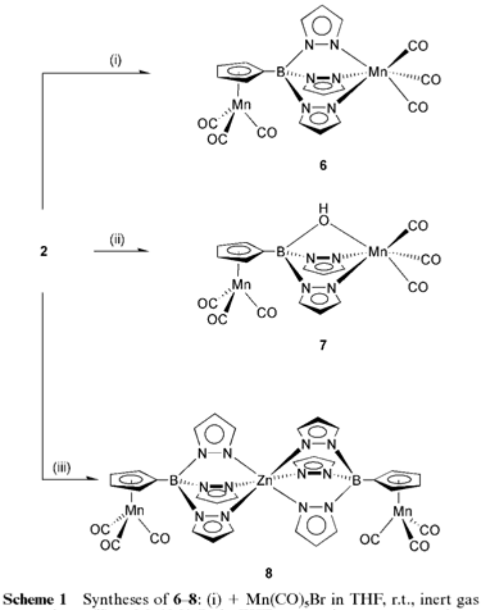

Scheme 1 Syntheses of **6**–**8**: (i) + $Mn(CO)_5Br$ in THF, r.t., inert gas atmosphere; (ii) + $Mn(CO)_5Br$ in THF, r.t., no inert gas atmosphere; (iii) + 0.5 equiv. $ZnBr_2$ in THF, r.t., inert gas atmosphere.

DOI: 10.1039/b212356h

obtained in 32% yield. The compound crystallized from $CHCl_3$ together with one equiv. of pyrazole (**7**·pzH). Since THF solutions of **6** were found to be stable towards air and moisture, **7** is probably formed at an earlier stage *via* the hydrolysis of a reaction intermediate in which a $Mn(CO)_5$ [$Mn(CO)_4$] fragment is coordinated to only one [two] pyrazolyl ring[s] of the cymantrenyl scorpionate ligand. The heterotrimetallic compound **8** can be synthesized from two equiv. of **2** and one equiv. of $ZnBr_2$ in THF in a very clean reaction.

The carbonyl ligands of parent cymantrene give rise to two bands in the infrared spectrum [A_1, E; ν(CO) = 2035, 1949 cm^{-1}],[9] thereby indicating the $Mn(CO)_3$ fragment to possess local C_{3v} symmetry. Three rather than two bands appear in the IR spectrum of the cymantrenyl scorpionate complex **2** bearing a sterically demanding [Bpz_3Tl] substituent on its cyclopentadienyl ring [**2**: ν(CO) = 2019, 1944, 1922 cm^{-1} (in TlBr)].[4] There is a pronounced red-shift of these frequencies compared to the bands recorded for cymantrene [see above; *cf.* methylcymantrene:[9] ν(CO) = 2030, 1942 cm^{-1}; **3**:[4] ν(CO) = 2003, 1933, 1917 cm^{-1} (in TlBr)]. The $Mn(CO)_3$ complex **6** exhibits carbonyl bands at ν(CO) = 2030, 2023, 1933 (two shoulders at ca. 1945 and 1925) and 1908 cm^{-1} (in KBr). We tentatively assign the signal at ν(CO) = 2030 cm^{-1} to the $Mn(CO)_3$ fragment coordinated by the scorpionate ligand while the band at ν(CO) = 2023 cm^{-1} is likely due to the cymantrenyl substituent of **6** {*cf.* $Mn(CO)_3[HB(pz)_3]$:[10] ν(CO) = 2041, 1941 cm^{-1}}. There is obviously only little difference between the CO stretching frequencies of the two manganese tricarbonyl units, which leads to the conclusion that the charge density on both manganese centres is rather similar. Broad and poorly resolved signals are obtained for the heteroscorpionate complex **7** [ν(CO) = 2014, 1931 (shoulder at *ca.* 1905 cm^{-1}) while the expected set of three bands is observed in the case of the trinuclear Mn_2Zn aggregate **8** [ν(CO) = 2021, 1944 (shoulder at 1934), 1918 cm^{-1}].

The ^{11}B NMR signals of **6**, **7** and **8** occur in a range typical of tetra-coordinated boron nuclei[11] [$\delta(^{11}B, CDCl_3)$ = −2.2 (**6**), 0.7 (**7**) and −1.6 (**8**)]. In the ^1H NMR spectra of **6** and **8**, two resonances are found for the magnetically non-equivalent α and β protons of the cyclopentadienyl ring(s) while the C_5H_4 protons of **7** give rise to only one resonance possessing an intermediate shift value [*cf.* **6**: $\delta(^1H, CDCl_3)$ = 4.87, 5.13; **7**: $\delta(^1H, CDCl_3)$ = 4.95]. In all three molecules, the pyrazolyl rings give rise to the expected set of three resonances which appear in the usually observed spectral regions. The corresponding integral values are consistent with the assumption that **6** and **8** are cymantrenyl-substituted tris(1-pyrazolyl)borates, whereas **7** clearly contains only two pyrazolyl rings per molecule. A common feature of carbon atoms attached to a boron centre is an extreme broadening of their ^{13}C NMR signals, which has to be attributed to the quadrupolar relaxation of the boron nucleus.[11] Consequently, only two rather than three ^{13}C NMR resonances have been found for the cyclopentadienyl rings of **6**, **7** and **8**. Signals assignable to carbonyl ligands were also not detected in the ^{13}C NMR spectra of these molecules. The same is true for the Tl(I) salts **2** and **3**,[4] and even in the case of parent cymantrene ^{13}C(CO) resonances are not readily observed. However, IR spectroscopy (see above) as well as X-ray crystal structure analyses of **6**, **7** and **8** (see below) undoubtedly reveal the presence of three CO ligands on each of the manganese atoms. Only three ^{13}C NMR signals are visible for the pyrazolylborate groups of **6**, **7** and **8**, suggesting that the pyrazolyl rings are magnetically equivalent in these compounds, which is consistent with the proposed molecular structures (Scheme 1).

Crystal structure determination

The dinuclear manganese complex **6** crystallizes from $CDCl_3$ in the monoclinic space group $P2_1$ with two crystallographically independent molecules (**6a**, **b**) in the asymmetric unit (Table 1, Fig. 2). Since there are no significant differences between corresponding bond lengths, angles and torsion angles of the two molecules, only **6a** will be discussed in detail here (Table 2). Contrary to the related Tl^I salt **2**, which forms polymeric chains with bridging tris(1-pyrazolyl)borate ligands in the solid state, the scorpionate fragment of **6a** binds to the Mn(2) atom in an η^3 fashion. One of the three pyrazolyl rings is placed in a position almost orthogonal to the cyclopentadienyl moiety [dihedral angle: 94.8°]. The carbonyl ligand C(3)O(3) is pointing into the empty space between the two other pyrazolyl groups. The Mn–C as well as the C–O bond lengths of the two $Mn(CO)_3$ fragments are identical within experimental error (Table 2). This indicates a similar degree of Mn–CO back bonding in both cases as has already been deduced from the IR spectra of **6**. The manganese centre Mn(2) is surrounded by three nitrogen atoms and three carbon atoms in an almost perfect octahedral geometry [deviations from the ideal ligand–Mn(2)–ligand angles of 180 and 90° are smaller than 5°]. The same is true for the pseudo-octahedral coordination sphere of Mn(1) [angles OC–Mn(1)–CO 90.1(2), 91.2(3) and 91.5(3)°]. Compound **6a** contains a tetra-coordinated boron atom, which is in accord with the results obtained by ^{11}B NMR spectroscopy. Most likely due to steric repulsion, the angles C(11)–B(1)–N(31) and C(11)–B(1)–N(41) possess values of 115.2(4) and 114.7(4)°, respectively, and are thus significantly larger than to be expected for a tetrahedral geometry.

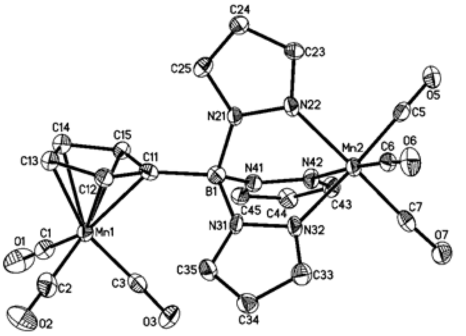

Fig. 2 Structure plot of **6a** in the solid state. Displacement ellipsoids are drawn at the 50% probability level.

Compound **7**·pzH crystallizes from $CHCl_3$ in the monoclinic space group *C2/c* (Table 1). The molecule has to be addressed as a *hetero*scorpionate complex in which the Mn(2) centre is coordinated by two pyrazolyl rings and one hydroxy substituent. In the solid state, each molecule of **7** is linked to a second molecule of **7** *via* two bridging pyrazole heterocycles and by four N–H–O hydrogen bonds. Two different structural types of these dimeric aggregates are observed. One, which is depicted in Fig. 3, possesses an inversion centre while the building blocks of the other dimer are not symmetry related. This results in an overall number of three crystallographically independent molecules **7a**·pzH, **7b**·pzH and **7c**·pzH in the asymmetric unit. A schematic sketch of the arrangement of these molecules in the crystal lattice is given in Fig. 4. **7a**·pzH, **7b**·pzH and **7c**·pzH exhibit very similar structural parameters. Any further structure description will therefore be restricted to molecule **7c**·pzH (Table 2, Fig. 3). The molecular structure of **7c**·pzH closely resembles that of **6a** apart from the fact that a hydroxy group is substituted for the pyrazolyl ring N(21)N(22)C(23)C(24)C(25). Again, the octahedral coordination sphere around Mn(2) is largely unperturbed, except of the bond angle O(8)–Mn(2)–C(7) which is reduced to a value of 168.0(2). There are no significant differences between the structural features of the C(7)O(7) ligand located in a position *trans* to the hydroxy donor [Mn(2)–C(7) 1.787(5) Å, C(7)–O(7) 1.155(5) Å] and the other two carbonyl groups that coordinate *trans* to a pyrazolyl

Table 1 Crystallographic data for **6**,**7**·pzH and **8**

Compound	**6**	**7**·pzH	**8**
Formula	$C_{20}H_{13}BMn_2N_6O_6$	$C_{20}H_{15}BMn_2N_6O_7$	$C_{34}H_{26}B_2Mn_2N_{12}O_6Zn$
M	554.05	572.07	895.54
Crystal system	Monoclinic	Monoclinic	Triclinic
Space group	$P2_1$	$C2/c$	$P\bar{1}$
a/Å	9.3830(9)	56.691(4)	8.5125(6)
b/Å	22.907(2)	13.2772(6)	8.6745(6)
c/Å	10.5301(9)	19.5660(10)	12.3157(9)
α/°	90	90	98.556(6)
β/°	105.298(7)	103.776(5)	96.647(6)
γ/°	90	90	92.171(6)
V/Å^3	2183.1(3)	14303.6(14)	891.84(11)
Z	4	24	1
D_c/g cm^{-3}	1.686	1.594	1.667
F(000)	1112	6912	452
μ(Mo-Kα)/cm^{-1}	0.1209	0.1113	0.1430
$2\theta_{max}$/°	51.06	52.48	64.32
Measured reflections	22577	74118	35033
Unique reflections (R_{int})	7920 (0.0651)	14138 (0.1263)	6175 (0.0597)
Observed reflections [$I > 2\sigma(I)$]	6496	7786	5233
Parameters refined	631	997	259
*R*1 [I>2σ(I)]	0.0415	0.0462	0.0498
*wR*2 [I>2σ(I)]	0.0794	0.0650	0.1551
GOOF on F^2	0.939	0.817	1.068
Largest diff. peak and hole/e$^-$ Å^{-3}	0.605, −0.519	0.473, −0.359	0.563, −1.965

Table 2 Selected bond lengths (Å), angles (°) and torsion angles (°) of **6a**, **7c**·pzH and **8**; *x*: in the case of **7c**·pzH

Compound	**6a**	**7c**·pzH	**8**
Mn(1)–C(1)	1.796(6)	1.772(4)	1.800(2)
Mn(1)–C(2)	1.801(6)	1.804(5)	1.802(2)
Mn(1)–C(3)	1.788(6)	1.796(5)	1.805(2)
Mn(2)–C(5)	1.819(6)	1.816(5)	–
Mn(2)–C(6)	1.790(6)	1.810(5)	–
Mn(2)–C(7)	1.809(5)	1.787(5)	–
C(1)–O(1)	1.165(7)	1.175(4)	1.147(3)
C(2)–O(2)	1.153(7)	1.148(5)	1.148(3)
C(3)–O(3)	1.155(6)	1.154(5)	1.153(3)
C(5)–O(5)	1.140(7)	1.146(5)	–
C(6)–O(6)	1.171(6)	1.161(5)	–
C(7)–O(7)	1.160(6)	1.155(5)	–
B(1)–C(11)	1.602(7)	1.594(6)	1.605(3)
B(1)–N(21)[O(8)^x]	1.548(6)	1.496(5)	1.567(3)
B(1)–N(31)	1.559(7)	1.557(6)	1.557(3)
B(1)–N(41)	1.559(7)	1.542(5)	1.567(3)
Mn(2)–N(22)[O(8)^x]	2.035(4)	2.090(3)	–
Mn(2)–N(32)	2.046(5)	2.047(3)	–
Mn(2)–N(42)	2.058(4)	2.055(3)	–
Zn(1)–N(22)	–	–	1.995(2)
Zn(1)–N(32)	–	–	2.002(2)
Zn(1)–N(42)	–	–	1.988(2)
C(11)–B(1)–N(21)[O(8)^x]	107.0(4)	112.2(4)	107.1(2)
C(11)–B(1)–N(31)	115.2(4)	114.4(3)	115.4(2)
C(11)–B(1)–N(41)	114.7(4)	115.4(3)	114.0(2)
N(31)–B(1)–N(21)[O(8)^x]	107.5(4)	103.9(3)	106.6(1)
N(41)–B(1)–N(21)[O(8)^x]	106.5(4)	102.0(3)	106.6(2)
N(41)–B(1)–N(31)	105.5(4)	107.7(4)	106.5(2)
C(12)–C(11)–B(1)–N(21)[O(8)^x]	77.3(6)	−79.7(5)	89.9(2)
C(12)–C(11)–B(1)–N(31)	−42.1(6)	38.3(6)	−28.7(3)
C(12)–C(11)–B(1)–N(41)	−164.9(4)	164.1(4)	−152.4(2)
C(11)–B(1)–N(21)–N(22)	−177.3(4)	–	175.3(2)
C(11)–B(1)–N(31)–N(32)	175.1(4)	162.6(3)	168.3(2)
C(11)–B(1)–N(41)–N(42)	−171.3(4)	−161.8(4)	−176.3(2)

ring [Mn(2)–C(5) 1.816(5) Å, C(5)–O(5) 1.146(5) Å; Mn(2)–C(6) 1.810(5) Å, C(6)–O(6) 1.161(5) Å]. As already observed for **6a**, the bond angles C(11)–B(1)–N(31) and C(11)–B(1)–N(41) of **7c**·pzH are stretched to values of 114.4(3) and 115.4(3)°, respectively. The C(11)–B(1)–O(8) angle is also quite large [112.2(4)°], which is clearly due to the fact that the small μ-hydroxy bridge has to span the same distance between B(1) and Mn(2) as the much bigger μ-pyrazolyl ligands. The conformation of the heteroscorpionate fragment in **7c**·pzH and the tris(1-pyrazolyl)borate ligand in **6a** relative to their adjacent cymantrenyl units is very similar [torsion angles: C(12)–C(11)–B(1)–O(8) −79.7(5)° (**7c**·pzH); C(12)–C(11)–B(1)–N(21) 77.3(6)° (**6a**)].

The heterotrinuclear complex **8** crystallizes from C_6D_6 in the triclinic space group $P\bar{1}$ (Table 1, Fig. 5). The Zn^{II} ion is located at a crystallographic inversion centre and coordinated by the six nitrogen atoms of two cymantrenyl scorpionate ligands [Zn(1)–N(22) 1.995(2) Å, Zn(1)–N(32) 2.002(2) Å, Zn(1)–N(42)

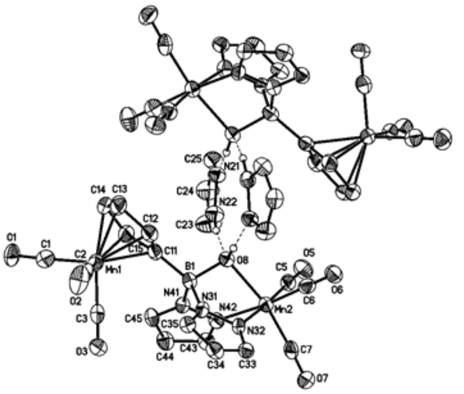

Fig. 3 Structure plot of **7c**·pzH in the solid state. Displacement ellipsoids are drawn at the 50% probability level.

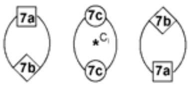

Fig. 4 Crystal packing scheme of **7**·pzH. **7a**–**c**: Three crystallographically independent molecules in the asymmetric unit; C_i : inversion centre.

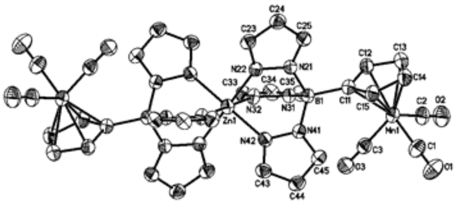

Fig. 5 Structure plot of **8** in the solid state. Displacement ellipsoids are drawn at the 50% probability level.

1.988(2) Å; average value 1.996 Å; Table 2]. There is only negligible deviation from an ideal octahedral coordination sphere around the zinc atom. The conformation of the cymantrenyl scorpionate moiety in **8** is similar to that observed in the case of **6a** [*cf.* torsion angles: C(12)–C(11)–B(1)–N(21) 89.9(2)° (**8**), 77.3(6)° (**6a**)], and the overall molecular structure of **8** closely resembles that of the related Cu^{II} complex Cu[FcB(pz*)$_3$]$_2$ [Fc = ferrocenyl; pz* = (cyclohexylmethyl)pyrazolyl].[8]

Reactivity of 6. A solution of **6** in CHCl$_3$, which was exposed to air over a period of several days, did not show signs of hydrolysis or oxidative decomposition (IR and NMR spectroscopic monitoring). Upon irradiation of a CD$_3$CN solution of **6** with UV light (λ = 254 nm) in an NMR tube, a pale yellow microcrystalline precipitate formed. The ^{1}H and ^{13}C NMR spectra of the supernatant did not give any signals except those of the solvent molecules. The precipitate proved to be insoluble in all common organic solvents. Its IR spectrum in KBr revealed absorption bands at ν(CO) = 2019, 1933 (very broad) and 1862 cm^{-1} [*cf.* **6**: ν(CO) = 2030, 2023, 1933 (two shoulders at *ca.* 1945 and 1925), 1908 cm^{-1}; in KBr]. The complex (MeC$_5$H$_4$)Mn(CO)$_2$CH$_3$CN exhibits a signal at ν(CO) = 1886 cm^{-1} in the IR spectrum.[12] Thus, the infrared data obtained for the precipitate indicate the presence of Mn(CO)$_2$Do fragments in the photolysis product(s) of **6** (Do: CD$_3$CN or another σ-donor, most likely pyrazole). When the experiment was repeated in the presence of 1 equiv. of PPh$_3$, qualitatively similar results were obtained [absorption bands of the precipitate in KBr: ν(CO) = 2019, 1948, 1927, 1913, 1856 cm^{-1}; *cf.* (C$_5$H$_5$)Mn(CO)$_2$PPh$_3$:[13] ν(CO) = 1931, 1864 cm^{-1}, in CH$_2$Cl$_2$].

MALDI mass spectra of **6** gave peaks at m/z = 488 [M$^+$ − 3 CO + H$_2$O], 771, 1056, 1338, 1625 and 1910 (6-aza-2-thiothymine matrix). A peak assignable to [M$^+$] (m/z = 554) was not observed. The signal intensities decrease continuously with increasing ion masses. It is interesting to note that the differences between the m/z values of adjacent peaks are 283, 285, 282, 287 and 285, thereby indicating that the heavier ions may be generated by the consecutive addition of always the same molecular fragment. Since complex **6** possesses a strong absorption band in the UV/vis spectrum at the wavelength of the laser beam (λ = 337 nm), the experiment was repeated with neat **6** which was not embedded into a polymer matrix. In this spectrum, the peaks at m/z = 488, 771 and 1056 occurred again. Given the fact that (i) **6** contains six carbonyl ligands at two different sites in the molecule, (ii) the molecular mass of a pyrazolyl ring [m/z (C$_3$H$_3$N$_2$) = 67] is similar to that of the cyclopentadienyl group [m/z (C$_5$H$_4$) = 64] and (iii) water molecules may become attached to the ions in the course of the measurement, an unambiguous assignment of the peaks was found to be rather difficult. It is, however, obvious that **6** has a pronounced tendency to form larger aggregates, as has already been observed in the case of the Tl^I complexes **2** and **3**.[4]

To get more insight into the thermal stability of **6**, differential thermal scans (DSC)[14] and thermogravimetric measurements (TG)[15] were performed [heating rate: 10 K min^{-1}; inert gas flow: Ar]. The compound loses about 45% of its original weight in the temperature range between 165 °C and 400 °C. Four well-resolved steps are clearly visible which correspond to weight losses of 8.5% (T = 165–190 °C), 8.5% (T = 205–245 °C), 12% (T = 285–320 °C) and 16% (T = 340–400 °C). Since liberation of two CO ligands from **6** leads to a mass reduction of 10%, the first three steps in the TG curve are likely due to the consecutive loss of all six carbonyl groups. This interpretation is further supported by the fact that no carbonyl bands appear in the infrared spectrum of the material obtained from the crucible after the DTA–TG measurements. It is interesting to note in this context that the endothermic peak in the DTA curve, which is associated with the loss of the first two CO ligands, is significantly smaller than in the case of the other two CO liberation steps.

Conclusion

The di- and trinuclear complexes Mn(CO)$_3$[CymB(pz)$_3$] **6**, Mn(CO)$_3$[CymB(pz)$_2$(OH)] **7** and Zn[CymB(pz)$_3$]$_2$ **8** have been synthesized and structurally characterized by X-ray crystallography (Cym = cymantrenyl, pz = pyrazolyl). **7** represents a rare example of a heteroscorpionate ligand featuring a hydroxy donor functionality. In contrast to the corresponding cymantrene-based Tl^I scorpionates **2** and **3**, which form polymeric chains and cyclic tetramers with bridging tris(1-pyrazolyl)borate moieties in the solid state, a tridentate coordination mode is preferred by the scorpionate ligands in **6**–**8**. The compounds are stable towards air and moisture. Irradiation of **6** with UV light in the presence of acetonitrile or PPh$_3$ leads to substitution reactions within the carbonyl ligand spheres. We have not been able to identify the molecular structure and precise chemical composition of the reaction product(s) but rather obtained microcrystalline precipitates which proved to be insoluble in all common organic solvents. MALDI mass spectrometry indicates the removal of carbonyl ligands from **6** to be accompanied by the formation of larger aggregates.

Experimental

General considerations

All reactions and manipulations of air-sensitive compounds were carried out in dry, oxygen-free argon using standard

Schlenk ware unless mentioned otherwise. Solvents were freshly distilled under argon from Na/benzophenone (THF, hexane, C_6D_6) or passed through a 4 Å molecular sieves column ($CHCl_3$, $CDCl_3$) prior to use. IR: Nicolet MAGNA-IR 550. Abbreviations: w = weak, m = medium, s = strong, sh = shoulder. NMR: Bruker AMX 250, AMX 400, Bruker DPX 250. ^{11}B NMR spectra were reported relative to external $BF_3 \cdot Et_2O$. Abbreviations: d = doublet; n.r. = multiplet expected in the ^1H NMR spectrum but not resolved; n.o. = signal not observed; Cym = cymantrenyl; pz = pyrazolyl. MS: Fisons, VG Tofspec. Elemental analyses were performed by the microanalytical laboratory of the University of Frankfurt.

Tl[CymB(pz)$_3$] **2** has been synthesized according to a literature procedure.[4]

Syntheses

Synthesis of 6. A mixture of Tl[CymB(pz)$_3$] **2** (0.61 g, 0.99 mmol) and $Mn(CO)_5Br$ (0.27 g, 0.99 mmol) in dry THF (40 ml) was stirred at room temperature for 24 h, whereupon a colourless precipitate formed (TlBr). The insoluble material was collected on a frit and the yellow filtrate evaporated to dryness *in vacuo*. The resulting yellow residue was triturated with hexane (10 ml) and dried *in vacuo* again. Yield: 0.44 g (80%). X-Ray quality crystals of **2** were obtained from $CDCl_3$ at ambient temperature.

IR ($CDCl_3$, cm^{-1}): ν(CO) 2036 (w), 2023 (s), 1942 (s; sh at *ca*. 1935); IR (KBr, cm^{-1}): ν(CO) 2030 (m), 2023 (s), 1933 (s; with two sh at *ca*. 1945 and 1925), 1908 (w). ^{11}B NMR ($CDCl_3$, 128.3 MHz): δ −2.2 ($w_{1/2}$ = 90 Hz). ^1H NMR ($CDCl_3$, 250.1 MHz): δ 4.87, 5.13 (2 × n.r., 2 × 2H, C_5H_4), 6.24 (n.r., 3H, pz-H4), 7.65, 7.89 (2 × n.r., 2 × 3H, pz-H3,5). ^{13}C NMR ($CDCl_3$, 62.9 MHz): δ 86.4, 86.7 (C_5H_4), n.o. (Cp–*C*B), 105.9 (pz-C4), 135.0, 144.9 (pz-C3,5), n.o. (CO). Calc. for $C_{20}H_{13}BMn_2N_6O_6$ (554.05): C, 43.36; H, 2.37; N, 15.17. Found: C, 43.01; H, 2.22; N, 14.95%.

Synthesis of 7. Complex **7** was prepared similarly to **6**, but without exclusion of air and moisture. Tl[CymB(pz)$_3$] **2** (0.31 g, 0.50 mmol), $Mn(CO)_5Br$ (0.14 g, 0.51 mmol), THF (20 ml). Yield: 0.09 g (32%). Yellow X-ray quality crystals of **7**·pzH were obtained from $CHCl_3$ at ambient temperature.

IR (KBr, cm^{-1}): ν(CO) 2014 (s), 1931 (s; sh at *ca*. 1905). ^{11}B NMR ($CDCl_3$, 128.3 MHz): δ 0.7 ($w_{1/2}$ = 100 Hz). ^1H NMR ($CDCl_3$, 250.1 MHz): δ 4.95 (n.r., 4H, C_5H_4), 6.26 (n.r., 2H, pz-H4), 7.57, 7.85 (2 × d, 2 × 2H, J_{HH} = 2.2 Hz, pz-H3,5). ^{13}C NMR ($CDCl_3$, 62.9 MHz): δ 84.8, 87.0 (C_5H_4), n.o. (Cp–*C*B), 106.7 (pz-C4), 132.3, 142.8 (pz-C3,5), n.o. (CO). Calc. for $C_{17}H_{11}BMn_2N_4O_7$ (503.99)·$C_3H_4N_2$ (68.08): C, 41.99; H, 2.64; N, 14.69. Found: C, 41.55; H, 2.60; N, 14.43%.

Synthesis of 8. A mixture of Tl[CymB(pz)$_3$] **2** (0.090 g, 0.145 mmol) and $ZnBr_2$ (0.016 g, 0.071 mmol) in dry THF (20 ml) was stirred at room temperature for 30 h, whereupon a colourless precipitate formed (TlBr). The insoluble material was collected on a frit and the yellow filtrate evaporated to dryness *in vacuo*. The yellow residue was triturated with hexane (2 × 15 ml) and dried *in vacuo* again. Yield: 0.054 g (85%). X-Ray quality crystals of **8** were grown by slow evaporation of its solution in C_6D_6 at ambient temperature.

IR ($CDCl_3$, cm^{-1}): ν(CO): 2021 (s), 1944 (s, sh at *ca*. 1934), 1918 (s). ^{11}B NMR ($CDCl_3$, 128.3 MHz): δ −1.6 ($w_{1/2}$ = 200 Hz). ^1H NMR ($CDCl_3$, 400.1 MHz): δ 5.07, 5.18 (2 × n.r., 2 × 4H, C_5H_4), 6.09 (n.r., 6H, pz-H4), 7.14, 7.75 (2 × n.r., 2 × 6H, pz-H3,5). ^{13}C NMR ($CDCl_3$, 100.6 MHz): δ 86.1, 87.7 (C_5H_4), n.o. (Cp–*C*B), 103.6 (pz-C4), 133.9, 139.7 (pz-C3,5), n.o. (CO). CI-MS: *m/z* 895 [M^+]. Calc. for $C_{34}H_{26}B_2Mn_2N_{12}O_6Zn$ (895.54): C, 45.60; H, 2.93; N, 18.77. Found: C, 45.28; H, 2.74; N, 18.59%.

Crystal structure determinations of 6, 7 and 8. Crystal data and details of the structure determinations are summarised in Table 1. Plots of the molecular structures of **6a**,**7c**·pzH and **8** are shown in Figs. 2, 3 and 5. The measurements were performed at 100 K using a STOE-IPDS-II two-circle diffractometer with graphite-monochromated Mo-Kα radiation (λ = 0.71073 Å). Empirical absorption corrections were made.[16,17] The structures were determined by direct methods using the programs SHELXS and SHELXL.[18,19] Hydrogen atoms bonded to C were placed at calculated positions and were not refined. Hydrogen atoms bonded to O and N were refined isotropically.

CCDC reference numbers 196636 (**6**), 196635 (**7c**·pzH) and 196637 (**8**).

See http://www.rsc.org/suppdata/dt/b2/b212356h/ for crystallographic data in CIF or other electronic format.

Acknowledgements

The authors wish to thank Fariba Maysamy Tmar for the thermoanalytical measurements and Dr. Lothar Fink for helpful discussions. This research was generously supported by the Deutsche Forschungsgemeinschaft (DFG).

References

1 S. Trofimenko, *Chem. Rev.*, 1993, **93**, 943.
2 S. Trofimenko, *Scorpionates – The Coordination Chemistry of Polypyrazolylborate Ligands*, Imperial College Press, London, 1999.
3 F. T. Edelmann, *Angew. Chem., Int. Ed.*, 2001, **40**, 1656.
4 S. L. Guo, J. W. Bats, M. Bolte and M. Wagner, *J. Chem. Soc., Dalton Trans.*, 2001, 3572.
5 F. Jäkle, K. Polborn and M. Wagner, *Chem. Ber.*, 1996, **129**, 603.
6 F. Fabrizi de Biani, F. Jäkle, M. Spiegler, M. Wagner and P. Zanello, *Inorg. Chem.*, 1997, **36**, 2103.
7 E. Herdtweck, F. Peters, W. Scherer and M. Wagner, *Polyhedron*, 1998, **17**, 1149.
8 S. L. Guo, F. Peters, F. Fabrizi de Biani, J. W. Bats, E. Herdtweck, P. Zanello and M. Wagner, *Inorg. Chem.*, 2001, **40**, 4928.
9 T. Renk, W. Ruf and W. Siebert, *J. Organomet. Chem.*, 1976, **120**, 1.
10 S. Trofimenko, *J. Am. Chem. Soc.*, 1969, **91**, 588.
11 H. Nöth and B. Wrackmeyer, *Nuclear Magnetic Resonance Spectroscopy of Boron Compounds*, in *NMR Basic Principles and Progress*, ed. P. Diehl, E. Fluck and R. Kosfeld, Springer, Berlin, 1978.
12 J. W. Hershberger, R. J. Klingler and J. K. Kochi, *J. Am. Chem. Soc.*, 1983, **105**, 61.
13 C. G. Atwood, W. E. Geiger and T. E. Bitterwolf, *J. of Electroanal. Chem.*, 1995, **397**, 279.
14 P. J. Haines, *Thermal Methods of Analysis: Principles, Applications, and Problems*, Kluwer Academic Publishers, Dordrecht, 1994.
15 H.-G. Wiedemann and G. Bayer, *Top. Curr. Chem.*, 1978, **77**, 67.
16 R. Blessing, *Acta Crystallogr., Sect. A.*, 1995, **51**, 33.
17 A. L. Spek, *Acta Crystallogr., Sect. A.*, 1990, **46**, C34.
18 G. M. Sheldrick, *Acta Crystallogr., Sect. A.*, 1990, **46**, 467.
19 G. M. Sheldrick, SHELXL-97. A Program for the Refinement of Crystal Structures, Universität Göttingen, 1997.

6.2 „On the way to ferrocene-based multiple-decker sandwich complexes“

Alireza Haghiri Ilkhechi, Matthias Scheibitz, Michael Bolte, Hans-Wolfram Lerner, Matthias Wagner,

Polyhedron., **2004**, 23, 2597-2604.

ELSEVIER

Available online at www.sciencedirect.com
SCIENCE DIRECT

Polyhedron 23 (2004) 2597–2604

POLYHEDRON
www.elsevier.com/locate/poly

On the way to ferrocene-based multiple-decker sandwich complexes ☆

Alireza Haghiri Ilkhechi, Matthias Scheibitz, Michael Bolte, Hans-Wolfram Lerner, Matthias Wagner *

Institut für Anorganische Chemie, J.W. Goethe-Universität Frankfurt, Marie-Curie-Strasse 11, D-60439 Frankfurt (Main), Germany

Received 11 February 2004; accepted 19 May 2004
Available online 15 July 2004

Dedicated to Professor Malcolm L.H. Green on the occasion of his retirement

---

Abstract

Three ferrocene derivatives, Li[FcBH$_3$], Li$_2$[1,1′-fc(BMe$_3$)$_2$] and Li$_2$[1,1′-fc(BMe$_2$pz)$_2$] [Fc = (C$_5$H$_5$)Fe(C$_5$H$_4$), fc = (C$_5$H$_4$)$_2$Fe, pz = pyrazolyl], have been synthesized and structurally characterized to investigate the interaction of the negatively charged sandwich complex with its Li$^+$ counterion(s) in the solid state. Single crystals of Li[FcBH$_3$] · (12-crown-4), obtained from a THF solution after addition of 12-crown-4, contain hexacoordinated Li$^+$ ions, which are bonded to one molecule of crown ether and to two hydrogen atoms of the BH$_3$ fragment. The compound Li$_2$[1,1′-fc(BMe$_3$)$_2$] crystallized from THF as solvent-separated ion pairs with each Li$^+$ being encapsulated by four THF molecules. Single crystals of Li$_2$[1,1′-fc(BMe$_2$pz)$_2$] were grown from diethyl ether. In this compound, the lithium ions are coordinated by two solvent molecules, the pyrazolyl side-arm and the cyclopentadienyl ring. Thus, Li$_2$[1,1′-fc(BMe$_2$pz)$_2$] can be regarded as a trinuclear segment of the polymeric structure [–(C$_5$H$_4$R)Li(C$_5$H$_4$R)Fe–]$_\infty$ with R = BMe$_2$pz.

Keywords: Multiple-decker sandwich complex; Ferrocene; Boron; Lithium; Crystal structure

---

1. Introduction

For more than 30 years, multiple-decker sandwich complexes have been in the focus of attention due to their promising potential as building blocks for nanoscale applications (e.g., one-dimensional wires and spin-chains) [1]. A most remarkable representative of this class of compounds was reported in 1985 by Siebert [2,3], who succeeded in the synthesis of extended columnar structures from Ni ions and η^5,μ-2,3-dihydro-1,3-diborolyl ligands. Later, this one-dimensional system was shown to possess semiconducting properties in the solid state [4–6]. For practical reasons, it would, however, be desirable to substitute simple cyclopentadienyl ligands for the sophisticated boron heterocycle. Numerous triple-decker sandwich complexes of the permethylated cyclopentadienyl derivative [C$_5$Me$_5$]$^-$ have already been isolated and structurally characterized [1]. In contrast, the number of known examples featuring exclusively the unsubstituted [C$_5$H$_5$]$^-$ ligand is still rather small (e.g., [Ni$_2$(C$_5$H$_5$)$_3$]$^+$ [7,8], [Tl$_2$(C$_5$H$_5$)$_3$]$^-$ [9]). Even though Schildcrout [10] reported as early as 1973 the detection of [Fe$_2$(C$_5$H$_5$)$_3$]$^+$ in the high-pressure electron-impact mass spectrum of ferrocene, this compound has not been isolated yet. However, clusters of the general formula V$_n$[Fe(C$_5$H$_5$)$_2$]$_{n+1}$ (n = 1–3) have recently been generated by two-laser vaporization of vanadium and ferrocene targets. Time-of-flight mass spectra measured with and without the addition of NH$_3$ gas indicate that these species possess multiple-decker sandwich structures rather than consisting of a central core of vanadium atoms capped by ferrocene molecules [11].

☆ Supplementary data associated with this article can be found, in the online version, at doi:10.1016/j.poly.2004.05.017.

* Corresponding author. Tel.: +49-69-798-29156; fax: +49-69-798-29260.

E-mail address: Matthias.Wagner@chemie.uni-frankfurt.de (M. Wagner).

0277-5387/$ - see front matter © 2004 Elsevier Ltd. All rights reserved.
doi:10.1016/j.poly.2004.05.017

Our group has published the synthesis and X-ray crystal structure analysis of compound **I** (Fig. 1), in which an array of alternating Ga(I) and Fe(II) ions is connected by η^5,μ-$[C_5H_5]^-$ moieties [12]. According to density functional (DFT) calculations, the binding energy of two ferrocenes to Ga^+ is about 80 kJ mol^{-1} higher than that for the formation of $[Ga(C_6H_6)_2]^+$ from Ga^+ and two benzene molecules. Fragment analysis of $\{[Fe(C_5H_5)_2]_2Ga\}^+$ indicated a transfer of 0.4 electrons into the gallium 4p orbitals compared with a zero occupancy for the isolated ion. More detailed insight into the gas phase basicity of ferrocene toward metal cations is provided by a recent DFT study on the ferrocene–Li^+ complex [13]. Two minima have been located on the energy surface: in the lower energy structure, the lithium cation is coordinated on top of one of the cyclopentadienyl rings (cf. **II**; Fig. 1), whereas the second minimum structure **III**, being 33 kJ mol^{-1} higher in energy, has the Li^+ ion bonded laterally to the iron atom. We found a similar structural motif as predicted for the hypothetical aggregate **III** in the [1.1]diborataferrocenophane **IV**, which crystallizes with one lithium cation inside its molecular cavity [d(Fe···Li): 2.4 Å (**III**); 2.706(5), 2.720(6) Å (**IV**)] [14,15]. ^7Li NMR spectroscopy shows this ferrocenophane–Li^+ complex to be stable in THF solution even in the presence of excess 12-crown-4.

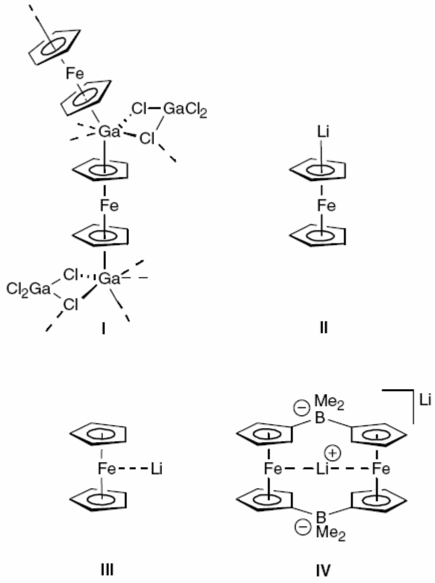

Fig. 1. The Ga^+–ferrocene multiple-decker sandwich complex **I**, the two calculated minimum structures **II** and **III** of the Li^+···ferrocene complex in the gas phase, and the lithium [1.1]diborataferrocenophane **IV**.

The purpose of this paper is to describe the synthesis and structural characterization of type-**II** ferrocene–Li^+ adducts, which appears to be a realistic goal given the fact that the ferrocene–Ga^+ fragments in **I** already resemble the geometry of our target structure. It has, however, to be borne in mind that the synthesis protocol leading to **I** is quite unique in that we are starting from the covalent molecule $GaCl_3$ which is readily soluble in non-coordinating solvents. Consequently, there is no competition between the ferrocene donor and Lewis basic solvent molecules for the Ga(I) ion formed in situ in the course of the reaction. Moreover, in the calculated gas phase structure **II** any possible perturbations of the molecular geometry caused by the presence of solvent molecules are necessarily neglected. For a more general approach to ferrocene–metal multiple-decker sandwich complexes, however, we will have to use transition metal salts as starting materials which usually require strongly coordinating solvents as the reaction media. It therefore seemed reasonable to employ ferrocene derivatives equipped with suitable functional groups able to assist the cyclopentadienyl ring in metal ion binding. Such auxiliary substituents will greatly enhance the stability of the ferrocene–metal aggregate but still allow for those metal···Cp interactions that have been theoretically predicted and experimentally proven to exist in the solid state (cf. the unsupported multiple-decker complex **I**).

2. Results and discussion

To bring about close contacts between a lithium cation and the ferrocene cyclopentadienyl ring, we decided to introduce substituents into the ferrocene core that (i) increase the electron density on the organometallic moiety and (ii) bear a negative charge able to attract Li^+ electrostatically. It is important to know in this context, that the Fe(II)/Fe(III) redox potentials of ferrocenylborane-amine adducts have a pronounced shift to cathodic values with respect to the parent ferrocene [cf. $FcBMe_2$–picoline: $E^{0'} = -0.33$ V, 1,1′-fc(BMe_2–picoline)$_2$: $E^{0'} = -0.56$ V; in CH_2Cl_2 vs. FcH/FcH$^+$, Fc = $(C_5H_5)Fe(C_5H_4)$, fc = $(C_5H_4)_2Fe$] [16,17]. This effect becomes even stronger when the amine base is replaced by a negatively charged organyl group [14,15]. Thus, tetra-coordinated boryl substituents appear to be particularly well-suited to meet the two requirements outlined above. Starting from the well-known ferrocenylboranes FcB(Br)OEt (**1**) [18] and 1,1′-fc$(BMe_2)_2$ (**2**) [19], three derivatives of ferrocenylborates were chosen for our further investigations (Scheme 1): Li[$FcBH_3$] (**3**), Li_2[1,1′-fc$(BMe_3)_2$] (**4**) and Li_2[1,1′-fc$(BMe_2pz)_2$] (**5**; pz = pyrazolyl), in which the aimed-for Li···Cp coordination may be stabilized by a chelating pyrazolyl side-arm.

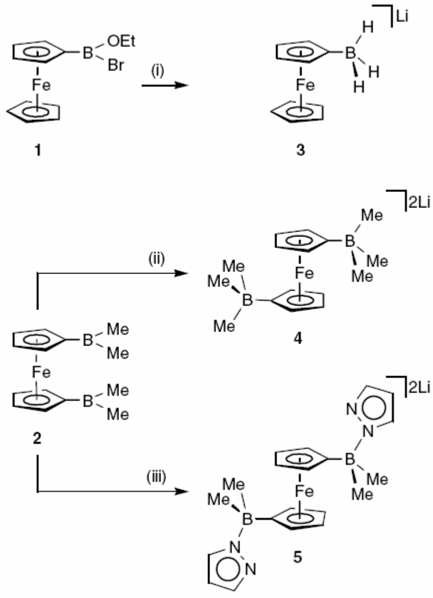

Scheme 1. Syntheses of the lithium ferrocenylborates **3**, **4** and **5**: (i) +Li[AlH$_4$], Et$_2$O/C$_5$H$_{12}$, 0 °C; (ii) +2LiMe, Et$_2$O, −78 °C; (ii) +2Lipz, Et$_2$O, −78 °C.

2.1. Syntheses and NMR spectroscopic characterization

FcB(OEt)Br (**1**) and 1 equiv. of Li[AlH$_4$] in ether/pentane gave lithium ferrocenylborohydride **3** in excellent yield (Scheme 1). Details of the synthesis procedure and NMR data of **3** have been published elsewhere [20]. Single crystals of Li[FcBH$_3$] · (12-crown-4) were grown by gas phase diffusion of diethyl ether onto a THF solution of **3**, to which a small amount of 12-crown-4 had been added. In the absence of the crown ether, no single crystalline material could be obtained. Reaction of 1,1′-fc(BMe$_2$)$_2$ (**2**) with either 2 equiv. of LiMe or 2 equiv. of Lipz in diethyl ether at −78 °C gave Li$_2$[1,1′-fc(BMe$_3$)$_2$] (**4**) and Li$_2$[1,1′-fc(BMe$_2$pz)$_2$] (**5**). The ^{11}B NMR spectra of **4** and **5** show resonances at $\delta = -21.8$ and −9.0, respectively, which agree nicely with those of Li[BMe$_4$] [$\delta(^{11}B) = -20.2$] [21] on one hand and Na[B(NH$_2$)Et$_3$] [$\delta(^{11}B) = -9.8$] [22] on the other. The ^{11}B NMR signal of **4** possesses a narrow linewidth ($h_{1/2}$ = 25 Hz) testifying to a high local symmetry at the boron atom. In contrast, the less symmetrical boron coordination sphere in **5** results in a significantly broader ^{11}B NMR resonance ($h_{1/2}$ = 300 Hz). In the ^{1}H NMR spectrum of **4**, three signals appear at −0.47, 3.55 and 3.75 ppm (integral ratio = 9:2:2), which are assigned to the methyl protons and the two types of magnetically non-equivalent ferrocene hydrogen atoms. In the ^{1}H NMR spectrum of

Table 1
Selected crystallographic data for **3** · (12-crown-4), **4** · (THF)$_8$ and **5** · (Et$_2$O)$_4$

Compound	**3** · (12-crown-4)	**4** · (THF)$_8$	**5** · (Et$_2$O)$_4$
Formula	C$_{18}$H$_{28}$BFeLiO$_4$	C$_{48}$H$_{90}$B$_2$FeLi$_2$O$_8$	C$_{36}$H$_{66}$B$_2$FeLi$_2$N$_4$O$_4$
Molecular weight	382.00	886.55	710.28
Crystal size (mm)	0.46 × 0.35 × 0.19	0.42 × 0.33 × 0.28	0.41 × 0.36 × 0.33
Crystal system	orthorhombic	orthorhombic	triclinic
Space group	*Pnma*	*Pca*2$_1$	$P\bar{1}$
Unit cell dimensions			
a (Å)	20.629(5)	17.4302(16)	10.6219(8)
b (Å)	10.3594(15)	17.5219(13)	13.1216(11)
c (Å)	8.6903(11)	17.2759(14)	15.2509(13)
α (°)	90	90	98.722(7)
β (°)	90	90	97.012(7)
γ (°)	90	90	93.914(6)
V (Å^3)	1857.2(6)	5276.2(8)	2077.1(3)
Z	4	4	2
D_c (g cm^{-3})	1.366	1.116	1.136
T (K)	100(2)	173(2)	173(2)
μ(Mo Kα) (mm^{-1})	0.830	0.332	0.402
$2\theta_{max}$ (°)	54.56	51.80	53.08
Measured reflections	6792	22966	33516
Unique reflections (R_{int})	2095 (0.0534)	8934 (0.0638)	8567 (0.0476)
Observed reflections [$I > 2\sigma(I)$]	1252	5285	6765
Parameters refined	167	551	442
R_1 [$I > 2\sigma(I)$; all data]	0.0259; 0.0584	0.1337; 0.1690	0.0577; 0.0709
wR_2 [$I > 2\sigma(I)$; all data]	0.0438; 0.0481	0.3402; 0.3603	0.1645; 0.1718
Goodness-of-fit on F^2	0.568	1.198	1.073
Largest difference peak and hole (e Å^{-3})	0.21 and −0.31	0.52 and −1.01	1.075 and −1.131

5, the corresponding signals are visible at 0.11, 4.05 and 4.19 ppm. This time, an integral ratio of 6:2:2 reveals the presence of only two methyl substituents at each boron atom. Moreover, the electronegative pyrazolyl groups lead to a downfield shift of the methyl and ferrocenyl resonances of **5** compared to **4** and to a pattern of three signals in the aromatic region of the proton spectrum [$\delta(^1H) = 5.95, 7.01, 7.48$]. In the ^{13}C NMR spectrum of **4**, a 1:1:1:1 quadruplet for the methyl groups is observed [$\delta(^{13}C) = 16.4$, $^1J_{BC} = 40$ Hz] as a result of ^{11}B ($I = 3/2$) coupling. The methyl resonance of the less symmetrically substituted derivative **5** [$\delta(^{13}C) = 12.8$] is severely broadened and its multiplet structure was not resolved, which was attributed to the quadrupolar relaxation of the adjacent boron nucleus [22].

2.2. X-ray crystal structure determinations

Selected crystallographic data are summarized in Table 1. Lithium ferrocenylborohydride **3** crystallizes together with 1 equiv. of 12-crown-4 in the orthorhombic space group *Pnma* (Fig. 2). Each Li^+ ion is complexed by four oxygen atoms of a crown ether molecule and establishes close contacts to two hydrogen atoms of the BH_3 fragment [Li(1)–H(1A) = 1.97(2) Å]. The Li···H distance to the third hydrogen atom is almost 1 Å longer [Li(1)···H(1B) = 2.94(2) Å]. Thus, $[FcBH_3]^-$ acts as a bidentate ligand toward the lithium cation. In metal borohydrides, this is the most common binding mode [23]. The coordination geometry of Li^+ in **3**·(12-crown-4) is reminiscent of the structure determined for $Li[BH_4]\cdot 2DME$ in the solid state (DME = dimethoxyethane) [23]. Here, the hexacoordinated Li ion is surrounded by four oxygen atoms of two DME molecules and two hydrogen atoms from a μ_2-$[BH_4]^-$ group. Consequently, the Li–H bond lengths {**3**·(12-crown-4): 1.97(2) Å; $Li[BH_4]\cdot 2DME$: 2.02(2) Å}, as well as the Li–H–B bond angles {**3**·(12-crown-4): 96.4(12)°; $Li[BH_4]\cdot 2DME$: 98.1(9)°} are rather similar in both compounds. A significantly shorter B···Li distance is found in **3**·(12-crown-4) [2.382(4) Å] compared to $Li[BH_4]\cdot 2DME$ [2.470(4) Å]. Using Edelstein's correlation of metal–boron distances as a measure of the denticity of borohydride groups [24], values of 1.6 ± 0.1 and 1.36 ± 0.06 Å are estimated for the ionic radii of bidentate and tridentate borohydride ligands, respectively. Thus, B···Li distances of about 2.50 and 2.26 Å are to be expected for Li-μ_2-BH_3R and Li-μ_3-BH_3R coordination modes [ionic radius of hexacoordinated $Li^+ = 0.90$ Å [25]]. It may therefore be concluded, that the $[BH_4]^-$ ion in $Li[BH_4]\cdot 2DME$ represents the ideal Li-μ_2-BH_3R arrangement, whereas the BH_3 fragment in **3**·(12-crown-4) is slightly tilted in the direction of a Li-μ_3-BH_3R coordination {cf. the distance between Li^+ and the non-coordinating H atom(s) is shorter in **3**·(12-crown-4) than in $Li[BH_4]\cdot 2DME$ with values of 2.94(2) and 3.27(2) Å, respectively}. This effect is most likely caused by steric repulsion between the crown ether ligand and the bulky ferrocenyl substituent in **3**·(12-crown-4).

The molecular structure of **3**·(12-crown-4) indicates coordination of Li^+ to the BH_3 group via two hydride bridges to be preferred over $Li^+\cdots\eta^5$-ferrocene bonding. The system was therefore developed further by replacing the hydrogen substituents with methyl groups, which can be expected to interact less strongly with lithium cations. Moreover, two borate substituents were introduced into the ferrocene core in order to increase the electrostatic attraction of Li^+ ions. Single crystals of the resulting compound **4** were obtained from THF [$\mathbf{4}\cdot(THF)_8$: orthorhombic, *Pca*2_1; Fig. 3]; addition of 12-crown-4 was not required. The crystal lattice of $\mathbf{4}\cdot(THF)_8$ consists of solvent-separated ions with each Li^+ being coordinated to four THF molecules in a tetrahedral fashion. The $[1,1'\text{-fc}(BMe_3)_2]^{2-}$ ion adopts a conformation in which the BMe_3 substituents are pointing away from each other [C(11)–COG–COG′–C(21) = 154.1°; COG: centre of gravity of a cyclopentadienyl ring].

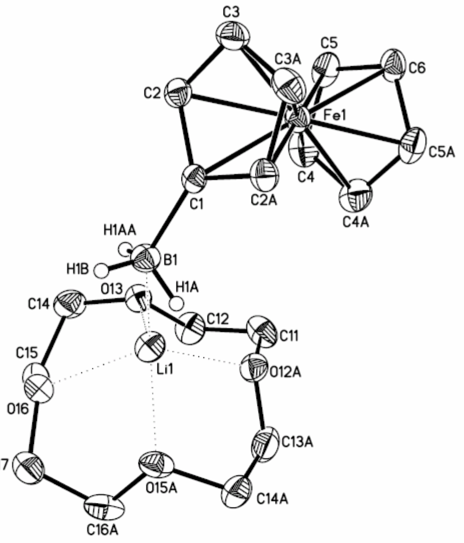

Fig. 2. Molecular structure of compound **3**·(12-crown-4); thermal ellipsoids are shown at the 50% probability level. Selected bond lengths (Å), atom···atom distances (Å), angles (°), torsion angles (°) and dihedral angles (°): B(1)–C(1) = 1.600(4), B(1)···Li(1) = 2.382(4), B(1)–H(1A) = 1.14(2), B(1)–H(1B) = 1.15(3), Li(1)–H(1A) = 1.97(2), Li(1)···H(1B) = 2.94(2); C(2)–C(1)–C(2A) = 104.2(2), C(2)–C(1)–B(1) = 127.8(1), C(1)–B(1)···Li(1) = 141.3(2), C(1)–B(1)–H(1A) = 112.6(10), C(1)–B(1)–H(1B) = 111.6(14), H(1A)–B(1)–H(1B) = 105.1(12), Li(1)–H(1A)–B(1) = 96.4(12); COG–C(1)–B(1) = 176.5; C(2)–C(1)–B(1)···Li(1) = 92.4(2), C(2)–C(1)–B(1)–H(1B) = −87.6(2), C(1)–COG–COG′–C(4A) = −36.1; C(1)C(2)C(3)C(3A)C(2A)//C(4)C(5)C(6)C(5A)C(4A) = 0.2. COG: centre of gravity of a C_5H_4 ring. Symmetry transformation used to generate equivalent atoms: $x, -y+3/2, z$.

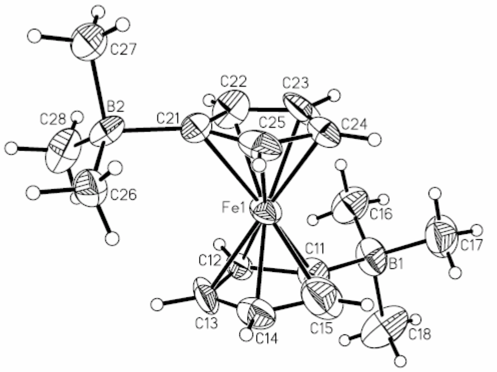

Fig. 3. Molecular structure of the anionic part of compound $\mathbf{4}\cdot(\mathrm{THF})_8$; thermal ellipsoids are shown at the 30% probability level. Selected bond lengths (Å), angles (°), torsion angles (°) and dihedral angles (°): B(1)–C(11) = 1.734(16), B(2)–C(21) = 1.634(16); C(12)–C(11)–C(15) = 102.7(11), C(12)–C(11)–B(1) = 127.6(10), C(15)–C(11)–B(1) = 129.7(13), C(22)–C(21)–C(25) = 101.7(10), C(22)–C(21)–B(2) = 126.4(11), C(25)–C(21)–B(2) = 131.9(11), COG–C(11)–B(1) = 174.9, COG–C(21)–B(2) = 177.7; C(12)–C(11)–B(1)–C(18) = −94.3(14), C(22)–C(21)–B(2)–C(27) = −88.5(13), C(11)–COG–COG′–C(21) = 154.1; C(11)C(12)C(13)C(14)C(15)// C(21)C(22)C(23)C(24)C(25) = 2.2.

Since the desired Li–ferrocene interaction could not be achieved just by increasing the number of negatively charged side-chains, each of the borate groups was equipped with a Lewis-basic pyrazolyl substituent in order to anchor the Li$^+$ ion via a Li–N adduct bond. The lithium pyrazolylborate **5** crystallizes from diethyl ether together with four solvent molecules in the triclinic space group $P\bar{1}$ [$\mathbf{5}\cdot(\mathrm{Et_2O})_4$; Fig. 4]. This time, each Li$^+$ ion is bonded to two ether molecules and to the nitrogen lone-pair of the pyrazolyl side-arm [Li(1)–N(32) = 1.998(5), Li(2)–N(42) = 1.999(6) Å], which places it on top of the cyclopentadienyl ring [C(12)–C(11)–B(1)–N(31) = 97.7(3)°, C(22)–C(21)–B(2)–N(41) = −81.3(3)°]. As a consequence, three lithium–carbon contacts [Li(1)–C(11) = 2.646(5), Li(1)–C(12) = 2.395(5), Li(1)–C(13) = 2.910(6), Li(2)–C(21) = 2.475(5), Li(2)–C(22) = 2.496(5), Li(2)–C(25) = 2.730(6) Å] are established by Li(1) as well as Li(2). As the internal angles of the C(Cp)–B–N–N–Li chains do not depart appreciably from the ideal values of 109° [C(11)–B(1)–N(31) = 105.3(2)°, C(21)–B(2)–N(41) = 106.6(2)°] and 120° [B(1)–N(31)–N(32) = 121.9(2)°, N(31)–N(32)–Li(1) = 124.0(2)°, B(2)–N(41)–N(42) = 124.2(2)°, N(41)–N(42)–Li(2) = 122.3(2)°], the molecular framework of the heterotrimetallic aggregate is apparently free of ring strain. Compound **5** is related to the ferrocene-based tris(1-pyrazolyl)borates **V** [26] (Fig. 5), of which several metal complexes [27,28] (including one Li$^+$ salt) [29] have been synthesized and structurally characterized. In all these cases, the tris(1-pyrazolyl)borate units act as di- or trihapto ligand toward the metal centre, which in turn was never found to interact with the ferrocene backbone. Thus, as is to be expected, Li$^+$–ferrocene bonding appears to be less favourable than lithium-pyrazolyl adduct formation. Some key structural features of $\mathbf{5}\cdot(\mathrm{Et_2O})_4$ resemble Laguna's coordination polymer **VI** [30] (Fig. 5), consisting of 1,1′-ferrocenediyl bis(dialkyldithiocarbamate) ligands [31] and Ag(I) ions. Here, each silver ion is not only bonded to two sulfur atoms of different ferrocene moieties but also to two cyclopentadienyl rings in an η^2 fashion. In 1998, **VI** represented the first example where an η^5-cyclopentadienyl ring of ferrocene was shared with another metal atom via the π-system.

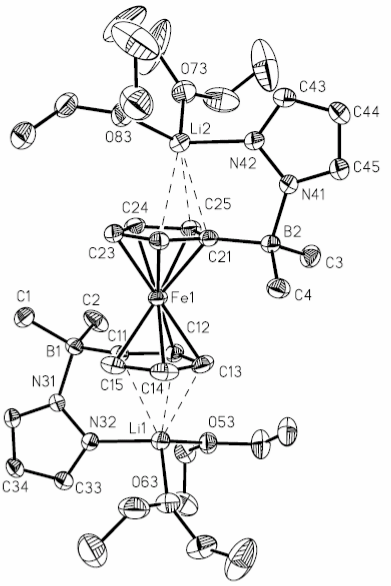

Fig. 4. Molecular structure of compound $\mathbf{5}\cdot(\mathrm{Et_2O})_4$; thermal ellipsoids are shown at the 30% probability level. Selected bond lengths (Å), angles (°), torsion angles (°) and dihedral angles (°): B(1)–C(11) = 1.617(4), B(1)–N(31) = 1.611(3), B(2)–C(21) = 1.621(4), B(2)–N(41) = 1.610(3), Li(1)–N(32) = 1.998(5), Li(1)–C(11) = 2.646(5), Li(1)–C(12) = 2.395(5), Li(1)–C(13) = 2.910(6), Li(2)–N(42) = 1.999(6), Li(2)–C(21) = 2.475(5), Li(2)–C(22) = 2.496(5), Li(2)–C(25) = 2.730(6); C(12)–C(11)–C(15) = 104.5(2), C(12)–C(11)–B(1) = 128.8(2), C(15)–C(11)–B(1) = 126.7(2), C(22)–C(21)–C(25) = 104.9(2), C(22)–C(21)–B(2) = 127.0(2), C(25)–C(21)–B(2) = 128.1(2), C(11)–B(1)–N(31) = 105.3(2), B(1)–N(31)–N(32) = 121.9(2), N(31)–N(32)–Li(1) = 124.0(2), C(21)–B(2)–N(41) = 106.6(2), B(2)–N(41)–N(42) = 124.2(2), N(41)–N(42)–Li(2) = 122.3(2), N(32)–Li(1)–O(53) = 109.0(3), N(32)–Li(1)–O(63) = 106.3(3), O(53)–Li(1)–O(63) = 111.2(2), N(42)–Li(2)–O(73) = 105.4(3), N(42)–Li(2)–O(83) = 109.4(3), O(73)–Li(2)–O(83) = 107.1(2), COG–C(11)–B(1) = 177.5, COG–C(21)–B(2) = 179.3; C(12)–C(11)–B(1)–N(31) = 97.7(3), C(11)–B(1)–N(31)–N(32) = −35.4(3), B(1)–N(31)–N(32)–Li(1) = 14.2(4), C(22)–C(21)–B(2)–N(41) = −81.3(3), C(21)–B(2)–N(41)–N(42) = 4.0(3), B(2)–N(41)–N(42)–Li(2) = −9.2(4), C(11)–COG–COG′–C(21) = −157.9; C(11)C(12)C(13)C(14)C(15)// C(21)C(22)C(23)C(24)C(25) = 1.0.

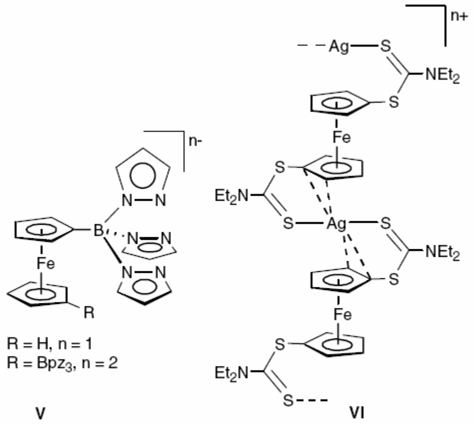

Fig. 5. Ferrocene-based tris(1-pyrazolyl)borate derivatives **V** and a double sandwich silver(I)–ferrocene polymer **VI**.

3. Conclusions

Inspired by a DFT study on the ferrocene–Li^+ complex in the gas phase [13], we synthesized three ferrocene derivatives, $Li[FcBH_3]$, $Li_2[1,1'\text{-}fc(BMe_3)_2]$ and $Li_2[1,1'\text{-}fc(BMe_2pz)_2]$ [$Fc = (C_5H_5)Fe(C_5H_4)$, $fc = (C_5H_4)_2Fe$, pz = pyrazolyl], in order to establish the structural motif of a Li^+ cation located on top of a ferrocene–Cp ring. Our rationale was to stabilize a potential interaction between both components by introducing negatively charged substituents into the ferrocene core. Initially, it appeared to be of prime importance to use anionic side-chains that do *not* possess electron lone pairs able to compete with the cyclopentadienyl π-system for Li^+ coordination. Thus, borate substituents were chosen for all further investigations. A crystal structure analysis of $Li[FcBH_3] \cdot$(12-crown-4), obtained from a THF solution after addition of 12-crown-4, revealed hexacoordinated Li^+ ions bonded to one molecule of crown ether and two hydrogen atoms of the BH_3 fragment. Even a hydridoborate fragment is thus preferred over the Cp π-system for Li^+ coordination. Attempts to block this coordination site by substitution of methyl groups for the hydrogen atoms failed, since the related methylborate crystallized from THF as solvent-separated ion pairs $\{[Li(THF)_4]^+\}_2[1,1'\text{-}fc(BMe_3)_2]^{2-}$. Single crystals of this compound from less strongly coordinating solvents (e.g., diethyl ether) could not be obtained up to now. Contrary to our a priori assumptions, we thus came to the conclusion that a Lewis-basic functionality might be required to stabilize the aimed-for Li^+–ferrocene complex, provided the electron lone pair is part of a side-arm designed to put the Li^+ ion on the cyclopentadienyl ring. From molecular modelling studies, the rigid pyrazolyl ring appeared to be well-suited for this purpose. Single crystals of $Li_2[1,1'\text{-}fc(BMe_2pz)_2]$ were grown from diethyl ether. In this compound, the lithium ions are coordinated by two solvent molecules, the pyrazolyl side-arm and the cyclopentadienyl ring. Thus, $Li_2[1,1'\text{-}fc(BMe_2pz)_2]$ can be regarded as a trinuclear segment of the polymeric structure $[\text{–}(C_5H_4R)\text{-}Li(C_5H_4R)Fe\text{–}]_\infty$ with $R = BMe_2pz$. In the future, we are planning to employ the $[1,1'\text{-}fc(BMe_2pz)_2]^{2-}$ ligand in combination with metals other than Li^+ for the synthesis of ferrocene-based multiple-decker complexes.

4. Experimental section

4.1. General remarks

All reactions and manipulations of air-sensitive compounds were carried out in dry, oxygen-free argon using standard Schlenk ware. Solvents were freshly distilled under N_2 from Na–benzophenone (diethyl ether, THF) prior to use. NMR: Bruker DPX 400, Bruker DPX 250. ^{11}B NMR spectra are reported relative to external $BF_3 \cdot Et_2O$. Unless stated otherwise, all NMR spectra were run at ambient temperature; abbreviations: s, singlet, d, doublet, vtr, virtual triplet, q, quadruplet, n.r., multiplet expected in the ^1H NMR spectrum but not resolved, n.o., signal not observed. Compounds **1** [18] and **2** [19] were synthesized according to the literature procedures.

4.2. Preparation of 3

For the synthesis of compound **3** see [20]. Single crystals of **3** · (12-crown-4) were grown by gas phase diffusion of diethyl ether onto a THF solution of **3** to which a small amount of 12-crown-4 had been added. Compound **3** is sensitive to air and moisture. *Anal*. Calc. for $C_{18}H_{28}BFeLiO_4$ [382.00]: C, 56.60; H, 7.39. Found: C, 56.33; H, 7.12%.

4.3. Preparation of 4

LiMe (1.6 M, 4.42 mL, 7.07 mmol) in Et_2O was added dropwise with stirring at −78 °C to **2** (0.94 g, 3.54 mmol) in Et_2O (20 mL). The mixture was slowly warmed to room temperature and the solvent removed under reduced pressure. The remaining highly viscous oily residue was dissolved in THF (20 ml) and the solution stored at 5 °C overnight, whereupon dark red X-ray quality crystals of **4** · $(THF)_8$ formed. Yield: 2.79 g (89%). ^{11}B NMR (128.4 MHz, d_8-THF): δ −21.8 ($h_{1/2} = 25$ Hz). ^1H NMR (400.1 MHz, d_8-THF): δ −0.47 (s, 18H, CH_3), 3.55, 3.75 (2 × n.r., 2 × 4H, C_5H_4). ^{13}C NMR (100.6 MHz, d_8-THF): δ 16.4 (q, $^1J_{BC} = 40$ Hz, CH_3), 67.8, 70.7 (C_5H_4), n.o. C_5H_4-C_{ipso}. The compound is extremely sensitive to air and the crystals lose THF rapidly when isolated at ambient temperature; a decent elemental analysis was therefore not obtained.

*4.4. Preparation of **5***

Lipz (0.34 g, 4.60 mmol) in Et_2O (15 mL) was added dropwise with stirring at −78 °C to **2** (0.61 g, 2.30 mmol) in Et_2O (15 mL). The mixture was slowly warmed to room temperature, filtered and the clear yellow filtrate stored at 5 °C overnight, whereupon yellow–orange X-ray quality crystals of $\mathbf{5} \cdot (Et_2O)_4$ formed. Yield: 1.52 g (93%). ^{11}B NMR (128.4 MHz, d_8-THF): δ −9.0 ($h_{1/2} = 300$ Hz). ^1H NMR (400.1 MHz, d_8-THF): δ 0.11 (s, 12H, CH_3), 4.05, 4.19 ($2 \times$ vtr, $2 \times 4H$, $^3J_{HH} = {}^4J_{HH} = 1.6$ Hz, C_5H_4), 5.95 (vtr, 2H, $^3J_{HH} = 1.9$ Hz, pz–H4), 7.01, 7.48 ($2 \times$ d, $2 \times 2H$, $^3J_{HH} = 1.7$, 2.0 Hz, pz–H3,5). ^{13}C NMR (100.6 MHz, d_8-THF): δ 12.8 (n.r., CH_3), 71.0, 72.2 (C_5H_4), 102.8 (pz–C4), 131.9, 135.4 (pz–C3,5), n.o. C_5H_4-C_{ipso}. The compound is sensitive to air and the crystals lose diethyl ether rapidly when isolated at ambient temperature; a decent elemental analysis was therefore not obtained.

4.5. X-ray crystal structure analyses

The crystals of $\mathbf{3} \cdot$(12-crown-4), $\mathbf{4} \cdot (THF)_8$ and $\mathbf{5} \cdot (Et_2O)_4$ were measured on a STOE IPDS II two-circle diffractometer with graphite-monochromated Mo Kα radiation. An empirical absorption correction was performed using the MULABS [32] option in the program PLATON [33]. The structures were solved by direct methods using the program SHELXS [34] and refined against F^2 with full-matrix least-squares techniques using the program SHELXL [35]. The crown ether ring in $\mathbf{3} \cdot$(12-crown-4) is located on a crystallographic mirror plane and therefore disordered over two equally occupied sites. $\mathbf{4} \cdot (THF)_8$ is a racemic twin composed of two domains with an occupancy ratio of 0.70(6)/0.30(6). All non-H atoms of $\mathbf{3} \cdot$(12-crown-4), $\mathbf{4} \cdot (THF)_8$ and $\mathbf{5} \cdot (Et_2O)_4$ were refined with anisotropic displacement parameters. The BH_3 hydrogen atoms of $\mathbf{3} \cdot$(12-crown-4) could be located in the difference Fourier map and were freely refined. All other H atoms were refined using a riding model.

5. Supplementary material

Crystallographic data for the structural analyses have been deposited with the Cambridge Crystallographic Data Centre, CCDC reference numbers: 230425 [$\mathbf{3} \cdot$(12-crown-4)], 230426 [$\mathbf{4} \cdot (THF)_8$], 230427 [$\mathbf{5} \cdot (Et_2O)_4$]. Copies of this information may be obtained free of charge from The Director, CCDC, 12 Union Road, Cambridge, CB2 1EZ, UK (fax: +44-1223-336033; email: deposit@ccdc.cam.ac.uk or www: http://www.ccdc.cam.ac.uk).

Acknowledgements

M.W. is grateful to the Deutsche Forschungsgemeinschaft (DFG) for financial support and to Chemetall for generous gifts of organolithium compounds. M.S. thanks the Fonds der Chemischen Industrie (FCI) and the Bundesministerium für Bildung und Forschung (BMBF) for a Ph.D. grant.

References

[1] N.J. Long, Metallocenes, Blackwell Science, London, 1998.
[2] W. Siebert, Angew. Chem. 97 (1985) 924.
[3] W. Siebert, Angew. Chem., Int. Ed. Engl. 24 (1985) 943.
[4] T. Kuhlmann, S. Roth, J. Rozière, W. Siebert, Angew. Chem. 98 (1986) 87.
[5] T. Kuhlmann, S. Roth, J. Rozière, W. Siebert, Angew. Chem., Int. Ed. Engl. 25 (1986) 105.
[6] M.Y. Lavrentiev, H. Köppel, M.C. Böhm, Chem. Phys. 169 (1993) 85.
[7] A. Salzer, H. Werner, Angew. Chem. 84 (1972) 949.
[8] A. Salzer, H. Werner, Angew. Chem., Int. Ed. Engl. 11 (1972) 930.
[9] D.R. Armstrong, A.J. Edwards, D. Moncrieff, M.A. Paver, P.R. Raithby, M.-A. Rennie, C.A. Russell, D.S. Wright, J. Chem. Soc., Chem. Commun. (1995) 927.
[10] S.M. Schildcrout, J. Am. Chem. Soc. 95 (1973) 3846.
[11] S. Nagao, A. Kato, A. Nakajima, K. Kaya, J. Am. Chem. Soc. 122 (2000) 4221.
[12] S. Scholz, J.C. Green, H.-W. Lerner, M. Bolte, M. Wagner, Chem. Commun. (2002) 36.
[13] A. Irigoras, J.M. Mercero, I. Silanes, J.M. Ugalde, J. Am. Chem. Soc. 123 (2001) 5040.
[14] M. Scheibitz, R.F. Winter, M. Bolte, H.-W. Lerner, M. Wagner, Angew. Chem. 115 (2003) 954.
[15] M. Scheibitz, R.F. Winter, M. Bolte, H.-W. Lerner, M. Wagner, Angew. Chem., Int. Ed. Engl. 42 (2003) 924.
[16] M. Fontani, F. Peters, W. Scherer, W. Wachter, M. Wagner, P. Zanello, Eur. J. Inorg. Chem. (1998) 1453.
[17] M. Fontani, F. Peters, W. Scherer, W. Wachter, M. Wagner, P. Zanello, Eur. J. Inorg. Chem. (1998) 2087.
[18] T. Renk, W. Ruf, W. Siebert, J. Organomet. Chem. 120 (1976) 1.
[19] W. Ruf, T. Renk, W. Siebert, Z. Naturforsch. B 31 (1976) 1028.
[20] M. Scheibitz, J.W. Bats, M. Bolte, H.-W. Lerner, M. Wagner, Organometallics 23 (2004) 940.
[21] R.J. Thompson, J.C. Davis Jr., Inorg. Chem. 4 (1965) 1464.
[22] H. Nöth, B. Wrackmeyer, in: P. Diehl, E. Fluck, R. Kosfeld (Eds.), NMR Basic Principles and Progress, vol. 14, Springer, Berlin, 1978.
[23] H.-H. Giese, H. Nöth, H. Schwenk, S. Thomas, Eur. J. Inorg. Chem. (1998) 941.
[24] N. Edelstein, Inorg. Chem. 20 (1981) 297.
[25] R.D. Shannon, Acta Crystallogr. Sect. A 32 (1976) 751.
[26] F. Jäkle, K. Polborn, M. Wagner, Chem. Ber. 129 (1996) 603.
[27] F. Fabrizi de Biani, F. Jäkle, M. Spiegler, M. Wagner, P. Zanello, Inorg. Chem. 36 (1997) 2103.
[28] E. Herdtweck, F. Peters, W. Scherer, M. Wagner, Polyhedron 17 (1998) 1149.
[29] S.L. Guo, F. Peters, F. Fabrizi de Biani, J.W. Bats, E. Herdtweck, P. Zanello, M. Wagner, Inorg. Chem. 40 (2001) 4928.

[30] O. Crespo, M.C. Gimeno, P.G. Jones, A. Laguna, C. Sarroca, Chem. Commun. (1998) 1481.
[31] B. McCulloch, C.H. Brubaker Jr., Organometallics 3 (1984) 1707.
[32] R.H. Blessing, Acta Crystallogr. Sect. A 51 (1995) 33.
[33] A.L. Spek, Acta Crystallogr. Sect. A 46 (1990) C34.
[34] G.M. Sheldrick, Acta Crystallogr. Sect. A 46 (1990) 467.
[35] G.M. Sheldrick, SHELXL-97. A Program for the Refinement of Crystal Structures, Unversität Göttingen, Göttingen, Germany, 1997.

6.3 „A Joint Experimental and Theoretical Study of Cation-π Interactions: Multiple-Decker Sandwich Complexes of Ferrocene with Alkali Metal Ions (Li^+, Na^+, K^+, Rb^+, Cs^+)"

Alireza Haghiri Ilkhechi, Jose M. Mercero, Iñaki Silanes, Michael Bolte, Matthias Scheibitz, Hans-Wolfram Lerner, Jesus M. Ugalde and Matthias Wagner,

J. Am. Chem. Soc., **2005**, im Druck.

A Joint Experimental and Theoretical Study of Cation-π Interactions: Multiple-Decker Sandwich Complexes of Ferrocene with Alkali Metal Ions (Li^+, Na^+, K^+, Rb^+, Cs^+).

Alireza Haghiri Ilkhechi[a], Jose M. Mercero[b], Iñaki Silanes[b], Michael Bolte[a], Matthias Scheibitz[a], Hans-Wolfram Lerner[a], Jesus M. Ugalde[b*], and Matthias Wagner[a*]

[a] Institut für Anorganische Chemie, J.W. Goethe-Universität Frankfurt, Marie-Curie-Strasse 11, D-60439 Frankfurt (Main), Germany.

Fax: +49 6979829260; E-mail: Matthias.Wagner@chemie.uni-frankfurt.de

[b] Kimika Fakultatea, Euskal Herriko Unibertsitatea, and Donostia International Physics Center DIPC, P. K. 1072, 20080 Donostia Euskadi, Spain.

Fax: +34 943015270; E-mail: ugalde@sq.ehu.es

Abstract: The alkali metal (Li^+, Na^+, K^+, Rb^+, Cs^+) salts of the ditopic mono(pyrazol-1-yl)borate ligand $[1,1'\text{-fc}(BMe_2pz)_2]^{2-}$ crystallize from dimethoxyethane as multiple-decker sandwich complexes with the M^+ ions bound to the π faces of the ferrocene cyclopentadienyl rings in an η^5 manner (fc = $(C_5H_4)_2Fe$; pz = pyrazolyl). X-ray crystallography of the lithium complex reveals discrete trimetallic entities with each lithium ion being coordinated by only one cyclopentadienyl ring. The sodium salt forms polyanionic zig-zag chains where each Na^+ ion bridges the cyclopentadienyl rings of two ferrocene moieties. Linear columns $[\text{-CpR-Fe-CpR-}M^+\text{-CpR-Fe-CpR-}M^+\text{-}]_\infty$ (R = $[\text{-}BMe_2pz]^-$) are established by the K^+-, Rb^+-, and Cs^+ derivatives in the solid state. According to DFT calculations, the binding enthalpies of M^+-η^5(ferrocene) model complexes are about 20 % higher compared to the corresponding M^+-η^6(benzene) aggregates when M^+ = Li^+, Na^+. For K^+ and Rb^+, the degree of cation-π interaction with both aromatics is about the same. The binding sequence along the M^+-η^5(ferrocene) series follows a classical electrostatic trend with the smaller ions being more tightly bound.

Introduction

Alkali metal cations, as well as tetraalkylammonium groups, are attracted to the π face of aromatic structures through a strong non-covalent binding force. During the past 20 years, both experimental and theoretical evidence has been gathered that suggests these cation-π interactions to play a prominent role in various areas of chemistry and biology [1-5]. For example, cation-π interactions appear to contribute to the ion selectivity in potassium channels[6], they are important for the binding of acetylcholine to the active site of the enzyme acetylcholine esterase[7], and they guide the stereoselective cyclization of squalene epoxide in the enzymatically catalyzed process of steroid biosynthesis[7]. Even though cation-π interactions involving arene molecules have been studied extensively, only very little is known about the degree of cation binding to organometallic structures like the cyclopentadienyl ring of sandwich complexes. In this context, ferrocene, being the prototypical sandwich complex and said to be even more aromatic than benzene[8], is of particular interest for further studies.[9] This is the more so as ferrocene-based planar-chiral ligands and ferrocenyl-substituted crown ethers are important in homogeneous catalysis and alkali metal complexation, respectively.[10] In both cases it may be interesting to explore the potential of cation-π interactions involving the ferrocene cyclopentadienyl rings for the design of improved ligand systems and redox-switchable alkali metal receptors.

The main focus of this paper is on the role of cation-π interactions for the development of ferrocene-containing multiple-decker sandwich complexes. Even though $[Fe_2(C_5H_5)_3]^{+}$[11] and clusters of the general formula $V_n[Fe(C_5H_5)_2]_{n+1}$ (n = 1-3)[12] have been detected in the gas phase, it was for a long time not possible to stabilize any of these aggregates in the condensed phase. In 1998, Laguna et al. reported on a double sandwich silver(I) complex with 1,1'-bis(diethyldithiocarbamate)ferrocene. This ligand-supported polymer represented the first isolable compound where an η^5-cyclopentadienyl ring of ferrocene was shared with another metal atom via the π system.[13] More recently, Enders et al. synthesized the $ZnCl_2$ complex of η^5-1-(8-quinolyl)-2,3,4,5-tetramethylcyclopentadienyl- η^5-cyclopentadienyliron in which the zinc ion is surrounded tetrahedrally by two chlorine atoms, the nitrogen atom of the 8-quinolyl sidearm and one carbon atom of the tetramethylcyclopentadienyl ring.[14] Our group published the synthesis and X-ray crystal structure analysis of compound **I** (Figure 1) consisting of a ligand-unsupported array of alternating Ga(I) and Fe(II) ions connected by η^5,μ-$[C_5H_5]^-$ moieties.[15] According to density functional (DFT) calculations, the binding energy of two ferrocenes to Ga^+ is about 80 kJ mol^{-1} higher than that for the formation of $[Ga(C_6H_6)_2]^+$ from Ga^+ and two benzene molecules. Fragment analysis of $\{[Fe(C_5H_5)_2]_2Ga\}^+$ indicated a transfer of 0.4 electrons into the gallium 4p orbitals compared with a zero occupancy for the isolated ion. These encouraging results prompted us to start a systematic search for more one-dimensional solids exhibiting the structural motif of ferrocene-containing multiple-decker sandwich complexes. It is important to note in this context that the synthesis protocol developed for the ligand-unsupported polymer **I** [15] is unique in that it starts from the covalent molecule $GaCl_3$ which readily dissolves in non-coordinating solvents. For a more general approach it will, however, become necessary to use ionic metal salts that usually require strongly coordinating solvents as reaction media. We therefore decided to follow Laguna's approach and employ ferrocene derivatives equipped with Lewis-basic substituents designed to stabilize the aimed-for metal···Cp interactions.

Ferrocene- and cymantrene-based tris(pyrazol-1-yl)borate (scorpionate) ligands **II**[16, 17] and **III**[18] (Figure 2) are readily available and have been used for the preparation of heterooligonuclear transition metal complexes[19-21]. Cyclic voltammetric measurements on (**IIa**)ML_n and (**IIa**)$_2$M revealed the oxidation state of the ferrocenyl substituent(s) to have a significant influence on the redox potential of M and *vice versa*. Notably, the heterotrinuclear complex (**IIa**)$_2$Cu exhibits two well-resolved Fe(II)/Fe(III) redox waves thereby indicating an electronic communication between the two ferrocenyl substituents. Starting from the ditopic scorpionate ligand **IIb** and divalent transition metal ions, polymers of the general formula $[(\mathbf{IIb})M]_n$ are accessible. In an attempt to further increase the degree of metal-metal interaction along the chain and to promote direct bonding between the ferrocenyl Cp rings and the coordinated metal atom,[22] the *tris*(pyrazol-1-yl)borate substituents of **IIb** (Figure 2) are now replaced by *mono*(pyrazol-1-yl)borate fragments, thereby creating the novel ligand $[\mathbf{2}]^{2-}$ (Scheme 1). In the following we report on the synthesis and structural characterization of the complete series $\mathbf{2Li_2}$, $\mathbf{2Na_2}$, $\mathbf{2K_2}$, $\mathbf{2Rb_2}$, $\mathbf{2Cs_2}$ and give some insight into the different structural effects exerted by coordinated dimethoxyethane (DME) and tetrahydrofurane (THF) molecules. The experimental investigations are augmented with density functional (DFT) calculations on model complexes between ferrocene and alkali metal ions ($M^+ = Li^+, Na^+, K^+, Rb^+$) in order to get deeper insight into the nature of the interaction between these two components.

Results and Discussion

Syntheses and NMR-spectroscopic Characterization: Upon treatment of 1,1'-bis(dimethylboryl)ferrocene **1** with two equivalents of the appropriate alkali metal pyrazolide (Mpz) in diethyl ether, the respective complexes $\mathbf{2M_2}$ ($M^+ = Li^+, Na^+, K^+, Rb^+, Cs^+$) readily precipitate from the reaction mixtures (Scheme 1). X-ray quality crystals of $\mathbf{2M_2}$·(THF)$_4$ ($M^+ = Na^+, K^+, Rb^+$) were obtained from THF at –30 °C, room temperature, and 5 °C, respectively. Recrystallization of $\mathbf{2Li_2}$·(Et$_2$O)$_4$, $\mathbf{2M_2}$·(THF)$_4$ ($M^+ = Na^+, K^+, Rb^+$) and crude $\mathbf{2Cs_2}$·(Et$_2$O)$_x$ from DME gave single-crystalline materials of the composition $\mathbf{2Li_2}$·(DME)$_2$ and $\mathbf{2M_2}$·(DME)$_3$ ($M^+ = Na^+, K^+, Rb^+, Cs^+$). The complexes $\mathbf{2K_2}$·(THF)$_4$, $\mathbf{2Rb_2}$·(THF)$_4$, and $\mathbf{2Cs_2}$·(Et$_2$O)$_x$ are only poorly soluble in DME. Elevated temperatures and the use of an ultrasonic bath was thus required to prepare saturated solutions.

All NMR spectra were run at ambient temperature in d$_8$-THF. The ^{11}B NMR resonances of $\mathbf{2M_2}$ lie in the range between –9.4 ($\mathbf{2K_2}$) and –7.6 ppm ($\mathbf{2Rb_2}$, $\mathbf{2Cs_2}$), thereby testifying to the presence of tetra-coordinated boron nuclei.[23] Both in the ^{1}H- and in the ^{13}C NMR spectra, the two fragments [$C_5H_4B(Me_2)pz$] of **2M₂** give rise to six signals only (C_5H_4-C*ipso* is generally not observed as a result of quadrupolar broadening[23]). This leads to the conclusion that there are no restrictions to intramolecular motion on the NMR timescale as was also observed for the quinolylferrocene-$ZnCl_2$[14] complex mentioned above. Moreover, no systematic changes of the C_5H_4 chemical shift values, which might indicate Cp···metal coordination in solution, are evident from a comparison of the NMR spectra of **2Li₂**, **2Na₂**, **2K₂**, **2Rb₂**, and **2Cs₂**. The ^{7}Li NMR spectrum of **2Li₂** reveals one broad resonance at $\delta(^{7}Li) = -1.30$ ($h_{1/2}$ = 37 Hz). From a comparison of these data with the chemical shift values of LiCl in d_8-THF before ($\delta(^{7}Li) = -1.54$; $h_{1/2}$ = 0.6 Hz) and after ($\delta(^{7}Li) = -1.26$; $h_{1/2}$ = 0.6 Hz) the addition of one equivalent of pyrazole, we may safely conclude that **2Li₂** does not form completely solvent separated ion pairs in THF solution but rather exists with the Li^+ ion bound to the pyrazolyl substituent. The large width at half height of the ^{7}Li resonance indicates a dynamic process to go on in **2Li₂** solutions which possesses a significantly different rate constant or is even absent in the case of the Li^+-pyrazole complex.

Electrochemical Investigations: In THF solution, **2Li₂**·$(DME)_2$ gives rise to one ferrocenylene-centred oxidation with an Fe(II)/Fe(III) redox potential of E°' = -0.99 V. An analysis of the cyclic voltammogram measured at room temperature with scan rates varying from 0.05 Vs^{-1} to 1.00 Vs^{-1} not only confirms the chemical reversibility of the one-electron oxidation (i_{pc}/i_{pa} constantly equal to 1), but also proves its electrochemical reversibility (ΔE_p constantly close to 60 mV), thereby suggesting that no significant structural reorganization occurs upon electron removal. It is revealing to compare the redox potential of **2Li₂**·$(DME)_2$ with the electrochemical data of the dianionic [1.1]diborataferrocenophane $[\{Fe(C_5H_4)_2\}_2(BMe_2)_2]^{2-}$ (E°' = –1.02, –1.33 V)[24] and of the neutral boron-nitrogen adduct $Fe(C_5H_4BMe_2{\cdot}DMAP)_2$ (E°' = -0.64 V; DMAP: 4-dimethylaminopyridine)[25]. In all three cases, the introduction of tetracoordinated substituents into the ferrocene core leads to a substantial cathodic shift of the Fe(II)/Fe(III) transition. As to be expected for electrostatic reasons, this effect is more pronounced for negatively charged borate groups than for neutral sidechains. Moreover, the borate substituents of [**2**]$^{2-}$ are obviously weaker electron donors than that of $[\{Fe(C_5H_4)_2\}_2(BMe_2)_2]^{2-}$, which is most likely due to the high group electronegativity of the pyrazolide ring [cf. $Fe(C_5H_4B(pz)_3Tl)_2$: E°' = -0.02 V][19].

X-ray Crystal Structure Determinations: Selected crystallographic data of **2Li₂**·(DME)$_2$, **2Na₂**·(DME)$_3$, **2K₂**·(DME)$_3$, **2Rb₂**·(DME)$_3$, **2Cs₂**·(DME)$_3$, **2Na₂**·(THF)$_4$, **2K₂**·(THF)$_4$, and **2Rb₂**·(THF)$_4$ are summarized in Table 1. **2Li₂**·(DME)$_2$ crystallizes in the triclinic space group *P*-1. The asymmetric unit contains two complete and two half-molecules, which are both located on a center of inversion. As a result, there are six molecules in the unit cell. Since the structural parameters of all four molecules are rather similar, bond lengths and angles of only one of them are given in Figure 3. **2Li₂**·(DME)$_2$ forms heterotrimetallic aggregates in the solid state (Figure 3). Each Li^+ ion is bonded to one chelating DME molecule and to the nitrogen lone-pair of one pyrazolyl sidearm [Li(1)-N(12) = 2.04(3) Å, Li(2)-N(22) = 1.98(3) Å], which places it on-top of the cyclopentadienyl ring [C(12)-C(11)-B(1)-N(11) = 98(2)°, C(22)-C(21)-B(2)-N(21) = 81.3(19)°; B(1)-N(11)-N(12)-Li(1) = -6(2)°, B(2)-N(21)-N(22)-Li(2) = 2(2)°]. As a consequence, short distances are established between the Li^+ cations and the geometric centers (COG) of the cyclopentadienyl rings (Li(1)···COG(1) = 2.26 Å, Li(2)···COG(2) = 2.32 Å; the corresponding distances in the other three molecules are 2.26 Å, 2.44 Å, 2.30 Å, and 2.51 Å; mean value: 2.35 Å). As the internal angles of the C(Cp)-B-N-N-Li chains do not depart appreciably from the ideal values of 109° (C(11)-B(1)-N(11) = 100.4(15)°, C(21)-B(2)-N(21) = 108.2(16)°) and 120° (B(1)-N(11)-N(12) = 123.6(13)°, N(11)-N(12)-Li(1) = 124.2(11)°, B(2)-N(21)-N(22) = 122.3(14)°, N(21)-N(22)-Li(2) = 123.0(13)°), the molecular framework is apparently not suffering from internal strain.

The crystal lattice of the sodium derivative **2Na₂**·(DME)$_3$ (orthorhombic space group *Pbca*) consists of polyanionic zig-zag chains [**2**Na]$_n^{n-}$ and distorted octahedral $[Na(DME)_3]^+$

counterions (Figure 4). A major difference in the overall conformation of the ferrocene ligand $[\mathbf{2}]^{2-}$ in **2Na₂**·(DME)₃ and **2Li₂**·(DME)₂ lies in the torsion angle C(11)-COG(1)-COG(2)-C(21) which possesses values of –135.4° and 178.8°, respectively. Within the zig-zag chains, each Na^+ ion binds to two pyrazolyl substituents of adjacent $[\mathbf{2}]^{2-}$ ligands ($Na(1)-N(12^{\#})$ = 2.382(5) Å, Na(1)-N(22) = 2.405(6) Å; $N(12^{\#})-Na(1)-N(22)$ = 122.2(2)°) and establishes short contacts to two cyclopentadienyl rings ($Na(1)\cdots COG(1^{\#})$ = 2.561, $Na(1)\cdots COG(2)$ = 2.590). Thus, the polymeric subunit $[\mathbf{2}Na]_n^{n-}$ can be regarded as a bent multiple-decker sandwich complex of ferrocene with sodium ions (dihedral angle $C(11^{\#})C(12^{\#})C(13^{\#})C(14^{\#})C(15^{\#})$// C(21)C(22)C(23)C(24)C(25) = 48.0°).

The complexes of the heavier alkali metal ions, **2K₂**·(DME)₃ (triclinic, *P*-1), **2Rb₂**·(DME)₃ (triclinic, *P*-1), and **2Cs₂**·(DME)₃ (monoclinic, *C*2/*c*) are largely isostructural. Representative for these three compounds, the molecular structure of **2K₂**·(DME)₃ is depicted in Figure 5 (selected bond lengths, angles and dihedral angles of **2K₂**·(DME)₃, **2Rb₂**·(DME)₃, and **2Cs₂**·(DME)₃ are given in the caption). In contrast to the bent polymer **2Na₂**·(DME)₃, linear columns of alternating ferrocene units and alkali metal ions are established by the complexes of the higher homologues in the solid state [dihedral angle between the cyclopentadienyl rings of adjacent ferrocenylene fragments: 2.7° (**2K₂**·(DME)₃), 2.5° **2Rb₂**·(DME)₃), 1.7° (**2Cs₂**·(DME)₃)]. The conformation of the ferrocenylene fragment in **2K₂**·(DME)₃ (C(11)-COG(1)-COG(2)-C(21) = 92.1°; corresponding value in **2Rb₂**·(DME)₃: -93.2°, **2Cs₂**·(DME)₃: 86.7°) leads to a closer approach of the boryl substituents as compared to **2Na₂**·(DME)₃ (C(11)-COG(1)-COG(2)-C(21) = -135.4°) and **2Li₂**·(DME)₂ (C(11)-COG(1)-COG(2)-C(21) = 178.8°). Moreover, the pyrazolyl substituents now adopt bridging positions between two alkali metal ions M(1) and M(2). In the case of **2K₂**·(DME)₃ and **2Rb₂**·(DME)₃, one pyrazolyl bridge is roughly symmetric (cf. B(1)-N(11)-N(12)-K(1) = -66.0(4), B(1)-N(11)-N(12)-K(2) = 47.3(4); B(1)-N(11)-N(12)-Rb(1) = 68.3(13), B(1)-N(11)-N(12)-Rb(2) = -43.9(15)), while the other pyrazolyl ring binds in a π,σ-fashion to the two alkali metal ions (cf. B(2)-N(21)-N(22)-

K(1*) = -86.3(3), B(2)-N(21)-N(22)-K(2*) = 10.1(6); B(2)-N(21)-N(22)-Rb($1^{\#}$) = 86.2(11), B(2)-N(21)-N(22)-Rb($2^{\#}$) = -11.4(18)). The latter coordination mode is also apparent in **2Cs₂**·(DME)₃ (B(1)-N(11)-N(12)-Cs(1) = -90.3(3), B(1)-N(11)-N(12)-Cs(2) = 12.0(7)). In addition to the pyrazolyl moieties, M(1) is bonded to one DME molecule and two cyclopentadienyl rings, whereas the coordination sphere of M(2) is completed by two DME ligands. The distances between M(1) and the geometric centers of the neighboring C_5H_4 ligands are 3.228 Å / 3.298 Å (K(1)), 3.265 Å / 3.285 Å (Rb(1)), and 3.283 Å / 3.283 Å (Cs(1)). Apart from **2K₂**·(DME)₃ there is only one example of an η^5-ferrocene-K^+ complex known in the literature, namely $[K(ferrocene)_2(toluene)_2]^+[Mg(HMDS)_3]^-$ (HMDS = hexamethyldisilazide).[26] Here, the cationic moiety consists of a potassium ion coordinated by the centroids of two toluene π systems and two ferrocenyl cyclopentadienyl rings in a distorted-tetrahedral geometry with a bond angle COG(FcH(1))-K^+-COG(FcH(2)) of 106.08° (FcH = ferrocene; cf. COG(FcH(1))-Na^+-COG(FcH(2) in the bent polymer **2Na₂**·(DME)₃ = 132.0°). The average distance K^+···COG(FcH) in $[K(ferrocene)_2(toluene)_2]^+$ equals to 2.964 Å, 0.3 Å (about 10 %) shorter than the corresponding value in **2K₂**·(DME)₃ (3.263 Å) which more closely approaches the K^+···COG(C_6H_5) distance of $[K(ferrocene)_2(toluene)_2]^+$ (3.143 Å). Several reasons can be suggested for the difference in the K^+···ferrocene bond lengths of $[K(ferrocene)_2(toluene)_2]^+$ and **2K₂**·(DME)₃: (i) the $B(Me)_2pz$ sidearm may not be perfectly adjusted to the geometric requirements of the aggregate, (ii) the bulky DME molecule at K(1) can be expected to push the ferrocenylene moieties away from the alkali metal ion, (iii) the oxygen- and nitrogen donors may lower the Lewis acidity of K^+ to such an extent that the K^+···ferrocene π interaction is weakened, and (iv) in contrast to $[K(ferrocene)_2(toluene)_2]^+$, which features only one K^+ ion bonded to the ferrocene molecule, two potassium ions have to share the electron density provided by the ferrocenylene fragment in **2K₂**·(DME)₃.

As in the case of **2M₂**·(DME)₃ (M^+ = Na^+, K^+, Rb^+, Cs^+), polymeric aggregates are observed for **2Na₂**·(THF)₄ (orthorhombic, *Pbcn*), **2K₂**·(THF)₄ (monoclinic, *P*2₁/*n*), and **2Rb₂**·(THF)₄ (monoclinic, $P2_1/n$) in the solid state. Because of the similarity of all three structures, only **2Na$_2$**·(THF)$_4$ is plotted in Figure 6 (selected bond lengths, angles and dihedral angles of **2Na$_2$**·(THF)$_4$, **2K$_2$**·(THF)$_4$, and **2Rb$_2$**·(THF)$_4$ are given in the caption). In contrast to **2K$_2$**·(DME)$_3$ with its columnar structure, **2Na$_2$**·(THF)$_4$, **2K$_2$**·(THF)$_4$, and **2Rb$_2$**·(THF)$_4$ are arranged in a stepped formation. Much alike **2K$_2$**·(DME)$_3$, each pyrazolyl substituent bridges two alkali metal ions. Unlike **2K$_2$**·(DME)$_3$, these ions are now symmetry-related and coordinated to two THF molecules. The most important difference in the crystal structures of **2M$_2$**·(DME)$_3$ (M^+ = Na^+, K^+, Rb^+, Cs^+) on one hand and **2Na$_2$**·(THF)$_4$, **2K$_2$**·(THF)$_4$, and **2Rb$_2$**·(THF)$_4$ on the other arise from the way in which the M^+ ions are coordinated to the ferrocene fragments. The THF complexes have each alkali metal ion bonded to *one* cyclopentadienyl ring only, which is reminiscent of the structural motif exhibited by the trimetallic aggregate **2Li$_2$**·(DME)$_2$ (Figure 3). In the DME complexes of the higher homologues, however, all M^+ ions are located in close proximity to *two* cyclopentadienyl rings. Moreover, the alkali metal ions in **2Na$_2$**·(THF)$_4$, **2K$_2$**·(THF)$_4$, and **2Rb$_2$**·(THF)$_4$ are shifted away from the center of the C_5H_4 ring towards the boryl substituent which results in large differences between the individual $M^+\cdots$Cp(carbon) distances. The shortest contacts observed, Na(1)-C(15$^\#$) = 2.848(3) Å, K(1)-C(12) = 2.953(4) Å, and Rb(1)-C(12) = 3.156(12) Å), tend to be closer than the average $M^+\cdots$Cp(carbon) distances in the corresponding complexes **2Na$_2$**·(DME)$_3$ (2.84(9) Å), **2K$_2$**·(DME)$_3$ (3.48(9) Å), and **2Rb$_2$**·(DME)$_3$ (3.50(4) Å).

DFT Calculations: So far, we have gathered evidence that the ligand [**2**]$^{2-}$ is well-suited for the generation of low-dimensional solids featuring stacks of alternating Fe(II)- and alkali metal cations sandwiched between cyclopentadienyl rings. In the next step it has to be investigated whether this structural motif is merely due to crystal packing effects or whether alkali metal cation-ferrocene π interactions do play a major role. We therefore performed DFT calculations on the model complexes **5M**, **6M$_2$** (M^+ = Li^+, Na^+, K^+, Rb^+; Figure 7), and

7M ($M^+ = Li^+, Na^+, K^+$; Figure 7) to get insight into the gas-phase geometries and binding enthalpies of alkali metal cation-η^5(ferrocene) complexes not perturbed by negatively charged substituents or the presence of adjutant sidearms. However, before elaborating further our effort to obtain theoretical data on cation-*ferrocene* π interactions, some discussion is in order for the corresponding cation-*benzene* π complexes, which have been studied in detail both by theoretical means[27, 28] and experimentally by various gas-phase techniques[27, 29-31].

Let us first consider the energy optimized structures of $M^+(C_6H_6)$ (**3M**, C_{6v}, $M^+ = Li^+, Na^+, K^+, Rb^+, Cs^+$; Figure 7) and $M^+(C_6H_6)_2$ (**4M**, D_{6h}, $M^+ = Li^+, Na^+, K^+, Rb^+, Cs^+$; Figure 7) and compare them with the geometries obtained by X-ray crystal structure analysis of **2M₂**·(DME)$_x$ ($M^+ = Li^+, Na^+, K^+, Rb^+, Cs^+$; x = 2, 3) as well as by our DFT calculations on the respective model complexes (Figure 7). The most revealing structural feature, the $M^+\cdots$COG(benzene) and $M^+\cdots$COG(cyclopentadienyl) distances, are compiled in Table 2. The $M^+\cdots$COG(benzene) contacts in **3M**, as calculated by Feller[28] and Armentrout[27] (Table 2), are consistently smaller than the sum of the half-thickness of benzene (1.7 Å)[3] and the ionic radii[6] of Li^+ (0.60 Å + 1.7 Å = 2.30 Å), Na^+ (0.95 Å + 1.7 Å = 2.65 Å), K^+ (1.33 Å + 1.7 Å = 3.03 Å), Rb^+ (1.48 Å + 1.7 Å = 3.18 Å), Cs^+ (1.66 Å + 1.7 Å = 3.36 Å; note that the values employed for these calculations are at the lower limit of the alkali metal ion radii given by Shannon[32]). The difference between the $M^+\cdots$COG(benzene) distances (cf. the first two columns of Table 2) and the van der Waals contacts of M^+ and benzene (cf. the third column of Table 2) decreases monotonously from **3Li** to **3Cs**. This structural feature indicates the M^+-π interaction to be disproportionately larger for the smaller alkali metal cations. The $M^+\cdots$COG(benzene) distances in the monobenzene complexes **3M** and in the dibenzene sandwich compounds **4M** are very similar.[27] The largest deviations are found for **3Li** (1.842 Å) / **4Li** (1.917 Å), which show a 4% increase of the $M^+\cdots$COG(benzene) distance upon complexation of the second benzene ring, and **3Rb** (3.165 Å) / **4Rb** (3.105 Å), where a 2% decrease is observed. In the case of **4Li-4K**, the somewhat larger $M^+\cdots$COG(benzene) contacts may be due to intramolecular steric repulsion of the two benzene rings which becomes smaller with increasing size of the central metal ion. Michl et al. recently determined the crystal structures of $[M(benzene)_2]^+[CB_{11}Me_{12}]^-$ ($M^+ = Na^+, K^+, Rb^+, Cs^+$).[33] The crystals containing K^+, Rb^+, and Cs^+ are isomorphous with the metal cations being apically η^6-coordinated to two disordered, symmetry equivalent, nearly parallel benzene molecules in an essentially linear arrangement ($COG\text{-}M^+\text{-}COG = 180 \pm 3°$) with $M^+\cdots$COG(benzene) distances of 3.14 Å (K^+), 3.19 Å (Rb^+), and 3.28 Å (Cs^+). Even though the structures of $[M(benzene)_2]^+$ in the condensed phase are influenced by the presence of the counterions as well as by crystal packing forces, the measured data are in reasonably good agreement with the $M^+\cdots$COG(benzene) distances calculated for **4M** (K^+: 2.832 / 2.917 Å, Rb^+: 3.105 Å, Cs^+: 3.392 Å; Table 2). Interestingly, compound $[Na(benzene)_2]^+[CB_{11}Me_{12}]^-$ adopts a different geometry in the solid state since it is coordinated to two benzene molecules in a tilted-sandwich arrangement (dihedral angle between the benzene rings: 55.9°) with distances $Na^+\cdots$COG(benzene) of 2.69 Å and 2.71 Å (cf. **4Na**: 2.421 Å). A similar structural motif as in $[Na(benzene)_2]^+[CB_{11}Me_{12}]^-$ has also been observed in the compound $[Na(toluene)_2]^+[Al(SiMe_3)_4]^-$ (dihedral angle between the toluene ligands: 61.6°).[34] Other useful data for comparison are provided by the X-ray crystal structure analyses of the salts $K[B(C_6H_5)_4]$[35] and $Rb[B(C_6H_5)_4]$[36], since they give insight into π interactions between alkali metal cations and an arene equipped with an anionic borate substituent reminiscent to the borate sidearm of $[\mathbf{2}]^{2-}$. In both crystal structures, the respective alkali metal ion is embedded between two phenyl rings of the tetraphenyl borate anion at a distance of $M^+\cdots COG(C_6H_5)$ = 2.986 Å (average value K^+) and 3.060 Å (average value Rb^+).

Turning to the alkali metal cation-η^5(ferrocene) compounds **5M** (C_{5v}), we find that the π contacts calculated on the B3LYP//DZ level of theory tend to be slightly larger than the values obtained with the same hybrid functional and a basis set of triple-ζ quality (cf. Table 2). Moreover, the $M^+\cdots$COG(benzene) distances in **3M** and the $M^+\cdots$COG(cyclopentadienyl) distances in **5M** are pretty much alike. In this context, it is important to compare the theoretically obtained data for **3M** and **5M** with the experimentally determined values in Honeyman's cation [K(ferrocene)$_2$(toluene)$_2$]$^{+26}$, featuring $K^+\cdots\pi$ interactions to ferrocene ($M^+\cdots$COG(cyclopentadienyl): mean value = 2.964 Å) and toluene ($M^+\cdots$COG(C_6H_5): mean value = 3.143 Å) in the same molecule. For the K^+-ferrocene fragment, the difference between the theoretical and experimental results is only 0.131 Å (ca. 5%; DZ basis set) and 0.161 Å (ca. 6%; TZ basis set). Larger discrepancies are observed for the K^+-toluene fragment [between 0.247 Å (ca. 9%) and 0.357 Å (ca. 13%) depending on the level of theory applied]. Given the fact, that any cation-π interaction in [K(ferrocene)$_2$(toluene)$_2$]$^+$ is certainly hampered by steric crowding absent in the model complexes **3M** and **5M**, the larger experimental distances are not surprising [Note that the toluene ligands coordinate to K^+ in a limited η^3 manner which leads to a larger $M^+\cdots$COG(C_6H_5) distance even though the potassium ion approaches C_{meta} (average distance: 3.331 Å) and C_{para} (average distance: 3.247 Å) of the toluene ring rather closely]. All in all we note a pleasingly good agreement between theory and experiment which leads to the conclusion that the level of theory applied for the description of our alkali metal ion-η^5(ferrocene) interactions is adequate and leads to reliable structure predictions.

As in **3M**, the $M^+\cdots$COG(cyclopentadienyl) distances in **5M** are smaller than the calculated van der Waals contacts, and this feature is most pronounced for the smaller alkali metal ions (we assume that the half thickness of benzene equals the half thickness of the Cp ring in ferrocene). Coordination of a second ferrocene molecule to the same alkali metal ion (**7M**; D_{5h}) causes a small increase in the $M^+\cdots$COG(cyclopentadienyl) contacts of about 7% (**7Li**), 3% (**7Na**), and 2% (**7K**; Table 2) as has already been observed upon going from **3Li** – **3K** to **4Li** – **4K**. $M^+\cdots$COG(cyclopentadienyl) distances do also increase upon addition of a second metal ion to the same ferrocene moiety (cf. **6M$_2$**; D_{5h}). In this case, however, the degree of bond stretching is rather independent from the nature of the alkali metal ion (i.e. 8-10% upon going from **5M** to **$6M_2$**).

The molecular structure of the experimentally accessible system **$2Li_2$**·$(DME)_2$ is best compared with the hypothetical gas-phase aggregate **$6Li_2$**. The measured $Li^+\cdots$COG(cyclopentadienyl) distance of 2.29 Å (Table 2) is significantly longer than the corresponding value calculated for **$6Li_2$** (2.018 Å, DZ basis set; 1.971, TZ basis set). In **$2Na_2$**·$(DME)_3$, the experimentally obtained $Na^+\cdots$COG(cyclopentadienyl) contact of 2.576 Å (Table 2) fits nicely to the corresponding distances in **$6Na_2$** (2.506 Å, DZ basis set; 2.518, TZ basis set) and **7Na** (2.427 Å; note that the dihedral angle $Cp(Fc^1)//Cp(Fc^2)$ is 0° in the case of **7Na**, but 48.0° in **$2Na_2$**·$(DME)_3$, which is, however, not likely to have a large impact on the $Na^+\cdots$COG(cyclopentadienyl) distances since alkali metal ions are essentially featureless spheres). The potassium ions in **$2K_2$**·$(DME)_3$ ($K^+\cdots$COG(cyclopentadienyl) = 3.263 Å; Table 2) are slightly further apart from the ferrocene cyclopentadienyl rings (7-9% deviation) than in the model complexes **$6K_2$** (3.060 / 3.030 Å) and **7K** (2.903 Å). In contrast, somewhat shorter $Rb^+\cdots$COG(cyclopentadienyl) contacts are found in **$2Rb_2$**·$(DME)_3$ (3.275 Å) as compared to **$6Rb_2$** (3.478 Å). Apart from these subtle differences, both the absolute experimental values and the general trends upon variation of the alkali metal cation are very well reproduced by density functional theory, especially if one takes into account that gas-phase structures are compared with condensed-phase structures.

In order to get insight into the effects of Lewis-base coordination on the structural properties of $M^+\cdots\eta^5$(ferrocene) complexes, we have calculated the systems **8Li** and **9Li** (Figure 8). As to be expected, the $Li^+\cdots$COG(cyclopentadienyl) distance increases substantially upon going from **5Li** (1.870 Å, DZ basis set; 1.837 Å, TZ basis set) to **8Li** (2.915 Å, DZ basis set) and **9Li** (2.715 Å, DZ basis set). Moreover, the lithium ion is shifted away from the center of the cyclopentadienyl ring (**8Li**: Li-COG-Fe = 149.7°; **9Li**: Li-COG-Fe = 147.3°).

Binding enthalpies of **3M** ($M^+ = Li^+, Na^+, K^+, Rb^+, Cs^+$) at 0 K ($\Delta H_0$) in the complete basis set limit[28] are compiled in Table 3. These values agree well with experimental data determined by collision induced dissociation (CID) of **3M** with Xe in a guided ion beam mass spectrometer[27] (Table 3, second column). Experimental bond dissociation enthalpies for the respective bisbenzene complexes **4M** are also available[27] (Table 3, third column). The investigations on alkali metal-benzene complexes can be summarized as follows: (i) Bond dissociation enthalpies M^+-C_6H_6 as well as $(C_6H_6)M^+$-C_6H_6 decrease monotonically with increasing size of M^+. (ii) CID experiments on **4M** indicate that the benzene rings are lost sequentially. The second benzene ring is generally less tightly bound to the metal ion than the first benzene ligand (Table 3), however, the difference between the first and the second dissociation enthalpy decreases along the sequence **4Li/3Li** – **4Cs/3Cs**. (iii) Comparisons drawn between the bond dissociation enthalpies of **3M**/**4M** on the one hand and alkali metal-water complexes $M^+(H_2O)_x$ (x = 1, 2) on the other reveal comparable ΔH_0 values when $M^+ = Li^+, Na^+, K^+$ and larger bond dissociation enthalpies for **3M** / **4M** when $M^+ = Rb^+, Cs^+$.

Bond dissociation enthalpies for the alkali metal-ferrocene aggregates **5M** follow the same general trend as described for the alkali metal-benzene complexes **3M** (Table 3). By far the most pronounced interaction is thus predicted for **5Li** (ΔH_0 = -44.0 kcal/mol, DZ basis set; ΔH_0 = -45.3 kcal/mol, TZ basis set), while Rb^+ bonding to ferrocene is considerably weaker (ΔH_0 = -14.8 kcal/mol, DZ basis set). In the case of **5Li** and **5Na**, the bond dissociation enthalpies are significantly higher than in the corresponding benzene complexes **3Li** and **3Na** which indicates ferrocene to be superior over benzene as ligand to these alkali metal ions. Addition of a second ferrocene molecule to **5M** is exothermic by –27.7 kcal/mol, –21.8 kcal/mol, and –15.9 kcal/mol for Li^+, Na^+, and K^+, respectively. As in the case of the benzene aggregates, the second ferrocene ligand generally appears to be less strongly bound to the alkali metal ion than the first one. The reaction of a second alkali metal ion M^+ with **5M** to give **6M₂** is strongly endothermic (ΔH_0 = 26.4 kcal/mol, 27.9 kcal/mol, 28.5 kcal/mol, and

24.7 kcal/mol for **$6Li_2$**, **$6Na_2$**, **$6K_2$**, and **$6Rb_2$**, respectively; DZ basis set). One obvious reason is that introduction of the additional positive charge leads to Coulomb repulsion within the molecule. Since the ferrocene-based ligand [**2**]$^{2-}$ is equipped with two anionic substituents, destabilization of the aggregates **$6M_2$** due to unfavourable electrostatic interactions is probably not a major issue in this system.

So far, it became evident that both the structural characteristics (e.g. $M^+\cdots$COG distances) and the thermodynamic features (i.e. ΔH_0 values) of $M^+\cdots$(benzene) and $M^+\cdots$(ferrocene) complexes resemble each other. The question thus arises, whether the nature of the interaction of an alkali metal ion with benzene and the ferrocene cyclopentadienyl ring is also similar. The potential energy curves of **5Li–5Rb** together with those of **3Li** and **3Rb** calculated at the same level of theory are plotted in Figure 9. The largest differences between the shape of the potential energy surfaces of (i) **3Li** / **5Li** and (ii) **3Rb** / **5Rb** occur at longer $M^+\cdots$COG distances, where the $M^+\cdots\eta^6$(benzene) potential appears to be softer (cf. to stretch the optimal $Li^+\cdots$COG(cyclopentadienyl) contact by 0.5 Å, an energy input of 8.7 kcal/mol is required, 3.5 kcal/mol more than in the case of $Li^+\cdots$COG(benzene)).

It is widely accepted that, to first order, the binding sequence of Li^+-Cs^+ to benzene represents a classical electrostatic trend and that the cation interacts with the large permanent quadrupole moment of the aromatic.[2] As a rough estimate for **3Na**, 60% of the binding is due to electrostatics.[37] Even though a purely electrostatic model is thus not valid to explain the *absolute* values of cation-π interactions, *variations* in ion-binding energies across a series of different π donor molecules are faithfully mirrored by the electrostatic term.[2] Interestingly, the well-known aromatic substituent effects derived from studies of electrophilic aromatic substitution reactions (Hammett parameters) fail to provide a reliable tool for the prediction of trends in cation-π interactions. For example, even though phenol is much more prone to electrophilic attack than benzene, it turns out not to be superior when it comes to alkali metal ion binding.[2] Dougherty managed to rationalize differences in the degree of cation π binding among selected aromatics by an inspection of their electrostatic potential surfaces (EPS): The more negative the maximum electrostatic potential above the center of the aromatic, the stronger the $M^+\cdots$arene interaction.[7] We therefore calculated the EPS of ferrocene and benzene (B3LYP, TZ basis set) in order to see whether the higher ΔH_0 values obtained for compounds **5M** as compared to **3M** can be assigned to differences in the electrostatic potential of the two ligands. The EPSs of ferrocene and benzene are shown in Figure 10. There is a clear similarity between the two, but ferrocene has more negative charge localized at the center of the ring. The largest density at the given contour value, calculated at the B3LYP/TZ level of theory, corresponds to -17.3 kcal/mol for ferrocene and -14.6 kcal/mol for benzene. For the fragment $\{[Fe(C_5H_5)_2]_2Ga\}^+$, our previous DFT calculations[15] indicated a transfer of 0.4 electrons into the gallium 4p orbitals. In contrast, the natural charges[38, 39] of the alkali metal ions in **5M** and **7M** are uniformly close to +1 with the largest deviations being found for **5Li** (0.97) and **7Li** (0.93). This population analysis thus adds further support to the proposition that the interaction between M^+ and ferrocene is mainly electrostatic. However, the nature of the bonding will most likely change when the alkali metal ions are replaced by transition metal ions, because now d orbital contributions may lead to a more covalent interaction.

Conclusions

The alkali metal salts **2M₂** ($M^+ = Li^+, Na^+, K^+, Rb^+, Cs^+$) of the ditopic mono(pyrazol-1-yl)borate ligand $[1,1'\text{-fc}(BMe_2pz)_2]^{2-}$, $[\mathbf{2}]^{2-}$, crystallize from dimethoxyethane as multiple-decker sandwich complexes $\mathbf{2M_2}\cdot(DME)_x$ with alkali metal ions bound to the π faces of the ferrocene cyclopentadienyl rings in an η^5 manner. X-ray crystallographic analysis of $\mathbf{2Li_2}\cdot(DME)_2$ revealed discrete trinuclear complexes in which each lithium ion interacts with only one cyclopentadienyl ring. In contrast, infinite zig-zag chains are formed by

$2Na_2$ $\cdot$(DME)$_3$ in the solid state. Here, each sodium ion bridges the cyclopentadienyl rings of two different ferrocene moieties whereas each cyclopentadienyl ring is coordinated by Fe(II) at one π face and by Na^+ at the other. The polyanionic charge of the macromolecular backbone is counterbalanced by $[Na(DME)_3]^+$ complexes. **$2K_2$**$\cdot$(DME)$_3$, **$2Rb_2$**$\cdot$(DME)$_3$, and **$2Cs_2$**$\cdot$(DME)$_3$ establish very similar crystal structures consisting of linear columns $[\text{-CpR-Fe-CpR-M}^+\text{-CpR-Fe-CpR-M}^+\text{-}]_\infty$ (R = $[\text{-BMe}_2\text{pz}]^-$). We speculate that one reason for the different solid state structures established by **$2Li_2$**$\cdot$(DME)$_2$, **$2Na_2$**$\cdot$(DME)$_3$, and **$2K_2$**$\cdot$(DME)$_3$ lies in the ionic radii of the constituent alkali metal ions. When in a linear aggregate of the form CpFeCp$\cdots K^+\cdots$CpFeCp the potassium ion is replaced by a sodium ion, the distance between the cyclopentadienyl rings of the two coplanar coordinating ferrocene fragments is reduced by about 0.95 Å [cf. Table 2: calculated $M^+\cdots$COG distances in **7K** (2.903 Å) and **7Na** (2.427 Å); COG: centroid of the cyclopentadienyl ring]. Due to the presence of the $[\text{-BMe}_2\text{pz}]^-$ substituents in the real system **$2M_2$**$\cdot$(DME)$_3$, a substitution of Na^+ for K^+ would thus lead to severe steric congestion between adjacent $[\mathbf{2}]^{2-}$ ligands. This problem can be overcome when the coordination polymer is bent which allows more space for the pyrazolyl rings but still maintains two energetically favourable cation-π bonds *per* sodium ion. In the case of **$2Li_2$**$\cdot$(DME)$_2$, the yet smaller radius of the lithium ion is no longer compatible with the simultaneous coordination of two ligands $[\mathbf{2}]^{2-}$ so that only a trinuclear aggregate is formed [cf. Table 2: calculated $M^+\cdots$COG distances in **3Li** (1.842 Å) and **7Li** (1.995 Å)]. Thus, the structural characteristics of **$2Li_2$**$\cdot$(DME)$_2$, **$2Na_2$**$\cdot$(DME)$_3$, and **$2K_2$**$\cdot$(DME)$_3$ provide some experimental evidence that cation-π interactions are operative in these compounds because otherwise the M^+ radii and the $M^+\cdots$COG distances would not be structure-determining factors.

DFT calculations on $M^+\cdots\eta^5$(ferrocene) complexes **5M** in the gas phase give binding enthalpies of ΔH_0 = -44.0 kcal mol^{-1}, -30.0 kcal mol^{-1}, -20.1 kcal mol^{-1}, and -14.8 kcal mol^{-1} for **5Li**, **5Na**, **5K**, and **5Rb**, respectively (B3LYP, double-ζ basis set; Figure 7, Table 3). In the case of **5Li** and **5Na**, these enthalpies are significantly larger than the values calculated for the corresponding $M^{+}\cdots\eta^{6}$(benzene) complexes **3Li** (ΔH_0 = -36.1 kcal mol^{-1}) and **3Na** (ΔH_0 = -24.2 kcal mol^{-1}; Figure 7, Table 3).[28] A comparison of **5K** (ΔH_0 = -20.1 kcal mol^{-1}) / **3K** (ΔH_0 = -20.0 kcal mol^{-1})[28] and **5Rb** (ΔH_0 = -14.8 kcal) / **3Rb** (ΔH_0 = -16.4 kcal mol^{-1})[28], however, reveals cation-π interactions of similar strength in the ferrocene and benzene aggregates (note that the calculated binding enthalpies of **3Li** – **3Rb** are in nice agreement with experimentally determined ΔH_0 values[27] for these complexes). We therefore conclude that ferrocene is not only able to establish strong $M^{+}\cdots\eta^{5}$(cyclopentadienyl) interactions to alkali metal ions but that to Li^{+} and Na^{+} it presents an even more attractive π-face than benzene. This view is further supported by an inspection of the electrostatic potential surfaces of ferrocene and benzene, since the strongest attraction of a point-like +1 probe charge at the given contour value is -17.3 kcal/mol for ferrocene and -14.6 kcal/mol for benzene (B3LYP, triple-ζ basis set, Figure 10). Looking at the mean experimental $M^{+}\cdots$COG distances in **2M$_2$**·(DME)$_x$ (Li^{+}: 2.29 Å, Na^{+}: 2.576 Å, K^{+}: 3.263 Å, Rb^{+}: 3.275 Å, Cs^{+}: 3.283 Å) and the corresponding calculated distances in the model complexes **5M** (Li^{+}: 1.870 Å, Na^{+}: 2.350 Å, K^{+}: 2.833 Å, Rb^{+}: 3.147 Å), we find the $M^{+}\cdots$COG contacts in the real compounds to be longer. However, these bond stretches do not correspond to large energies. For example, even in the most strongly bound complex **5Li** an energy input of only 7.4 kcal mol^{-1} is required to increase the $Li^{+}\cdots$COG distance from the optimal (1.870 Å) to the experimentally determined value (2.29 Å). It is thus apparent that the ligand system [**2**]$^{2-}$ is well-suited for the promotion of π-interactions between metal atoms and the ferrocene cyclopentadienyl ring.

Work is currently in progress to employ [**2**]$^{2-}$ for the synthesis of multiple-decker sandwich complexes consisting of ferrocene and transition metal atoms. While metal binding in **2M$_2$**·(DME)$_x$ is largely due to electrostatics, a more covalent binding mode may be envisaged if d-block metals are used, which could in turn lead to a more pronounced metal-iron interaction along the polymer backbone.

Experimental Section

General remarks: All reactions and manipulations of air-sensitive compounds were carried out in dry, oxygen-free nitrogen using standard Schlenk ware. Solvents were freshly distilled under argon from Na-benzophenone (diethyl ether, THF, DME) prior to use. NMR: Bruker DPX 400, Bruker DPX 250. ^{11}B NMR spectra are reported relative to external $BF_3 \cdot Et_2O$, ^{7}Li NMR spectra are reported relative to external LiCl in D_2O. Unless stated otherwise, all NMR spectra were run at ambient temperature; abbreviations: s = singlet, d = doublet, vtr = virtual triplet, br = broad, n.r. = multiplet expected in the NMR spectrum but not resolved, n.o. = signal not observed. Compound **1**[40] was synthesized according to a literature procedure.

Preparation of 2Li₂: A slurry of Lipz (0.34 g, 4.60 mmol) in Et_2O (15 ml) was added with stirring at –78 °C via a dropping funnel to **1** (0.61 g, 2.30 mmol) in Et_2O (15 ml). The mixture was slowly warmed to room temperature, whereupon a yellow-orange precipitate of $\mathbf{2Li_2}\cdot(Et_2O)_4$ formed (the amount of ether solvate molecules was determined by integration of the ^{1}H NMR spectrum in d_8-THF). After filtration, the mother liquor was stored at 5 °C overnight to yield a second crop. Yield of $\mathbf{2Li_2}\cdot(Et_2O)_4$: 1.52 g (93 %). X-ray quality crystals of $\mathbf{2Li_2}\cdot(DME)_2$ were obtained after a saturated solution of $\mathbf{2Li_2}\cdot(Et_2O)_4$ in DME had been stored at 5 °C over a period of several days. ^{11}B-NMR (128.4 MHz, d_8-THF): δ -9.0 ($h_{1/2}$ = 300 Hz). ^{1}H-NMR (400.1 MHz, d_8-THF): δ 0.11 (s, 12H, CH_3), 4.05, 4.19 (2 × vtr, 2 × 4H, $^{3}J_{HH} = {}^{4}J_{HH}$ = 1.6 Hz, C_5H_4), 5.95 (vtr, 2H, $^{3}J_{HH}$ = 1.9 Hz, pz-H4), 7.01, 7.48 (2 × d, 2 × 2H, $^{3}J_{HH}$ = 1.7, 2.0 Hz, pz-H3,5). ^{13}C-NMR (100.6 MHz, d_8-THF): δ 12.8 (n.r., CH_3), 71.0, 72.2 (C_5H_4), 102.8 (pz-C4), 131.9, 135.4 (pz-C3,5), n.o. (C_5H_4-C*ipso*). ^{7}Li-NMR (155.5 MHz, d_8-THF): δ –1.30 ($h_{1/2}$ = 37 Hz). Anal. Calcd for $\mathbf{2Li_2}\cdot(DME)_2$, $C_{28}H_{46}B_2FeLi_2N_4O_4$, (594.04): C, 56.61; H, 7.81; N, 9.43. Found : C, 56.33; H, 7.72; N, 9.09.

Preparation of 2Na₂: A slurry of Napz (0.24 g, 2.70 mmol) in Et_2O (20 ml) was added with stirring via a dropping funnel at –78 °C to **1** (0.36 g, 1.35 mmol) in Et_2O (20 ml). The mixture was slowly warmed to room temperature, whereupon a yellow-orange precipitate formed which was isolated by filtration. The microcrystalline solid was dissolved in THF (20 ml), the solution stirred for 24 hours and evaporated to dryness in vacuo to substitute THF for Et_2O in the coordination sphere of the Na^+ ions. Yield of **2Na₂**·(THF)₄: 0.94 g (95 %). X-ray quality crystals of **2Na₂**·(THF)₄ formed from a saturated THF solution at -30 °C over a period of several days. X-ray quality crystals of **2Na₂**·(DME)₃ formed from a saturated solution of **2Na₂**·(THF)₄ in DME at -30 °C over a period of several days.

^{11}B-NMR (128.4 MHz, d_8-THF): δ -9.1 ($h_{1/2}$ = 250 Hz). ^{1}H-NMR (400.1 MHz, d_8-THF): δ 0.03 (s, 12H, CH_3), 3.86, 3.98 (2 × n.r., 2 × 4H, C_5H_4), 5.84 (n.r., 2H, pz-H4), 6.99, 7.44 (2 × n.r., 2 × 2H, pz-H3,5). ^{13}C-NMR (100.6 MHz, d_8-THF): δ 13.2 (br, CH_3), 69.3, 72.0 (C_5H_4), 101.9 (pz-C4), 131.7, 136.2 (pz-C3,5), n.o. (C_5H_4-C*ipso*). Anal. Calcd for **2Na₂**·(DME)₃, $C_{32}H_{56}B_2FeN_4Na_2O_6$, (716.26): C, 53.66; H, 7.88; N, 7.82. Found : C, 53.38; H, 7.72; N, 7.49.

Preparation of 2K₂: The compound was synthesized similar to **2Na₂** from Kpz (0.80 g, 7.54 mmol) and **1** (1.00 g, 3.76 mmol) in Et_2O (60 ml). Yield of **2K₂**·(THF)₄: 2.65 g (92 %). Recrystallization of **2K₂**·(THF)₄ from hot THF afforded orange blocks suitable for single crystal X-ray diffraction. To obtain X-ray quality crystals of **2K₂**·(DME)₃, **2K₂**·(THF)₄ was dissolved in DME at 40 °C in an ultrasonic bath and the resulting clear yellow-orange solution slowly concentrated in vacuo. ^{11}B-NMR (128.4 MHz, d_8-THF): δ -9.4 ($h_{1/2}$ = 250 Hz). ^{1}H-NMR (400.1 MHz, d_8-THF): δ 0.11 (s, 12H, CH_3), 3.96, 4.00 (2 × vtr, 2 × 4H, $^3J_{HH}$ = $^4J_{HH}$ = 1.5 Hz, C_5H_4), 5.85 (vtr, 2H, $^3J_{HH}$ = 1.4 Hz, pz-H4), 7.06, 7.48 (n.r., d, 2 × 2H, $^3J_{HH}$ = 1.9 Hz, pz-H3,5). ^{13}C-NMR (62.9 MHz, d_8-THF): δ 13.2 (br, CH_3), 69.2, 73.2 (C_5H_4), 101.5 (pz-C4), 131.2, 136.1 (pz-C3,5), n.o. (C_5H_4-C*ipso*). Anal. Calcd for **2K₂**·(DME)₃,

$C_{32}H_{56}B_2FeK_2N_4O_6$, (748.48): C, 51.35; H, 7.54; N, 7.49. Found : C, 51.26; H, 7.51; N, 7.19.

Preparation of 2Rb₂: The compound was synthesized similar to **2Na₂** from Rbpz (1.00 g, 6.56 mmol) and **1** (0.87 g, 3.28 mmol) in Et_2O (50 ml). Yield of **2Rb₂**·$(THF)_4$: 2.64 g (94 %). X-ray quality crystals of **2Rb₂**·$(THF)_4$ formed from a saturated THF solution at 5 °C over a period of several days. **2Rb₂**·$(THF)_4$ was dissolved in DME at 70 °C in an ultrasonic bath. After cooling to room temperature, the clear yellow-orange solution was slowly concentrated in vacuo, whereupon orange platelets of **2Rb₂**·$(DME)_3$ formed.
^{11}B-NMR (128.4 MHz, d_8-THF): δ -7.6 ($h_{1/2}$ = 370 Hz). ^{1}H-NMR (400.1 MHz, d_8-THF): δ 0.14 (s, 12H, CH_3), 3.95 (n.r., 8H, C_5H_4), 5.87 (vtr, 2H, $^{3}J_{HH}$ = 1.6 Hz, pz-H4), 7.15, 7.49 (n.r., d, 2 × 2H, $^{3}J_{HH}$ = 1.6 Hz, pz-H3,5). ^{13}C-NMR (100.6 MHz, d_8-THF): δ 12.9 (br, CH_3), 69.4, 73.1 (C_5H_4), 99.7 (br, C_5H_4-C*ipso*), 101.0 (pz-C4), 130.5, 135.7 (pz-C3,5). Anal. Calcd for **2Rb₂**·$(DME)_3$, $C_{32}H_{56}B_2FeN_4O_6Rb_2$, (841.22): C, 45.69; H, 6.71; N, 6.66. Found : C, 45.45; H, 6.59; N, 6.30.

Preparation of 2Cs₂: The compound was synthesized similar to **2Na₂** from Cspz (0.78 g, 3.90 mmol) and **1** (0.52 g, 1.95 mmol) in Et_2O (45 ml). Since the crude product is only poorly soluble in THF, it was recrystallized from DME at 40 °C in an ultrasonic bath. Yield of **2Cs₂**·$(DME)_3$: 1.75 g (96 %). ^{11}B-NMR (128.4 MHz, d_8-THF): δ -7.6 ($h_{1/2}$ = 210 Hz). ^{1}H-NMR (400.1 MHz, d_8-THF): δ 0.17 (s, 12H, CH_3), 3.94, 3.99 (2 × vtr, 2 × 4H, $^{3}J_{HH} = {}^{4}J_{HH}$ = 1.6 Hz, C_5H_4), 5.85 (vtr, 2H, $^{3}J_{HH}$ = 1.5 Hz, pz-H4), 7.13, 7.48 (n.r., d, 2 × 2H, $^{3}J_{HH}$ = 1.9 Hz, pz-H3,5). ^{13}C-NMR (100.6 MHz, d_8-THF): δ 11.5 (br, CH_3), 70.1, 72.5 (C_5H_4), 100.9 (pz-C4), 130.1, 135.3 (pz-C3,5), n.o. (C_5H_4-C*ipso*). Anal. Calcd for **2Cs₂**·$(DME)_3$,

$C_{32}H_{56}B_2Cs_2FeN_4O_6$, (936.10): C, 41.06; H, 6.03; N, 5.99. Found : C, 40.88; H, 6.10; N, 5.71.

X-ray Crystal Structure Analyses: The data collections for all structures were performed on a STOE IPDS-II two-circle diffractometer with graphite-monochromated MoK_α-radiation ($\lambda = 0.71073$). The structures were solved by direct methods using the program SHELXS[41] and refined by full-matrix least-squares calculations on F^2 using the program SHELXL97[42]. All absorption corrections were performed with the MULABS[43] option in PLATON[44]. All non-H atoms (with the exception of **2Li₂**·(DME)₂; see below) have been refined anisotropically, whereas the H atoms have been treated as riding atoms with their displacement parameters fixed to 1.2 or 1.5 (for methyl groups) of the value of their parent atom. The C atoms of **2Li₂**·(DME)₂ were restrained in a way that their U_{ij} components approximate to isotropic behaviour. B and Li atoms were refined isotropically. The THF rings of **2Rb₂**·(THF)₄ were restrained to have equal bond lengths and angles. CCDC reference numbers: 246210 (**2Li₂**·(DME)₂), 246213 (**2Na₂**·(DME)₃), 246212 (**2K₂**·(DME)₃), 246211 (**2Rb₂**·(DME)₃), 246208 (**2Cs₂**·(DME)₃), 246207 (**2Na₂**·(THF)₄), 246206 (**2K₂**·(THF)₄), 246209 (**2Rb₂**·(THF)₄).

Electrochemistry: Cyclic voltammetry was performed in THF solutions containing $[NBu_4][PF_6]$ (0.1 mol l^{-1}) as the supporting electrolyte. All potential values are reported relative to the FcH/FcH^+ redox couple. The cell for voltammetric studies was designed as detailed in ref.[45]. Voltammetric scans were referenced by addition of a small amount of ferrocene as internal standard at an appropriate time of the experiment.

Computational Details: Calculations were performed using Gaussian 98[46] and 03,[47] program packages. Based on our previous experience with similar systems,[9] we chose the B3LYP hybrid functional[48-50] together with basis sets of double-ζ quality (the DZVP basis set given by Salahub et al.[51, 52] for iron and Pople's 6-31++G** for the rest of the atoms; this basis set combination will be denoted as DZ) to generate educated guesses for starting stationary points and reoptimization with triple-ζ quality basis sets. For iron, the TZVP basis given by Schäfer et al.[53] was employed, supplemented with a diffuse *s* function (with an exponent 0.33 times that of the most diffuse *s* function on the original set), two sets of *p* functions (optimized by Wachters)[54] for the excited states, one set of diffuse pure angular momentum *d* functions (optimized by Hay)[55], and three sets of uncontracted pure angular momentum *f* functions, including both tight and diffuse exponents, as recommended by Ragavachari and Trucks[56]; Pople's 6-311++G(2df,2p) basis was used for the rest of the atoms. This basis set will be hereafter denoted as TZ. As shown below, both basis sets give similar results which compare well with theoretical and experimental values available from other sources. Supported by the good agreement of data obtained at the DZ and TZ level of theory, the DZ basis set was used in the computations of the larger systems and all the Rb containing structures (with the Hay and Watt effective core pseudopotentials for Rb[57]). DFT methods are known to have smaller basis set superposition errors (BSSE) than other theoretical methods like MP2[58]. Thus, combinations of DFT with large polarized basis functions (as the TZ used in the present manuscript) guarantee the BSSE to be negligible[59]. Nevertheless, since a DZ basis set is used in the largest molecules, the BSSE was evaluated for **7Na** (**7M** column of Table 3) and, as expected, the calculated value was very small (1.12 kcal/mol). All structures were verified to represent minima of the potential energy surface by vibrational frequency analysis. The zero-point vibrational energies ZPVEs were calculated in the rigid rotor-harmonic oscillator approximation. The rotational and translational energies were treated classically as ½ RT per degree of freedom.

The electrostatic potentials (ESP, Figure 10) have been calculated on selected points F belonging to the isodensity surface with constant electron density $\rho(\bar{r}) = 0.02$ bohr^{-3} as

$$V(\bar{r}) = \int \frac{\rho(F')}{|\bar{r} - \bar{r}'|} d\bar{r}$$

where the electron density has been written in terms of the N/2 lowest energy Kohn-Sham orbitals as

$$\rho(\bar{r}) = 2\sum_{1>1}^{occ.} \phi_i(\bar{r})\phi_i^*(\bar{r})$$

with N being the number of electrons of the system.

Acknowledgements

M.W. is grateful to the *Deutsche Forschungsgemeinschaft* (DFG) for financial support and to *Chemetall* for generous gifts of organolithium compounds. M.S. wishes to thank the *Fonds der Chemischen Industrie* (FCI) and the *Bundesministerium für Bildung und Forschung* (BMBF) for a Ph.D. grant. The SGI/IZO-SGIker UPV/EHU (supported by European Social Fund and MCyT) is greatfully aknowledged by J.M.M, I.S.C and J.M.U. for the generous allocation of computational resources.

References

(1) Schade, C.; Schleyer, P. v. R. *Adv. Organomet. Chem.* **1987**, *27*, 169-278.

(2) Ma, J. C.; Dougherty, D. A. *Chem. Rev.* **1997**, *97*, 1303-1324.

(3) Gokel, G. W.; Wall, S. L. D.; Meadows, E. S. *Eur. J. Org. Chem.* **2000**, 2967-2978.

(4) Gokel, G. W.; Barbour, L. J.; Wall, S. L. D.; Meadows, E. S. *Coord. Chem. Rev.* **2001**, *222*, 127-154.

(5) Gokel, G. W.; Barbour, L. J.; Ferdani, R.; Hu, J. *Acc. Chem. Res.* **2002**, *35*, 878-886.

(6) Kumpf, R. A.; Dougherty, D. A. *Science* **1993**, *261*, 1708-1710.

(7) Dougherty, D. A. *Science* **1996**, *271*, 163-168.

(8) Laskoski, M.; Steffen, W.; Smith, M. D.; Bunz, U. H. F. *Chem. Commun.* **2001**, 691-692.

(9) Irigoras, A.; Mercero, J. M.; Silanes, I.; Ugalde, J. M. *J. Am. Chem. Soc.* **2001**, *123*, 5040-5043.

(10) Togni, A.; Hayashi, T., *Ferrocenes*. ed.; VCH: Weinheim, **1995**; 'Vol.' p.

(11) Schildcrout, S. M. *J. Am. Chem. Soc.* **1973**, *95*, 3846-3849.

(12) Nagao, S.; Kato, A.; Nakajima, A.; Kaya, K. *J. Am. Chem. Soc.* **2000**, *122*, 4221-4222.

(13) Crespo, O.; Gimeno, M. C.; Jones, P. G.; Laguna, A.; Sarroca, C. *Chem. Comm.* **1998**, 1481-1482.

(14) Enders, M.; Ludwig, G.; Pritzkow, H. *Organometallics* **2002**, *21*, 3856-3859.

(15) Scholz, S.; Green, J. C.; Lerner, H.-W.; Bolte, M.; Wagner, M. *J. Chem. Soc., Chem. Commun.* **2002**, 36-37.

(16) Jäkle, F.; Polborn, K.; Wagner, M. *Chem. Ber.* **1996**, *129*, 603-606.

(17) Herdtweck, E.; Peters, F.; Scherer, W.; Wagner, M. *Polyhedron* **1998**, *17*, 1149-1157.

(18) Guo, S. L.; Bats, J. W.; Bolte, M.; Wagner, M. *J. Chem. Soc., Dalton Trans.* **2001**, 3572-3576.

(19) Biani, F. F. d.; Jäkle, F.; Spiegler, M.; Wagner, M.; Zanello, P. *Inorg. Chem.* **1997**, *36*, 2103-2111.

(20) Guo, S. L.; Peters, F.; Biani, F. F. d.; Bats, J. W.; Herdtweck, E.; Zanello, P.; Wagner, M. *Inorg. Chem.* **2001**, *40*, 4928-4936.

(21) Haghiri Ilkhechi, A.; Guo, S.; Bolte, M.; Wagner, M. *Dalton Trans.* **2003**, 2303-2307.

(22) Haghiri Ilkhechi, A. ; Scheibitz, M.; Bolte, M.; Lerner, H.-W.; Wagner, M. *Polyhedron* **2004**, *23*, 2597-2604.

(23) Nöth, H.; Wrackmeyer, B., *Nuclear Magnetic Resonance Spectroscopy of Boron Compounds.* ed.; Springer: Berlin, **1978**; 'Vol.' p.

(24) Scheibitz, M.; Winter, R. F.; Bolte, M.; Lerner, H.-W.; Wagner, M. *Angew. Chem.* **2003**, *115*, 954-957.

(25) Fontani, M.; Peters, F.; Scherer, W.; Wachter, W.; Wagner, M.; Zanello, P. *Eur. J. Inorg. Chem.* **1998**, 1453-1465.

(26) Honeyman, G. W.; Kennedy, A. R.; Mulvey, R. E.; Sherrington, D. C. *Organometallics* **2004**, *23*, 1197-1199.

(27) Amicangelo, J. C.; Armentrout, P. B. *J. Phys. Chem. A* **2000**, *104*, 11420-11432.

(28) Feller, D.; Dixon, D. A.; Nicholas, J. B. *J. Phys. Chem. A* **2000**, *104*, 11414-11419.

(29) Woodin, R. L.; Beauchamp, J. L. *J. Am. Chem. Soc.* **1978**, *100*, 501-508.

(30) Sunner, J.; Nishizawa, K.; Kebarle, P. *J. Phys. Chem.* **1981**, *85*, 1814-1820.

(31) Armentrout, P. B.; Rodgers, M. T. *J. Phys. Chem. A* **2000**, *104*, 2238-2247.

(32) Shannon, R. D. *Acta Crystallogr. Sect. A.* **1976**, *32*, 751-767.

(33) King, B. T.; Noll, B. C.; Michl, J. *Collect. Czech. Chem. Commun.* **1999**, *64*, 1001-1012.

(34) Rösch, L.; Altnau, G.; Krüger, C.; Tsay, Y. H. *Z. Naturforsch. B* **1983**, *38*, 34-41.

(35) Hoffmann, K.; Weiss, E. *J. Organomet. Chem.* **1974**, *67*, 221-228.

(36) Pajzderska, A.; Maiuszynska, H.; Wasicki, J. *Z. Naturforsch.* **2002**, *57a*, 847-853.

(37) Mecozzi, S.; Jr., A. P. W.; Dougherty, D. A. *J. Am. Chem. Soc.* **1996**, *118*, 2307-2308.

(38) Reed, A. E.; Curtiss, L. A.; Weinhold, F. *Chem. Rev.* **1988**, *88*, 899-926.

(39) Glendening, A. E.; Reed, A. E.; Carpenter, J. E.; Weinhold, F. *NBO Version 3.1.*

(40) Ruf, W.; Renk, T.; Siebert, W. *Z. Naturforsch.* **1976**, *31b*, 1028-1034.

(41) Sheldrick, G. M. *Acta Crystallogr. Sect. A.* **1990**, *46*, 467-473.

(42) Sheldrick, G. M. *SHELXL-97. A Program for the Refinement of Crystal Structures.*, Unversität Göttingen, **1997**.

(43) Blessing, R. H. *Acta Crystallogr. Sect. A.* **1995**, *51*, 33-38.

(44) Spek, A. L. *Acta Crystallogr. Sect. A.* **1990**, *46*, C34.

(45) Winter, R. F.; Hornung, F. M. *Organometallics* **1999**, *18*, 4005-4014.

(46) Frisch, M. J.; Trucks, G. W.; Schlegel, H. B.; Scuseria, G. E.; Robb, M. A.; Cheeseman, J. R.; Zakrzewski, V. G.; Montgomery, J. A.; Stratmann, R. E.; Burant, J. C.; Dapprich, S.; Millam, J. M.; Daniels, A. D.; Kudin, K. N.; Strain, M. C.; Farkas, O.; Tomasi, J.; Barone, V.; Cossi, M.; Cammi, R.; Mennucci, B.; Pomelli, C.; Adamo, C.; Clifford, S.; Ochterski, J.; Petersson, G. A.; Ayala, P. Y.; Cui, Q.; Morokuma, K.; Malick, D. K.; Rabuck, A. D.; Raghavachari, K.; Foresman, J. B.; Cioslowski, J.; Ortiz, J. V.; Stefanov, B. B.; Liu, G.; Liashenko, A.; Piskorz, P.; Komaromi, I.; Gomperts, R.; Martin, R. L.; Fox, D. J.; Keith, T.; Al-Laham, M. A.; Peng, C. Y.; Nanayakkara, A.; Gonzalez, C.; Challacombe, M.; Gill, P. M. W.; Johnson, B. G.; Chen, W.; Wong, M. W.; Andres, J. L.; Head-Gordon, M.; Replogle, E. S.; Pople, J. A. *Gaussian 98, Revision A.11*, Gaussian, Inc.: Pittsburgh, PA, **1998**.

(47) Frisch, M. J.; Trucks, G. W.; Schlegel, H. B.; Scuseria, G. E.; Robb, M. A.; Cheeseman, J. R.; J. A. Montgomery, J.; Vreven, T.; Kudin, K. N.; Burant, J. C.; Millam, J. M.; Iyengar, S. S.; Tomasi, J.; Barone, V.; Mennucci, B.; Cossi, M.; Scalmani, G.; Rega, N.; Petersson, G. A.; Nakatsuji, H.; Hada, M.; Ehara, M.; Toyota, K.; Fukuda, R.; Hasegawa, J.; Ishida, M.; Nakajima, T.; Honda, Y.; Kitao, O.; Nakai, H.; Klene, M.; Li, X.; Knox, J. E.; Hratchian, H. P.; Cross, J. B.; Bakken, V.; Adamo, C.; Jaramillo, J.; Gomperts, R.; Stratmann, R. E.; Yazyev, O.; Austin, A. J.; Cammi, R.; Pomelli, C.; Ochterski, J. W.; Ayala, P. Y.; Morokuma, K.; Voth, G. A.; Salvador, P.; Dannenberg, J. J.; Zakrzewski, V. G.; Dapprich, S.; Daniels, A. D.; Strain, M. C.; Farkas, O.; Malick, D. K.; Rabuck, A. D.; Raghavachari, K.; Foresman, J.

B.; Ortiz, J. V.; Cui, Q.; Baboul, A. G.; Clifford, S.; Cioslowski, J.; Stefanov, B. B.; Liu, G.; Liashenko, A.; Piskorz, P.; Komaromi, I.; Martin, R. L.; Fox, D. J.; Keith, T.; Al-Laham, M. A.; Peng, C. Y.; Nanayakkara, A.; Challacombe, M.; Gill, P. M. W.; Johnson, B.; Chen, W.; Wong, M. W.; Gonzalez, C.; Pople, J. A. *Gaussian 03, Revision C.02*, Gaussian, Inc.: Wallingford, CT, **2004**.

(48) Becke, A. D. *Phys. Rev. A* **1988**, *38*, 3098-3100.

(49) Lee, C.; Yang, W.; Parr, R. G. *Phys. Rev. B* **1988**, *37*, 785-789.

(50) Becke, A. D. *J. Chem. Phys.* **1993**, *98*, 5648-5652.

(51) Sim, F.; Salahub, D. R.; Chin, S.; Dupuis, M. *J. Chem. Phys.* **1991**, *95*, 4317-4326.

(52) Godbout, N.; Salahub, D. R.; Andzelm, J.; Wimmer, E. *Can. J. Chem.* **1992**, *70*, 560-571.

(53) Schäfer, A.; Huber, C.; Ahlrichs, R. *J. Chem. Phys.* **1994**, *100*, 5829-5835.

(54) Wachters, A. J. *J. Chem. Phys.* **1970**, *52*, 1033-1036.

(55) Hay, P. J. *J. Chem. Phys.* **1977**, *66*, 4377-4384.

(56) Raghavachari, K.; Trucks, G. W. *J. Chem. Phys.* **1989**, *91*, 1062-1065.

(57) Hay, P. J.; Wadt, W. R. *J. Chem. Phys.* **1985**, *82*, 299-310.

(58) Andzelm, J.; Wimmer, E. *J. Chem. Phys.* **1992**, *96*, 1280-1303.

(59) Mercero, J. M.; Matxain, J. M.; López, X.; York, D. M.; Largo, A.; Eriksson, L. A.; Ugalde, J. M. *Int. J. Mass Spectrom.* **2005**, *240*, 37-99.

Figure captions

Scheme 1: Synthesis of **$2Li_2$**, **$2Na_2$**, **$2K_2$**, **$2Rb_2$**, and **$2Cs_2$**; (i) + Mpz, Et_2O, -78 °C to r.t..

Figure 1: A Ga^+-ferrocene multiple-decker sandwich complex **I**.

Figure 2: Ferrocene- and cymantrene-based tris(pyrazol-1-yl)borate derivatives **IIa**, **IIb**, and **III**.

Figure 3: Molecular structure of **$2Li_2$**·$(DME)_2$ (hydrogen atoms omitted for clarity); selected bond lengths [Å], angles [°], torsion angles [°], and dihedral angles [°]: B(1)-C(11) = 1.69(3), B(1)-N(11) = 1.66(2), B(2)-C(21) = 1.64(2), B(2)-N(21) = 1.58(2), Li(1)-N(12) = 2.04(3), Li(2)-N(22) = 1.98(3), Li(1)-O(102) = 1.97(3), Li(1)-O(105) = 1.97(3), Li(2)-O(202) = 2.06(3), Li(2)-O(205) = 1.94(3), Li(1)···COG(1) = 2.26, Li(2)···COG(2) = 2.32; C(11)-B(1)-N(11) = 100.4(15), B(1)-N(11)-N(12) = 123.6(13), N(11)-N(12)-Li(1) = 124.2(11), C(21)-B(2)-N(21) = 108.2(16), B(2)-N(21)-N(22) = 122.3(14), N(21)-N(22)-Li(2) = 123.0(13); C(12)-C(11)-B(1)-N(11) = 98(2), C(11)-B(1)-N(11)-N(12) = 2.7(19), B(1)-N(11)-N(12)-Li(1) = -6(2), C(22)-C(21)-B(2)-N(21) = 81.3(19), C(21)-B(2)-N(21)-N(22) = 4(2), B(2)-N(21)-N(22)-Li(2) = 2(2), C(11)-COG(1)-COG(2)-C(21) = 178.8; C(11)C(12)C(13)C(14)C(15)// C(21)C(22)C(23)C(24)C(25) = 0.5. COG(1): geometric center of C(11)C(12)C(13)C(14)C(15), COG(2): geometric center of C(21)C(22)C(23)C(24)C(25).

Figure 4: Molecular structure of **$2Na_2$**·$(DME)_3$ (hydrogen atoms omitted for clarity); selected bond lengths [Å], angles [°], torsion angles [°], and dihedral angles [°]: B(1)-C(11) = 1.631(9), B(1)-N(11) = 1.617(9), B(2)-C(21) = 1.644(8), B(2)-N(21) = 1.604(9), Na(1)-N($12^{\#}$) = 2.382(5), Na(1)-N(22) = 2.405(6), Na(1)···COG($1^{\#}$) = 2.561, Na(1)···COG(2) = 2.590; C(11)-B(1)-N(11) = 105.4(5), B(1)-N(11)-N(12) = 125.5(5), N(11)-N(12)-Na(1*) = 127.2(4), C(21)-B(2)-N(21) = 106.1(5), B(2)-N(21)-N(22) = 124.0(5), N(21)-N(22)-Na(1) = 124.1(4), N($12^{\#}$)-Na(1)-N(22) = 122.2(2); C(12)-C(11)-B(1)-N(11) = -89.4(7), C(11)-B(1)-N(11)-N(12) = 7.4(8), B(1)-N(11)-N(12)-Na(1*) = -18.0(8), C(22)-C(21)-B(2)-N(21) =

100.0(7), C(21)-B(2)-N(21)-N(22) = -29.5(8), B(2)-N(21)-N(22)-Na(1) = 26.7(8), C(11)-COG(1)-COG(2)-C(21) = -135.4; C(11)C(12)C(13)C(14)C(15)// C(21)C(22)C(23)C(24)C(25) = 1.2, C(11$^{\#}$)C(12$^{\#}$)C(13$^{\#}$)C(14$^{\#}$)C(15$^{\#}$)// C(21)C(22)C(23)C(24)C(25) = 48.0. COG(1$^{\#}$): geometric center of C(11$^{\#}$)C(12$^{\#}$)C(13$^{\#}$)C(14$^{\#}$)C(15$^{\#}$), COG(2): geometric center of C(21)C(22)C(23)C(24)C(25). Symmetry transformation used to generate equivalent atoms: x - ½, y, -z + ½ (#); x + ½, y, -z + ½ (*).

Figure 5: Molecular structure of **2K$_2$**·(DME)$_3$ (hydrogen atoms omitted for clarity); selected bond lengths [Å], angles [°], torsion angles [°], and dihedral angles [°]: B(1)-C(11) = 1.625(6), B(1)-N(11) = 1.604(6), B(2)-C(21) = 1.623(6), B(2)-N(21) = 1.618(6), K(1)-N(12) = 2.969(3), K(1)-N(22$^{\#}$) = 2.987(4), K(2)-N(22$^{\#}$) = 2.853(3), K(2)-N(12) = 2.929(4), K(1)-O(102) = 2.766(3), K(1)-O(105) = 2.866(3), K(2)-O(202) = 2.768(4), K(2)-O(205) = 2.867(4), K(2)-O(212) = 2.963(4), K(2)-O(215) = 2.768(3), K(1)···COG(1) = 3.228, K(1)···COG(2$^{\#}$) = 3.298; C(11)-B(1)-N(11) = 106.9(3), B(1)-N(11)-N(12) = 122.5(3), N(11)-N(12)-K(1) = 116.1(2), N(11)-N(12)-K(2) = 127.3(3), C(21)-B(2)-N(21) = 106.0(3), B(2)-N(21)-N(22) = 123.0(3), N(21)-N(22)-K(1*) = 93.3(2), N(21)-N(22)-K(2*) = 136.4(2), K(1)-N(12)-K(2) = 90.89(9), K(1*)-N(22)-K(2*) = 92.03(9), N(12)-K(1)-N(22$^{\#}$) = 86.89(9), N(12)-K(2)-N(22$^{\#}$) = 90.19(10); C(12)-C(11)-B(1)-N(11) = 70.5(5), C(11)-B(1)-N(11)-N(12) = 56.8(5), B(1)-N(11)-N(12)-K(1) = -66.0(4), B(1)-N(11)-N(12)-K(2) = 47.3(4), C(22)-C(21)-B(2)-N(21) = 68.0(5), C(21)-B(2)-N(21)-N(22) = 87.3(4), B(2)-N(21)-N(22)-K(1*) = -86.3(3), B(2)-N(21)-N(22)-K(2*) = 10.1(6), C(11)-COG(1)-COG(2)-C(21) = 92.1; C(11)C(12)C(13)C(14)C(15)// C(21)C(22)C(23)C(24)C(25) = 2.7, C(11$^{\#}$)C(12$^{\#}$)C(13$^{\#}$)C(14$^{\#}$)C(15$^{\#}$)// C(21)C(22)C(23)C(24)C(25) = 2.7. COG(1): geometric center of C(11)C(12)C(13)C(14)C(15), COG(2$^{\#}$): geometric center of C(21$^{\#}$)C(22$^{\#}$)C(23$^{\#}$)C(24$^{\#}$)C(25$^{\#}$). Symmetry transformation used to generate equivalent atoms: x – 1, y, z (#); x + 1, y, z (*).

Molecular structure of **2Rb$_2$**·(DME)$_3$ (hydrogen atoms omitted for clarity); selected bond lengths [Å], angles [°], torsion angles [°], and dihedral angles [°]: B(1)-C(11) = 1.623(17), B(1)-N(11) = 1.602(16), B(2)-C(21) = 1.608(19), B(2)-N(21) = 1.613(14), Rb(1)-N(12) = 3.087(11), Rb(1)-N(22*) = 3.130(12), Rb(2)-N(22*) = 2.998(10), Rb(2)-N(12) = 3.050(11), Rb(1)-O(202) = 3.008(11), Rb(1)-O(205) = 2.939(12), Rb(2)-O(102) = 3.043(12), Rb(2)-O(105) = 2.911(13), Rb(2)-O(112) = 2.912(10), Rb(2)-O(115) = 3.018(10), Rb(1)···COG(1) = 3.285, Rb(1)···COG(2*) = 3.265; C(11)-B(1)-N(11) = 107.4(10), B(1)-N(11)-N(12) = 123.4(9), N(11)-N(12)-Rb(1) = 112.9(7), N(11)-N(12)-Rb(2) = 129.1(8), C(21)-B(2)-N(21) = 105.0(9), B(2)-N(21)-N(22) = 124.5(9), N(21)-N(22)-Rb(1$^{\#}$) = 95.0(7), N(21)-N(22)-Rb(2$^{\#}$) = 136.6(7), Rb(1)-N(12)-Rb(2) = 91.4(3), Rb(1$^{\#}$)-N(22)-Rb(2$^{\#}$) = 91.5(3), N(12)-Rb(1)-N(22*) = 87.0(3), N(12)-Rb(2)-N(22*) = 90.1(3); C(12)-C(11)-B(1)-N(11) = 107.3(13), C(11)-B(1)-N(11)-N(12) = -61.2(15), B(1)-N(11)-N(12)-Rb(1) = 68.3(13), B(1)-N(11)-N(12)-Rb(2) = -43.9(15), C(22)-C(21)-B(2)-N(21) = -69.6(13), C(21)-B(2)-N(21)-N(22) = -83.5(13), B(2)-N(21)-N(22)-Rb(1$^{\#}$) = 86.2(11), B(2)-N(21)-N(22)-Rb(2$^{\#}$) = -11.4(18), C(11)-COG(1)-COG(2)-C(21) = -93.2; C(11)C(12)C(13)C(14)C(15)// C(21)C(22)C(23)C(24)C(25) = 2.5, C(11*)C(12*)C(13*)C(14*)C(15*)// C(21)C(22)C(23)C(24)C(25) = 2.5. COG(1): geometric center of C(11)C(12)C(13)C(14)C(15), COG(2*): geometric center of C(21*)C(22*)C(23*)C(24*)C(25*). Symmetry transformation used to generate equivalent atoms: x – 1, y, z (#); x + 1, y, z (*).

Molecular structure of **2Cs$_2$**·(DME)$_3$ (hydrogen atoms omitted for clarity); selected bond lengths [Å], angles [°], torsion angles [°], and dihedral angles [°]: B(1)-C(11) = 1.609(7), B(1)-N(11) = 1.632(5), Cs(1)-N(12) = 3.331(4), Cs(2)-N(12) = 3.101(4), Cs(1)-O(42) = 3.156(4), Cs(2)-O(32) = 3.102(4), Cs(2)-O(35) = 3.146(4), Cs(1)···COG(1) = 3.283; C(11)-B(1)-N(11) = 104.9(3), B(1)-N(11)-N(12) = 121.6(3), N(11)-N(12)-Cs(1) = 89.9(2), N(11)-N(12)-Cs(2) = 141.9(3), Cs(1)-N(12)-Cs(2) = 97.57(10), N(12)-Cs(1)-N(12*) = 78.85(14), N(12)-Cs(2)-N(12*) = 86.01(15); C(12)-C(11)-B(1)-N(11) = 70.9(5), C(11)-B(1)-N(11)-

N(12) = 88.2(5), B(1)-N(11)-N(12)-Cs(1) = -90.3(3), B(1)-N(11)-N(12)-Cs(2) = 12.0(7), C(11)-COG(1)-COG(1#)-C(11#) = 86.7; C(11)C(12)C(13)C(14)C(15)// C(11$^{\#}$)C(12$^{\#}$)C(13$^{\#}$)C(14$^{\#}$)C(15$^{\#}$) = 1.7, C(11*)C(12*)C(13*)C(14*)C(15*)// C(21)C(22)C(23)C(24)C(25) = 1.7. COG(1): geometric center of C(11)C(12)C(13)C(14)C(15). Symmetry transformation used to generate equivalent atoms: -x +1, y, -z + $^{3}/_{2}$ (*); -x +2, y, -z + $^{3}/_{2}$ (#).

Figure 6: Molecular structure of **2Na$_2$**·(THF)$_4$ (hydrogen atoms omitted for clarity); selected bond lengths [Å], angles [°], torsion angles [°], and dihedral angles [°]: B(1)-C(11) = 1.612(4), B(1)-N(11) = 1.613(4), Na(1)-N(12) = 2.534(2), Na(1)-N(12$^{\#}$) = 2.532(2), Na(1)-O(31) = 2.348(2), Na(1)-O(41) = 2.332(2), Na(1)-C(15$^{\#}$) = 2.848(3); C(11)-B(1)-N(11) = 106.2(2), B(1)-N(11)-N(12) = 122.88(19), N(11)-N(12)-Na(1) = 118.75(15), N(11)-N(12)-Na(1$^{\#}$) = 112.81(16), Na(1)-N(12)-Na(1$^{\#}$) = 86.46(7), N(12)-Na(1)-N(12$^{\#}$) = 93.54(7), O(31)-Na(1)-O(41) = 87.51(8); C(12)-C(11)-B(1)-N(11) = -86.1(3), C(11)-B(1)-N(11)-N(12) = -83.9(3), B(1)-N(11)-N(12)-Na(1) = -45.2(3), B(1)-N(11)-N(12)-Na(1$^{\#}$) = 53.6(3), C(11)-COG(1)-COG(1*)-C(11*) = -144.8; C(11)C(12)C(13)C(14)C(15)// C(11*)C(12*)C(13*)C(14*)C(15*) = 1.9, C(11)C(12)C(13)C(14)C(15)// C(11$^{\#}$)C(12$^{\#}$)C(13$^{\#}$)C(14$^{\#}$)C(15$^{\#}$) = 0.0. COG(1): geometric center of C(11)C(12)C(13)C(14)C(15), COG(1*): geometric center of C(11*)C(12*)C(13*)C(14*)C(15*). Symmetry transformation used to generate equivalent atoms: -x + 1, -y + 1, -z + 1(#), -x + 1, y, -z + $^{3}/_{2}$ (*).

Molecular structure of **2K$_2$**·(THF)$_4$; selected bond lengths [Å], angles [°], torsion angles [°], and dihedral angles [°]: B(1)-C(11) = 1.660(7), B(1)-N(11) = 1.628(7), K(1)-N(12) = 2.863, K(1)-N(12$^{\#}$) = 2.807(4), K(1)-O(31) = 2.700(4), K(1)-O(41) = 2.647(4), K(1)-C(12) = 2.953(4); C(11)-B(1)-N(11) = 103.4(4), B(1)-N(11)-N(12) = 122.1(4), N(11)-N(12)-K(1) = 109.6(3), N(11)-N(12)-K(1$^{\#}$) = 123.2(3), K(1)-N(12)-K(1$^{\#}$) = 96.71(12), N(12)-K(1)-N(12$^{\#}$) = 83.3(2), O(31)-K(1)-O(41) = 84.63(13); C(12)-C(11)-B(1)-N(11) = -111.1(5), C(11)-B(1)-

N(11)-N(12) = 79.3(5), B(1)-N(11)-N(12)-K(1) = -59.7, B(1)-N(11)-N(12)-K($1^{\#}$) = 52.7(5), C(11)-COG(1)-COG(1*)-C(11*) = 180.0; C(11)C(12)C(13)C(14)C(15)// C(11*)C(12*)C(13*)C(14*)C(15*) = 0.0, C(11)C(12)C(13)C(14)C(15)// C($11^{\#}$)C($12^{\#}$)C($13^{\#}$)C($14^{\#}$)C($15^{\#}$) = 0.0. COG(1): geometric center of C(11)C(12)C(13)C(14)C(15), COG(1*): geometric center of C(11*)C(12*)C(13*)C(14*)C(15*). Symmetry transformation used to generate equivalent atoms: -x + 1, -y + 1, -z + 1 (#), -x, -y + 1, -z + 1 (*).

Molecular structure of **$2Rb_2$**·$(THF)_4$; selected bond lengths [Å], angles [°], torsion angles [°], and dihedral angles [°]: B(1)-C(11) = 1.69(2), B(1)-N(11) = 1.57(2), Rb(1)-N(12) = 3.090(12), Rb(1)-N($12^{\#}$) = 2.955(12), Rb(1)-O(31) = 2.865(12), Rb(1)-O(41) = 2.852(13), Rb(1)-C(12) = 3.156(12); C(11)-B(1)-N(11) = 104.3(14), B(1)-N(11)-N(12) = 123.5(16), N(11)-N(12)-Rb(1) = 90.8(8), N(11)-N(12)-Rb($1^{\#}$) = 134.4(11), Rb(1)-N(12)-Rb($1^{\#}$) = 99.1(3), N(12)-Rb(1)-N($12^{\#}$) = 80.9(15), O(31)-Rb(1)-O(41) = 82.1(4); C(12)-C(11)-B(1)-N(11) = -114.6(16), C(11)-B(1)-N(11)-N(12) = 98.0(17), B(1)-N(11)-N(12)-Rb(1) = -80.6(14), B(1)-N(11)-N(12)-Rb($1^{\#}$) = 23(2), C(11)-COG(1)-COG(1*)-C(11*) = 180.0; C(11)C(12)C(13)C(14)C(15)// C(11*)C(12*)C(13*)C(14*)C(15*) = 0.0, C(11)C(12)C(13)C(14)C(15)// C($11^{\#}$)C($12^{\#}$)C($13^{\#}$)C($14^{\#}$)C($15^{\#}$) = 0.0. COG(1): geometric center of C(11)C(12)C(13)C(14)C(15), COG(1*): geometric center of C(11*)C(12*)C(13*)C(14*)C(15*). Symmetry transformation used to generate equivalent atoms: -x + 1, -y + 1, -z + 1 (#), -x, -y + 1, -z + 1 (*).

Figure 7: Schematic representations of the alkali metal ion-benzene complexes **3M**, **4M**, and of the alkali metal ion-ferrocene complexes **5M**, **$6M_2$**, **7M**, **8Li**, and **9Li**.

Figure 8: Optimized gas phase structures of **8Li** and **9Li** (B3LYP/TZ level of theory).

Figure 9: Potential energy curves of the M^+-ferrocene (**5M**) and Li^+/Rb^+-benzene (**3Li**/**3Rb**) complexes over the M···COG coordinate at the B3LYP/TZ level of theory (DZ basis and pseudopotentials for Rb complexes).

Figure 10: Electrostatic potential surface (EPS) of ferrocene (left) and benzene (right). The surfaces are calculated at the B3LYP/TZ level of theory, with a contour value of 0.02 bohr^{-3}. The colors represent the following energies (in kcal/mol): Red < -19 kcal/mol, yellow = -9 kcal/mol, green = 0.0 kcal/mol, light-blue = +9 kcal/mol, blue > 19 kcal/mol.

Table 1. Selected crystallographic data of **2Li₂**·(DME)₂, **2Na₂**·(DME)₃, **2K₂**·(DME)₃, **2Rb₂**·(DME)₃, **2Cs₂**·(DME)₃, **2Na₂**·(THF)₄, **2K₂**·(THF)₄, and **2Rb₂**·(THF)₄.

compound	**2Li₂**·(DME)₂	**2Na₂**·(DME)₃	**2K₂**·(DME)₃
formula	$C_{28}H_{46}B_2FeLi_2N_4O_4$	$C_{32}H_{56}B_2FeN_4Na_2O_6$	$C_{32}H_{56}B_2FeK_2N_4O_6$
f_w	594.04	716.26	748.48
color, shape	orange, block	orange, plate	orange, block
temp (K)	173(2)	173(2)	173(2)
radiation	MoK$_\alpha$, 0.71073 Å	MoK$_\alpha$, 0.71073 Å	MoK$_\alpha$, 0.71073 Å
cryst syst	triclinic	orthorhombic	triclinic
space group	*P*-1	*Pbca*	*P*-1
a (Å)	15.721(5)	15.584(3)	9.8339(16)
b (Å)	16.515(6)	32.374(4)	13.083(2)
c (Å)	21.159(7)	15.4767(16)	16.826(3)
α (deg)	84.86(3)	90	86.743(15)
β (deg)	83.56(3)	90	75.024(13)
γ (deg)	65.71(3)	90	71.342(13)
V (Å^3)	4970(3)	7808.4(19)	1980.6(6)
Z	6	8	2
$D_{\mathrm{calcd.}}$ (g cm^{-3})	1.191	1.219	1.255
F(000)	1896	3056	796
μ (mm^{-1})	0.491	0.452	0.634
crystal size (mm^3)	0.16×0.14×0.06	0.42×0.12×0.03	0.23×0.20×0.16
no. of rflns collected	23624	29580	14842
no. of indep rflns (R_{int})	15786 (0.1466)	7280 (0.0954)	7148 (0.0815)
data/restraints/params	15786/504/1051	7280/0/424	7148/0/424
GOOF on F^2	0.840	0.840	0.829
R_1, wR_2 (I>2σ(I))	0.1207, 0.2640	0.0737, 0.1491	0.0529, 0.1107
R_1, wR_2 (all data)	0.3584, 0.3683	0.1884, 0.1917	0.1072, 0.1263
largest diff. peak and hole (eÅ^{-3})	0.478, -0.355	0.954, -0.366	0.539, -0.546

Table 1. continued

compound	**2Rb₂**·(DME)₃	**2Cs₂**·(DME)₃	**2Na₂**·(THF)₄
formula	$C_{32}H_{56}B_2FeN_4O_6Rb_2$	$C_{32}H_{56}B_2Cs_2FeN_4O_6$	$C_{36}H_{58}B_2FeN_4Na_2O_4$
f_w	841.22	936.10	734.31
color, shape	orange, plate	light orange, block	light brown, block
temp (K)	173(2)	173(2)	173(2)
radiation	MoK_α, 0.71073 Å	MoK_α, 0.71073 Å	MoK_α, 0.71073 Å
cryst syst	triclinic	monoclinic	orthorhombic
space group	*P*-1	C*2*/c	*Pbcn*
a (Å)	9.8596(18)	9.8708(12)	20.6370(16)
b (Å)	13.136(3)	24.313(3)	11.5631(7)
c (Å)	17.292(4)	17.594(2)	16.2548(10)
α (deg)	85.950(18)	90	90
β (deg)	75.063(16)	103.180(10)	90
γ (deg)	69.938(15)	90	90
V (Å^3)	2032.2(8)	4111.1(9)	3878.8(5)
Z	2	4	4
$D_{\text{calcd.}}$ (g cm^{-3})	1.375	1.512	1.257
F(000)	868	1880	1568
μ (mm^{-1})	2.793	2.154	0.453
crystal size (mm^3)	0.36×0.34×0.12	0.19×0.14×0.12	0.42×0.32×0.28
no. of rflns collected	20674	14494	36382
no. of indep rflns (R_{int})	7152 (0.1091)	3941 (0.0755)	3779 (0.0715)
data/restraints/params	7152/0/424	3941/0/214	3779/0/222
GOOF on F^2	1.084	0.815	1.031
R_1, wR_2 (I>2σ(I))	0.1057, 0.2712	0.0345, 0.0582	0.0484, 0.1333
R_1, wR_2 (all data)	0.1571, 0.3005	0.0692, 0.0638	0.0674, 0.1417
largest diff. peak and hole (eÅ^{-3})	3.025, -1.338	0.386, -0.652	1.026, -0.430

Table 1. continued

compound	**2K$_2$**·(THF)$_4$	**2Rb$_2$**·(THF)$_4$
formula	$C_{36}H_{58}B_2FeK_2N_4O_4$	$C_{36}H_{58}B_2FeN_4O_4Rb_2$
f_w	766.53	859.27
color, shape	yellow, plate	orange, needle
temp (K)	173(2)	173(2)
radiation	MoK$_\alpha$, 0.71073 Å	MoK$_\alpha$, 0.71073 Å
cryst syst	monoclinic	monoclinic
space group	$P2_1/n$	$P2_1/n$
a (Å)	11.0876(19)	11.309(3)
b (Å)	14.624(3)	15.248(5)
c (Å)	12.7422(18)	12.259(4)
α (deg)	90	90
β (deg)	99.159(13)	96.13(3)
γ (deg)	90	90
V (Å^3)	2039.7(6)	2101.9(11)
Z	2	2
$D_{calcd.}$ (g cm^{-3})	1.248	1.358
F(000)	816	888
μ (mm^{-1})	0.614	2.699
crystal size (mm^3)	0.22×0.18×0.12	0.22×0.18×0.12
no. of rflns collected	15298	10870
no. of indep rflns (R_{int})	3732 (0.0828)	3700 (0.1834)
data/restraints/params	3732/0/223	3700/10/223
GOOF on F^2	0.797	0.965
R_1, wR_2 ($I>2\sigma(I)$)	0.0524, 0.0738	0.0978, 0.1932
R_1, wR_2 (all data)	0.1495, 0.0886	0.2266, 0.2475
largest diff. peak and hole (eÅ^{-3})	0.340, -0.257	0.694, -0.932

Table 2. Distances $M^+\cdots$COG [Å] between the alkali metal ions M^+ and the centroid (COG) of the coordinated benzene or cyclopentadienyl ring [B3LYP hybrid functional, double-ζ (DZ) and triple-ζ (TZ) basis sets].

[a]ref.[28]; [b]MP2/CBS; [c]MP2/aVQZ; [d]ref.[27]; [e]MP2(full)/6-311+G*; [f]The Hay-Wadt ECP/valence basis set was used for the metal atom; [g]sum of the ionic radius of M^+ and the half-thickness of benzene; [h]mean experimental value.

M	**3M**[a]	**3M**[d]	r(M^+)	**4M**[d]	**5M**	**5M**	**6M$_2$**	**6M$_2$**	**7M**	**2M$_2$**
			+1.7 Å[g]		DZ	TZ	DZ	TZ	DZ	exptl.[h]
Li	1.879[b]	1.842[e]	2.30	1.917[e]	1.870	1.837	2.018	1.971	1.995	2.29
Na	2.390[b]	2.394[e]	2.65	2.421[e]	2.350	2.350	2.506	2.518	2.427	2.576
K	2.786[b]	2.810[e]	3.03	2.832[e]	2.833	2.803	3.060	3.030	2.903	3.263
	2.786[c]	2.896[e,f]		2.917[e,f]						
Rb	3.100[c]	3.165[e,f]	3.18	3.105[e,f]	3.147	--	3.478	--	--	3.275
Cs	3.313[c]	3.417[e,f]	3.36	3.392[e,f]	--	--	--	--	--	3.283

Table 3. M^+(benzene) and M^+(ferrocene) binding enthalpies [kcal/mol].

[a]theoretical value according to ref.[28], CCSD(T) / est. CBS; [b]experimental value obtained from CID measurements according to ref.[27]; [c]experimental value for the reaction **3M** + C_6H_6 → **4M**; [d]B3LYP hybrid functional, double-ζ (DZ) basis set; [e]B3LYP hybrid functional, triple-ζ (TZ) basis set; [f]theoretical value for the reaction **5M** + M^+ → **6M₂**, B3LYP hybrid functional, double-ζ (DZ) basis set; [g]theoretical value for the reaction **5M** + M^+ → **6M₂**, B3LYP hybrid functional, triple-ζ (TZ) basis set; [h]theoretical value for the reaction **5M** + $(C_5H_5)_2Fe$ → **7M**, B3LYP hybrid functional, double-ζ (DZ) basis set.

M	**3M**	**3M**	**4M**	**5M**	**5M**	**6M₂**	**6M₂**	**7M**
	ΔH_0^a	ΔH_0^b	ΔH_0^c	ΔH_0^d	ΔH_0^e	ΔH_0^f	ΔH_0^g	ΔH_0^h
Li	-36.1	-38.5±3.2	-24.9±1.6	-44.0	-45.3	26.4	25.6	-27.7
Na	-24.2	-22.1±1.4	-19.1±1.4	-30.0	-29.5	27.9	28.0	-21.8
K	-20.0	-17.5±0.9	-16.1±1.6	-20.1	-20.3	28.6	29.0	-15.9
Rb	-16.4	-16.4±0.9	-15.0±1.8	-14.8	--	24.7	--	--
Cs	-12.4	-15.4±1.1	-14.0±1.8	--	--	--	--	--

Scheme 1:

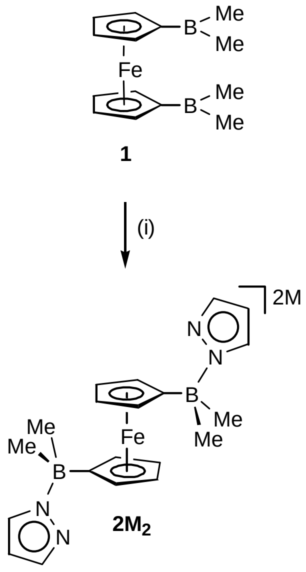

M = Li$^+$, Na$^+$, K$^+$, Rb$^+$, Cs$^+$

Figure 1:

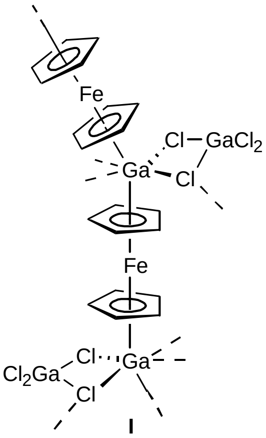

Figure 2:

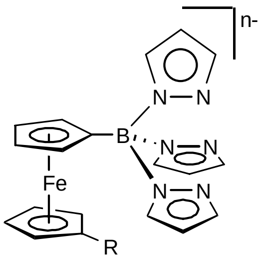

IIa: R = H, n = 1
IIb: R = Bpz_3, n = 2

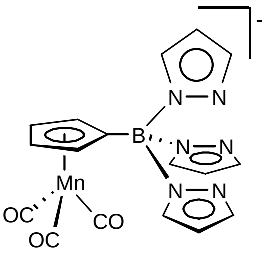

III

Figure 3:

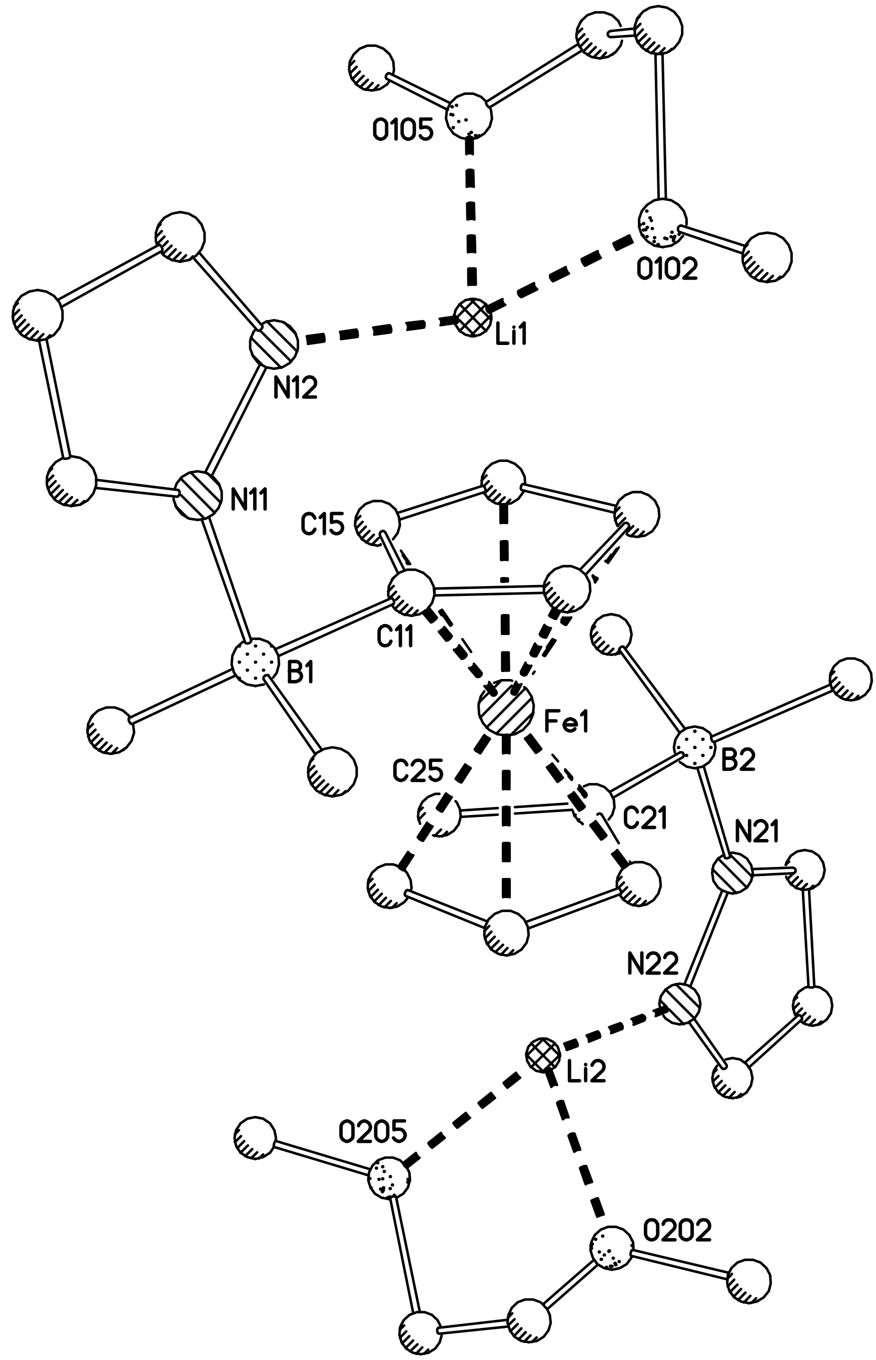
0105
0102
Li1
N12
N11
C15
C11
B1
Fe1
C25
C21
B2
N21
N22
Li2
0205
0202

Figure 4:

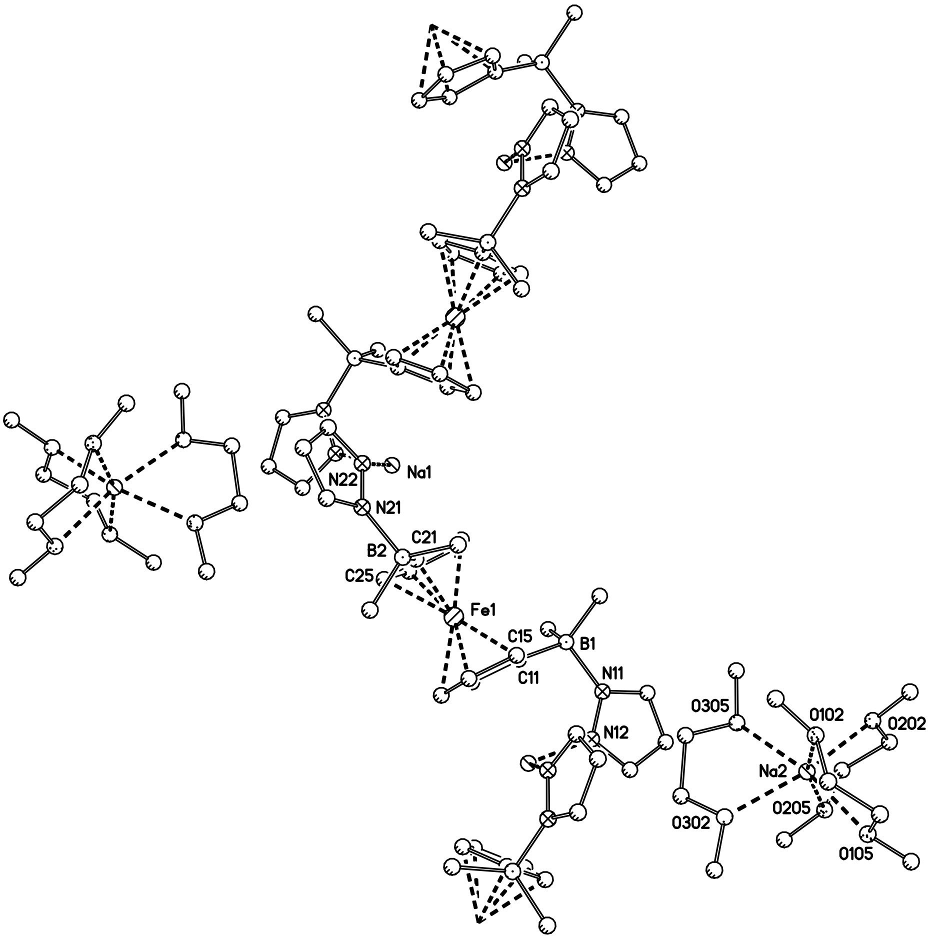
Na1
N22
N21
B2
C21
C25
Fe1
C15
B1
C11
N11
N12
0305
0102
0202
Na2
0205
0302
0105

Figure 5:

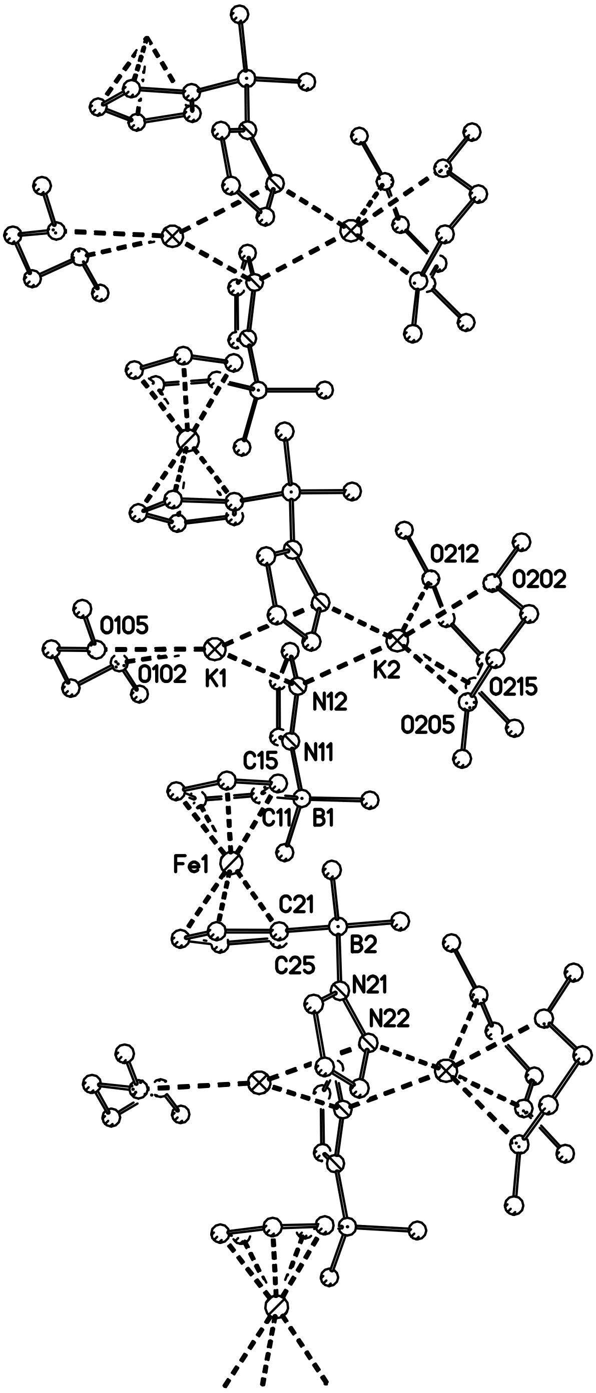
O212
O202
O105
O102
K1
K2
N12
O215
O205
N11
C15
C11
B1
Fe1
C21
B2
C25
N21
N22

Figure 6 :

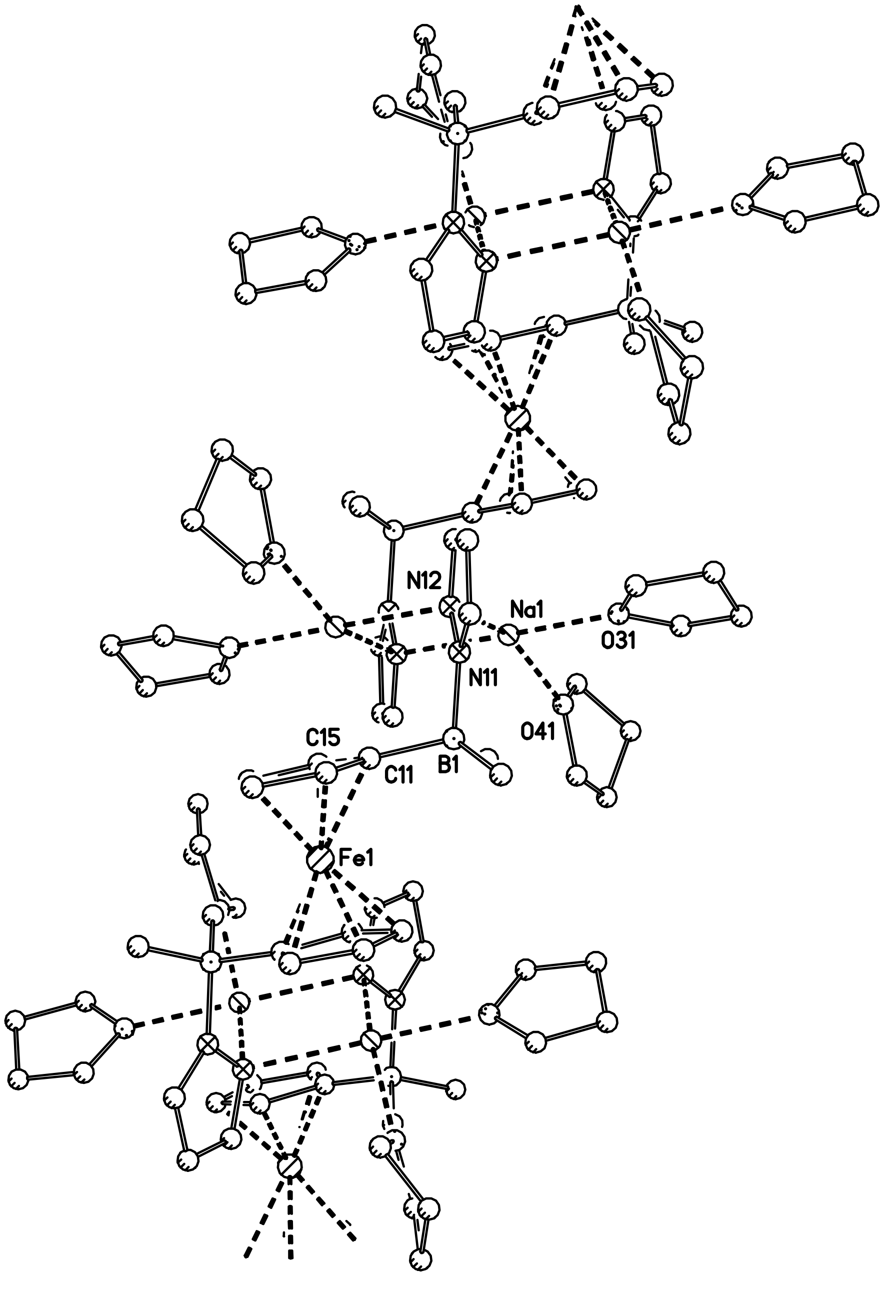

Figure 7:

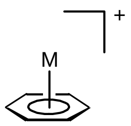

3M

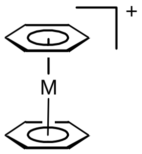

4M

$M^+ = Li^+, Na^+, K^+, Rb^+, Cs^+$

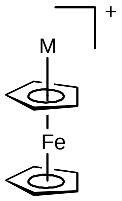

5M

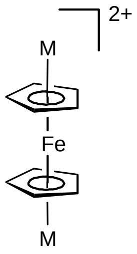

$6M_2$

$M^+ = Li^+, Na^+, K^+, Rb^+$

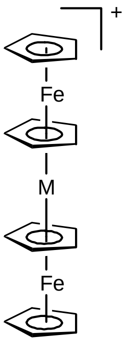

7M

$M^+ = Li^+, Na^+, K^+$

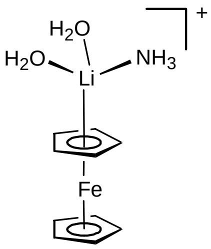

8Li

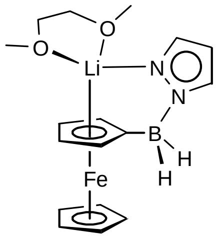

9Li

Figure 8:

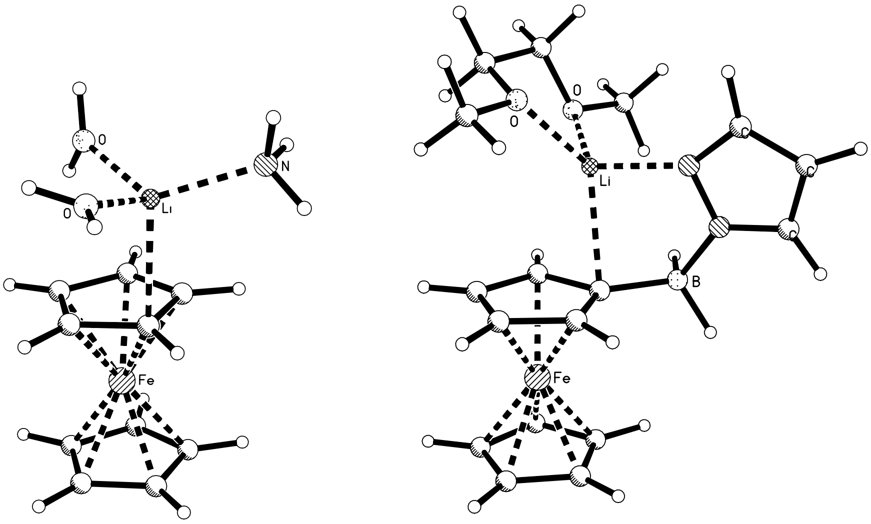

Figure 9:

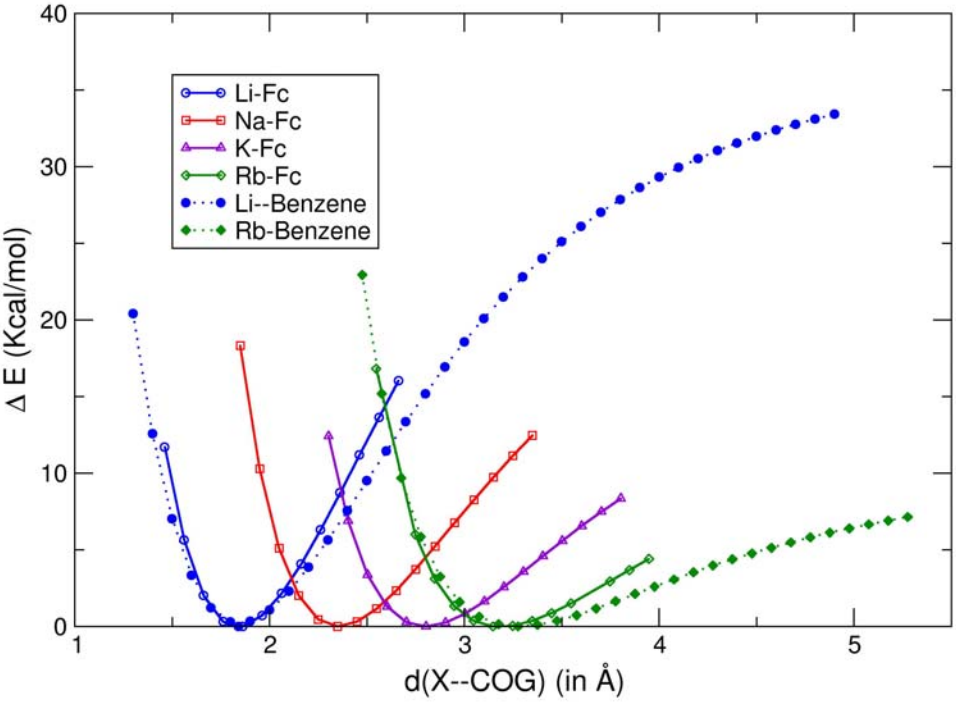
Li-Fc
Na-Fc
K-Fc
Rb-Fc
Li--Benzene
Rb-Benzene
Δ E (Kcal/mol)
d(X--COG) (in Å)
0
10
20
30
40
1
2
3
4
5

Figure 10:

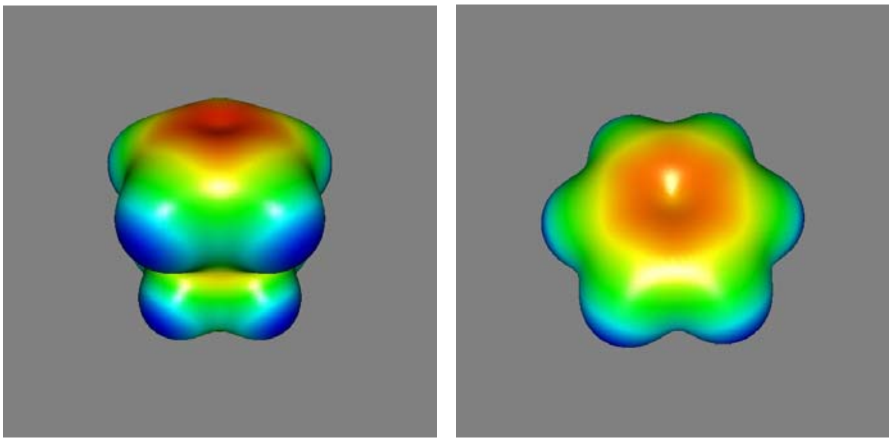

6.4 „Synthesis and structural characterization of ferrocene-based bis(pyrazol-1-yl)borate ligands: $FcB(Me)pz_2K$, Fc_2Bpz_2K, and 1,1´-$fc[B(Me)pz_2]_2K_2$ (Fc: ferrocenyl, fc: ferrocenylene, pz: pyrazolyl)“

Alireza Haghiri Ilkhechi, Michael Bolte, Hans-Wolfram Lerner and Matthias Wagner,

J. Organomet. Chem., **2005**, 690, 1971-1977.

ELSEVIER

Available online at www.sciencedirect.com

SCIENCE DIRECT®

Journal of Organometallic Chemistry 690 (2005) 1971–1977

Journal of Organometallic Chemistry

www.elsevier.com/locate/jorganchem

Synthesis and structural characterization of ferrocene-based bis(pyrazol-1-yl)borate ligands: $FcB(Me)pz_2K$, Fc_2Bpz_2K, and $1,1'$-$fc[B(Me)pz_2]_2K_2$ (Fc: ferrocenyl, fc: ferrocenylene, pz: pyrazolyl)

Alireza Haghiri Ilkhechi, Michael Bolte, Hans-Wolfram Lerner, Matthias Wagner *

Institut für Anorganische Chemie, J.W. Goethe-Universität Frankfurt, Marie-Curie-Strasse 11, D-60439 Frankfurt (Main), Germany

Received 10 November 2004; accepted 10 November 2004
Available online 11 February 2005

Abstract

Reaction of the ferrocenyl(dimethylamino)boranes $FcB(Me)NMe_2$, Fc_2BNMe_2, and $1,1'$-$fc[B(Me)NMe_2]_2$ with 1:1 mixtures of pyrazole and potassium pyrazolide in refluxing THF gave the potassium salts of the ferrocene-based bis(pyrazol-1-yl)borate ligands $FcB(Me)pz_2K$, Fc_2Bpz_2K, and $1,1'$-$fc[B(Me)pz_2]_2K_2$ in good yield (Fc: ferrocenyl, fc: ferrocenylene, pz: pyrazolyl). In the solid state, $FcB(Me)pz_2K$ and Fc_2Bpz_2K form centrosymmetric dimers with short K···Cp contacts suggesting an η^5 coordination mode of the potassium ion. The crystal lattice of the ditopic ligand $1,1'$-$fc[B(Me)pz_2]_2K_2$ consists of coordination polymer strands featuring essentially the same structural motif that has been observed for the monotopic derivatives. All three scorpionate ligands are thus promising building blocks for the preparation of ferrocene-containing multiple-decker sandwich complexes.

Keywords: Ferrocene; Nitrogen ligand; Bis(pyrazol-1-yl)borate; X-ray crystallography

---

1. Introduction

Our group is interested in the development of poly(pyrazol-1-yl)borate ligands [1] ("scorpionates") as bridging elements for the generation of oligonuclear hybrid compounds consisting of organometallic entities (e.g., ferrocene, cymantrene) on one hand and classical Werner-type complexes on the other. For start, we prepared derivatives of the mono- and ditopic tris(pyrazol-1-yl)borates **I** and **II** (Fig. 1), which were subsequently employed for the assembly of various di- and trinuclear transition metal complexes [2–5]. Even though, in most cases, the nature of the complexed transition metal centre M had some influence over the redox potential of the ferrocene iron atom, the degree of electronic communication was generally low [3,5]. We therefore decided to reduce the number of pyrazolyl substituents in **I** and **II**, assuming that a lack of σ-donor sites might force the complexed metal atom to bind directly to the cyclopentadienyl ring of the ferrocene backbone which could in turn lead to a more pronounced Fe/M interaction. The general validity of our concept was proven by an X-ray single crystal structure determination of the ditopic lithium mono(pyrazol-1-yl)borate **III** (Fig. 1) that revealed the desired multiple-decker sandwich arrangement in the solid state [6]. In order to see whether an additional chelating sidearm *per* borate unit would also lead to the aimed-for η^5 M···Cp coordination, it appeared to be worthwhile to investigate the corresponding ferrocene-based bis(pyrazol-1-yl) borate ligands (note that an analogous bitopic ferrocenylene-linked bis(pyrazol-1-yl)methane **IV** has recently been published by Reger et al. [7]; Fig. 1). Thus, the methyl

---

* Corresponding author. Tel.: 49 69 798 29156; fax: 49 69 798 29260.
E-mail address: matthias.wagner@chemie.uni-frankfurt.de (M. Wagner).

0022-328X/$ - see front matter © 2004 Elsevier B.V. All rights reserved.
doi:10.1016/j.jorganchem.2004.11.016

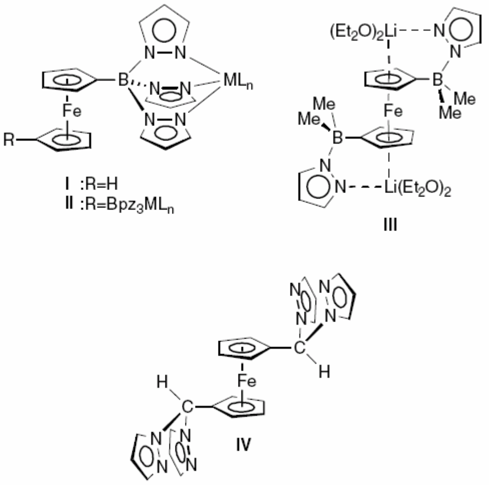

Fig. 1. Mono- and ditopic ferrocene-based tris(pyrazol-1-yl)borates **I** and **II**, the analogous lithium mono(pyrazol-1-yl)borate **III** and Reger's ferrocenylene-linked bis(pyrazol-1-yl)methane ligand **IV**.

derivatives **4** and **6** (Scheme 1) were selected as target molecules since they are closely related to **III**. In addition, the diferrocenyl ligand **5** was prepared, because the presence of *two* ferrocenyl substituents in the ligand molecule may be expected to increase the number of conformations allowing for close M· · ·Cp contacts.

2. Results and discussion

2.1. Syntheses and spectroscopy

The starting materials **1** and **3** (Scheme 1) are available by published procedures [8]. The diferrocenyl complex **2** (Scheme 1) was prepared from Fc$_2$BBr [8] and Me$_3$SiNMe$_2$ in 86% yield (Fc: ferrocenyl). Further reaction of **1**–**3** with one (**1**, **2**) or two (**3**) equivalents of Kpz/Hpz in refluxing THF readily leads to the desired heteroscorpionates **4**–**6**. The ligands are sensitive to air; **4** and **5** are readily soluble in THF, whereas **6** is only moderately soluble in all common organic solvents.

The ^{11}B NMR resonances of **4**–**6** appear in the range between −1.4 and 1.0 ppm thereby testifying to the presence of four-coordinate boron nuclei. In all three cases, only one set of signals is observed for the pyrazolyl rings in the ^{1}H as well as in the ^{13}C NMR spectrum. The same is true for the ferrocenyl resonances of **5**. Thus, even though **5** and **6** are sterically quite crowded, rotation about the B–N– and the B–C bonds is obviously fast on the NMR timescale. All proton and carbon resonances appear in the usually observed region and therefore do not merit detailed discussion.

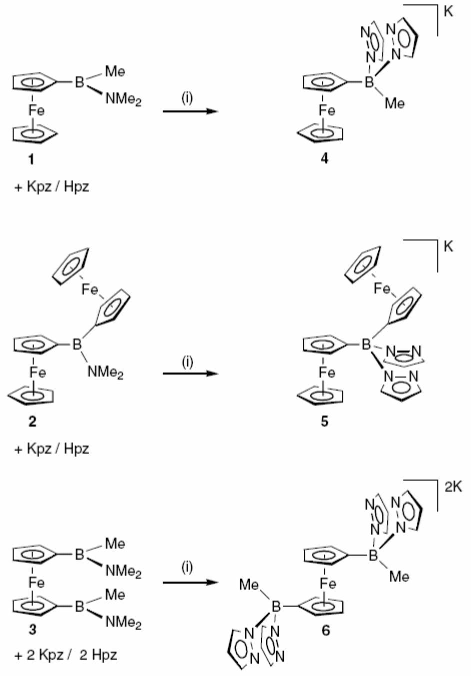

Scheme 1. Synthesis of the ferrocene–based heteroscorpionate ligands **4**, **5** and **6**. (i) THF, −78 °C to reflux temperature.

2.2. X-ray crystallography

Crystal data and structure refinement details for **4** (monoclinic, $P2_1/n$), **5** (triclinic, $P\bar{1}$), and **6** (monoclinic, $P2_1/n$) are compiled in Table 1.

FcB(Me)pz$_2$K, **4**, forms centrosymmetric dimers (**4**THF)$_2$ in the solid state (Fig. 2). Both pyrazolyl rings of the B(1)-scorpionate fragment bind to the potassium ion K(1) but in different manners: While the N(12)-pyrazolyl ring merely acts as a σ-donor (K(1)–N(12) = 2.806(5) Å), the N(22)-pyrazolyl ring coordinates in a distorted η^5 mode (K(1)· · ·COG(pz) = 2.958 Å; COG: centre of gravity). The B(1$^{\#}$)-scorpionate ligand binds to K(1) via one pyrazolyl ring (η^1 mode; K(1)–N(22$^{\#}$) = 2.797(5) Å) and its ferrocenyl–Cp unit (η^5 mode; K(1)· · ·COG(Cp$^{\#}$) = 2.942 Å). Thus, if we just regard N(22)-pyrazolyl and C(31$^{\#}$)–Cp as pentagonal π electron systems, the coordination modes of both scorpionate fragments are very much alike. The ligand sphere of K(1) is completed by one THF molecule. While the N(12)-pyrazolyl ring is bonded to one potassium ion only, N(22)-pyrazolyl acts as a bridging ligand between two K$^+$ ions. One of them is coordinated via the N(22)

Table 1
Crystal data and structure refinement details for compounds $(\mathbf{4}\mathrm{THF})_2$, $[\mathbf{5}(\mathrm{THF})_2]_2$ and $[\mathbf{6}(\mathrm{THF})_4]_\infty$

	$(\mathbf{4}\mathrm{THF})_2$	$[\mathbf{5}(\mathrm{THF})_2]_2$	$[\mathbf{6}(\mathrm{THF})_4]_\infty$
Formula	$C_{42}H_{52}B_2Fe_2K_2N_8O_2$	$C_{72}H_{88}B_2Fe_4K_2N_8O_5$	$C_{40}H_{58}B_2FeK_2N_8O_4$
F_w	912.44	1468.72	870.61
Colour, shape	Orange, plate	Orange, block	Orange, block
Crystal size (mm)	0.24 × 0.16 × 0.08	0.35 × 0.33 × 0.26	0.16 × 0.15 × 0.12
Temperature (K)	173(2)	173(2)	173(2)
Radiation Mo Kα (Å)	0.71073	0.71073	0.71073
Crystal syst.	Monoclinic	Triclinic	Monoclinic
Space group	$P2_1/n$	$P\bar{1}$	$P2_1/n$
Unit cell dimensions			
a (Å)	9.8960(11)	10.0893(15)	10.6714(12)
b (Å)	21.711(2)	13.4257(19)	15.6115(17)
c (Å)	10.5580(13)	13.502(2)	13.3795(17)
α (°)	90	67.942(11)	90
β (°)	107.834(9)	84.113(12)	94.535(10)
γ (°)	90	88.370(12)	90
V (Å^3)	2159.4(4)	1686.0(4)	2222.0(4)
Z	2	1	2
D_{calc} (g cm^{-3})	1.403	1.447	1.301
μ (mm^{-1})	0.910	1.025	0.575
No. of reflections collected	21877	23581	18561
No. of independent reflections	4106	6390	4242
R_{int}	0.0935	0.0749	0.0781
Data/restraints/parameters	4106/0/262	6390/0/433	4242/0/259
GOF	0.989	0.912	0.844
R_1, wR_2 ($I > 2\sigma(I)$)	0.0727, 0.1289	0.0418, 0.1024	0.0408, 0.0748
R_1, wR_2 (all data)	0.1344, 0.1487	0.0620, 0.1105	0.0878, 0.0848
Largest differences in peak and hole (e Å^{-3})	0.471, −0.290	0.542, −0.381	0.309, −0.282

electron lone pair, whereas the other is embedded in the π electron cloud.

In the solid state, $\mathrm{Fc_2Bpz_2K}$, **5**, adopts a structure very similar to $(\mathbf{4}\mathrm{THF})_2$ apart from the fact that the methyl group has been replaced by a ferrocenyl substituent and that each of the two potassium ions now bears two THF ligands (i.e. $[\mathbf{5}(\mathrm{THF})_2]_2$; Fig. 3). As a result of the higher coordination number, all K–N and K···COG values are significantly elongated in $[\mathbf{5}(\mathrm{THF})_2]_2$ as compared to $(\mathbf{4}\mathrm{THF})_2$ (cf. $[\mathbf{5}(\mathrm{THF})_2]_2$: K(1)–N(12) = 2.821(3) Å, K(1)–N(22$^{\#}$) = 2.871(3) Å; K(1)···COG(pz) = 3.168 Å, K(1)···COG(Cp$^{\#}$) = 3.171 Å). The conformation of the scorpionate ligand is such that the planes of the C(31)–Cp–, the C(51)–Cp– and the N(21)–pyrazolyl ring are all orthogonal to each other (dihedral angles: C(31)C(32)C(33)C(34)C(35)//C(51)C(52)C(53)C(54)C(55) = 82.7°, N(21)N(22)C(23)-C(24)C(25)//C(31)C(32)C(33)C(34)C(35) = 94.2°, N(21)-N(22)C(23)C(24)C(25)//C(51)C(52)C(53)C(54)C(55) = 84.2°).

The crystal lattice of the discorpionate complex 1,1′-$\mathrm{fc[B(Me)pz_2]_2K_2}$, **6**, consists of coordination polymer strands ($[\mathbf{6}(\mathrm{THF})_4]_\infty$; Figs. 4 and 5). Within these strands, the individual $\mathrm{CpB(Me)pz_2K}$ fragments are again arranged into dinuclear potassium complexes giving rise to essentially the same structural motif as has already been described for $(\mathbf{4}\mathrm{THF})_2$ (cf. $[\mathbf{6}(\mathrm{THF})_4]_\infty$: K(1)–N(12) = 2.787(3) Å, K(1)–N(22$^{\#}$) = 2.786(3) Å; K(1)···COG(pz) = 3.069 Å, K(1)···COG(Cp$^{\#}$) = 3.020 Å). Similar to $[\mathbf{5}(\mathrm{THF})_2]_2$, the ligand environment of the K$^+$ ion of $[\mathbf{6}(\mathrm{THF})_4]_\infty$ contains two THF molecules.

3. Conclusion

We have prepared a series of ferrocene-based bis(pyrazol-1-yl)borate ligands $\mathrm{FcB(Me)pz_2K}$ (**4**), $\mathrm{Fc_2Bpz_2K}$ (**5**) and 1,1′-$\mathrm{fc[B(Me)pz_2]_2K_2}$ (**6**; Fc: ferrocenyl, fc: ferrocenylene, pz: pyrazolyl). Single crystal X-ray structure analyses revealed **4** and **5** to exist as centrosymmetric dimers whereas **6** forms coordination polymer chains. In all three cases, each potassium ion is not only bonded to the pyrazolyl rings but also η^5-coordinated to one ferrocene fragment. The respective distance between the metal atom and the centre of gravity of the cyclopentadienyl ring is 2.942 Å (**4**), 3.171 Å (**5**) and 3.020 Å (**6**). There is only one example of an η^5-ferrocene–K$^+$ complex known in the literature up to now, namely $[\mathrm{K(ferrocene)_2(toluene)_2}]^+$. [9] Here, the average length of the ligand-unsupported K$^+$···COG(Cp) bond equals to 2.964 Å, which is in very good agreement with our findings. This leads to the conclusion that ligands **4**–**6** are well-designed to promote direct bonding interactions between metal atoms and the electron π systems of the ferrocenyl substituents and thus to generate multiple-decker sandwich structures. Work is in progress to synthesize transition metal complexes of our compounds

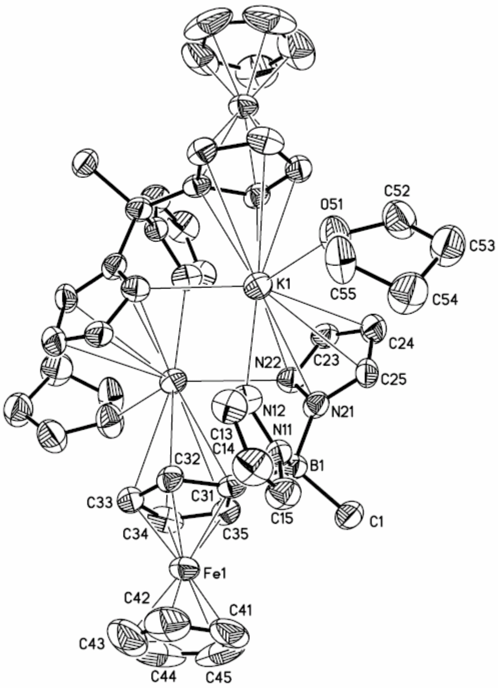

Fig. 2. Molecular structure and numbering scheme of compound $(4THF)_2$. Hydrogen atoms are omitted for clarity. Thermal ellipsoids are shown at the 50% probability level. Selected bond lengths (Å), atom···atom distances (Å), angles (°), torsion angles (°) and dihedral angles (°): B(1)–C(31) = 1.610(9), B(1)–N(11) = 1.568(8), B(1)–N(21) = 1.583(7), K(1)–N(12) = 2.806(5), K(1)–N(22) = 3.145(5), K(1)–N($22^{\#}$) = 2.797(5), K(1)···COG($Cp^{\#}$) = 2.942, K(1)···COG-(pz) = 2.958, K(1)···K($1^{\#}$) = 4.155; N(11)–B(1)–N(21) = 106.4(4), N(12)–K(1)–N(22) = 78.4(1), N(12)–K(1)–N($22^{\#}$) = 91.6(1); N(11)–B(1)–C(31)–C(32) = 15.6(7), N(21)–B(1)–C(31)–C(32) = −100.3(6), N(22)–N(21)–B(1)–C(31) = −7.0(7), N(12)–N(11)–B(1)–C(31) = −72.2(6), N(12)–N(11)–B(1)–N(21) = 45.7(6); N(11)N(12)C(13)C(14)C(15)//C(31)C(32)C(33)C(34)C(35) = 104.9, N(21)N(22)C(23)C(24)C(25)//C(31)C(32)C(33)C(34)C(35) = 71.5, C(31)C(32)C(33)C(34)C(35)//C(41)C(42)C(43)C(44)C(45) = 3.6. COG($Cp^{\#}$): centre of gravity of the C($31^{\#}$)C($32^{\#}$)C($33^{\#}$)C($34^{\#}$) C($35^{\#}$) ring; COG(pz): centre of gravity of the N(21)N(22)C(23)C(24)C(25) ring. Symmetry transformation used to generate equivalent atoms: $-x+1$, $-y+1$, $-z+1$ (#).

and to investigate the degree of electronic metal–ferrocene communication.

4. Experimental

4.1. General remarks

All reactions and manipulations of air-sensitive compounds were carried out in dry, oxygen-free nitrogen using standard Schlenk ware. Solvents were freshly distilled under argon from Na-benzophenone (diethyl ether, THF, toluene) or dried over molecular sieves ($CDCl_3$) prior to use. NMR: Bruker DPX 400, Bruker DPX 250. ^{11}B NMR spectra are reported relative to external $BF_3 \cdot Et_2O$. All NMR spectra were run at ambient temperature; abbreviations: s = singlet, d = doublet, vtr = virtual triplet, br = broad, n.r. = multiplet expected in the NMR spectrum but not resolved, n.o. = signal not observed. $FcB(Me)NMe_2$ [8], 1,1′-$fc[B(Me)NMe_2]_2$ [8], and Fc_2BB_r [8] were synthesized according to the literature procedures.

4.2. Preparation of **2**

A solution of Me_3SiNMe_2 (0.48 g, 4.10 mmol) in toluene (10 ml) was added dropwise with stirring at −78 °C to Fc_2BBr (1.89 g, 4.10 mmol) in toluene (20 ml). The mixture was slowly warmed to room temperature and stirred for 12 h. After the solvent had been removed in vacuo, the product was obtained as a dark orange solid. Yield: 1.50 g (86%). ^{11}B NMR (128.4 MHz, $CDCl_3$): δ 41.0 ($h_{1/2}$ = 330 Hz). ^{1}H NMR (250.1 MHz, $CDCl_3$): δ 3.22 (s, 6H, CH_3), 4.10 (s, 10H, C_5H_5), 4.37, 4.46 (2 × vtr, 2 × 4H, $^3J_{HH} = {}^4J_{HH} = 1.8$ Hz, C_5H_4). ^{13}C NMR (62.9 MHz, $CDCl_3$): δ 42.5 (CH_3), 67.7 (C_5H_4), 68.4 (C_5H_5), 69.8 (C_5H_4), n.o. (C_5H_4–C*ipso*).

4.3. Preparation of **4**

Kpz (0.35 g, 3.33 mmol) and Hpz (0.23 g, 3.33 mmol) were combined in THF (20 ml) and the resulting slurry added dropwise with stirring at −78 °C to **1** (0.85 g, 3.33 mmol) in THF (20 ml). The mixture was slowly warmed to room temperature, refluxed for 24 h and cooled to room temperature again. All volatiles were removed under reduced pressure, the solid residue washed with Et_2O (40 ml) and dried in vacuo. Yield of **4** · THF: 1.35 g (89%). X-ray quality crystals of $(\mathbf{4}THF)_2$ gradually formed when a saturated solution of **4** in THF was stored at 5 °C for a period of several days. ^{11}B NMR (128.4 MHz, d_8-THF): δ − 1.4 ($h_{1/2}$ = 150 Hz). ^{1}H NMR (400.1 MHz, d_8-THF): δ 0.65 (s, 3H, CH_3), 3.84 (s, 5H, C_5H_5), 3.99 (n.r., 4H, C_5H_4), 5.98 (dd, 2H, $^3J_{HH}$ = 2.1 Hz, $^3J_{HH}$ = 1.6 Hz, pzH-4), 7.31∗ (dd, 2H, $^3J_{HH}$ = 1.6 Hz, $^4J_{HH}$ = 0.6 Hz, pzH-3 or 5), $7.45^{\#}$ (dd, 2H, $^3J_{HH}$ = 2.1 Hz, $^4J_{HH}$ = 0.6 Hz, pzH-5 or 3). ^{13}C NMR (100.6 MHz, d_8-THF): δ 10.6 (very br, CH_3), 68.1 (C_5H_4), 68.4 (C_5H_5), 73.6 (C_5H_4), 102.5 (pzC-4), $132.9^{\#}$, 138.1∗ (pzC-3,5), n.o. (C_5H_4-C*ipso*). The two signals (∗) on one hand and the two signals (#) on the other are correlated via crosspeaks in the HSQC spectrum. The compound is sensitive to air and its crystals lose THF when isolated at ambient temperature; a decent elemental analysis was therefore not obtained.

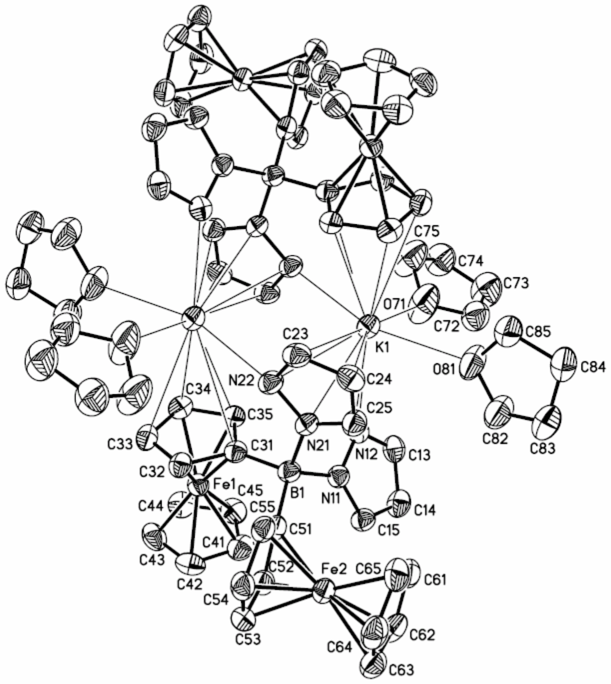

Fig. 3. Molecular structure and numbering scheme of compound [**5**$(THF)_2]_2$. Hydrogen atoms are omitted for clarity. Thermal ellipsoids are shown at the 50% probability level. Selected bond lengths (Å), atom···atom distances (Å), angles (°), torsion angles (°) and dihedral angles (°): B(1)–C(31) = 1.621(4), B(1)–C(51) = 1.619(4), B(1)–N(11) = 1.563(4), B(1)–N(21) = 1.591(4), K(1)–N(12) = 2.821(3), K(1)–N(22) = 3.359(3), K(1)–N(22$^{\#}$) = 2.871(3), K(1)···COG(Cp$^{\#}$) = 3.171, K(1)···COG(pz) = 3.168, K(1)···K(1$^{\#}$) = 4.330; N(11)–B(1)–N(21) = 104.5(2), N(12)–K(1)–N(22) = 76.8(1), N(12)–K(1)–N(22$^{\#}$) = 105.4(1); N(11)–B(1)–C(31)–C(32) = 149.2(3), N(21)–B(1)–C(31)–C(32) = −96.3(3), N(22)–N(21)–B(1)–C(31) = 18.6(4), N(12)–N(11)–B(1)–C(31) = 65.9(3); N(11)N(12)C(13)C(14)C(15)//C(31)C(32)C(33)C(34)C(35) = 60.2, N(21)N(22)C(23)C(24)C(25)//C(31)C(32)C(33)C(34)C(35) = 94.2, N(21)N(22)C(23)C(24)C(25)//C(51)C(52)C(53)C(54)C(55) = 84.2, C(31)C(32)C(33)C(34)C(35)//C(41)C(42)C(43)C(44)C(45) = 2.3, C(31)C(32)C(33)C(34)C(35)//C(51)C(52)C(53)C(54)C(55) = 82.7. COG(Cp$^{\#}$): centre of gravity of the C(31$^{\#}$)C(32$^{\#}$) C(33$^{\#}$)C(34$^{\#}$) C(35$^{\#}$) ring; COG(pz): centre of gravity of the N(21)N(22)C(23)C(24)C(25) ring. Symmetry transformation used to generate equivalent atoms: $-x + 1, -y + 1, -z$ (#).

4.4. Preparation of ***5***

The compound was prepared similar to **4** from Kpz (0.18 g, 1.70 mmol), Hpz (0.12 g, 1.70 mmol) and **2** (0.72 g, 1.70 mmol) in THF. Yield of **5** · 2THF: 1.00 g (84%). X-ray quality crystals of [**5**$(THF)_2]_2$ gradually formed when a saturated solution of **5** in THF was stored at 5 °C for a period of several days. ^{11}B NMR (128.4 MHz, d_8-THF): δ 1.0 ($h_{1/2}$ = 230 Hz). ^{1}H NMR (400.1 MHz, d_8-THF): δ 3.69 (s, 10H, C_5H_5), 4.08, 4.52 (2 × vtr, 2 × 4H, $^{3}J_{HH} = {}^{4}J_{HH}$ = 1.7 Hz, C_5H_4), 6.01 (vtr, 2H, $^{3}J_{HH}$ = 1.7 Hz, pzH-4), 7.36 (d, 2H, $^{3}J_{HH}$ = 1.9 Hz, pzH-3 or 5), 7.41 (br, 2H, pzH-5 or 3). ^{13}C NMR (100.6 MHz, d_8-THF): δ 68.4 (C_5H_4), 68.6 (C_5H_5), 74.9 (C_5H_4), 102.1 (pzC-4), 135.1, 138.0 (pzC-3,5), n.o. (C_5H_4-C*ipso*). The compound is sensitive to air and its crystals lose THF when isolated at ambient temperature; a decent elemental analysis was therefore not obtained.

4.5. Preparation of ***6***

Kpz (0.33 g, 3.08 mmol) and Hpz (0.21 g, 3.08 mmol) were combined in THF (20 ml) and the resulting slurry added with stirring at −78 °C via a dropping funnel to **3** (0.50 g, 1.54 mmol) in THF (20 ml). The mixture was slowly warmed to room temperature, stirred for 11 h, refluxed for 34 h and cooled to room temperature again. The solvent was driven off under reduced pressure, the solid residue washed with Et_2O (40 ml) and dried in vacuo. Yield of **6** · 4THF: 1.00 g (75%). A suspension of **6** in THF was heated at 60 °C in an ultrasonic bath. Cooling of the resulting clear solution to room temperature led to the deposition of X-ray quality crystals of

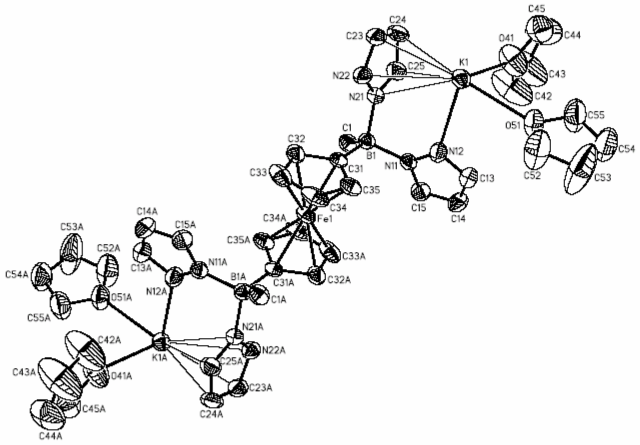

Fig. 4. Molecular structure and numbering scheme of compound [**6**$(THF)_4]_\infty$. Hydrogen atoms are omitted for clarity. Thermal ellipsoids are shown at the 50% probability level. Selected bond lengths (Å), atom···atom distances (Å), angles (°), torsion angles (°), and dihedral angles (°): B(1)–C(31) = 1.606(4), B(1)–N(11) = 1.569(4), B(1)–N(21) = 1.584(4), K(1)–N(12) = 2.787(3), K(1)–N(22) = 3.243(2), K(1)–N($22^{\#}$) = 2.786(3), K(1)···COG(Cp$^{\#}$) = 3.020, K(1)···COG(pz) = 3.069, K(1)···K($1^{\#}$) = 4.558; N(11)–B(1)–N(21) = 104.8(2), N(12)–K(1)–N(22) = 72.3(1), N(12)–K(1)–N($22^{\#}$) = 94.5(1); N(11)–B(1)–C(31)–C(32) = −169.7(2), N(21)–B(1)–C(31)–C(32) = 76.1(3), N(22)–N(21)–B(1)–C(31) = 2.5(4), N(12)–N(11)–B(1)–C(31) = −77.6(3); N(11)N(12)C(13)C(14)C(15)//C(31)C(32)C(33)C(34)C(35) = 104.4, N(21)N(22)C(23)C(24)C(25)//C(31)C(32)-C(33)C(34)C(35) = 102.3. COG(Cp$^{\#}$): centre of gravity of the C($31^{\#}$)C($32^{\#}$) C($33^{\#}$)C($34^{\#}$) C($35^{\#}$) ring; COG(pz): centre of gravity of the N(21)N(22)C-(23)C(24)C(25) ring. Symmetry transformation used to generate equivalent atoms: $-x + 1$, $-y + 1$, $-z + 1$ (#).

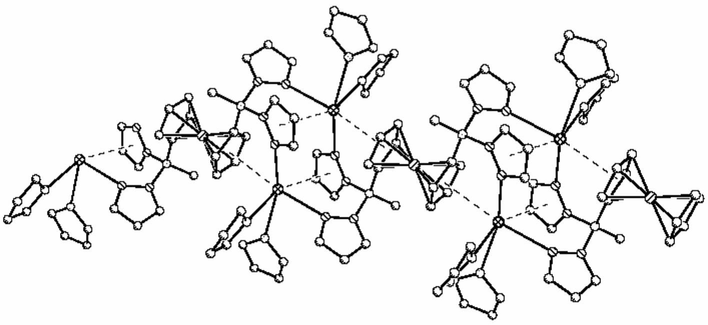

Fig. 5. View of one polymer strand of [**6**$(THF)_4]_\infty$; hydrogen atoms omitted for clarity.

[**6**$(THF)_4]_\infty$. ^{11}B NMR (128.4 MHz, d_8-THF): δ-1.3 ($h_{1/2}$ = 250 Hz). ^{1}H NMR (250.1 MHz, d_8-THF): δ 0.67 (s, 6H, CH_3), 3.75, 3.80 (2 × vtr, 2 × 4H, $^{3}J_{HH} = {}^{4}J_{HH}$ = 1.7 Hz, C_5H_4), 5.90 (dd, 4H, $^{3}J_{HH}$ = 2.1 Hz, $^{3}J_{HH}$ = 1.6 Hz, pzH-4), 7.21* (dd, 4H, $^{3}J_{HH}$ = 1.6 Hz, $^{4}J_{HH}$ = 0.7 Hz, pzH-3 or 5) 7.47$^{\#}$ (dd, 4H, $^{3}J_{HH}$ = 2.1 Hz, $^{4}J_{HH}$ = 0.7 Hz, pzH-5 or 3). ^{13}C NMR (62.9 MHz, d_8-THF): δ 11 (very br, CH_3), 68.9, 73.7 (C_5H_4), 102.0 (pz-C4), 132.3$^{\#}$, 137.6* (pz-C3,5), n.o. (C_5H_4-C*ipso*). The two signals (*) on one hand and the two signals (#) on the other are correlated via crosspeaks in the HSQC spectrum. The compound is sensitive to air and its crystals lose THF when isolated at ambient temperature; a decent elemental analysis was therefore not obtained.

5. X-ray crystal structure determination of $(\mathbf{4}THF)_2$, [**5**$(THF)_2]_2$ and [**6**$(THF)_4]_\infty$

Data collection for all structures was performed on a STOE-IPDS-II diffractometer with graphite-monochromated MoK_α-radiation. The structures were solved with direct methods [10] and refined against F^2 using full-matrix least-squares [11]. Absorption corrections were performed with the MULABS [12] option in PLATON [13]. All non-H atoms have been refined anisotropically, whereas the H atoms have been treated with a riding model, fixing their displacement parameter to 1.2 or 1.5 (for methyl groups) of the value of their parent atom. The asymmetric unit of [**5**$(THF)_2]_2$ contains a

THF molecule which is disordered about a centre of inversion.

Crystallographic data for the structure analyses have been deposited with the Cambridge Crystallographic Data Centre, CCDC Nos. 253747 ((**4**THF)$_2$), 253749 ([**5**(THF)$_2$]$_2$), 253748 ([**6**(THF)$_4$]$_\infty$).

Acknowledgement

This work was generously supported by the *Deutsche Forschungsgemeinschaft* (DFG).

References

[1] S. Trofimenko, Scorpionates - The Coordination Chemistry of Polypyrazolylborate Ligands, Imperial College Press, London, 1999.
[2] F. Jäkle, K. Polborn, M. Wagner, Chem. Ber. 129 (1996) 603–606.
[3] F. Fabrizi de Biani, F. Jäkle, M. Spiegler, M. Wagner, P. Zanello, Inorg. Chem. 36 (1997) 2103–2111.
[4] E. Herdtweck, F. Peters, W. Scherer, M. Wagner, Polyhedron 17 (1998) 1149–1157.
[5] S.L. Guo, F. Peters, F. Fabrizi de Biani, J.W. Bats, E. Herdtweck, P. Zanello, M. Wagner, Inorg. Chem. 40 (2001) 4928–4936.
[6] A. Haghiri Ilkhechi, M. Scheibitz, M. Bolte, H.-W. Lerner, M. Wagner, Polyhedron 23 (2004) 2597–2604.
[7] D.L. Reger, K.J. Brown, J.R. Gardinier, M.D. Smith, Organometallics 22 (2003) 4973–4983.
[8] (a) T. Renk, W. Ruf, W. Siebert, J. Organomet. Chem. 120 (1976) 1–25;
(b) M. Scheibitz, J.B. Heilmann, R.F. Winter, M. Bolte, J.W. Bats, M. Wagner, Dalton Trans., in press.
[9] G.W. Honeyman, A.R. Kennedy, R.E. Mulvey, D.C. Sherrington, Organometallics 23 (2004) 1197–1199.
[10] G.M. Sheldrick, Acta Crystallogr. Sect. A. 46 (1990) 467–473.
[11] G.M. Sheldrick, SHELXL-97. A Program for the Refinement of Crystal Structures, Universität Göttingen, Göttingen, 1997.
[12] R.H. Blessing, Acta Crystallogr. Sect. A. 51 (1995) 33–38.
[13] A.L. Spek, Acta Crystallogr. Sect. A. 46 (1990) C34.

6.5 „Multiply Borylated Arenes: X-ray Crystal Structure Analyses and Quantum Chemical Calculations“

Monika C. Haberecht, Julia B. Heilmann, Alireza Haghiri Ilkhechi, Michael Bolte, Jan W. Bats, Hans-Wolfram Lerner, Max C. Holthausen and Matthias Wagner,

Z. Anorg. Allg. Chem., **2004**, 630, 904-913.

Multiply Borylated Arenes: X-ray Crystal Structure Analyses and Quantum Chemical Calculations

Monika C. Haberecht[a], **Julia B. Heilmann**[a], **Alireza Haghiri**[a], **Michael Bolte**[a], **Jan W. Bats**[b], **Hans-Wolfram Lerner**[a], **Max C. Holthausen**[c,*] **and Matthias Wagner**[a,*]

Frankfurt am Main, [a] Institut für Anorganische Chemie and [b] Institut für Organische Chemie der J. W. Goethe-Universität
Marburg, [c] Fachbereich Chemie der Philipps-Universität

Received January 30th, 2004.

Abstract. Optimised synthesis procedures and results of X-ray single crystal structure analyses for 4-(dibromoboryl)toluene, 1,3-bis(dibromoboryl)benzene, 1,4-bis(dibromoboryl)benzene, and 1,3,5-tris(dibromoboryl)benzene are reported. These compounds have also been studied by Hartree-Fock (HF), density functional theory (DFT), and Møller-Plesset second-order perturbation (MP2) methods in combination with the polarized double-ζ valence (SVP) and polarized triple-ζ valence (TZVP) basis sets of *Ahlrichs* and coworkers. A comparison of the quantum chemical results for optimised geometries and computed NMR chemical shifts with experiment is presented to test the quality of the various methods for this class of compounds. All DFT methods tested yield optimised geometries within the experimental error bars of 3σ for bond lengths, whereas larger deviations among the methods are observed for computed NMR chemical shifts. This calibration recommends the B3LYP/SVP combination as a reliable and computationally efficient level of theory to assess the structures and absolute and relative ^{1}H-, ^{13}C- and ^{11}B NMR shift values of borylated aromatic compounds in future investigations.

Keywords: Lewis acids; Arylboranes; Crystal structures; Quantum chemical calculations

Mehrfach borylierte Arene: Kristallstrukturanalysen and quantenchemische Rechnungen

Inhaltsübersicht. Wir berichten über optimierte Synthesevorschriften und die Ergebnisse der Kristallstrukturanalysen von 4-(Dibromoboryl)toluol, 1,3-Bis(dibromoboryl)benzol, 1,4-Bis(dibromoboryl)benzol und 1,3,5-Tris(dibromoboryl)benzol. Diese Verbindungen wurden weiterhin mittels Hartree-Fock (HF), Dichtefunktionaltheorie (DFT) und Møller-Plesset-Störungstheorie (MP2) in Kombination mit dem polarisierten Double-ζ Valenz- (SVP) und dem polarisierten Triple-ζ Valenzbasissatz (TZVP) von *Ahlrichs* et al. untersucht. Ein Vergleich der optimierten Geometrien und berechneten NMR-Verschiebungen mit den entsprechenden experimentellen Daten dient als Test für die Qualität der unterschiedlichen theoretischen Methoden im Hinblick auf eine zuverlässige Behandlung der hier untersuchten Verbindungsklasse. Alle eingesetzten DFT-Methoden liefern optimierte Molekülstrukturen, deren Bindungslängen im Rahmen des 3σ-Fehlerintervalls mit dem Experiment übereinstimmen. Bei der Berechnung von NMR-Verschiebungen treten signifikante Abweichungen zwischen den einzelnen Methoden auf. Für zukünftige Untersuchungen borylierter aromatischer Verbindungen empfiehlt sich die Verwendung der B3LYP/SVP Kombination als zuverlässiges und effizientes theoretisches Niveau zur Berechnung von Molekülstrukturen sowie absoluter und relativer ^{1}H-, ^{13}C- und ^{11}B NMR-Verschiebungen.

1 Introduction

Molecules containing several Lewis acidic functional groups (e.g. BR_2) are currently gaining growing attention due to potential applications as (co)catalysts in organic transformations [1]. Among the smaller molecules that may serve as backbones of multiply borylated compounds, ferrocene is of particular interest since it can conveniently be substituted 1-4 times upon reaction with the appropriate amount of BBr_3 (**Ia-d**, Figure 1) [2−6]. The resulting ferrocenylboranes have been successfully employed for the generation of charge transfer polymers, redox-active macrocycles and ferrocenophanes with switchable *ansa* bridges (see refs [7, 8] for reviews). Recently, even polymeric boron-containing Lewis acids (e.g. dibromoborylated polystyrene **II**, Fig. 1) have been reported by *Jäkle* et al. [9].

Our group is interested in borylarene derivatives, which may serve as useful building blocks for the synthesis of oligonuclear Lewis acids and oligotopic tris(1-pyrazolyl)borate ligands [10]. In contrast to ferrocene, borylation of benzene is not achieved by the direct reaction of the aromatic compound with boron trihalides. However, treatment of (trimethylsilyl)arenes with BX_3 (X = Cl, Br, I) results in the clean substitution of the silyl group for a BX_2 substituent (Scheme 1) [11]. Using this method, various monoborylated, 1,2-, 1,3- and 1,4-diborylated as well as 1,3,5-triboryl-

---

* Prof. Dr. M. Wagner
Institut für Anorganische Chemie
der J. W. Goethe-Universität
Marie-Curie-Str. 11
D-60439 Frankfurt (Main)
Fax: +49(0)69-79829260
E-mail: Matthias.Wagner@chemie.uni-frankfurt.de

* Dr. M. C. Holthausen
Fachbereich Chemie der Philipps-Universität
D-35032 Marburg

DOI: 10.1002/zaac.200400021

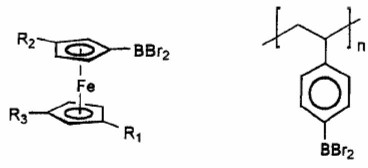

Ia: $R_1 = R_2 = R_3 = H$
Ib: $R_1 = BBr_2$; $R_2 = R_3 = H$
Ic: $R_1 = R_2 = BBr_2$; $R_3 = H$
Id: $R_1 = R_2 = R_3 = BBr_2$

II

Figure 1 Mono- to tetraborylated ferrocene derivatives (**Ia** − **Id**) and the polymeric Lewis acid **II**.

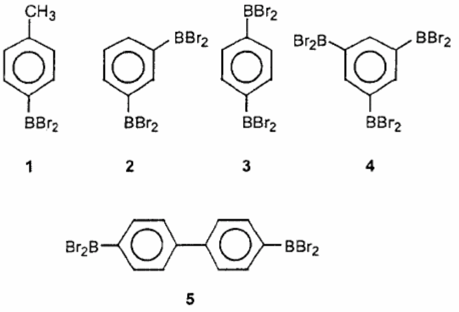

1 **2** **3** **4**

5

$\text{Aryl-SiMe}_3 + BBr_3 \longrightarrow \text{Aryl-BBr}_2 + BrSiMe_3$

Scheme 1 Borylated arenes **1**−**5** and the general synthesis strategy via silyl/boryl exchange.

ated benzene derivatives have been synthesized by *Kaufmann* [11] and *Siebert* [12]. *Siebert* et al. also obtained hexaborylbenzenes by the $CpCo(CO)_2$-catalysed cyclotrimerisation of diborylacetylenes [13].

The purpose of this paper is to summarize optimised synthetic procedures for the (dibromoboryl)arenes **1-5** (Scheme 1), to provide a full NMR spectroscopical characterization of these compounds, and to discuss their molecular structures in the solid state. The experimental data is augmented with density functional (DFT) calculations [14] on **1-4** to unambiguously assign ^{1}H- and ^{13}C NMR chemical shifts and to get insight into the degree of aryl-boron π bonding within these compounds. In order to test the applicability of contemporary DFT for this class of compounds, several density functionals widely in use have been tested in combination with standard basis sets.

2 Results and Discussion

2.1 Synthesis and Spectroscopy

All borylarenes **1**−**5** were synthesized by treating the corresponding aryl(trimethyl)silanes with excess BBr_3 (**1**: 1.5 equiv.; **2**, **3**, **5**: 3-4 equiv.; **4**: 6 equiv.) The general reaction is outlined in Scheme 1. The first BBr_2 group is easily introduced into the aryl ring already at ambient temperature, whereas further substitution generally requires higher temperatures.

Note: For the assignment of ^{1}H- and ^{13}C NMR resonances, a numbering scheme following the standard IUPAC nomenclature is employed, which is different from the atom labelling in the crystal structure analyses. The ^{11}B NMR signals of **1-5** lie in the range between 56.6 ppm (**1**) and 58.3 ppm (**3**) characteristic of trivalent aryl-BBr_2 species [15]. Since the boron atoms possess rather uniform coordination spheres in **1-5**, the strongest influence on the magnetic shielding can be expected to come from the π charge density on the boron nuclei which is obviously very similar in all five compounds. As an experimental probe for the charge density distribution within the aromatic rings, ^{13}C NMR spectroscopy provides a more reliable diagnostic tool than ^{1}H NMR spectroscopy, because proton shift values may be greatly influenced by magnetic anisotropy effects [16]. In the monoborylated derivative **1**, the carbon atoms C-3 and C-5 appear at δ = 138.3 and are thus deshielded by 9.8 ppm compared to the corresponding carbon nuclei in parent toluene (δ = 128.5 [16]). In contrast, only a negligible shift difference is observed between the carbon atoms C-2 and C-6 of **1** (δ = 129.4) and the complementary carbon atoms of toluene (δ = 129.3 [16]). Introduction of a second BBr_2 substituent into the 3-position of the benzene ring (**2**) leads to three ^{13}C NMR resonances with chemical shift values of δ = 147.0 (C-2), 143.5 (C-4,6) and 128.1 (C-5; C-1,3 are not observed due to an extreme broadening of their ^{13}C NMR signals, which has to be attributed to the quadrupolar relaxation of the boron nucleus [15]). Again, the chemical shift of the carbon atom in the *meta* position to both boryl substituents (C-5) is virtually unchanged compared to the benzene molecule [$\delta(C_6H_6)$ = 128.5 [16]]. The other three carbon nuclei, which experience a π electron-withdrawing effect of *two* boryl groups, show an additional deshielding of 8.7 ppm (C-2) and 5.2 ppm (C-4,6) with respect to the monoborylated species **1** (18.5 ppm and 15.0 ppm with respect to benzene). In the 1,4-diborylated derivative **3**, the atoms C-2,3,5,6 give rise to one ^{13}C NMR signal at δ = 136.5 in agreement with the resonances of C-3,5 in **1** (δ = 138.3). In the triborylated molecule **4**, each of the carbon atoms C-2, C-4 and C-6 is located in a position *ortho* to two boryl substituents and *para* to the third one. Consequently, the respective NMR resonance appears at extremely low field [δ(C-2,4,6) = 151.4; $\Delta\delta$(**4**-benzene) = 22.9]. As to be expected, the ^{13}C NMR spectrum of the biphenyl derivative **5** [δ(C-3,3′,5,5′) = 138.6, δ(C-2,2′,6,6′) = 127.1], which bears one BBr_2 substituent per C_6H_4 ring, closely resembles the spectrum of 4-(dibromoboryl)toluene **1** [δ(C-3,5) = 138.3, δ(C-2,6) = 129.4]. Qualitatively similar trends as discussed for the ^{13}C NMR shifts are observed for the proton resonances of **1** − **5** (see Experimental Section).

Table 1 Crystallographic data of the compounds **1** − **5**

	1	**2**	**3**	**4**	**5**
formula	$C_7H_7BBr_2$	$C_6H_4B_2Br_4$	$C_6H_4B_2Br_4$	$C_6H_3B_3Br_6$	$C_{12}H_8B_2Br_4$
fw	261.76	417.35	417.35	586.97	493.44
colour, shape	colourless, plate	colourless, needle	colourless, needle	colourless, needle	colourless, plate
crystal size /mm	0.45×0.28×0.06	0.49×0.11×0.09	0.26×0.09×0.07	0.28×0.05×0.03	0.33×0.25×0.05
temp /K	143(2)	100(2)	173(2)	173(2)	173(2)
radiation (MoK_α) /Å	0.71073	0.71073	0.71073	0.71073	0.71073
crystal syst.	orthorhombic	orthorhombic	monoclinic	hexagonal	monoclinic
space group	$Pca2_1$	$Pna2_1$	$P2_1/c$	$P6_122$	$P2_1/n$
a /Å	20.161(4)	20.1283(15)	4.0998(10)	11.0560(9),	4.0864(12)
b /Å	4.0467(7)	4.0393(3)	10.805(2)	11.0560(9),	20.970(4)
c /Å	10.542(2)	13.0422(13)	12.275(3)	20.376(2),	8.573(3)
β /deg			91.54(2)		100.66(3)
V /Å^3	860.1(3)	1060.39(15)	543.6(2)	2157.0(3)	722.0(4)
Z	4	4	2	6	2
$D_{calcd.}$ /g cm^{-3}	2.021	2.614	2.550	2.711	2.270
μ /mm^{-1}	9.344	15.121	14.749	16.715	11.124
no. of rflns. coll.	10551	11711	4399	15122	3139
no. of rflns. obs. (I > 2σ(I))	1888	1878	787	1042	745
no. of indep. rflns.	2643	2064	1098	1297	1296
R(int)	0.0848	0.0610	0.0728	0.1511	0.1909
data/restr./ param.	2643/1/ 92	2064/1/109	1098/0/55	1297/0/70	1296/0/82
GOF	1.044	0.995	1.005	1.045	0.983
F(000)	496	760	380	1584	460
$R1$, $wR2$ (I > 2σ(I))	0.0498, 0.0947	0.0261,0.0589	0.0420, 0.0832	0.0507, 0.0719	0.1058, 0.2578
$R1$, $wR2$ (all data)	0.0838, 0.1047	0.0294, 0.0598	0.0685, 0.0921	0.0730, 0.0771	0.1473, 0.2879
largest diff. peak and hole /e Å^{-3}	0.896, −0.891	0.660, −0.330	0.701, −0.714	0.382, −0.573	1.287, −1.377

2.2 *X-ray crystallography*

X-ray quality crystals of **1** (orthorhombic; $Pca2_1$) were obtained by slow evaporation of its *n*-pentane solution. **2** (orthorhombic; $Pna2_1$), **3** (monoclinic; $P2_1/c$), **4** (hexagonal; $P6_122$) and **5** (monoclinic; $P2_1/n$) precipitated from the reaction mixtures [solvents: pentane (**2**), toluene (**3**, **4**, **5**)] upon cooling from reflux temperature to ambient temperature. Details of the crystal structure analyses of **1**-**5** are summarized in Table 1.

1 (Figure 2) adopts an almost planar conformation in the solid state (dihedral angle between the plane of the phenyl ring and the plane spanned by the BBr_2 substituent: 6.5°). The Br(1)-B(1)-Br(2) angle of 114.4(4)° is significantly smaller than the adjacent angles C(1)-B(1)-Br(1) [122.4(5)°] and C(1)-B(1)-Br(2) [123.3(5)°; sum of angles around the boron atom 360°]. The angle with the boryl substituent attached to its vertex [C(2)-C(1)-C(6) = 116.6(5)°], deviates by 3.4° from the value of 120° expected for an ideal sp^2-hybridized carbon atom. The crystal lattice features intermolecular C-H···Br contacts with distances ranging from 3.18 Å to 3.23 Å, and C-H···π(phenyl) contacts of about 3.0 Å.

The planar 1,3-diborylated compound **2** [dihedral angles: C(1)C(2)C(3)C(4)C(5)C(6)//B(1)Br_2 = 5.6(5)°; C(1)C(2)C(3)C(4)C(5)C(6)//B(2)Br_2 = 6.0(5)°] exhibits structural features similar to **1** (Figure 3). **2** crystallizes in parallel stacks and shows intermolecular C-H···Br contacts in a range from 3.08 Å to 3.12 Å.

Compound **3** (Figure 4) contains an inversion center in the solid state and features an almost planar molecular structure similar to **1** and **2** [dihedral angle between the plane of the phenyl ring and the plane spanned by the BBr_2 substituent: 4.3(5)°]. The carbon-carbon bonds C(1)-C(2) = 1.405(9) Å and C(1)-C(3A) = 1.412(9) Å are somewhat longer than those bonds of the aromatic ring which connect non-borylated carbon atoms [C(2)-C(3) = 1.385(9) Å]. **3** forms a layer structure in the solid state. Within these layers, the B···B axis of each molecule is oriented orthogonal to the B···B axes of its four next neighbors. This arrangement results in intermolecular C-H···Br contacts of 3.98(1) Å, 3.89(1) Å and 3.76(3) Å. Consecutive layers are shifted with respect to each other in such a way that the bromine atoms of one layer are placed on top of the boron atoms of the other.

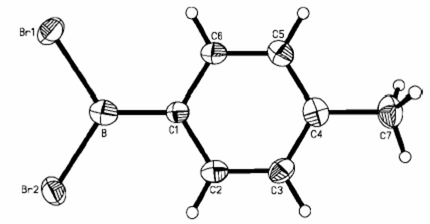

Figure 2 Structure plot of **1** in the solid state. Displacement ellipsoids are drawn at the 50 % probability level.

Bond lengths/Å, angles/° and dihedral angles/°: B(1)-C(1) 1.499(9), B(1)-Br(1) 1.943(7), B(1)-Br(2) 1.931(7), C(1)-C(2) 1.421(8), C(2)-C(3) 1.373(9), C(3)-C(4) 1.383(9), C(4)-C(5) 1.384(9), C(5)-C(6) 1.369(9), C(6)-C(1) 1.395(8); Br(1)-B(1)-Br(2) 114.4(4), C(1)-B(1)-Br(1) 122.4(5), C(1)-B(1)-Br(2) 123.3(5), C(1)-C(2)-C(3) 120.8(6), C(2)-C(3)-C(4) 121.3(6), C(3)-C(4)-C(5) 118.2(6), C(4)-C(5)-C(6) 121.3(6), C(5)-C(6)-C(1) 121.6(5), C(6)-C(1)-C(2) 116.6(5); C(1)C(2)C(3)C(4)C(5)C(6)//B(1)Br_2 6.5.

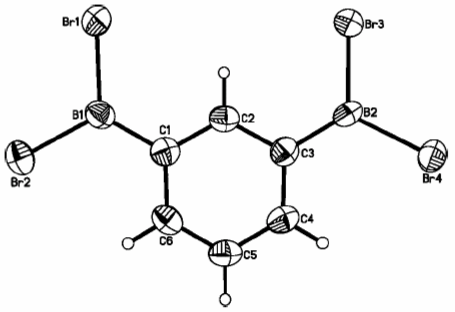

Figure 3 Structure plot of **2** in the solid state. Displacement ellipsoids are drawn at the 50 % probability level.

Bond lengths/Å, angles/° and dihedral angles/°: B(1)-C(1) 1.543(9), B(2)-C(3) 1.526(9), B(1)-Br(1) 1.919(7), B(1)-Br(2) 1.910(7), B(2)-Br(3) 1.921(6), B(2)-Br(4) 1.919(6), C(1)-C(2) 1.401(9), C(2)-C(3) 1.422(8), C(3)-C(4) 1.404(8), C(4)-C(5) 1.385(10), C(5)-C(6) 1.382(10), C(6)-C(1) 1.410(9); Br(1)-B(1)-Br(2) 116.7(4), C(1)-B(1)-Br(1) 121.0(5), C(1)-B(1)-Br(2) 122.3(5), C(1)-C(2)-C(3) 122.3(5), C(2)-C(3)-C(4) 117.3(5), C(3)-C(4)-C(5) 121.3(6), C(4)-C(5)-C(6) 120.1(6), C(5)-C(6)-C(1) 121.6(6), C(6)-C(1)-C(2) 117.3(5); C(1)C(2)C(3)C(4)C(5)C(6)//B(1)Br_2 5.6(5)°, C(1)C(2)C(3)C(4)C(5)C(6)//B(2)Br_2 6.0(5)°.

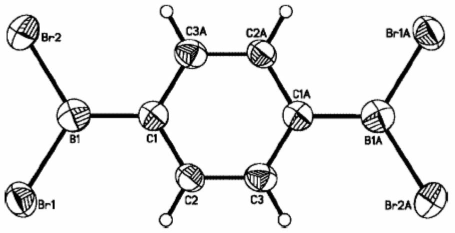

Figure 4 Structure plot of **3** in the solid state. Displacement ellipsoids are drawn at the 50 % probability level.

Bond lengths/Å, angles/° and dihedral angles/°: B(1)-C(1) 1.559(11), B(1)-Br(1) 1.925(8), B(1)-Br(2) 1.920(9), C(1)-C(2) 1.405(9), C(2)-C(3) 1.385(9), C(1)-C(3A) 1.412(9); Br(1)-B(1)-Br(2) 116.6(4), C(1)-B(1)-Br(1) 121.4(6), C(1)-B(1)-Br(2) 122.0(5), C(1)-C(2)-C(3) 120.5(6), C(2)-C(3)-C(1A) 121.2(6), C(2)-C(1)-C(3A) 118.3(6); C(1)C(2)C(3)C(1A)C(2A)C(3A)//B(1)Br_2 4.3(5). Symmetry transformations used to generate equivalent atoms: 2−x, 1−y, 1−z.

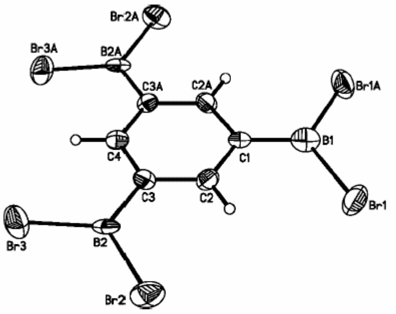

Figure 5 Structure plot of **4** in the solid state. Displacement ellipsoids are drawn at the 50 % probability level.

Bond lengths/Å, angles/° and dihedral angles/°: B(1)-C(1) 1.520(20), B(2)-C(3) 1.571(12), B(1)-Br(1) 1.908(11), B(2)-Br(2) 1.888(13), B(2)-Br(3) 1.903(14), C(1)-C(2) 1.418(13), C(2)-C(3) 1.423(16), C(3)-C(4) 1.388(13); Br(1)-B(1)-Br(1A) 117.3(11), Br(2)-B(2)-Br(3) 118.8(6), C(1)-B(1)-Br(1) 121.4(5), C(3)-B(2)-Br(2) 122.2(9), C(3)-B(2)-Br(3) 119.0(9), C(1)-C(2)-C(3) 122.7(8), C(2)-C(3)-C(4) 117.2(8), C(3)-C(4)-C(3A) 124.0(13), C(2A)-C(1)-C(2) 116.3(13); C(1)C(2)C(3)C(4)C(3A)C(2A)//B(1)Br_2 8.8(1), C(1)C(2)C(3)-C(4)C(3A)C(2A)//B(2)Br_2 5.8(1). Symmetry transformations used to generate equivalent atoms: −x, −x+y, −z+2/3.

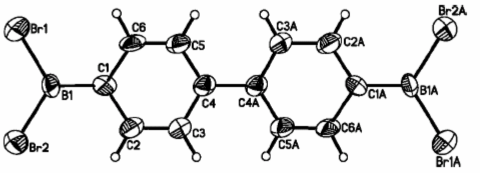

Figure 6 Structure plot of **5** in the solid state. Displacement ellipsoids are drawn at the 50 % probability level.

Bond lengths/Å, angles/° and dihedral angles/°: B(1)-C(1) 1.53(2), B(1)-Br(1) 1.90(2), B(1)-Br(2) 1.90(2), C(1)-C(2) 1.44(2), C(2)-C(3) 1.38(3), C(3)-C(4) 1.41(3), C(4)-C(5) 1.41(2), C(5)-C(6) 1.31(3), C(6)-C(1) 1.46(2), C(4)-C(4A) 1.50(3); Br(1)-B(1)-Br(2) 117.1(8), C(1)-B(1)-Br(1) 120.6(12), C(1)-B(1)-Br(2) 122.2(12), C(1)-C(2)-C(3) 122.9(17), C(2)-C(3)-C(4) 119.3(15), C(3)-C(4)-C(5) 118.5(15), C(4)-C(5)-C(6) 122.7(16), C(5)-C(6)-C(1) 122.5(15), C(6)-C(1)-C(2) 113.9(14); C(1)C(2)C(3)C(4)C(5)C(6)//B(1)Br_2 1(1), C(1)C(2)-C(3)C(4)C(5)C(6)//C(1A)C(2A)C(3A)C(4A)C(5A)C(6A) 0.0(9). Symmetry transformations used to generate equivalent atoms: 1−x, 2−y, 2−z.

Similar to **1**, **2**, and **3**, the 1,3,5-triborylated species **4** is effectively planar with dihedral angles between the BBr_2 substituents and the phenyl ring of 5.8(1)° and 8.8(1)° (Figure 5). A value of 1.520(20) Å is found for the B(1)-C(1) bond while the B(2)-C(3) bond length is 1.571(12) Å. The C-C bond lengths of the central six-membered ring fall in a range between 1.388(13) Å [C(3)-C(4)] and 1.423(16) Å [C(2)-C(3)]. The molecules are arranged into helical stacks, all of them having the same sense of rotation (chiral space group $P6_122$). The only symmetry element present in the solid state structure is a C_2 axis along the atoms B(1), C(1) and C(4). Given an essentially planar structure for **4**, however, we would expect an effective D_{3h} symmetry for this species. The lack of any obvious reason for the symmetry breaking in the crystal structure spurred us to perform quantum chemical calculations to gain further insights (see below).

The crystal structure analysis of **5** suffers from large error margins because the crystals were just weakly diffracting thin plates. Bond lengths and angles (Figure 6) will therefore not be discussed in any detail. **5** shows a dihedral angle between the BBr_2 substituent and the phenyl ring of only 1(1)°. The biphenyl backbone also adopts a planar conformation [C(1)C(2)C(3)C(4)C(5)C(6)//C(1A)C(2A)C(3A)-C(4A)C(5A)C(6A) = 0.0(9)°]. **5** crystallizes in parallel stacks featuring a herringbone pattern. There are several C-H···Br contacts with distances in the interval between 3.07 Å and 3.28 Å but no C-H···π(phenyl) interactions.

2.3 *Quantum Chemical Calculations*

Quantum chemical calculations have been performed by means of the programs Turbomole [17] and Gaussian 03 [18]. As 'production quality' method, for example, the B3LYP/cc-pVTZ functional/basis set combination could be considered the most reliable quality of approximation within the framework of DFT established so far [14]. Using contemporary workstation hardware, however, calculations at this level are computationally quite expensive already for the present systems. As we intend to study the chemistry of much larger borylated aromatic systems in the future we included other, potentially more efficient functional/basis set combinations in our study. At the GGA level we used the older BP86 and BLYP functionals, both of which are quite commonly in use, as well as the HCTH407 functional of *Boese* et al. [19], which has been newly implemented in the Gaussian 03 program (HCTH for short). All GGA functionals can make use of the resolution of identity (RI) approximation [20], which can improve the computational efficiency and scalability with system size substantially. However, use of the very small DGA1 Coulomb density fitting basis available in the program Gaussian 03 resulted in a substantial pyramidalisation of BBr_2 groups in several test calculations. This has been clearly identified as an artefact due to the neglect of higher angular momentum functions in the atomic fitting basis for Br. As we are interested here only in the general performance of functionals and basis sets, we avoided the use of the RI approach in the current study − more careful testing of available density fitting basis sets for use with Gaussian 03 is clearly indicated. As a newly developed hybrid method we employed the B98 functional of *Schmider* and *Becke* [21]. DFT results are compared to Hartree-Fock (HF) and Møller-Plesset second order perturbation theory (MP2) calculations − computationally the latter level is nearly prohibitively demanding for the present system size if used with basis sets of polarized triple-ζ quality, and not an efficient means to treat larger molecular systems. All calculations have been done in combination with the SVP and TZVP basis sets of *Ahlrichs* and coworkers [22, 23]. Additional B3LYP calculations have been performed using the large cc-pVTZ basis of *Dunning* [24]. All structures have been optimised within the highest applicable symmetry point group (C_s, C_{2v}, C_{2v}, and D_{3h} for **1**, **2**, **3** and **4**, respectively). The minimum character of the resulting stationary points has been confirmed by the absence of negative eigenvalues in the analytically computed Hessian matrices. Calculations of nuclear magnetic shielding tensors were performed based on the gauge-independent atomic orbital (GIAO) approach as implemented in Gaussian 03 [25].

For a comparison of calculated and experimental data a common numbering scheme following the standard IUPAC nomenclature is employed. Here, only the mean experimental values of symmetry-related bond lengths are discussed. First of all we note that for all computational models applied all trends observable in the experimental bond lengths (Tables 2−5), angles, and dihedral angles are reproduced within an interval of 3σ: e.g., C-C bonds involving the borylated carbon atom are significantly longer than bonds between non-borylated carbon atoms (e. g. **3**: 1.409 Å and 1.385 Å, respectively). Some trends become obvious from inspection of the computed data presented in Tables 2-5: quite independent of the method a minor but systematic shortening of C-C and C-B bonds (by 0.009−0.004 Å) occurs when going from the SVP to the TZVP basis, whereas for B-Br bonds an elongation (by 0.007−0.002 Å) is observed. For B3LYP, the choice of the larger cc-pVTZ basis does not lead to any significant changes of bond lengths in comparison to the computationally much more efficient TZVP basis. When going from HF to MP2, the inclusion of electron correlation leads to a constant elongation of C-C bonds by about 0.010 Å, whereas B-Br bonds are significantly shortened by 0.021 Å. C-B bonds hardly change at all. Only minor differences occur between MP2, HCTH, B98, and B3LYP calculations. In contrast, the older GGA functionals BP86 and BLYP give systematically longer C-C (by about 0.010 Å) and B-Br bonds (by about 0.024 Å). This observation is in line with the tendency quite commonly observed for these functionals to overestimate bond lengths [14]. With all other optimised parameters being virtually identical, the only difference in structures optimised with these two GGA functionals is the B-Br bond, which is systematically longer (by 0.012 Å) in BLYP calculations. Interestingly, all methods investigated give almost identical C-B bond lengths. All in all, the computational methods applied yield optimised geometries within the experimental error bars of 3σ (between 0.009 and 0.048 Å) − hence, based only on results from the present applications no method seems preferable over another in terms of quality. In terms of computational efficiency we note the excellent performance of the HCTH functional, which can make use of the RI approximation rendering the calculations faster by a factor of 2-3 for the present system sizes, and potentially more for larger species. Yet, this functional compares well with MP2 or the two hybrid functionals tested.

Trends in the computed data become obvious also for NMR shifts (Tables 6−9) [26]: When going from the SVP to the TZVP basis set a systematic low-field shift results for the ^{1}H NMR data (0.5-0.7 for MP2 and 0.2-0.5 for all other methods) and for ^{13}C NMR shifts. For the latter, however, low field shifts are much more pronounced for DFT methods compared to HF and MP2 (mean low field shifts SVP→TZVP in ppm: HF: 4.8, MP2: 3.5, BP86: 7.5, BLYP: 8.9, B98: 6.8, B3LYP: 7.8). This large dependence on the one-particle basis renders a comparison of computed data with experiment rather arbitrary: e.g., while for B3LYP the ^{13}C NMR results obtained with the SVP basis nicely agree with experiment (mean error −1.8 ppm) a significant deterioration results with the TZVP basis (shifts are systematically overestimated by a mean error of 5.9 ppm). A similar situation becomes visible for the B98 functional and for HF. The BLYP data, in turn, show a similar basis set dependence but both data sets are somewhat shifted with respect to experimental data (SVP: −4.2 ppm, TZVP: +2.6 ppm).

Table 2. Comparison between experimental and theoretical data for selected bond lengths in **1**

	Exp.	Mean	3σ	HF		MP2		BP86		BLYP		HCTH407		B98		B3LYP		
				SVP	TZVP	SVP	TZVP	SVP	TZVP	SVP	TZVP	SVP	TZVP	SVP	TZVP	SVP	TZVP	cc-pVTZ
C4-C5	1.421(8)	1.408	0.024	1.403	1.398	1.412	1.406	1.422	1.417	1.426	1.420	1.414	1.408	1.417	1.411	1.414	1.407	1.407
C3-C4	1.395(8)																	
C5-C6	1.373(9)	1.371	0.027	1.383	1.377	1.394	1.387	1.399	1.392	1.401	1.394	1.391	1.385	1.394	1.387	1.392	1.385	1.384
C2-C3	1.369(9)																	
C1-C6	1.383(9)	1.384	0.027	1.395	1.388	1.404	1.397	1.414	1.407	1.416	1.409	1.405	1.398	1.408	1.401	1.405	1.398	1.397
C1-C2	1.384(9)																	
C4-B1	1.499(9)	1.499	0.027	1.553	1.544	1.549	1.541	1.551	1.544	1.552	1.546	1.554	1.546	1.547	1.540	1.546	1.538	1.537
B1-Br1	1.943(7)	1.937	0.021	1.934	1.939	1.913	1.920	1.937	1.940	1.949	1.953	1.927	1.932	1.930	1.933	1.934	1.937	1.934
B1-Br2	1.931(7)																	

Table 3 Comparison between experimental and theoretical data for selected bond lengths in **2**

	Exp.	Mean	3σ	HF		MP2		BP86		BLYP		HCTH407		B98		B3LYP		
				SVP	TZVP	SVP	TZVP	SVP	TZVP	SVP	TZVP	SVP	TZVP	SVP	TZVP	SVP	TZVP	cc-pVTZ
C1-C2	1.401(9)	1.412	0.026	1.400	1.395	1.408	1.402	1.417	1.410	1.421	1.415	1.410	1.404	1.412	1.406	1.410	1.404	1.402
C2-C3	1.422(8)																	
C3-C4	1.404(8)	1.407	0.026	1.404	1.398	1.411	1.405	1.421	1.418	1.425	1.419	1.413	1.407	1.416	1.410	1.414	1.408	1.407
C1-C6	1.410(9)																	
C4-C5	1.385(10)	1.384	0.030	1.385	1.379	1.396	1.389	1.402	1.394	1.404	1.397	1.393	1.387	1.397	1.390	1.395	1.387	1.386
C5-C6	1.382(10)																	
C1-B1	1.543(9)	1.535	0.027	1.560	1.552	1.557	1.549	1.558	1.552	1.560	1.554	1.562	1.556	1.556	1.550	1.554	1.550	1.546
C3-B2	1.526(9)																	
B1-Br1	1.919(7)	1.920	0.020	1.929	1.932	1.908	1.911	1.929	1.931	1.942	1.946	1.922	1.925	1.924	1.926	1.927	1.929	1.927
B2-Br3	1.921(6)																	
B1-Br2	1.910(7)	1.915	0.020	1.931	1.936	1.910	1.913	1.932	1.934	1.946	1.949	1.924	1.928	1.927	1.930	1.931	1.933	1.930
B2-Br4	1.919(6)																	

Table 4 Comparison between experimental and theoretical data for selected bond lengths in **3**

	Exp.	Mean	3σ	HF		MP2		BP86		BLYP		HCTH407		B98		B3LYP		
				SVP	TZVP	SVP	TZVP	SVP	TZVP	SVP	TZVP	SVP	TZVP	SVP	TZVP	SVP	TZVP	cc-pVTZ
C1-C2	1.405(9)	1.409	0.009	1.401	1.396	1.413	1.407	1.421	1.414	1.425	1.418	1.413	1.407	1.416	1.409	1.413	1.407	1.406
C1-C6	1.412(9)																	
C2-C3	1.385(9)	1.385	0.027	1.384	1.380	1.393	1.386	1.398	1.391	1.400	1.393	1.390	1.384	1.394	1.387	1.392	1.385	1.384
C1-B1	1.559(11)	1.559	0.033	1.569	1.563	1.557	1.549	1.560	1.555	1.563	1.557	1.564	1.558	1.559	1.553	1.557	1.551	1.550
B1-Br1	1.925(8)	1.923	0.026	1.927	1.932	1.909	1.912	1.930	1.932	1.943	1.946	1.921	1.926	1.924	1.926	1.927	1.930	1.927
B1-Br2	1.920(9)																	

For MP2 best results are obtained with the larger TZVP basis. Interestingly, for the $^{13}C(CH_3)$ NMR shift in **1** substantially lower deviations from experiment are observed compared to the data for carbon nuclei of the aromatic rings (Table 6). These trends, together with the large dependency on the basis set, point to strong error compensation effects. In order to identify the source of these findings, we also computed the ^{13}C NMR shifts for benzene (Table 10). Indeed, a compilation of signed errors for the carbon nuclei constituting the aromatic subsystems (Table 11) reveals that error trends are already present in the parent benzene system to a large extent. In other words: most of the deviations

Table 5 Comparison between experimental and theoretical data for selected bond lengths in **4**

	Exp.	Mean	3σ	HF		MP2		BP86		BLYP		HCTH407		B98		B3LYP		
				SVP	TZVP	SVP	TZVP	SVP	TZVP	SVP	TZVP	SVP	TZVP	SVP	TZVP	SVP	TZVP	cc-pVTZ
C1-C2	1.418(13)	1.410	0.042	1.400	1.394	1.407	1.401	1.417	1.410	1.421	1.414	1.409	1.403	1.412	1.406	1.410	1.403	1.402
C2-C3	1.423(16)																	
C3-C4	1.388(13)																	
C1-B1	1.520(20)	1.546	0.048	1.562	1.554	1.561	1.554	1.561	1.556	1.564	1.559	1.565	1.559	1.559	1.553	1.557	1.552	1.550
C3-B2	1.571(12)																	
B1-Br1	1.908(11)	1.900	0.038	1.928	1.932	1.906	1.909	1.928	1.930	1.942	1.945	1.920	1.924	1.923	1.925	1.926	1.928	1.926
B2-Br2	1.888(13)																	
B2-Br3	1.903(14)																	

Table 6 Experimental and computed ^{1}H-, ^{13}C-, and ^{11}B NMR shifts for **1**

	Exp.	HF		MP2		BP86		BLYP		B98		B3LYP		
		SVP	TZVP	SVP	TZVP	SVP	TZVP	SVP	TZVP	SVP	TZVP	SVP	TZVP	cc-pVTZ
H-3,5	8.2	8.4	8.6	8.2	8.8	8.0	8.3	7.9	8.2	8.1	8.4	8.1	8.5	8.6
H-2,6	7.0	7.2	7.4	7.4	8.0	7.0	7.3	6.9	7.3	7.1	7.4	7.0	7.5	7.4
H-CH$_3$	2.0	2.2	2.4	2.2	2.7	2.1	2.3	2.1	2.3	2.1	2.3	2.1	2.4	2.3
C-1	146.8	152.8	159.8	135.6	141.1	141.5	151.9	142.2	154.3	145.1	154.8	144.9	155.8	154.9
C-3,5	138.3	145.2	150.4	128.8	131.9	133.2	140.3	133.3	141.9	136.9	143.7	136.7	144.5	144.3
C-2,6	129.4	126.7	131.3	125.7	129.3	123.9	131.1	123.5	132.2	125.8	132.5	125.6	133.3	133.3
C-4	n.o.	129.6	134.8	129.4	133.6	128.1	137.4	128.9	139.4	129.7	138.0	130.2	139.4	139.1
C-CH$_3$	21.8	20.6	21.0	22.7	19.0	23.0	23.6	22.8	23.9	23.0	23.4	22.6	23.2	23.8
B	56.6	55.6	54.8	54.8	55.7	49.5	50.3	54.2	55.3	52.6	52.8	55.1	55.8	54.9

from experiment observed above relate to shortcomings in the description of aromatic NMR shielding properties in relation to the TMS ^{13}C NMR standard. Much higher computational accuracy can be obtained by the choice of a benzene NMR-standard instead of TMS. While this is an observation quite typical for energies, vibrational frequencies, and other properties computed with contemporary density functional methods [14], also HF and MP2 follow these general trends here. However, particularly large deviations from experiment occur for **4** at the HF and MP2 levels of theory, whereas both methods show constantly smaller errors for computed ^{13}C NMR shifts in **1**, **2**, **3**. Apparently, the correlation problem is especially pronounced in **4**. The DFT methods applied, in turn, show rather constant errors, independent of the species studied. For computed ^{11}B NMR shifts the choice of a particular basis set has hardly any influence on the results (below 1 ppm in most cases, Table 12), and HF, MP2, BLYP, and B3LYP results nicely compare with experiment. Larger errors become visible for the B98 (-3.3 to -4.0 ppm) and BP86 (-5.4 to -7.1 ppm) functionals. Trends between the molecules, however, are equally well reproduced by all methods. This finding indicates a problem related to the choice of the B_2H_6 ^{11}B NMR standard for the latter two functionals.

In conclusion, for the present set of systems the best overall agreement with experiment is found for the B3LYP/SVP level for ^{1}H-, ^{13}C-, and ^{11}B NMR shifts alike. As alluded to above, we relate this good performance largely to fortuitous error compensation. Notwithstanding the limited physical basis underlying such a statement, in terms of practicability we find this level of theory computationally efficient and suitable to describe the NMR properties of the present set of systems.

Overall, theoretically predicted *relative* shift values within each molecule as well as between molecules are in excellent agreement with the experiment. For example, a pronounced deshielding of the carbon nuclei C-2,4,6 in compound **4** has not only been found experimentally [$\delta(^{13}\mathrm{C})_{\mathrm{exp}} = 151.4$] but is fully reproduced at all levels of theory [e.g. $\delta(^{13}\mathrm{C})_{\mathrm{B3LYP/SVP}} = 152.2$]. The finding of nearly identical ^{11}B NMR shifts for **1**-**4** is intuitively in agreement with essentially identical NBO charges on boron for all four species (**1**, **2**: +0.41; **3**, **4**: +0.40). Thus, substitution of the *para*-methyl group in **1** for a BBr_2 substituent has apparently no appreciable effect on the charge density around the boron centre. *Ipso* carbon atoms bearing a boryl substituent possess large negative NBO charges (**1**, **2**, **4**: -0.46; **3**: -0.41). Carbon atoms C-2,6 in **1** and C-5 in **2** bearing NBO charges of -0.22 and -0.21, respectively, are not affected by the presence of BBr_2 substituents in the *meta* position(s) of the aromatic ring (carbon NBO charges in benzene: -0.20). In contrast, charges of carbon atoms in a position *ortho* to one boryl group show a considerably reduced negative charge (e.g. C-3,5 in **1**: -0.12), which becomes even smaller upon introduction of a second *ortho* BBr_2 group (C-2 in **2**: -0.06). A Wiberg bond order analysis assigns a single bond between C and B (**1**: 0.98; **2**: 0.96; **3**: 0.95; **4**: 0.94) and a partial double bond character to the B-Br bonds (**1**: 1.19; **2**, **3**: 1.21; **4**: 1.22; for comparison C-C in benzene: 1.44).

Table 7 Experimental and computed ^{1}H-, ^{13}C-, and ^{11}B NMR shifts for **2**

	Exp.	HF		MP2		BP86		BLYP		B98		B3LYP		
		SVP	TZVP	SVP	TZVP	SVP	TZVP	SVP	TZVP	SVP	TZVP	SVP	TZVP	cc-pVTZ
H-2	8.9	9.6	9.8	9.2	9.9	9.0	9.3	8.9	9.3	9.2	9.5	9.1	9.6	9.8
H-4,6	8.1	8.8	9.1	8.4	9.1	8.2	8.6	8.1	8.5	8.4	8.8	8.4	8.8	9.0
H-5	6.9	7.4	7.6	7.7	8.3	7.2	7.6	7.1	7.6	7.4	7.7	7.3	7.7	7.8
C-2	147.0	158.0	162.9	137.5	139.5	143.2	150.0	143.6	151.9	147.7	154.1	147.4	154.8	154.6
C-4,6	143.5	153.2	158.5	132.9	135.8	138.4	145.9	138.4	147.3	142.7	149.7	142.3	150.3	150.3
C-5	128.1	123.8	128.5	125.4	128.7	122.5	130.2	122.1	131.1	124.1	131.2	124.0	131.9	131.9
C-1,3	n.o.	130.4	135.3	132.0	135.7	129.9	138.8	130.6	140.9	131.4	139.4	131.9	140.9	140.6
B	57.6	56.4	55.8	56.1	57.1	51.1	52.0	55.8	57.0	54.1	54.3	56.5	57.4	56.5

Table 8 Experimental and computed ^{1}H-, ^{13}C-, and ^{11}B NMR shifts for **3**

	Exp.	HF		MP2		BP86		BLYP		B98		B3LYP		
		SVP	TZVP	SVP	TZVP	SVP	TZVP	SVP	TZVP	SVP	TZVP	SVP	TZVP	cc-pVTZ
H-2,3,5,6	7.9	8.5	8.7	8.4	9.1	8.1	8.5	8.0	8.4	8.3	8.6	8.2	8.6	8.7
C-2,3,5,6	136.5	139.3	144.2	130.8	133.5	132.2	139.1	132.1	140.5	135.0	141.6	134.8	142.3	142.2
C-1,4	n.o.	140.8	146.5	133.6	137.6	134.1	143.6	134.9	145.7	136.8	145.3	137.2	146.7	146.2
B	58.3	57.6	56.3	56.2	57.2	51.7	52.4	56.3	57.4	54.8	55.0	57.2	57.9	57.2

Table 9 Experimental and computed ^{1}H-, ^{13}C-, and ^{11}B NMR shifts for **4**

	Exp.	HF		MP2		BP86		BLYP		B98		B3LYP		
		SVP	TZVP	SVP	TZVP	SVP	TZVP	SVP	TZVP	SVP	TZVP	SVP	TZVP	cc-pVTZ
H-2,4,6	9.0	9.9	10.1	9.4	10.0	9.2	9.5	9.0	9.4	9.4	9.7	9.3	9.7	10.0
C-2,4,6	151.4	165.7	170.7	140.6	142.5	147.3	154.3	147.7	156.0	152.5	159.0	152.2	159.7	159.5
C-1,3,5	n.o.	128.6	132.9	133.0	136.3	129.5	137.9	130.2	140.0	130.8	138.3	131.3	139.7	139.8
B	57.9	56.6	55.9	56.6	57.5	51.6	52.5	56.3	57.5	54.6	54.6	56.9	57.9	57.0

Table 10 Experimental and computed ^{1}H-, and ^{13}C NMR shifts for benzene.

	Exp.	HF		MP2		BP86		BLYP		B98		B3LYP		
		SVP	TZVP	SVP	TZVP	SVP	TZVP	SVP	TZVP	SVP	TZVP	SVP	TZVP	cc-pVTZ
H	7.3	7.3	7.6	7.3	7.9	7.1	7.4	7.0	7.4	7.2	7.5	7.1	7.6	7.5
C	128.5	130.1	135.7	121.3	125.2	122.7	130.8	122.5	132.1	125.3	132.9	125.2	133.8	133.4

Table 11 Deviations from experiment for computed ^{13}C NMR shifts (signed errors in ppm). For **1** and **2** a mean value only for the aromatic carbon nuclei (three data points) is given.

	HF		MP2		BP86		BLYP		B98		B3LYP		
	SVP	TZVP	SVP	TZVP	SVP	TZVP	SVP	TZVP	SVP	TZVP	SVP	TZVP	cc-pVTZ
benzene	1.6	7.2	−7.2	−3.3	−5.8	2.3	−6.0	3.6	−3.2	4.4	−3.3	5.2	4.9
1	3.4	9.0	−8.1	−4.1	−5.3	2.9	−5.2	4.6	−2.2	5.5	−2.4	6.4	6.0
2	5.5	10.4	−7.6	−4.9	−4.8	2.5	−4.8	3.9	−1.4	5.5	−1.6	6.1	6.1
3	2.8	7.8	−5.7	−3.0	−4.3	2.6	−4.4	4.0	−1.5	5.1	−1.7	5.8	5.7
4	14.3	19.3	−10.8	−8.9	−4.1	2.9	−3.7	4.6	1.1	7.6	0.8	8.3	8.1

As to an assessment of the quality of thermochemical properties of the present class of species, Table 13 presents a comparison of energy differences obtained at all levels of theory applied in this study. We note a pleasing agreement of all correlated methods in the description of the relative stabilisation of **2** compared to **3**: with the exception of HF

Table 12 Deviations from experiment for computed ^{11}B NMR shifts (signed errors in ppm).

	HF		MP2		BP86		BLYP		B98		B3LYP		
	SVP	TZVP	SVP	TZVP	SVP	TZVP	SVP	TZVP	SVP	TZVP	SVP	TZVP	cc-pVTZ
1	−1.0	−1.8	−1.8	−0.9	−7.1	−6.3	−2.4	−1.3	−4.0	−3.8	−1.5	−0.8	−1.7
2	−1.2	−1.8	−1.5	−0.5	−6.5	−5.6	−1.8	−0.6	−3.5	−3.3	−1.1	−0.2	−1.1
3	−0.7	−2.0	−2.1	−1.1	−6.6	−5.9	−2.0	−0.9	−3.5	−3.3	−1.1	−0.4	−1.1
4	−1.3	−2.0	−1.3	−0.4	−6.3	−5.4	−1.6	−0.4	−3.3	−3.3	−1.0	0.0	−0.9

Table 13 Energy difference between **2** and **3** and reaction energy for the isodesmic reaction: toluene + **4** → **1** + **2** (total energy differences in kcal/mol).

	HF		MP2		BP86		BLYP		HCTH		B98		B3LYP		
	SVP	TZVP	SVP	TZVP	SVP	TZVP	SVP	TZVP	SVP	TZVP	SVP	TZVP	SVP	TZVP	cc-pVTZ
ΔE(**3**−**2**)	2.0	6.0	0.2	0.3	0.6	0.6	0.5	0.5	0.5	0.5	0.8	0.8	0.8	0.8	0.8
ΔE(reaction)	2.2	2.4	1.8	1.7	2.7	3.0	2.6	3.1	2.5	2.8	2.7	2.9	2.6	3.0	3.1

[27], the results do not even show any significant basis set dependence. Excellent agreement is also found for the isodesmic reaction: toluene + **4** → **1** + **2** (Table 13). Although error compensation should be highly efficient for the cases studied, we take these results as a confirmation of the general reliability of the quantum chemical methods tested for the present class of systems.

3 Conclusions

The strong Lewis acids 4-(dibromoboryl)toluene (**1**), 1,3-bis(dibromoboryl)benzene (**2**), 1,4-bis(dibromoboryl)benzene (**3**), 1,3,5-tris(dibromoboryl)benzene (**4**), and 4,4′-bis(dibromoboryl)biphenyl (**5**) have been synthesized from the corresponding trimethylsilyl derivatives and boron tribromide. Each of the compounds adopts an almost perfectly planar conformation in the solid state. According to DFT calculations, any deviations of the molecular structures from the highest applicable symmetry point groups (C_s, C_{2v}, C_{2v}, and D_{3h} for **1**, **2**, **3**, and **4**, respectively) are due to crystal packing effects (e.g. compound **4** possesses only C_2 symmetry in the solid state). The ^{11}B NMR signals of **1-5** lie in the very narrow range between 56.6 ppm (**1**) and 58.3 ppm (**3**). Since the strongest influence on the magnetic shielding of three-coordinate boron nuclei usually comes from the π charge density, the boron p orbitals are obviously equally populated in all five compounds. This interpretation is supported by the finding of essentially identical NBO charges on boron for **1** (+0.41), **2** (+0.41), **3** (+0.40), and **4** (+0.40). ^{13}C NMR spectroscopy shows the resonances of carbon atoms in *ortho* and *para* position to the BBr_2 group(s) to experience a continuous downfield shift as the number of boryl substituents increases [cf. C_6H_6: $\delta(^{13}C) = 128.5$ [16]; **1**: $\delta(^{13}C\text{-}ortho) = 138.3$; **2**: $\delta(^{13}C\text{-}ortho) = 147.0, 143.5$; **4**: $\delta(^{13}C) = 151.4$], in agreement with decreasing NBO charges on these atoms. Interestingly, even the introduction of a second BBr_2 group into the *para* position of another boryl substituent (cf. **3**) does not reduce the charge density on this boron atom as compared to the corresponding monoborylated species but rather leads to a further depletion of the aromatic π electron system. DFT calculations on **1-4** (geometry optimisations; population analyses; prediction of ^{1}H-, ^{13}C- and ^{11}B NMR parameters) lead to the conclusion, that the best overall agreement with experimental data is found for the B3LYP/SVP level of theory.

Acknowledgement. This work was supported by the *Deutsche Forschungsgemeinschaft* (DFG). The generous allotment of computer time by the CSC Frankfurt is gratefully acknowledged.

4 Experimental Section

General Considerations. All reactions and manipulations of air-sensitive compounds were carried out in dry, oxygen-free argon using standard Schlenk ware. Solvents were freshly distilled under Ar from Na-benzophenone (toluene, *n*-pentane) or stored over 4 Å molecular sieves prior to use (C_6D_6). NMR: Bruker Avance 400, Bruker AMX 250, Bruker DPX 250 spectrometers. ^{11}B NMR spectra are reported relative to external $BF_3 \cdot Et_2O$. All NMR spectra were run at ambient temperature. Abbreviations: s = singlet; d = doublet; t = triplet; n.r. = multiplet expected in the ^{1}H NMR spectrum but not resolved; n.o. = signal not observed. **2**, **3** [11], and **5** [28] have been prepared previously by slightly different procedures.

Preparation of 1: 4-(Trimethylsilyl)toluene (3.28 g, 19.96 mmol) was dissolved in 10 ml of *n*-pentane. Boron tribromide (7.50 g, 29.95 mmol) was added via syringe at ambient temperature. The reaction mixture was stirred for 2 h. Slow evaporation of all volatiles *in vacuo* gave colourless crystals of **1**. Yield: 5.09 g (97 %).

^{1}H-NMR (250.1 MHz, C_6D_6): δ 8.15 (d, 2H, ^3J(H,H) = 7.9 Hz; H-3,5), 6.95 (d, 2H, ^3J(H,H) = 7.9 Hz; H-2,6), 2.02 (s, 3H; CH_3); ^{13}C-NMR (100.6 MHz,): δ 146.8 (C-1), 138.3 (C-3,5), 129.4 (C-2,6), 21.8 (CH_3), n.o. (C-4); ^{11}B-NMR (128.4 MHz,): δ 56.6 ($h_{1/2}$ = 150 Hz).

Preparation of 2: 1,3-Bis(trimethylsilyl)benzene (3.00 g; 13.48 mmol) was dissolved in 10 ml of *n*-pentane. After boron tribromide (14.56 g; 58.16 mmol) had been added via syringe, the resulting clear solution was heated at reflux temperature for 7 h. Colourless needles of **2** precipitated from the reaction mixture upon cooling to ambient temperature. Slow evaporation of the solvent from the mother liquor *in vacuo* gave a second crop. Yield: 4.50 g (80 %).

^{1}H-NMR (250.1 MHz, C_6D_6): δ 8.94 (n.r., 1H; H-2), 8.07 (dd, 2H, $^{3}J_{HH}$ = 7.6 Hz, $^{4}J_{HH}$ = 1.5 Hz; H-4,6), 6.87 (t, 1H, $^{3}J_{HH}$ = 7.6 Hz; H-5); ^{13}C-NMR (62.9 MHz, C_6D_6): δ 147.0 (C-2), 143.5 (C-4,6), 128.1 (C-5), n.o. (C-1,3); ^{11}B-NMR (128.4 MHz, C_6D_6): δ 57.6 ($h_{1/2}$ = 210 Hz).

Preparation of 3: 1,4-Bis(trimethylsilyl)benzene (4.80 g, 21.58 mmol) was dissolved in 10 ml of toluene. After boron tribromide (16.00 g, 63.87 mmol) had been added via syringe, the resulting clear solution was heated at reflux temperature for 3 h. Colourless needles of **3** precipitated from the reaction mixture upon cooling to ambient temperature. Slow evaporation of the solvent from the mother liquor *in vacuo* gave a second crop. Yield: 6.95 g (77 %).

^{1}H-NMR (400.1 MHz, C_6D_6): δ 7.86 (s, 4H, H-2,3,5,6); ^{13}C-NMR (100.6 MHz, C_6D_6): δ 136.5 (C-2,3,5,6), n.o. (C-1,4); ^{11}B-NMR (128.4 MHz, C_6D_6): δ 58.3 ($h_{1/2}$ = 240 Hz).

Preparation of 4: The compound was prepared similar to **3** from 1,3,5-tris(trimethylsilyl)benzene (3.11 g, 10.55 mmol) and boron tribromide (16.00 g, 63.87 mmol) in 10 ml of toluene. Colourless needles of **4** precipitated from the reaction mixture upon cooling to ambient temperature. Slow evaporation of the solvent from the mother liquor *in vacuo* gave a second crop. Yield: 5.90 g (95 %).

^{1}H-NMR (400.1 MHz, C_6D_6): δ 9.03 (s, 3H, H-2,4,6); ^{13}C-NMR (62.9 MHz, C_6D_6): δ 151.4 (C-2,4,6), n.o. (C-1,3,5); ^{11}B-NMR (128.4 MHz, C_6D_6): δ 57.9 ($h_{1/2}$ = 270 Hz).

Preparation of 5: The compound was prepared similar to **3** from 4,4′-bis(trimethylsilyl)biphenyl (0.60 g, 2.01 mmol) and boron tribromide (1.41 g, 5.63 mmol) in 5 ml of toluene. Colourless needles of **5** precipitated from the reaction mixture upon cooling to ambient temperature. Slow evaporation of the solvent from the mother liquor *in vacuo* gave a second crop. Yield: 0.85 g (86 %).

^{1}H-NMR (250.1 MHz, C_6D_6): δ 8.11 (d, 4H, $^{3}J_{HH}$ = 8.2 Hz, H-3,3′,5,5′), 7.23 (d, 4H, $^{3}J_{HH}$ = 8.2 Hz, H-2,2′,6,6′); ^{13}C-NMR (62.9 MHz, C_6D_6): δ 146.2 (C-1,1′), 138.6 (C-3,3′,5,5′), 127.1 (C-2,2′,6,6′), n.o. (C-4,4′); ^{11}B-NMR (128.4 MHz, C_6D_6): δ 57.0 ($h_{1/2}$ = not determined).

X-ray crystal structure determinations of 1−5

The data for **1** were collected on a SIEMENS SMART diffractometer, the data for **2**, **3**, **4** and **5** were collected on a STOE-IPDS two-circle diffractometer. All structures were solved by direct methods and refined with full-matrix least-squares techniques. Non-H atoms were refined anisotropically, whereas H atoms were refined using a riding model. The molecules of **3** are located on a centre of inversion with half a molecule in the asymmetric unit. The molecules of **4** are located on a two-fold rotation axis with half a molecule in the asymmetric unit.

CCDC reference numbers:212678 (**1**), 212676 (**2**), 212675 (**3**), 212677 (**4**), 229267 (**5**).

References

[1] E. H. Yamamoto, *Lewis Acid Reagents: A Practical Approach*, Oxford University Press, New York, 1999.
[2] T. Renk, W. Ruf, W. Siebert, *J. Organomet. Chem.* **1976**, *120*, 1.
[3] W. Ruf, T. Renk, W. Siebert, *Z. Naturforsch.* **1976**, *31b*, 1028.
[4] B. Wrackmeyer, U. Dörfler, M. Herberhold, *Z. Naturforsch.* **1993**, *48b*, 121.
[5] B. Wrackmeyer, U. Dörfler, J. Rinck, M. Herberhold, *Z. Naturforsch.* **1994**, *49b*, 1403.
[6] A. Appel, H. Nöth, M. Schmidt, *Chem. Ber.* **1995**, *128*, 621.
[7] S. Aldridge, C. Bresner, *Coord. Chem. Rev.* **2003**, *244*, 71.
[8] K. Ma, M. Scheibitz, S. Scholz, M. Wagner, *J. Organomet. Chem.* **2002**, *652*, 11.
[9] Y. Quin, G. Cheng, A. Sundararaman, F. Jäkle, *J. Am. Chem. Soc.* **2002**, *124*, 12672.
[10] S. Bieller, F. Zhang, M. Bolte, J. W. Bats, H.-W. Lerner, M. Wagner, *Organometallics* **2004**, *23*, 2107.
[11] D. Kaufmann, *Chem. Ber.* **1987**, *120*, 901.
[12] M. Bluhm, H. Pritzkow, W. Siebert, R. N. Grimes, *Angew. Chem.* **2000**, *112*, 4736; *Angew. Chem. Int. Ed.* **2000**, *39*, 4562.
[13] A. Maderna, H. Pritzkow, W. Siebert, *Angew. Chem.* **1996**, *108*, 1664; *Angew. Chem. Int. Ed.* **1996**, *35*, 1501.
[14] W. Koch, M. C. Holthausen, *A Chemist's Guide to Density Functional Theory*, 2nd ed., Wiley-VCH, Weinheim, 2001.
[15] H. Nöth, B. Wrackmeyer, *Nuclear Magnetic Resonance Spectroscopy of Boron Compounds*, in P. Diehl, E. Fluck, R. Kosfeld (Eds.), *NMR Basic Principles and Progress*, Springer, Berlin, Heidelberg, New York, 1978.
[16] M. Hesse, H. Meier, B. Zeeh, *Spektroskopische Methoden in der organischen Chemie*, Thieme, Stuttgart, 1987.
[17] R. Ahlrichs, M. Bär, M. Häser, H. Horn, C. Kölmel, *Chem. Phys. Lett.* **1989**, *162*, 165.
[18] M. J. Frisch, G. W. Trucks, H. B. Schlegel, G. E. Scuseria, M. A. Robb, J. R. Cheeseman, J. J. A. Montgomery, T. Vreven, K. N. Kudin, J. C. Burant, J. M. Millam, S. S. Iyengar, J. Tomasi, V. Barone, B. Mennucci, M. Cossi, G. Scalmani, N. Rega, G. A. Petersson, H. Nakatsuji, M. Hada, M. Ehara, K. Toyota, R. Fukuda, J. Hasegawa, M. Ishida, T. Nakajima, Y. Honda, O. Kitao, H. Nakai, M. Klene, X. Li, J. E. Knox, H. P. Hratchian, J. B. Cross, C. Adamo, J. Jaramillo, R. Gomperts, R. E. Stratmann, O. Yazyev, A. J. Austin, R. Cammi, C. Pomelli, J. W. Ochterski, P. Y. Ayala, K. Morokuma, G. A. Voth, P. Salvador, J. J. Dannenberg, V. G. Zakrzewski, S. Dapprich, A. D. Daniels, M. C. Strain, O. Farkas, D. K. Malick, A. D. Rabuck, K. Raghavachari, J. B. Foresman, J. V. Ortiz, Q. Cui, A. G. Baboul, S. Clifford, J. Cioslowski, B. B. Stefanov, G. Liu, A. Liashenko, P. Piskorz, I. Komaromi, R. L. Martin, D. J. Fox, T. Keith, M. A. Al-Laham, C. Y. Peng, A. Nanayakkara, M. Challacombe, P. M. W. Gill, B. Johnson, W. Chen, M. W. Wong, C. Gonzalez, J. A. Pople, Gaussian, Inc., Pittsburgh, PA, 2003.
[19] F. A. Hamprecht, A. J. Cohen, D. J. Tozer, N. C. Handy, *J. Chem. Phys.* **1998**, *109*, 6264; A. D. Boese, N. C. Handy, *J. Chem. Phys.* **2001**, *114*, 5497.
[20] R. A. Kendall, H. A. Früchtl, *Theor. Chem. Acc.* **1997**, *97*, 158.
[21] A. D. Becke, *J. Chem. Phys.* **1997**, *107*, 8554.
[22] A. Schäfer, H. Horn, R. Ahlrichs, *J. Chem. Phys.* **1992**, *97*, 2571.
[23] A. Schäfer, C. Huber, R. Ahlrichs, *J. Chem. Phys.* **1994**, *100*, 5829.
[24] T. H. Dunning Jr., *J. Chem. Phys.* **1989**, *90*, 1007.
[25] J. Gauss, *Phys. Chem. Chem. Phys.* **1995**, *99*, 1001.
[26] In the present version of Gaussian 03 the computation of NMR chemical shielding tensors is not implemented for the HCTH functional.
[27] Common wisdom has it that HF theory should not be used for thermochemical predictions with the exception of isodesmic (or isogyric) reactions (see: K. K. Irikura, D. J. Frurip (Eds.), *Computational Thermochemistry*, American Chemical Society Symposium Series, Washington DC,1998.
[28] U. Gross, D. Kaufmann, *Chem. Ber.* **1987**, *120*, 991.

7 Lebenslauf

Persönliche Daten:

Name: Alireza Haghiri Ilkhechi
Wohnort: Ben-Gurion-Ring 48a
60437 Frankfurt am Main
Geburtsdatum: 11. September 1968
Geburtsort: Teheran (Iran)
Staatsangehörigkeit: Deutsch (seit September 2003)
Familienstand: Ledig

Schule und Studium:

20.09.1974 - 01.06.1979	Grundschule: Mahde-Kudak-Schule in Teheran
20.09.1979 - 03.06.1982	Mittelstufengymnasium: Nowjavanan-Engelab-Gymnasium in Teheran
20.09.1982 - 04.06.1986	Oberstufengymnasium: Shahid-Ahadzadeh-Gymnasium in Teheran
04. Juni 1986	Schulabschluss: Abitur
10.10.1987 - 20.10.1989	Militärdienst im Iran
18.12.1989 - 12.02.1991	Vorbereitungskurse für das Hochschulstudium im Iran
21. September 1991	Erfolgreiche Aufnahmeprüfung für die Hochschulen im Iran
12. August 1992	Einreise in die Bundesrepublik Deutschland
22.10.1992 - 20.12.1993	Deutschkurse an der TH-Aachen und der TH-Darmstadt
07.01.1994 - 20.12.1994	Besuch des Studienkollegs für ausländische Studienbewerber in Frankfurt am Main
20. Dezember 1994	Erfolgreiche Hochschulreifeprüfung im Studienkolleg für ausländische Studienbewerber in Frankfurt am Main
15.04.1995 - 01.12.2001	Studium im Fach Diplom-Chemie; Johann Wolfgang Goethe-Universität Frankfurt am Main
02.01.2002 - 25.06.2002	Diplomarbeit, Thema: „Synthese und Reaktivität von Skorpionat-Liganden auf Cymantrenbasis“ im Arbeitskreis von Prof. Dr. M. Wagner - Johann Wolfgang Goethe-Universität Frankfurt am Main
01.08.2002 - 01.03.2005	Dissertation, Thema: „Cymantren- und Ferrocen-basierte Poly(pyrazol-1-yl)borate: Kation-π Wechselwirkungen und Multidecker-Sandwichkomplexe“ im Arbeitskreis von Prof. Dr. M. Wagner - Johann Wolfgang Goethe-Universität Frankfurt am Main

8 Eidesstattliche Versicherung

Eidesstattliche Versicherung

Ich erkläre hiermit an Eides statt, dass ich die vorgelegte Dissertation über

Cymantren- und Ferrocen-basierte Poly(pyrazol-1-yl)borate: Kation-π Wechselwirkungen und Multidecker-Sandwichkomplexe

selbständig angefertigt und mich anderer Hilfsmittel als der in ihr angegebenen nicht bedient habe, insbesondere, dass aus Schriften Entlehnungen, soweit sie in der Dissertation nicht ausdrücklich als solche mit Angabe der betreffenden Schrift bezeichnet sind, nicht stattgefunden haben.

Frankfurt am Main, 01. März 2005

Alireza Haghiri Ilkhechi